ACADEMY OF SCIENCES OF THE REPUBLIC OF UZBEKISTAN
PHYSICAL-TECHNICAL INSTITUTE OF SPA «PHYSICS-SUN»

A manuscript
UDC 539.172.12; 539.172.17

KHUSNIDDIN KOSIMOVICH OLIMOV

PRODUCTION OF NEGATIVE PIONS AND $\Delta^0(1232)$ RESONANCES IN p, d, ^{4}He, ^{12}C(^{12}C) AND ^{12}C^{181}Ta COLLISIONS AT 4.2 *A* GeV/*c*

01.04.08- Physics of atomic nucleus and elementary particles. Accelerator technique

DISSERTATION
written to get the Doctor of Science (DSc) degree of physical and mathematical sciences

Scientific consultant: Sagdulla Lutfullaevich Lutpullaev,
Doctor on physics and mathematics sciences,
Professor

Tashkent – 2018

CONTENTS

LIST OF ABBREVIATIONS

A+A or *AA*	Nucleus–Nucleus
cm	Centre-of-Mass
cms	Centre-of-Mass System
d	Deuteron (^{2}H nucleus)
EOS	Equation of State
h+A or *hA*	Hadron–Nucleus
h+h or *hh*	Hadron–Hadron
JINR	Joint Institute for Nuclear Research (Dubna, Russia)
CERN	Center of European Nuclear Research (Geneva, Switzerland)
LHC	Large Hadron Collider (Geneva, Switzerland)
RHIC	Relativistic Heavy Ion Collider (Brookhaven, USA)
N+N or *NN*	Nucleon–Nucleon
RHIC	Relativistic Heavy Ion Collider
GSI	Gesellschaft fur Schwerionenforschung (Darmstadt, Germany)
QGSM	Quark–Gluon String Model
$\sqrt{s_{nn}}$	Center-of-Mass Energy per nucleon pair

p^{12}C collisions	is equivalent to	$p+^{12}$C collisions
d^{12}C collisions	is equivalent to	$d+^{12}$C collisions
^{16}Op collisions	is equivalent to	^{16}O+p collisions
^{4}He^{12}C collisions	is equivalent to	^{4}He+^{12}C collisions
^{12}C^{12}C collisions	is equivalent to	^{12}C+^{12}C collisions
^{12}C^{181}Ta collisions	is equivalent to	^{12}C+^{181}Ta collisions
π^{-12}C collisions	is equivalent to	$\pi^{-}+^{12}$C collisions

INTRODUCTION

Topicality and demand of the theme of dissertation. Nowadays the experimental and theoretical investigations of the high energy nucleus-nucleus collisions are important for solution of the modern fundamental problems of physics in the world. Nucleus–nucleus collisions allow very high energy to be deposited within the small volume of space in a short interval of time. Analysis of this high energy density matter constitutes one of the priporiy directions of the modern fundamental nuclear physics. The central AuAu and PbPb collisions, where the nuclei are accelerated to a nearly speed of light prior to the collisions, generate temperatures more than 100 000 times hotter than that of the centre of the Sun and allow researchers to study a Quark-Gluon Plasma state of matter. Therefore it is of importance the investigations of dynamics of the central nucleus-nucleus collisions at high energies.

During the independence era, a big attention is given to the development of science, in particular, of the theoretical and experimental works in the field of nuclear and particle physics, in order to create conditions at the highest international level for the fundamental research. The main directions of the fundamental researches, having importance for a development of fundamental science in our country and its subsequent application to the real life, are highlighted in the Strategy of actions on the further development of the Republic of Uzbekistan in the years 2017-2021.

Nowadays the data on dynamics of high energy nucleus-nucleus collisions come mainly from analysis of the measured transverse momentum and rapidity distributions of hadrons. The biggest fraction of the energy spent on particle creation during high energy nuclear collisions is used for pion production. Hence knowledge of the properties of pion production is necessary in order to establish the global conditions created in the collision zone and to understand the dynamics of the collision process. The temperatures, extracted from transverse momentum or transverse mass (energy) distributions of pions, are important for probing the freeze-out conditions after expansion of a “fireball”, produced in central heavy ion collisions at high energies. The delta resonances play a dominant role in pion production in heavy ion collisions at the energies of the order of 1–10 GeV/nucleon. As deduced from analysis of the relativistic heavy ion collisions, delta resonances are produced at an early “hot” compressional phase of a collision. At a later expansion phase, these resonances decay into nucleons and pions as the collision system gets cooled down significantly. The kinematics of Δ decay was shown to be responsible for the low transverse momentum enhancement of the pion p_t distributions in hadron–nucleus and nucleus–nucleus collisions at incident beam energies from 1 to 15 GeV per nucleon.

The present investigation complies with the tasks stipulated in government regulatory documents and Decree of the President of the Republic of Uzbekistan № PD-4512 “On works of further development of alternative energy sources” of 1 March 2013, Resolution № PR-2789 “On measures of further improvement of the activities of the Academy of Sciences, organization, management and financing the scientific research works” of 17 February 2017, and Decree № PD-4947 “On the Strategy of Actions on the Further Development of the Republic of Uzbekistan” of 7 February 2017 and others.

Conformity of research to priority directions of development of science and technologies of the Republic of Uzbekistan. The dissertation was carried out in accordance with the priority directions of science and technologies development: II. “Energetics, energy and resource saving”.

Review of international scientific researches on dissertation subject. Investigations of the processes of production of pions and delta resonances in hadron- and nucleus-nucleus collisions at high energies are held at the Joint Institute for Nuclear Research (JINR, Dubna, Russia), Center of Heavy Ions (GSI, Darmstadt, Germany), Brookhaven National Laboratory (Brookhaven, USA), Center of European Nuclear Research (CERN, Geneva, Switzerland), Lawrence

Berkeley Laboratory of University of California (California, USA), Department of Natural Sciences of the University of Belgrade (Belgrade, Serbia), Institute of High Energy Physics of Tbilisi State University (Tbilisi, Georgia) and other research centers, which are the members of the International collaborations, involved in high energy physics experiments.

The above international centers of high energy physics and international collaborations involved in their experiments studied extensively the rapidity, transverse momentum and energy distributions of pions and Δ(1232) production in hadron-nucleus and nucleus-nucleus collisions at incident energies of the order of a few GeV per nucleon. The several important results were obtained, including: the rapidity distributions of pions produced in relativistic nuclear collisions were shown to have a Gaussian bell-like shapes; it was discovered that transverse momentum as well as the center-of-mass energy spectra of pions demonstrate the two slope structures, corresponding to two different temperatures; the contribution of the low temperature part to transverse momentum as well as center-of-mass energy spectrum of pions was dominant being of the order of 80-90%, while that of the high temperature part was about 10-20% (Joint Institute for Nuclear Research, Dubna, Russia; Center of European Nuclear Research, Geneva, Switzerland; Department of Natural Sciences of the University of Belgrade, Belgrade, Serbia; Institute of High Energy Physics of Tbilisi State University, Tbilisi, Georgia); it was found out that the main fraction of pions produced in central heavy ion collisions at energies of the order of several GeV/nucleon come from decay of baryon resonances, excited during the early compression phase of a collision (which decay into pions and nucleons in the later expansion phase); it was observed that the mass and width of the Δ(1232)'s produced in nuclear medium in relativistic hadron-nucleus and nucleus-nucleus collisions modify as compared to those of Δ(1232)'s produced in nucleon-nucleon collisions (Center of Heavy Ions, Darmstadt, Germany); the modification of Δ(1232) properties in dense hadron matter created in central heavy ion collisions was interpreted in terms of thermal and isobar models, and also related to the values of hadronic density, temperature, and various non-nucleon degrees of freedom in nuclear matter (Center of Heavy Ions, Darmstadt, Germany).

The following fundamental investigations are held nowadays on the processes and mechanisms of pion and delta resonance production in relativistic nuclear collisions: search for the pion bose-condensate and effects of pion identity; construction of the realistic potential of pion-nucleon interaction at high energies; investigations of the influence of the dense nuclear (hadron) matter on the properties of pions and Δ(1232) resonances; study of the role of Δ(1232) resonances in the processes of pion production.

Degree of study of the problem. To date, leading international scientists carried out a large number of the experimental and theoretical investigations devoted to the processes and mechanisms of pion and delta resonance production in relativistic nuclear collisions, although some important problems still remain unsolved.

The Serbian scientists (L. Simic, S. Backovic, D. Salihagic) investigated the collision centrality dependencies of the rapidity spectra of the negative pions in nucleus-nucleus collisions at 4.2 *A* GeV/*c* (at Joint Institute for Nuclear Research experiments, Russia, Serbia). However, due to quite low statistics of the experimental material, they could not make unambigious conclusions about the changes of the widths and centers of the rapidity distributions of the negative pions with the changes in the collision centrality and mass numbers of the colliding nuclei. The Uzbek and Russian scientists (M.M. Muminov, R.N. Bekmirzaev, S.A. Sharipova, E.N. Kladnitskaya) investigated qualitatively the dependencies of the rapidity distributions of the negative pions on their transverse momentum range in nucleus-nucleus collisions at 4.2 *A* GeV/*c* (at Joint Institute for Nuclear Research experiments, Russia, Uzbekistan). However, not sufficient statistics of the experimental material did not allow them to make quantitative conclusions on the dependencies of the rapidity spectra of pions on their transverse momenta and mass numbers of the colliding nuclei.

The Indian scientists (G. Sau, B. De, and S. Bhattacharyya) proposed Grand Combinational Model (GCM) for the systematic description of the center-of-mass (cm) rapidity distributions of different particles produced in central heavy ion collisions at high energies. Using GSM, they described successfully the cm rapidity distributions of the produced particles, including pions, in central PbPb collisions and central AuAu collisions at high energies (at the experiments of the Center of European Nuclear Research, Switzerland; Brookhaven National Laboratory, USA). However, they could not give the plausible physical interpretations of the parameters, used in the phenomenological Grand Combinational Model.

The European scientists (D. Pelte, M.A. Lisa, E.L. Hjort, B. Hong) studied intensively the delta resonance production and modification of delta properties in central heavy-ion collisions at incident energies 1-2 *A* GeV, revealing that the decays of baryon resonances give the largest contribution to pion production at these energies. However, the mass distributions of the delta resonances could not be reconstructed in relativistic nucleus-nucleus collisions at Joint Institute for Nuclear Research (Dubna, Russia) experiments with the 2-m propane and 1-m hydrogen bubble chambers, except the work of the Serbian scientists (D. Krpic, S. Backovic, L. Simic), where production of baryon resonances was analyzed successfully in carbon-carbon collisions at 4.2 GeV/*c* per nucleon.

In the works of Serbian scientists (S. Backovic, L. Simic), Georgian researchers (L.V. Chkhaidze, T. Djobava, L. Kharkhelauri, M. Mosidze), and German scientist (R. Brockmann), the temperatures were extracted from the the transverse momentum and center-of-mass energy spectra of pions for different sets of colliding nuclei at various energies. However, practically no collision centrality of these temperatures (slopes of pion spectra) could be revealed from analysis of the whole range of the transverse momentum and center-of-mass energy distributions of pions in the analyzed collisions.

Connection of dissertational research with the plans of scientific-research works of the scientific research institution, where the dissertation

was conducted is reflected in the following projects, implemented within the framework of the fundamental research topics of Physical-technical institute of Uzbek Academy of Sciences: F2-F029 “Investigation of the nuclear matter structure and collective effects at interactions of hadrons and nuclei with nuclei at high energies” (2007-2011); F2-F-0-42438 “Investigation of multiparticle states in interactions of hadrons and nuclei with nuclei at high energies” (2012-2016).

The aim of the investigation is to establish the regularities of production of the negative pions and Δ^0(1232) resonances in p^{12}C, d^{12}C, ^{4}He^{12}C, ^{12}C^{12}C, ^{12}C^{181}Ta collisions at 4.2 *A* GeV/*c* and reveal the role of the Δ^0(1232) resonances in production of the negative pions in the above collisions and in ^{16}O*p* collisions at 3.25 *A* GeV/*c* and π^{-12}C interactions at 40 GeV/*c*.

The tasks of the research:

extraction of the separate classes of inelastic interactions in the set of p(C_3H_8) collisions at 4.2 GeV/*c*, π^-(C_3H_8) interactions at 40 GeV/*c*, *d*(C_3H_8), α(C_3H_8), and C(C_3H_8) interactions at 4.2 *A* GeV/*c*;

accounting for the loss of particles with short tracks and those emitted under large angles with respect to the object plane of the chamber in p^{12}C, d^{12}C, ^{4}He^{12}C, ^{12}C^{12}C, ^{12}C^{181}Ta collisions at 4.2 *A* GeV/*c*, ^{16}O*p* collisions at 3.25 *A* GeV/*c*, π^{-12}C interactions at 40 GeV/*c*;

reconstruction of the mass distributions of Δ^0(1232) resonances, analyzing the angles between outgoing π^- mesons and protons, in p^{12}C, d^{12}C, ^{4}He^{12}C, ^{12}C^{181}Ta collisions at 4.2 *A* GeV/*c*, ^{16}O*p* collisions at 3.25 *A* GeV/*c*, π^{-12}C interactions at 40 GeV/*c*;

selection and analysis of the peripheral, semicentral and central collision events in the analyzed set of collisions;

analysis of the transverse momentum and rapidity distributions of the negative pions in the minimum bias, peripheral, semicentral and central collision events in the analyzed collisions by fitting these spectra by the theoretical (model) functions;

interpretation of the obtained results on the dependencies of the transverse momentum and rapidity distributions of the negative pions on the collision centrality and mass numbers of the colliding nuclei.

Object of research is the nuclear processes, induced by hadrons and nuclei at high energies.

Subject of research is the processes of pion and $\Delta^0(1232)$ resonance production in relativistic nuclear collisions.

Methods of research. An inclusive approach to the formation of particles in nuclear interactions at high energies using the methods of mathematical statistics; the experimental methods of analysis of film information, obtained from bubble chambers, irradiated by the beams of relativistic hadrons and nuclei in the strong magnetic field.

The scientific novelty of the dissertation research is expressed by the following results, obtained for the first time:

the masses and widths of the $\Delta^0(1232)$ resonances in the minimum bias p^{12}C, d^{12}C, ^{4}He^{12}C, ^{12}C^{181}Ta collisions at 4.2 A GeV/c, ^{16}Op collisions at 3.25 A GeV/c, π^{-12}C interactions at 40 GeV/c were determined from fitting the reconstructed $\Delta^0(1232)$ mass distributions by the relativistic Breit-Wigner function;

it was estimated that in p^{12}C, d^{12}C, α^{12}C, and^{12}C^{181}Ta collisions at 4.2 A GeV/c and in ^{16}Op collisions at 3.25 A GeV/c around (40-50)% of the produced negative pions come from decay of $\Delta^0(1232)$ resonances, whereas in $\pi^{-\,12}$C interactions at 40 GeV/c only about 6% of the negative pions originate from $\Delta^0(1232)$ decays;

it was obtained that the average decrease in the mass of the $\Delta^0(1232)$ resonances in the analyzed collisions agrees within the uncertainties with the average binding energy of the nucleons of the fragmenting nuclei, suggesting that the $\Delta^0(1232)$ resonances are produced mainly on the bound nucleons at the collective excitations of the fragmenting nuclei;

the widths of the experimental rapidity spectra of the negative pions were found to decrease by $(8\pm2)\%$, $(5\pm1)\%$, and $(15\pm2)\%$ in going from peripheral to central d^{12}C, ^{12}C^{12}C, and ^{12}C^{181}Ta collisions, respectively, and the centers of the experimental rapidity distributions of π^-mesons were found to shift by –0.32±0.04 and –0.44±0.02 units towards target fragmentation region while going from peripheral to central d^{12}C and ^{12}C^{181}Ta collisions, respectively;

the collision centrality as well as the system-size dependencies of the temperatures of soft and hard parts of the experimental transverse momentum distributions of the negative pions in ^{4}He^{12}C, ^{12}C^{12}C, and ^{12}C^{181}Ta collisions at 4.2 *A* GeV/*c* were established and the differences between extracted temperatures of both the soft and hard components of p_t distributions of π^--mesons in the studied collision systems were found to increase with an increase in collision centrality;

the temperature of the soft p_t component of the negative pions in ^{12}C^{12}C (^{12}C^{181}Ta) collisions was found to increase (decrease) with increasing of the collision centrality, and the temperature of the hard p_t component of π^--mesons in ^{12}C^{181}Ta (^{4}He^{12}C) collisions was found to increase (decrease) consistently with an increase in collision centrality;

the temperature of the soft p_t component for π^--mesons was found to decrease consistently with an increase in collision system-size in the semicentral and central nucleus-nucleus collisions at 4.2 *A* GeV/*c*, and the temperature of the hard p_t component of π^--mesons was found to increase consistently with an increase in system-size in central collisions.

Practical results of the investigation are as follows:

the method of reconstruction of the mass distributions of the Δ^0(1232) resonances produced in relativistic hadron- and nucleus-nucleus collisions, based on analysis of the angles between outgoing protons and negative pions, was developed;

the physical interpretation of the parameters of the Grand Combinational Model (GCM), used for description of rapidity distributions of hadrons in central nucleus-nucleus collisions at high energies, was obtained;

the method of the separate analysis of the “soft” and “hard” components of the transverse momentum distributions of hadrons for studying of their dependencies on the collision centrality was applied for the first time.

Reliability of the obtained results. Reliability of the obtained results is ensured by the quite high statistics of the data on nuclear collisions used in this work, reliable identification of the particles by their mass and charge, quite good precision in measuring the momenta and emission angles of the secondary particles, satisfactory agreement between the experimental and model data.

Scientific and practical significance of the results of research. The scientific significance of the results of the dissertation is given by that the new fundamental results on $\Delta^0(1232)$ resonance production in the studied collisions complement the world data base on production of particles in nuclear collisions at intermediate and high energies, and the established dependencies of the slopes (temperatures) of the transverse momentum distributions of the negative pions on the collision centrality in the analyzed collisions can be applied to obtain the information about the properties of the excited dense nuclear matter.

The practical significance of the dissertation results is given by that they can be used to reconstruct the mass distributions of unstable resonance particles produced in high energy nucleus-nucleus collisions, to check the adequacy of the new models and approaches used to describe the relativistic nucleus-nucleus collisions, and to plan the new experiments at the modern heavy ion facilities.

Application of the results of dissertation. Based on the results obtained from analysis of production of the negative pions and $\Delta^0(1232)$ resonances in the studied collisions:

for determining the dependence of the transverse momentum and rapidity distributions of the negative pions on the collision centrality and masses of the colliding nuclei in nucleus-nucleus collisions at 4.2 *A* GeV/*c* (results were published in international scientific journals: Physical Review C, 2015; International Journal of Modern Physics E, 2015; International Journal of Modern Physics E, 2014; Physical Review C, 2013; Physical Review C, 2012; The

European Physical Journal A, 2011; Central European Journal of Physics, 2011) the dissertant received the prestigious international award of the World Academy of Sciences (TWAS, Italy) in the field of physics and mathematics in 2016;

the new results on production and properties of delta resonances were used by international scientists in the international journals (Physical Review C, 2009; Physical Review C, 2011; Progress in Particle and Nuclear Physics, 2018; The Euroschool on Exotic Beams, 2018; Indian Journal of Physics, 2017) to test the new theoretical approaches and find the regularities of production of baryon resonances in elementary and heavy ion collisions in wide range of incident energies; to analyze Δ^0 production in peripheral CTa collisions; to analyze the results on the collective flow of protons and pions in relativistic nuclear collisions. Usage of these results allowed the international researchers to interpret the results on the collective flow of protons and pions and modification of the delta parameters in the dense nuclear medium in relativistic nuclear collisions;

for obtaining the mass distributions of the Δ^0(1232) resonances in *p*C and *d*C collisions at 4.2 *A* GeV/*c*, determining the kinematic properties and role of the Δ^0(1232) resonances in production of the negative pions (results were published in international scientific journals: Physical Review C, 2012; Physics of Atomic Nuclei, 2012; Physical Review C, 2013; International Journal of Modern Physics E, 2013; Physics of Atomic Nuclei, 2013) the dissertant was conferred twice (in 2012 and 2013) the award of the Comission of the Development of Science and Technologies in the South (COMSATS, Pakistan).

Approbation of the work. The results of the present dissertation were tested and presented at 8 international and republican conferences.

Publication of the results. On the theme of dissertation, 33 scientific works were published, out of which 20 in the international journals, recommended by the Supreme Attestation Commission of the Republic of Uzbekistan for publishing of the main scientific results of the doctoral dissertation.

The structure and volume of dissertation. The dissertation consists of an introduction, six chapters, conclusion, and a bibliography. The volume of the dissertation is 217 pages.

LIST OF THE PUBLISHED WORKS:

1. *Olimov Kh.K.*, Lutpullaev S.L., Olimov K., Gulamov K.G., Olimov J.K. Production of Δ^0 and Δ^{++} resonances in collisions of ^{4}He nuclei with carbon nuclei at 4.2 GeV/c per nucleon // Physical Review C. – American Physical Society (USA), 2007. – Vol. 75. – id.067901. – 4 p. (№ 1. Web of Science; IF=3.820).
2. *Olimov Kh.K.* Production of baryon resonances in $\pi^- + ^{12}\mathrm{C}$ interactions at 40 GeV/c // Physical Review C. – American Physical Society (USA), 2007. –Vol. 76. – id.055202. – 7 p. (№ 1. Web of Science; IF=3.820).
3. *Olimov Kh.K.* Production of baryon resonances in collisions of ^{4}He nuclei with carbon nuclei at 4.2 GeV/c per nucleon // Physics of Atomic Nuclei. – Pleiades Publishing (USA), 2008. – Vol. 71, N 1. – pp. 93-97 (№ 1. Web of Science; IF=0.411).
4. *Olimov Kh.K.* Production of delta isobars on tantalum nuclei in CTa-collisions at a projectile momentum of 4.2 GeV/c per nucleon // Physics of Atomic Nuclei. – Pleiades Publishing (USA), 2010. – Vol. 73, N 3. – pp. 433-442 (№ 1. Web of Science; IF=0.411)**.**
5. *Olimov Kh.K.*, Lutpullaev S.L., Yuldashev B.S., Huseynaliyev Y.H., Olimov A.K. Production of Δ(1232) resonances on oxygen nuclei in ^{16}O+p collisions at a momentum of 3.25 GeV/c per nucleon // The European Physical Journal A. – Springer Verlag (Germany), 2010– Vol. 44. – pp. 43-54 (№ 1.Web of Science; IF=2.373)**.**
6. *Olimov Kh.K.*, Haseeb M.Q., Olimov A.K., Khan I. Analysis of Δ^0(1232) production in collisions of protons with carbon nuclei at 4.2 GeV/*c* // Central

European Journal of Physics. – Springer Verlag (Germany), 2011. – Vol. 9. – pp. 1393-1409 (№ 1. Web of Science; IF=0.765).

7. *Olimov Kh.K.*, Haseeb M.Q. Production of Δ^0(1232)-resonances in p+^{12}C collisions at a momentum of 4.2 GeV/c // The European Physical Journal A. – Springer Verlag (Germany), 2011. –Vol. 47. – id.79. – p. 16. (№ 1. Web of Science; IF=2.373).
8. *Olimov Kh.K.*, Haseeb M.Q., Khan I. Comparison of characteristics of Δ^0(1232) produced in p^{12}C and d^{12}C collisions at 4.2 A GeV/c // Physics of Atomic Nuclei. – Pleiades Publishing (USA), 2012. – Vol. 75, N. 4. – pp. 479-487. (№ 1.Web of Science; IF=0.411).
9. *Olimov Kh.K.*, Haseeb M.Q., Khan I., Olimov A.K. Glagolev V.V. Δ^0(1232) production in d+^{12}C collisions at 4.2 A GeV/c // Physical Review C. – American Physical Society (USA), 2012. – Vol. 85. – id.014907. – 14 p. (№ 1.Web of Science; IF=3.820).
10. *Olimov Kh.K.*, Haseeb M.Q., Hadi S.A. Rapidity and angular dependences of spectral temperatures of negative pions produced in ^{12}C^{12}C collisions at 4.2 A GeV/c // International Journal of Modern Physics E. – World Scientific (Singapore), 2013. – Vol. 22, N. 4. – id.1350020. – 14 p. (№ 1.Web of Science; IF=1.198).
11. Khan I., *Olimov Kh.K.* Spectral temperatures of Δ^0(1232) resonances produced in p^{12}C and d^{12}C collisions at 4.2 GeV/c per nucleon // Physics of Atomic Nuclei. – Pleiades Publishing (USA), 2013. – Vol. 76, N. 7. –pp. 883-887. (№ 1. Web of Science; IF=0.411).
12. *Olimov Kh.K.*, Haseeb M.Q. On spectral temperatures of negative pions produced in d^{12}C, ^{4}He^{12}C, and ^{12}C^{12}C collisions at 4.2 A GeV/c // Physics of Atomic Nuclei. – Pleiades Publishing (USA), 2013. – Vol. 76, N. 5. –pp. 595-601. (№ 1. Web of Science; IF=0.411).
13. *Olimov Kh.K.*, Iqbal A., Glagolev V.V., Haseeb M.Q. Analysis of rapidity spectra of negative pions in d+^{12}C, ^{12}C+^{12}C, and ^{12}C+^{181}Ta collisions at 4.2

GeV/c per nucleon // Physical Review C. – American Physical Society (USA), 2013. –Vol. 88. –id.064903. – 11 p. (№ 1. Web of Science; IF=3.820).

14. *Olimov Kh.K.*, Hadi S.A., Haseeb M.Q. Centrality Dependence of Rapidity Spectra of Negative Pions in $^{12}C+^{12}C$ and $^{12}C+^{181}Ta$ Collisions at 4.2 GeV/c per Nucleon // Physics of Atomic Nuclei**.** – Pleiades Publishing (USA), 2014. – Vol. 77, N. 5. – pp. 613-622. (№ 1. Web of Science; IF=0.411).
15. Iqbal A., *Olimov Kh.K.*, Khan I., Yuldashev B.S., Haseeb M.Q. On centrality and rapidity dependences of transverse momentum spectra of negative pions in $^{12}C+^{12}C$ collisions at 4.2 GeV/c per nucleon. // International Journal of Modern Physics E. – World Scientific (Singapore), 2014. –Vol. 23, N. 9. – id.1450047. – 19 p. (№ 1. Web of Science; IF=1.198).
16. *Olimov Kh.K.*, Iqbal A., Lutpullaev S.L., Khan I., Glagolev V.V., Haseeb M.Q. On transverse momentum spectra of negative pions in $^{12}C+^{181}Ta$ collisions at 4.2A GeV/c per nucleon // International Journal of Modern Physics E. – World Scientific (Singapore), 2014. –Vol. 23, N. 12. –id.1450084. – 22 p. (№ 1. Web of Science; IF=1.198).
17. *Olimov Kh.K.*, Iqbal A., Lutpullaev S.L., Hadi S.A., Glagolev V.V., Yuldashev B.S., Haseeb M.Q. Centrality dependences of soft and hard components of p_t distributions of negative pions in $^{4}He+^{12}C$ collisions at 4.2 A GeV/c // International Journal of Modern Physics E. – World Scientific (Singapore), 2015. – Vol. 24, N. 5. –id.1550036. – 24 p. (№ 1. Web of Science; IF=1.198).
18. *Olimov Kh. K.*, Ali Q., Haseeb M.Q., Arif A., Lutpullaev S.L., and Yuldashev B.S. Phenomenological analysis of rapidity distributions of negative pions in central $^{12}C+^{12}C$ collisions at $\sqrt{s_{nn}}$ =3.14 GeV // International Journal of Modern Physics E. – World Scientific (Singapore), 2015. – Vol. 24, N. **7.** –id.1550049. – 21 p. (№ 1. Web of Science; IF=1.198).
19. *Olimov Kh. K.*,Olimov K., Gulamov K. G., Olimov A.K., Lutpullaev S.L., Yuldashev B.S., Haseeb M.Q. Partial inelasticity coefficients of negative pions in p, d, α, $^{12}C+^{12}C$ and p, $^{12}C+^{181}Ta$ at 4.2 GeV/*c* per nucleon // International

Journal of Modern Physics E. – World Scientific (Singapore), 2015. – Vol. 24, N.10. – id.1550070. – 9 p. (№ 1. Web of Science; IF=1.198).

20. *Olimov Kh.K.*, Iqbal A., Haseeb M.Q., Lutpullaev S.L., Yuldashev B.S. Centrality and system-size dependencies of temperatures of soft and hard components of p_t distributions of negative pions in $^{4}He+^{12}C$, $^{12}C+^{12}C$ and $^{12}C+^{181}Ta$ Collisions at $\sqrt{s_{nn}}$=3.14 GeV // Physical Review C. – American Physical Society (USA), 2015. – Vol. 92, N. 2. – id.024909. – 16 p. (№ 1. Web of Science; IF=3.820).

21. *Olimov Kh.K.*,Lutpullaev S.L., Olimov K., Petrov V.I., Gulamov K.G., Olimov J.K., Yuldashev B.S. The comparative analysis of production of the cumulative π^{+} and π^{-} mesons in interactions of protons and nuclei with nuclei at high energies// "Nuclear and Radiation Physics": Book of Abstracts of the VI International Conference June 4-7, 2007. - Almaty (Kazakhstan), 2007. - pp. 75-77.

22. Huseynaliyev Y.H., Suleymanov M.K., Khan. I., Olimov K., *Olimov Kh.K.* Production of Δ^{0}-isobar in multi-nucleon $\pi^{-12}C$ interactions at the momentum of 40 GeV/*c* // "Modern Problems of Nuclear Physics": Book of Abstracts of the VII International ConferenceSeptember 22-25, 2009. - Tashkent, 2009.- pp. 73-74.

23. *Olimov Kh.K.* Production of baryon resonances on tantalum nuclei in CTa-collisions at the momentum of 4.2 GeV/*c* per nucleon // "Modern Problems of Nuclear Physics": Book of Abstracts of the VII International Conference September 22-25, 2009. - Tashkent, 2009. - p. 81.

24. Huseynaliev Y.H., *Olimov Kh.K.*, Sattarov A.R. Production of Δ^{0}-isobars on oxygen nuclei in ^{16}Op-interactions at the momentum of 3.25 GeV/*c* per nucleon // "Modern Problems of Nuclear Physics": Book of Abstracts of the VII International Conference September 22-25, 2009. - Tashkent, 2009. - p. 20.

25. *Olimov Kh.K.*, Lutpullaev S.L., Yuldashev A.A., Olimov A.K., Huseynaliyev Y.H. Production of Δ-resonances in ^{16}Op interactions at a momentum of 3.25 GeV/c per nucleon //“Modern Problems of Nuclear Physics”: Proceedings of the VII International Conference September 22-25, 2009. - Tashkent, 2010. - pp. 269-279. (published in Uzbek Journal of Physics – 2010. – Vol.12, N 4-6. – pp. 269-279.)

26. *Olimov Kh.K.*, Olimov K. Correlations in azimuthal plane in production of cumulative pions in relativistic hadron-nucleus and nucleus-nucleus collisions // “Fundamental and applied problems of physics”: Proceedings of the international conference, dedicated to 80th anniversary of academician M. S. Saidov (in Russian) 24-25 November, 2010. - Tashkent, 2010. - pp. 36-38.

27. *Olimov Kh.K.*, Khan I. About spectral temperatures of Δ^0(1232) produced in p^{12}C and d^{12}C collisions at 4.2 *A* GeV/*c* // “Nuclear Science and Its Applications”: Book of Abstracts of the VI Eurasian Conference September 25-28, 2012. – Samarkand, 2012. - pp. 135-137.

28. *Olimov Kh.K.*, Haseeb M.Q. Spectral temperatures of π^- mesons produced in d^{12}C ^{4}He^{12}C, and ^{12}C^{12}C collisions at 4.2 A GeV/c // “Nuclear Science and Its Applications”: Book of Abstracts of the VI Eurasian Conference September 25-28, 2012. – Samarkand, 2012. - pp. 137-139.

29. Лутпуллаев С.Л., *Олимов Х.К.*, Олимов К., Петров В.И. Образование Δ^0 -и Δ^{++}-изобар в адрон- и ядро-ядерных соударениях при высоких энергиях // “Фундаментальные и прикладные вопросы физики”: Сборник обзорных статей республиканской конференции, посвящённой 100-летию академика С.А. Азимова 6–7 ноября, 2014. – Ташкент, 2014. – с. 9-21.

30. *Olimov Kh.*, Lutpullaev S., Kanokova Sh., Yuldashev B. Phenomenological Analysis of Rapidity Distributions of Negative Pions in Symmetric ^{12}C+^{12}C Collisions at $\sqrt{s_{nn}}$ = 3.14 GeV // “Fundamental and Applied Problems of

Physics": Proceedings of the International Conference November 5-6, 2015.- Tashkent, 2015.- pp. 4-9.

31. *Olimov Kh.*, Lutpullaev S., Kanokova Sh., Yuldashev B. System-size and centrality dependencies of temperatures of soft and hard components of p_t distributions of negative pions in ^{4}He+^{12}C, ^{12}C+^{12}C and ^{12}C+^{181}Ta collisions at $\sqrt{s_{nn}}$ = 3.14 GeV // "Fundamental and Applied Problems of Physics": Proceedings of the International Conference November 5-6, 2015.- Tashkent, 2015. - pp. 10-14.

32. *Olimov Kh.K.*, Lutpullaev S.L., Olimov K., Yuldashev B.S., Gulamov K.G. Recent results on relativistic hadron-nucleus and nucleus-nucleus collisions obtained from bubble chamber experiments // "New Tendencies of Developing Fundamental and Applied Physics: Problems, Achievements, Prospectives": Proceedings of the International Symposium November 10-11, 2016. - Tashkent, 2016. - pp. 10-12.

33. *Olimov Kh.K.* Recent results on investigation of relativistic hadron-nucleus and nucleus-nucleus collisions // "Fundamental and Applied Problems of Physics": International Conference Tashkent (Conference Programme, Plenary Section), June 13-14, 2017. - Tashkent, 2017. - p. 3.

I. BRIEF REVIEW OF WORKS ON PION PRODUCTION, EXPERIMENTAL MATERIAL AND METHODOLOGICAL PROCEDURES

§ 1.1. Brief Review of Works on Pion Production

For writing the Introduction part of the present dissertation we used the references given in [1–27]. The new results of the present dissertation [28–60] complement the existing data on regularities of pion and $\Delta^0(1232)$ production and properties of their kinematical spectra at intermediate energies, and can also be useful for analysis and interpretations of the mechanisms of pion and $\Delta^0(1232)$ production in heavy ion collisions in modern high energy facilities such as Large Hadron Collider (LHC, Geneva, Switzerland) and Relativistic Heavy Ion Collider (RHIC, Brookhaven, USA).

It is interesting to mention the results on pion suppression and enchancement in nucleus-nucleus collisions as compared to nucleon-nucleon collisions obtained from comparing the properly normalized data on pion multiplicity from nucleus-nucleus and nucleon-nucleon collisions. One expects that inelastic secondary interactions produce additional pions and, therefore, their number per participating nucleon should be larger in nucleus-nucleus as compared to nucleon-nucleon collisions at the same initial energy per nucleon [61; P. 129]. The experimental data on pion multiplicities do contradict this expectation [61; P. 129]. It was deduced [20; P. 215-223, 61; P. 129, 62; P. 659] for Brookhaven National Laboratory (BNL, Brookhaven, USA) AGS (Alternating Gradient Synchrotron) energies (2–15 A GeV) and below that the number of the produced pions per participating nucleon in central collisions of identical nuclei (A+A) is smaller (pion suppression) as compared to that in inelastic nucleon-nucleon (N+N) interactions. The suppression of the pion production per participating nucleon, which is observed in central A+A collisions at the energies of BNL AGS and below, was discussed using the thermodynamical approach [61]. An approximate independence of the pion suppression factor on the collision energy and the participant number agreed with a scenario of the heavy-ion collision, distinguishing the following three stages [61]:

[1] The initial preequilibrium stage when the nonequilibrium hadronic system is created by the superposition of N+N collisions (interactions).

[2] The equilibrium stage, when the number of deltas decreases to the equilibrium value, which leads to the reduction of the total number of pions.

[3] The expansion stage of locally equlibriated hot hadronic matter, causing the additional pion suppression.

It should be noted that at the CERN SPS (Super Proton Synchrotron) energies (160-200 A GeV) a pion enchancement occurs instead of the suppression when going from N+N to A+A collisions [20; P. 215-223]. This different behavior cannot be understood within the above thermodynamical approach [20; P. 215-223]. In A+A collisions at SPS energy the role of meson resonances becomes significantly more important than that at AGS energy and below: a number of mesons at the freeze-out in A+A collisions at SPS energy is several times larger as compared to the number of baryons. Probably, the explanation of the pion enhancement effect requires the introduction of the new mechanism(s) [20; P. 215-223]. Formation of the Quark-Gluon-Plasma at CERN SPS energies has been considered as a candidate [62; P. 659], however, other mechanism(s) could be also responsible for the pion enhancement at high energies.

One of the important problems while studying hadron-nucleus collisions at high energies is the establishment of the fraction of the incident energy going to production of the new particles and various fragments, and excitation of the intermediate nuclei. Here it is worth mentioning our results on partial inelasticity coefficients of the negative pions [29; P. 1-9]. The partial inelasticity coefficient is calculated as a ratio of a total energy of c-type particles, produced in an individual collision event, to a kinetic energy of the impinging hadron or projectile nucleus $K_c = \sum_i \frac{E_i}{T_0}$, where E_i is the total energy of the ith c-type particle, and T_0 is the kinetic energy of the impinging hadron or projectile nucleus. The partial inelasticity coefficients of the negative pions were determined [29; P. 1-9] in minimum bias *p, d, α,* $^{12}C+^{12}C$ and *p,* $^{12}C+^{181}Ta$ collisions at 4.2 *A* GeV/*c* taking into account the average number of participant nucleons of a projectile nucleus. In nucleus–nucleus collisions, the average values of partial inelasticity coefficients ($\langle K(\pi^-)\rangle$) of the negative pions did not depend on the mass numbers of the projectile and target nuclei. Increase of $\langle K(\pi^-)\rangle$ in going from $p^{12}C$ to *d, α,*$^{12}C(^{12}C)$ collisions was due to additional source of production of fast negative pions in nucleus–nucleus collisions — a charge exchange conversion of one or more neutrons of the projectile nucleus into the proton and π^-. Linking the experimental results of the present analysis at intermediate energy with those obtained at high and ultra-high energies, it was concluded that the average values of partial inelasticity coefficients of pions in nucleon–nucleus and nucleus–nucleus collisions manifest a transitive behavior. At intermediate energies, the values of $\langle K(\pi^-)\rangle$ were smaller by a factor of two and more as compared to those at high energies, and they increased further with an increase in incident energy, reaching a plateau at $E_0 > 100$ *A* GeV.

Characteristics of the highly excited compressed nuclear matter, created in central nucleus–nucleus collisions at relativistic energies, could be extracted from an analysis of the collision centrality and system-size dependencies of the rapidity and transverse momentum distributions of pions [22, 63–68]. Analysis of pion rapidity distribution in Mg+Mg collisions at 4.3 *A* GeV/*c* [68] showed that the central rapidity region was occupied predominantly with pions of significantly larger p_t in comparison to the fragmentation region of colliding nuclei. The rapidity distributions of the negative pions in (*p, d, α,* C)+C and (*d, α,* C)+Ta collisions at 4.2 *A* GeV/*c* were studied for different transverse momentum ranges of π^- mesons in Refs. [66, 67]. As the transverse momentum of π^- increased, their fraction in the central rapidity region increased, and the corresponding fractions in the fragmentation regions of the colliding nuclei decreased. Negative pions with the large p_t were concentrated mainly in the central rapidity range [66, 67]. The quantitative analysis of the centrality dependencies of the rapidity as well as $\langle p_t \rangle$ versus rapidity spectra of π^- mesons in d^{12}C, ^{12}C^{12}C, and ^{12}C^{181}Ta collisions at 4.2 *A* GeV/*c* was made in our works [34, 35] by fitting the pion spectra with the Gaussian distribution function. The widths of the rapidity distributions of π^- mesons decreased in going from peripheral to central *d*^{12}C, ^{12}C^{12}C, and ^{12}C^{181}Ta collisions [35; P. 1-11]. With an increase in collision centrality, the centers of the rapidity distributions of the negative pions remained at midrapidity position for symmetric ^{12}C^{12}C collisions, while they shifted towards the target fragmentation region in the case of asymmetric *d*^{12}C and ^{12}C+^{181}Ta collisions. The extracted widths and locations of centers of $\langle p_t \rangle$ versus rapidity spectra of negative pions did not depend, within the uncertainties, on the masses of the projectile and target nuclei and the collision centrality as well [35; P. 1-11]. The width of the rapidity distribution of the particles, produced in relativistic nucleus–nucleus collisions, was deduced to carry information on the longitudinal flow [69] and final state rescattering [70]. For a given freeze-out temperature, the width of the rapidity distribution was shown to be sensitive to the velocity of sound in a medium at freeze-out in the Landau hydrodynamical model [71]. In Ref. [30] we investigated the various aspects of the simple phenomenological model, the Grand Combinational Model (GCM), proposed for the systematic description of the center-of-mass (cm) rapidity distributions of different particles, produced in high energy heavy ion collisions. The values of the GCM parameters have been extracted from fitting the cm rapidity distributions of the negative pions in ^{12}C+^{12}C collisions at $\sqrt{s_{nn}}$ = 3.14 GeV. The GCM parameters extracted for the central ^{12}C+^{12}C collisions were compared with those obtained in central Pb+Pb collisions at SPS and AGS energies between $\sqrt{s_{nn}}$ = 6.3 GeV and $\sqrt{s_{nn}}$ = 12.3 GeV and in central Au+Au collisions at RHIC energies between $\sqrt{s_{nn}}$ = 19.6 GeV and $\sqrt{s_{nn}}$ = 200 GeV. The physical interpretations of the GCM parameters were given. The initial assumption that the parameter β of GCM should be zero for the symmetric systems with identical colliding nuclei was verified. The parameter γ of GCM was deduced to follow an approximate asymptotic behavior ($\gamma \to 0$ as $\sqrt{s_{nn}} \to \infty$) at very large cm energies, and $\gamma \cong 0$ could possibly be related to the complete dehadronization of the whole collision system, along with attaining its maximum possible energy density, in the central collisions of identical nuclei [30]. The behavior of the cm energy dependence of γ suggested that it could possibly be sensitive to deconfinement phase transition [30].

The temperatures of the pions were estimated and investigated for the different colliding nuclei at various collision energies in the past [28, 31, 32, 33, 36, 38, 72–78]. Transverse momentum and transverse mass distributions were preferrable for extraction of the hadron temperatures due to their Lorentz invariance with respect to longitudinal boosts [73, 75, 36, 77]. The spectral temperatures of π^- mesons, produced in d^{12}C, ^{4}He^{12}C, and ^{12}C^{12}C collisions at 4.2 *A* GeV/*c*, were extracted from fitting the noninvariant center-of-mass (c.m.) energy spectra of π^- mesons with the Maxwell-Boltzmann distribution function in Ref. [72]. We investigated the rapidity and angular dependencies of the spectral temperatures of π^- mesons produced in ^{12}C^{12}C collisions at 4.2 *A* GeV/*c* in Ref. [38]. The centrality and rapidity range dependencies of the shapes of p_t distributions of the negative pions were investigated separately in ^{12}C^{12}C [33] and ^{12}C^{181}Ta [32] collisions at 4.2 *A* GeV/*c*. The transverse momentum and energy spectra of pions, produced in relativistic hadron–nucleus and nucleus–nucleus collisions, demonstrated the two temperature shapes. The lower temperature (T_1) component was the main one contributing ~ (80–90)% to the total pion spectra, and the higher temperature (T_2) component accounted for the remaining ~ (10–20)% part [72, 73, 32, 33, 36, 78]. However, practically no centrality dependence of these temperatures were revealed from fitting the whole or main part of p_t and c.m. energy distributions of pions in the past [72, 73, 32, 33, 36, 78]. The interplay of the temperatures of the soft and hard parts of the pion spectra while performing the combined two temperature model fits could be the reason for this. Therefore it was of interest to investigate the centrality dependence of the shapes (temperatures) of p_t distributions of pions in relativistic nuclear collisions separately in soft and hard p_t regions. We studied the collision centrality as well as the system-size dependencies of the temperatures of soft (p_t = 0.1–0.5 GeV/c) and hard (p_t = 0.5–1.2 GeV/c) components of the experimental transverse momentum distributions of the negative pions produced in ^{4}He^{12}C, ^{12}C^{12}C, and ^{12}C^{181}Ta collisions at 4.2 *A* GeV/*c* ($\sqrt{s_{nn}}$ = 3.14 GeV) in Refs. [28, 31]. For the analyzed collision systems and selected collision centralities, the temperatures were obtained from fitting separately the soft and hard p_t components of the negative pions by one temperature Hagedorn and one temperature Boltzmann functions. The extracted temperatures of both soft and hard components of p_t distributions of π^- depended on the geometry and degree of overlap of colliding nuclei in peripheral, semicentral, and central nucleus–nucleus collisions at $\sqrt{s_{nn}}$ = 3.14 GeV [28]. The differences between extracted temperatures in the studied collision systems increased with increasing the degree of overlap of colliding nuclei, i.e., with an increase in collision centrality and corresponding increase in the numbers of participant nucleons and binary collisions. The temperature of soft p_t component of the negative pions in ^{12}C^{12}C (^{12}C^{181}Ta) collisions increased (decreased) with increasing of collision centrality. The temperature of hard p_t component of π^- in ^{12}C^{181}Ta (^{4}He^{12}C) collisions increased (decreased) consistently with an increase in collision centrality [28, 31]. The temperature of soft p_t component of π^- decreased with an increase in system-size in semicentral and central nucleus–nucleus collisions at $\sqrt{s_{nn}}$ = 3.14 GeV. In central collisions, the temperature of hard p_t component increased consistently with an increase in system-size [28]. The physical interpretations of the results obtained were given. The quantitative results on temperatures extracted from p_t spectra of negative pions in nucleus–nucleus collisions at 4.2 *A* GeV/*c* were compared with those obtained in lower, intermediate, and higher energies in other JINR, GSI, and SPS experiments.

Resonances with the short lifetime and their coupling to a nuclear medium have unique characteristics to probe the various characteristics of the medium resulting from relativistic hadron-nucleus and nucleus-nucleus collisions. A lot of experimental and theoretical research [24, 25, 27, 37–47, 79–105] has been devoted to investigation of the Δ(1232)-resonance production in various strong and electromagnetic processes involving pions, protons, photons, light nuclei, and heavy ions. The process responsible for the meson production in central heavy ion collisions at energies of the order of several GeV/nucleon is believed to be predominantly the excitation of the baryon resonances during the early compression phase of the collision [24]. In the later expansion phase, these resonances decay. The mass and width of Δ(1232) produced in nuclear medium in relativistic hadron-nucleus and nucleus-nucleus collisions modify as compared to the mass and width ($M_{\Delta_{NN}} = 1232$ MeV/c^2, Γ = 115–120 MeV/c^2) [106] of the Δ(1232) resonances, produced in nucleon-nucleon collisions. The significant decrease in the mass and width of the Δ(1232)-resonances produced in dense hadron matter created in central heavy ion collisions was interpreted in terms of the thermal and isobar models [24, 92]. The modification of the Δ(1232) properties was also related to the values of hadronic density, temperature, and various non-nucleon degrees of freedom in the nuclear matter [24, 92, 101, 107, 108]. However, still many experimental results on Δ(1232) production are nontrivial and there are ambiguities in their theoretical interpretations.

Identification of the structures in the invariant mass distribution of the correlated proton and pion pairs provides a direct proof that nucleons are excited to the high-lying resonances [24]. The main obstacle that should be overcome in reconstructing of the invariant mass is the large background of the non-correlated $p\pi$ pairs [24]. In the peripheral reactions with the very light projectiles, e.g., p [93, 94] or ^{3}He [95] induced reactions at around 2 GeV bombarding energy, the $p\pi$ correlations were successfully investigated and the mass distribution of the Δ(1232) resonance was reconstructed. The resonance mass was shown to be shifted by about –25 MeV/c^2 towards lower masses in the reactions on various targets, compared to those on protons [93–95]. The mass reduction of the Δ(1232)-resonance in $p+A$ collisions ($A = \mathrm{C, Nb, Pb}$) at 0.8 and 1.6 GeV incident energy [93] was traced back to the effects of Fermi motion, NN scattering, and pion reabsorption in nuclear matter. In nucleus-nucleus interactions, $\Delta(1232)$ resonances are assumed to be mostly produced in the reaction $NN \to \Delta N$, competing with the process of direct pion production: $NN \to NN\pi$, $NN \to NN\pi\pi$, etc. In this simple scenario, the Δ^0(1232)-resonances are produced via the reaction $NN \to \Delta^0 N + k\pi \quad (k = 0,1,...)$, decaying subsequently through $\Delta^0 \to p\pi^-$ channel. The observed final particles, protons and π^- mesons, were used by us to analyze Δ^0(1232) production and their reconstructed kinematical spectra in the analyzed minimum bias collisions in Refs. [37, 39–47]. In Refs. [39, 41, 42] we analyzed Δ^0(1232) production and its various properties separately for minimum bias p^{12}C and d^{12}C collisions at 4.2 *A* GeV/*c*. The mass distributions of the Δ^0(1232) resonances produced in minimum bias p^{12}C [41, 42], d^{12}C [39], ^{4}He^{12}C [45, 47], ^{12}C^{181}Ta [44] at 4.2 *A* GeV/*c* collisions, ^{16}Op collisions [43] at 3.25 *A* GeV/*c*, and π^{-12}C collisions [46] at 40 GeV/*c* were reconstructed and their masses and widths extracted. The kinematical distributions of the $\Delta^0(1232)$ resonances were reconstructed and their corresponding mean kinematical characteristics estimated in Refs. [39, 41, 42, 43]. The fractions of the charged π^- mesons coming from Δ^0(1232) decay as well as the relative numbers of the nucleons excited to Δ^0(1232) in freeze-out conditions were estimated for the analyzed minimum bias collisions [39, 41–47]. The freeze-out temperatures of the Δ^0(1232) resonances were estimated and compared to the results of the other experiments with the different sets of colliding nuclei and various incident energies. In Ref. [40] we recontructed the transverse momentum distributions of π^- mesons coming from the Δ^0(1232) decay and compared with those for all π^- mesons, produced in d^{12}C and p^{12}C collisions. This comparison showed that Δ^0(1232) decay kinematics was responsible for the low transverse momentum enhancement of the π^- spectra in d^{12}C and p^{12}C collisions, as was also noted earlier in Refs. [25, 26] for the incident beam energies from 1 to 15 A GeV. Comparison of the reconstructed rapidity distributions of Δ^0(1232)'s produced in d^{12}C and p^{12}C collisions revealed that in the case of d^{12}C collisions a major fraction of Δ^0 is produced on carbon nuclei, while still a noticeable number of Δ^0 originate from neutrons of the impinging deuterons [40].

In Ref. [37] we analyzed the reconstructed experimental transverse momentum (p_t) distributions of the Δ^0(1232) resonances, produced in p^{12}C and d^{12}C collisions at 4.2 A GeV/c, and the corresponding spectra calculated using Modified FRITIOF model in the framework of Hagedorn Thermodynamic Model. The spectral temperatures of the Δ^0(1232) resonances were extracted from fitting their p_t spectra with the one-temperature Hagedorn function. The extracted spectral temperatures of Δ^0(1232) were compared with the corresponding temperatures of the π^- mesons in p^{12}C and d^{12}C collisions at 4.2 A GeV/c, obtained similarly from fitting the p_t spectra of π^- mesons by the one-temperature Hagedorn function. The spectral temperatures of the Δ^0(1232) resonances agreed within uncertainties with the corresponding temperatures of the π^- mesons produced in p^{12}C and d^{12}C collisions at 4.2 A GeV/c.

§ 1.2. The Synchrophasotron and Accelerator complex and 2 meter propane bubble chamber of Laboratory of High Energies, Joint Institute for Nuclear Research, Dubna, Russia

The particle accelerator based upon synchrotron, Synchrophasotron, was established in the beginning for interactions of protons, at the Joint Institute for Nuclear Research (JINR, Dubna, Russia) in 1957 by the designer of synchrotron, V.I. Veksler [109]. The detailed information [109-113] about the synchrophasotron and accelerator complex and 2 meter bubble of LHE, JINR (Dubna, Russia) is given below.

Veksler discovered the principle of self phasing, used to operate the cyclic accelerators of high energies, at Lebedev Physical Institute (LPI), USSR Academy of Sciences, in Dubna in 1944. He was supervisor for the construction and developing of the new accelerator, synchrophasotron, at LPI in 1949–1950. To investigate the field of high energy physics at synchrophasotron, the Electro-Physical Laboratory (EPL) of the USSR Academy of Sciences was founded in 1953. The EPL was given the name of the Laboratory of High Energies (LHE) in March 1956, and it became a part of the JINR. V. I. Veksler was the first Director of JINR. The synchrophasotron began operations in April 1957 and produced protons with energies upto 10 GeV. It was the highest energy, and the synchrophasotron was the biggest colliding machine in the world at a time [109].

Fig. 1.1. The synchrophasotron accelerator, LHE, JINR, Dubna

Veksler with his colleagues, Makarov and Chuvilo, began the program of research at the synchrophasotron. The analysis of the elastic scattering processes at the minimal and maximal transfers of momenta and multiple particle productions in hadron–nucleon collisions were the aims of the research project initially. Under this project in many experiments, various discoveries, like anti Σ^- hyperon, decay of φ^0 meson into e^-e^+ pair, and many others were made [109].

The third Director of LHE, A.M. Baldin, suggested to start research in a new field, called relativistic nuclear physics (RNP), to reveal the quark structure of the nuclei. This project was initiated at the Laboratory of High Energies to analyze the cumulative production of particles in relativistic nuclear collisions. The synchrophasotron made it possible to accelerate the deuterons up to several GeV per nucleon and use them for the physical research in 1971. The synchrophasotron had worked until 1993. At the same time, the construction of a superconducting accelerator of relativistic nuclei, the Nuclotron, was also going on. In 1993, the Nuclotron became operational to continue the investigations in the field of relativistic nuclear physics. Analysis of the strongly interacting matter under high temperatures or high baryonic densities, or both of them, one of the main aims of the modern high energy physics. Scientists believe that such extreme conditions of the temperatures and densities existed at the initial stages of evolutions of the Universe. Such conditions may be present in neutron stars nowadays. These conditions can be created in the laboratory in central collisions of heavy ions at high energies. The above information motivated the centers of high energy physics to construct the new heavy ion accelerators and increase the energies of the existing accelerators [109].

According to the modern theoretical perceptions, the strongly interacting matter can undergo a phase transition by increasing either temperature or density of a nuclear matter (or both of them). Each heavy ion accelerator is designed to study some part of a phase diagram of a strongly interacting matter. The part of the phase diagram chosen for investigation is defined by the temperature and baryonic density of a matter, attained in collisions of the nuclei, which depend on the energies and atomic numbers of the colliding nuclei. The temperatures and baryonic densities occuring during the collisions of nuclei with atomic numbers ~200 at the greatest energies ~5 GeV/nucleon achievable at that time [109; P.407] should allow reaching the region of a mixed phase, which was estimated theoretically at the Bogolyubov Laboratory of Theoretical Physics of JINR.

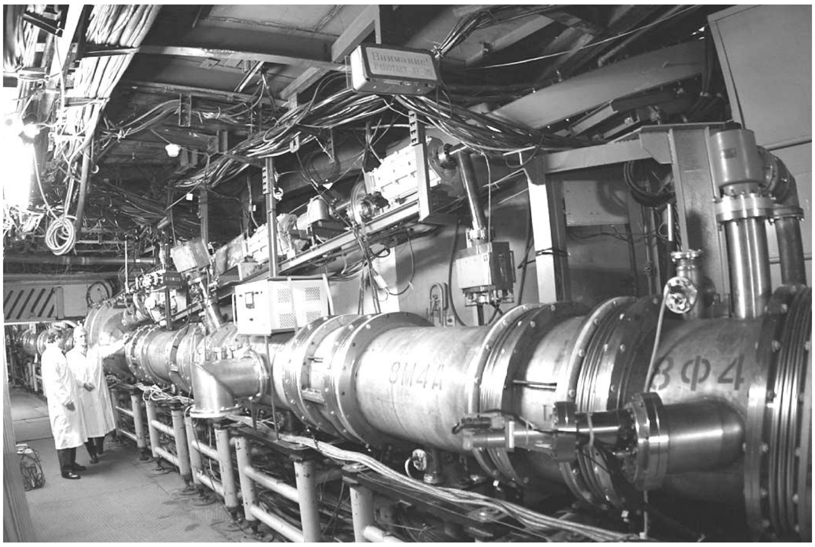

Fig. 1.2. The Nuclotron accelerator at LHE, JINR, Dubna

The first accelerator, providing the opportunity to obtain the beams of high energy particles, was the JINR synchrophasotron. The views of the synchrophasotron and Nuclotron accelerators are illustrated in Figs. 1.1 and 1.2 respectively. The accelerators were used to accelerate the singly charged particles, protons, and electrons for many years. It was suggested later that the heavy ions with the greater charges, instead of singly charged particles, could be used to accelerate in the accelerators to get collisions of higher energies. This is because if the accelerator accelerates a proton up to 10 GeV, then it could accelerate a heavy ion up to a greater energy, for example, ^{4}He nuclei could be accelerated up to 20 GeV. First a beam of deuterons was accelerated up to 9 GeV (4.5 GeV per nucleon) at JINR synchrophasotron in 1970s. Deuteron was chosen as the simplest nucleus having only two nucleons. This opened the way to carry out experiments on heavier relativistic nuclei. Under supervision of Stavinskii [110], a group of physicists found the nuclear cumulative effect in d + Cu collisions, in which the deuteron beam was incident on the copper target. When the summation or accumulation of many effects increases or enhances another effect, this phenomenon is called a cumulative effect. It was noticed that under special conditions the nucleons of the nuclei act differently from the free nucleons.

The accelerators complex at the LHE of JINR is the main part of JINR. It was founded to generate the proton, deuteron, polarized deuteron, and other nuclear beams. It could accelerate the light and heavier nuclei up to energies of 6 GeV per nucleon. The scheme of the Laboratory of High Energies accelerator complex is shown in Fig. 1.3. It includes the synchrophasotron and the Nuclotron. Nuclotron was constructed in the period from 1987 to 1992, becoming operational in March 1993. Fig. 1.4 illustrates the accelerator complex of the LHE, JINR. The Nuclotron was constructed in a tunnel below the ground floor of the building of the synchrophasotron.

The LHE of JINR comprises the Synchrophasotron, now Superconducting Nuclotron accelerator; Linear accelerator; Electrons beam source of high charge state ions; Laser source of light ions; Source of polarized deuterons; Source of heavy ions; System of slow beam extraction; System of extracted beam channels; Internal target complex.

The superconducting elements were cooled using two He liquefiers with the capacity of 1.6 kW each. The main characteristics of the accelerators are shown in Table 1.1. The presence of the extraction systems and a net of the external beam lines were the main advantages of the LHE accelerator complex. The beams could be extracted from the synchrophasotron in two directions, MV-1 and MV-2, as can be seen in Fig. 1.4, leading towards two experimental halls, Experimental Hall 205 and Hall 1B, respectively. The beams could be extracted in a relatively long time interval of 0.5 s and forwarded to the experimental area in the Hall 205, through the MV-1, up to maximum energy with efficiency of 95%. From MV-2 the beams could be extracted either fastly ($t < 10^{-3}$ s) or slowly ($t = 0.35$ s). These beams were then supplied to the physics setups in the experimental Hall 1B. Both extractions could operate simultaneously in the same cycle.

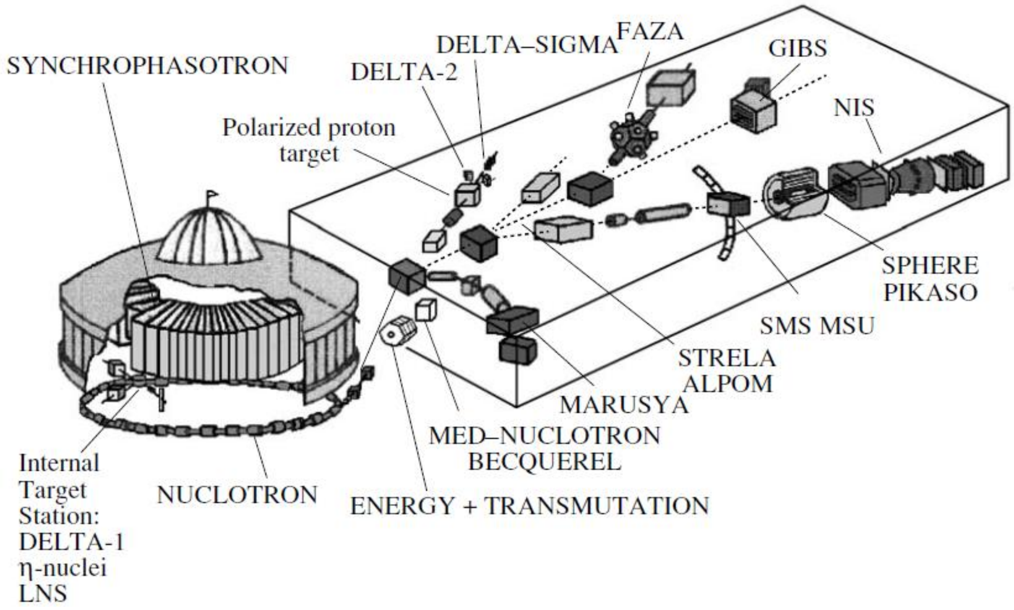

Fig. 1.3. Schematic diagram of the accelerator complex of the LHE at JINR, Dubna

Table 1.1

The comparison of the main characteristics of Synchrophasotron and Nuclotron accelerators

Parameter	Units	Synchrophasotron	Nuclotron
Energy (max)	*A* GeV	4.5	6
Extraction time (max)	S	0.5	10
Magnetic Field	T	1.5	2.1
Circumference	M	208	252
Chamber size	Cm	120	12

There are many arrangements at the Nuclotron to carry out the research. These are PIKASO, GIBS, FAZA, DELTA I and II, DISC, Leading Particles, MARUSYA, SCAN, STRELA, Polarized Proton Target, and Medium Resolution Spectrometer (MRS), as seen in Fig. 1.3. More detailed information is given in Ref. [111].

The bubble chamber is a particle detector which was used to record the passages of charged particles through the gas in high energy experiments. Donald Glaser formulated the work principle of a bubble chamber in 1952, and it remained in use for about forty years to investigate the complicated collisions of hadrons and nuclei with nuclei at various incident energies. It worked on a principle that when a charged particle passed through super heated liquid, kept under high pressure of about 5–20 atmospheres (1 atmospheres = 10^5 Pa), then gas bubbles were produced along the track of the particle [112], which were photographed by the cameras.

The bubble chambers were used for the pulsed, cyclic accelerators, and beams from fixed targets having repetition rates of a same order. Though the processes of taking pictures from bubble chambers were relatively slow, an experiment of many thousands of collision events took many months to complete. The numbers of the collision images were limited, and it was very intensive and time consuming task to analyze these pictures. However, the images from bubble chambers were very precious, because they provided a direct way to see the nuclear collision events by the naked eyes in a real world. The modern detectors allow detection of the several thousands of collision events in one second, and the pictures of interactions are reconstructed by computers. Therefore the use of the bubble chambers is practically stopped nowadays [113].

The bubble chambers were filled with the simplest nuclei like hydrogen, deuterium, or heavy liquids like a mixture of neon-hydrogen, or propane (C_3H_8). The bubble chamber was put in a strong magnetic field of the strength 1.5 − 3.5 T, produced by the electro-magnets. The magnetic field was used to measure the momenta of the secondary particles from the curvatures of their tracks via the relation

$$p = 0.3\rho B\,, \tag{1.1}$$

where B is the magnetic field’s strength in Tesla, p is the momentum of a particle in GeV/c, and ρ is the radius of the curvature of the particle track in meters. The pictures of the tracks having bubbles around were taken on photographic films with the help of the several cameras in three dimensions. The data obtained from the measurements of the images were converted into digital format. Different geometrical programs were used to reconstruct the tracks and the collision events in three dimensions. Using the bubble chambers, many particles were discovered, which made significant contribution to a quark model, making it possible to develop and establish this model.

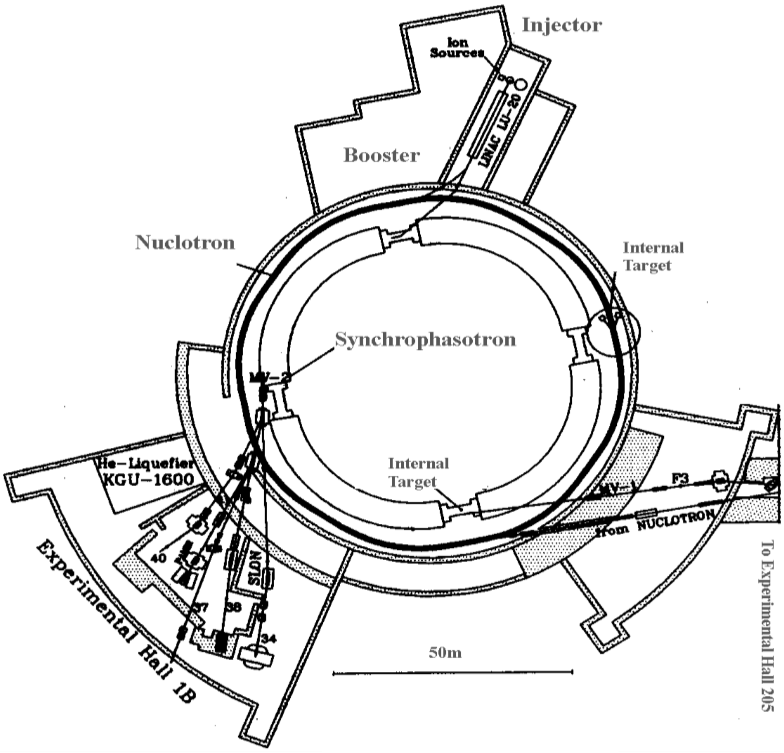

Fig. 1.4. Accelerator Complex of the LHE, JINR, Dubna

The Sketches of different decay signatures occurred during interaction (collision) processes [113] are illustrated in Table 1.2, which are helpful to identify the secondary particles. More details about the measurements and methodical analysis in bubble chamber experiments can be found in Ref. [113].

The 2 m (two meter) propane bubble chamber at JINR (Dubna, Russia) have a sensitive volume of (210 x 65 x 40) cm^3. Around 500 liters of propane (C_3H_8) were kept in liquid state under a high pressure (~ 20 atm) in the chamber. It operated at the temperature of about 58 °C. A constant magnetic field of 1.5 T (15 kG) was provided along the vertical direction. The piece of the upper magnetic pole was built as the construction part of the chamber. The piston to expand the liquid was located in the bottom of the chamber. The chamber was illuminated through 26 holes. Each hole had its own lighting system. There were two photographic systems having three cameras each. Every part of the system was controlled from the remote control table, specially constructed for the chamber.

Table 1.2

Sketches of different decay signatures

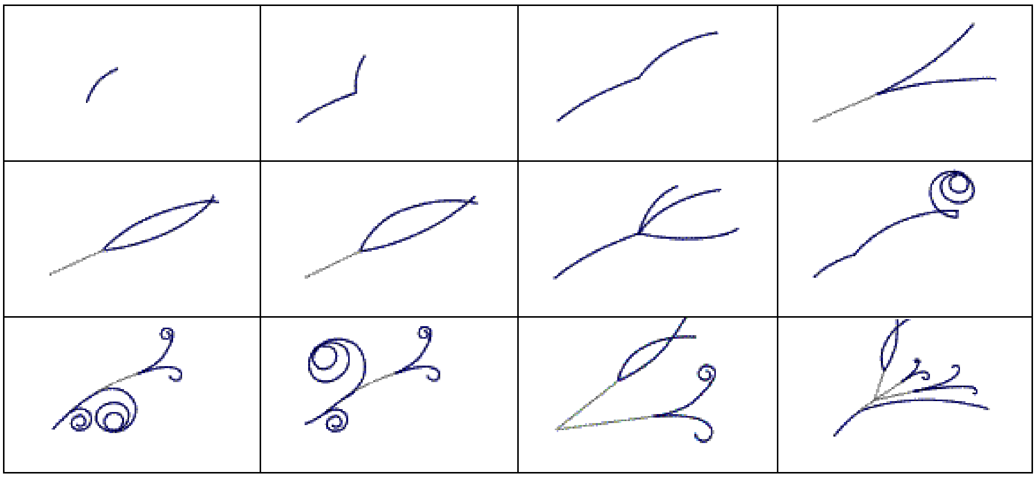

§1.3. Experimental Procedures

The experimental data obtained from analysis of the stereo photographs from 2 m propane (C_3H_8) bubble chamber (PBC-500) of the Laboratory of High Energies (LHE) of Joint Institute for Nuclear Research (JINR, Dubna, Russia), placed in a magnetic field of strength 1.5 Tesla and irradiated with beams of protons, deuterons, ^{4}He, and ^{12}C nuclei accelerated to the momentum of 4.2 GeV/*c* per nucleon at Dubna synchrophasotron accelerator, were investigated in the present work. Collision events of protons, deuterons, ^{4}He and ^{12}C nuclei with the propane (C_3H_8) nuclei were scanned, measured, reconstructed, and finally analyzed. The inelastic p+^{12}C, d+^{12}C, ^{4}He+^{12}C, and ^{12}C+^{12}C collision events on carbon nuclei of the propane were extracted from the total set of collisions with the propane, using the criteria based on the total charge of secondary particles, the total number of protons, the existence of protons bounced into the backward hemisphere in the laboratory system, and the number of π^- mesons produced, which is described in detail in Refs. [114–116]. Collisions were assumed to occur on the ^{12}C target in the propane if at least one condition out of the following ones was satisfied:

$$(n_+ - n_-) > (Z_{projectile} + 1);$$

$$n_{protons}\,(p_{lab} < 0.75\ \mathrm{GeV}/c) > 1;$$

$$n_{protons\ backward} > 0;$$

$n_- > 1$ (for p+^{12}C interactions) and $n_- > 2$ (for d, ^{4}He, ^{12}C +^{12}C collisions);

$$n_{ch} = even.$$

Here n_+ is the number of the positively charged particles, n_- represents the number of negatively charged particles, and n_{ch} represents the total number of the charged particles in a collision event. The detailed description of the used criteria can be found in Refs. [114; P.455, 116]. With the use of the above criteria, approximately 70% of all inelastic p+^{12}C, d+^{12}C, ^{4}He+^{12}C, and ^{12}C+^{12}C collision events on carbon nuclei were separated [114–116]. This was estimated using the known cross sections [117] for $p + p$, p+^{12}C, A+p, A+^{12}C collisions (A = d, ^{4}He, and ^{12}C) at a momentum of 4.2 A GeV/c and using the p:^{12}C and A:^{12}C ratios in a propane molecule [114, 116, 118, 119]. The remaining ~30% inelastic collision events of protons and nuclei with carbon nuclei were extracted statistically from $p + p$ and $A + p$ collisions on the quasi free protons of C_3H_8 molecules using the relevant weights. These weights were determined in such a way that the number of events produced on ^{12}C nuclei and hydrogens (protons of propane) corresponded to the number of the events expected for the inelastic collisions based on their cross sections [114, 116, 118, 119]. The numbers of such $p + p$ and $A + p$ collision events included into the data bases of p+^{12}C and A +^{12}C collisions were equal within statistical uncertainties to the numbers of $p + n$ and $A + n$ interaction events on the neutrons of ^{12}C nuclei, respectively. This is due to the coincidence of the number of protons and neutrons in the target ^{12}C nuclei and approximately the same cross sections of $p + p$ and $p + n$ collisions at 4.2 A GeV/c. The particles emitted under large angles (close to 90^0) to the photographic planes of the cameras were mostly lost due to their very short track lengths in a film, and therefore corrections were introduced to account for such losses. These corrections were ≈ 3% for protons having momentum $p_{lab} > 300\ \mathrm{MeV}/c$, and around 15% for protons having momentum $p_{lab} < 300\ \mathrm{MeV}/c$ (the so called slow protons) [114]. The protons and π^+ mesons up to a momentum of $p \approx 0.75\,\mathrm{GeV}/c$ can be separated visually based on their ionization in a chamber. However, in the present experiment, the protons and π^+ mesons could be separated with almost 100% efficiency up to a momentum of 0.5 GeV/c. Therefore all the positively charged particles with momenta higher than 0.5 GeV/c were assigned weights to give the probability that a certain particle was a proton or a π^+ meson. All the particles having negative charges were identified as π^- mesons. It is necessary to mention that π^- mesons make up the main fraction (> 95%) among the negatively charged particles produced in p+^{12}C and A+^{12}C collisions at a momentum of 4.2 A GeV/c. The admixture of fast electrons and strange particles among the negatively charged particles did not exceed 5%. Protons and charged pions having momenta less than 150 MeV/c and 70 MeV/c, respectively, were not registered because of their short track lengths in the propane bubble chamber. The average uncertainty in measurement of the angles $\langle \Delta\theta \rangle$ of the secondary particles was around 0.8 degree. The mean relative uncertainty in measuring the momenta of the protons and negative pions, $\left\langle \frac{\Delta p}{p} \right\rangle$, from the curvatures of their tracks in a magnetic field was about 11% and 6%, respectively [116]. The scanning of the stereo photographs of the p+^{12}C and A+^{12}C collision events were made in order to determine the experimental interaction cross sections [120]. The number of the incident beam tracks and the number of the collision events in the volume of a bubble chamber were counted and inserted in the following formula:

$$N = N_0\left[1 - \exp(-n\sigma x)\right] \quad (1.2)$$

Table 1.3

Mean experimental multiplicities per collision event of the negative pions and participant protons, experimental statistics and cross sections of inelastic collisions

Collision type and incident Momentum	$<n(\pi^-)>$	$<n(p_{partic.})>$	The number of inelastic collision events	Cross section of inelastic collisions (mb)
p^{12}C 4.2 GeV/c	0.36 ± 0.01	1.83 ± 0.04	6 736	265 ± 15
d^{12}C 4.2 *A* GeV/*c*	0.66 ± 0.01	1.94 ± 0.06	7 071	400 ± 20
^{4}He^{12}C 4.2 *A* GeV/*c*	1.02 ± 0.01	2.83 ± 0.02	11 692	450 ± 20
^{12}C^{12}C 4.2 *A* GeV/*c*	1.45 ± 0.01	4.35 ± 0.02	20 528	830 ± 50
^{12}C^{181}Ta 4.2 *A* GeV/*c*	3.50 ± 0.10	13.3 ± 0.20	2 420	3445 ± 40
^{16}Op 3.25 *A* GeV/*c*	0.30 ± 0.01	1.93 ± 0.02*	13 500	334 ± 6
π^{-12}C 40 GeV/*c*	3.22 ± 0.02	1.00 ± 0.01*	16 865	179 ± 2

*Here the mean multiplicities of all protons are given

Here N is the number of collision events on a length x in a propane chamber, N_0 is the initial number of the incident beam tracks, n is the number of nuclei in 1 cm^3 of the target, x is the propane layer thickness in the direction of the beam, and σ is the inelastic cross section. The density of the propane was 0.43 g/cm^3 in the PBC [116, 120].

To investigate ^{12}C+^{181}Ta collisions at 4.2 A GeV/c, three tantalum (^{181}Ta) foils were placed in the experimental set up of the 2 m propane bubble chamber of LHE of JINR, placed in a magnetic field of strength 1.5 Tesla. Thickness of each foil was 1 mm and the distance between the foils was 93 mm. The bubble chamber was irradiated with the beams of ^{12}C nuclei accelerated to a momentum of 4.2 GeV/c per nucleon at Dubna synchrophasotron. Methods of selection of the inelastic ^{12}C+^{181}Ta collision events in this experiment were given in detail in Refs. [32, 44, 121–123]. The momentum thresholds for the detection and measurement of the protons and π^- mesons in ^{12}C+^{181}Ta collisions in the propane bubble chamber were ~ 240 and ~ 80 MeV/*c*, respectively [44, 121–123].

In our experiment, in A+^{12}C and ^{12}C+^{181}Ta collisions at 4.2 *A* GeV/*c*, the spectator protons are the protons with momenta $p > 3$ GeV/c and emission angle $\theta < 4$ degrees (projectile spectators), and protons with momenta $p < 0.3$ GeV/c (target spectators) in the laboratory frame [116]. The participant protons are those protons which remain after elimination of the spectator protons.

The mean experimental multiplicities per collision event of the negative pions and participant protons along with the experimental statistics and cross sections of the minimum bias inelastic collisions analyzed in the doctoral dissertation are presented in Table 1.3.

II. DESCRIPTION OF THEORETICAL MODELS AND APPROACHES

§ 2.1. Modified FRITIOF Model

To compare with the experimental data, hadron–hadron (*h*+*h*), hadron–nucleus (*h*+*A*), and nucleus–nucleus (*A*+*A*) collisions are simulated (modeled) using various Monte Carlo programs, which generate the simulated collision events [118]. The FRITIOF model [118, 119, 124–127] is also based on a Monte Carlo technique and used to simulate the relativistic *h*+*h*, *h*+*A*, and *A*+*A* collisions. FRITIOF model is based on a two-body kinematics of inelastic collisions. If we deal with *h*+*h* collisions, it can then be described as $a+b \rightarrow a'+b'$, where *a* and *b* are the incident and target hadrons, and a' and b' are the excited hadrons, formed after a collision. These a' and b' hadrons have masses greater than those of the initial colliding hadrons, that is, $m_{a'} > m_a$ and $m_{b'} > m_b$. The laws of conservation of energy and momentum in the center of mass frame of the interacting hadrons are as follows:

$$E_a + E_b = E_{a'} + E_{b'} = \sqrt{s_{ab}}\ , \qquad (2.1)$$

$$p_{al} + p_{bl} = p_{a'l} + p_{b'l} = 0, \qquad (2.2)$$

$$0 = \vec{p}_{a't} + \vec{p}_{b't}\,, \qquad (2.3)$$

where E_a, E_b and p_{al}, p_{bl} are the energies and longitudinal momenta of initial interacting hadrons *a* and *b*, and $E_{a'}$, $E_{b'}$ and $p_{a'l}$ $p_{b'l}$ are the energies and longitudinal momenta of the final state excited hadrons, a' and b', respectively, $\sqrt{s_{ab}}$ is the total center-of-mass energy of the colliding system, and $\vec{p}_{a't}$, $\vec{p}_{b't}$ are the transverse momenta of final state excited hadrons. The initial interacting hadrons have zero transverse momenta, because we assume that both the colliding hadrons move towards each other along the same line in the center-of-mass frame. Addition and subtraction of the relations in Eqs. (2.1) and (2.2) result in

$$P_a^+ + P_b^+ = P_{a'}^+ + P_{b'}^+ , \tag{2.4}$$

$$P_a^- + P_b^- = P_{a'}^- + P_{b'}^- . \tag{2.5}$$

Here $P^+ = E + p_l$ and $P^- = E - p_l$.

The probability distributions of $P_{b'}^+$ and $P_{a'}^-$ employed in the FRITIOF model are as follows:

$$dW \sim \frac{dP_{b'}^+}{P_{b'}^+} \tag{2.6}$$

$$dW \sim \frac{dP_{a'}^-}{P_{a'}^-} \tag{2.7}$$

The permissible ranges for $P_{a'}^-$ and $P_{b'}^+$ are

$$[P_a^-, P_{\mathrm{b}}^-], [P_b^+, P_a^+]. \tag{2.8}$$

In case of h+A and A+A collisions, we assume that the excited nucleons of the initial collisions can make interactions with each other and with the other nucleons of nuclei, and, as a result of these subsequent interactions, the masses of the interacting nucleons increase. If the projectile hadron a interacts initially with any nucleon of the colliding nuclei, then their reaction can be expressed as $a + N_1 \rightarrow a' + N_1'$, here a and a' are the incident and the finally excited hadron, and N_1 and N_1' are the initial and final nucleon. Now if this excited hadron a' makes another interaction with any other intra-nuclear nucleon, then their collision can be described as $a' + N_2 \rightarrow a'' + N_2'$, where a' is the initially excited hadron, a'' is the doubly excited hadron, and N_2 and N_2' are the initial and final (excited) states of the second nucleon. As a result of successive collisions, the mass of the hadron a increases gradually. The same equations (2.4)−(2.6) are used for h+A interactions, however the relation in Eq. (2.8) is replaced by

$$[P_{a'}^-, P_{N2}^-], [P_{N2}^+, P_{a'}^+] \tag{2.9}$$

The similar approach is employed to simulate the nucleus–nucleus (A+A) collisions.

The distribution in the value of the transverse momentum, exchanged between the interacting (colliding) nucleons, used in the model is

$$dW = b^2 e^{-B p_t^2} p_t dp_t \,. \tag{2.10}$$

The Modified FRITIOF model, which is used for a comparison with the experimental data in the doctoral dissertation, was obtained by introducing the several modifications in the original FRITIOF model. The Glauber approximation [127,128] was used in the Modified FRITIOF model to obtain the time sequence of nucleon–nucleon collisions in case of h+A and A+A interactions. The properties of slow particles produced during the disintegration of nuclei are not described in the original model. This is because of neglecting the cascade processes caused by the secondary particles. For removing this discrepancy, the Reggeon model of nuclear breakup [127] was incorporated into the Modified FRITIOF model. In the model, the breakup of a nucleus is considered in two steps. In the first step, the number of inelastically interacting nucleons, called as hit nucleons, is determined with the use of the Glauber approach [128]. In the second step, the nucleons which are not taking part in the interactions are considered. If the distance between a non-interacting nucleon and a hit nucleon is r, then the probability of involvement of this non-interacting nucleon in a Reggeon cascade is

$$W = C_{nd} \; e^{-r^2/r_{nd}^2} \,. \tag{2.11}$$

Then this nucleon can involve another spectator nucleon, which can involve another one, and so on and so forth. All the interacting and hit nucleons leave the nucleus. The values of parameters C_{nd} and r_{nd} were taken as 1 and 1.2 fm, respectively, for correct description of the multiplicities of protons participating in the collisions of protons and nuclei with ^{12}C nuclei. The excitation energies of the residual nuclei were calculated using the approach presented in Ref. [129]. The simulations of the relaxations of excited nuclei were implemented using the evaporation model [130,131]. The Glauber cross sections were used for making the absolute normalizations of the spectra in the model. To determine these cross sections [128], one should specify some characteristics of $N+N$ interactions. These are the total cross section (σ_{NN}^{total}), the slopes of differential cross section for elastic scattering (B_{NN}), and, ρ_{NN}, the ratio of the real to the imaginary part of the amplitude of the elastic scattering at zero momentum transfer given by

$$\rho_{NN} = \frac{\mathrm{Re}\, f_{NN}(0)}{\mathrm{Im}\, f_{NN}(0)}. \tag{2.12}$$

Here f_{NN} denotes the elastic scattering amplitude. The amplitude $f_{NN}(b)$ of elastic $N+N$ scattering in terms of impact parameter representation was parameterized in the form standard for Glauber approximation:

$$f_{NN}(b) = \frac{\sigma_{NN}^{total}(1 - i\rho_{NN})}{4\pi B_{NN}} e^{-b^2/2B_{NN}}. \tag{2.13}$$

The values of the parameters used were identical to those given in Ref. [117]:

σ_{NN}^{total} = 42 mb, B_{NN} = 7.8 (GeV/c)$^{-2}$, and ρ_{NN} = – 0.23.

The single particle densities of nuclei heavier than helium nucleus used in the model are given by

$$\rho(r) = \frac{const}{1 + e^{\left(\frac{r - R_A}{c}\right)}}. \tag{2.14}$$

Here $R_A = 1.07 A^{1/3}$ fm, and c = 0.545 fm.

§ 2.2. Quark-Gluon String Model adapted to intermediate energies

The Quark-Gluon String Model (QGSM) [132; P.172] is a microscopic model, using the Regge and strings phenomenology of particle production. In this model, the formation of quark gluon plasma is not assumed. Strings are produced in $h+h$, $h+A$, and $A+A$ interactions, which decay later to form the secondary hadrons. The particles coming from string decays in QGSM can be also scattered. The strings can interact with each other forming di-quarks [133; P.1541].

The models depicting the decay of baryon resonances can be used to investigate the production of pions in these interactions. The QGSM [132] takes into account the production and decay of baryon resonances. The QGSM was extrapolated to the range of intermediate energies ($\sqrt{s_{nn}} \leq 4$ GeV). The QGSM can be useful to understand and interpret the characteristics of hadrons produced in relativistic *h*+*A* and *A*+*A* collisions, and its validity can also be checked comparing its results with the experimental data. The nuclear collisions were treated as a superposition of the independent collisions of the nucleons of the projectile and target nuclei, stable hadrons, and short lived resonances. In this model, the resonant reactions like $\pi + N \rightarrow \Delta$, absorption of pions by *N*+*N* quasi deuteron pairs, and also $\pi + \pi \rightarrow \rho$ reactions were included. The formation time of hadrons was also taken into account in this model. The strings have small masses at intermediate energies, and at $\sqrt{s_{nn}} = 3.14$ GeV they fragment through two particle decay channel in approoximately 90% cases. The coordinates of the nucleons are calcuulated using the realistic densities of a nuclear matter. The spheres of the nuclei are supposed to be fully occupied by the nucleons provided that the nucleons should be located at a distance not less than 0.8 fm from each other. The momenta (p) of nucleons are distributed in the range from “0” to a maximum Fermi momentum of a nucleon, p_F, calculated for a given nucleus from its nuclear density. In QGSM the collision events are generated in three steps: [1] The configurations of the interacting nucleons are defined; [2] Quark gluon strings are formed; [3] The produced strings fragment into hadrons, which are finally observed.

The topological quark diagrams used for the principal *N*+*N* and π+*N* interactions are illustrated in Fig. 2.1. Figure 2.1*a* presents the binary process, which is proportional to $1/p_{\text{lab}}$, making the main contribution in QGSM. This binary process corresponds to a rearrangement of quarks without direct particle emission during string fragmentation (decay). It results mainly in resonance production (like in reaction $p + p \rightarrow N + \Delta^{++}$). The produced resonances are the main sources of the pions. The angular dependence of the binary process (Fig. 2.1*a*) is defined by

$$\frac{d\sigma}{dt} \cong e^{-bt} \text{ , where } b(s) = 2.5 + 0.7 \ln(s/2). \quad (2.15)$$

Here t is the four-momentum transfer. The “undeveloped” cylindrical diagrams (Fig. 2.1*b*) and diffractive processes (Figs. 2.1*c* and 2.1*d*) contribute also to the inelastic cross section. Their contributions decrease as p_{lab} decreases.

The transverse momenta of pions created via quark-gluon string fragmentation are the product of the two factors: [1] String motion on the whole due to the transverse motion of constituent quarks; [2] Production of $q\bar{q}$ pairs from the string breakup. Transverse motion of quarks inside the hadrons was parameterized with the Gaussian distribution with the variance $\sigma^2 \cong 0.3$ (GeV/c)^2.

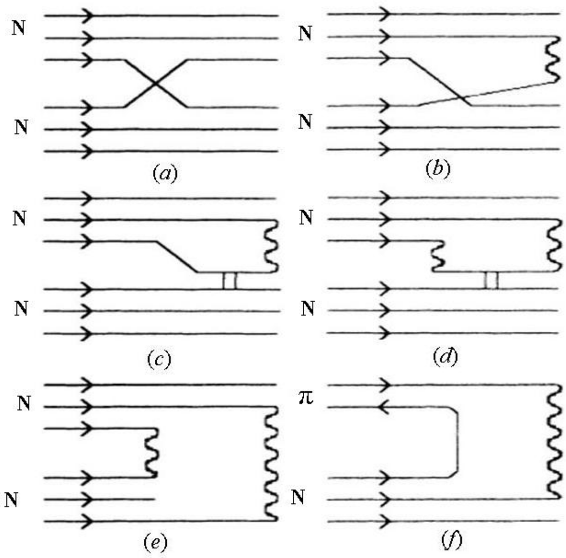

Fig. 2.1. Topological quark diagrams for main processes taken in QGSM: (*a*) binary, (*b*) “undeveloped” cylindrical, (*c*) and (*d*) diffractive, (*e*) cylindrical, and (*f*) planar. The solid lines show quarks and the wavy curves represent strings

The transverse momenta k_T of the created $q\bar{q}$ pairs in the center-of-mass system of a string were described by

$$W(k_T) = \frac{3b}{\pi \left(1 + bk_T^2\right)^4}. \quad (2.16)$$

Here b = 0.34 (GeV/c)$^{-2}$. The experimental cross sections were used for hadron interactions. The predictions of the additive quark model and isotopic invariance were used in the QGSM to determine the meson–meson cross sections and other necessary parameters, which are not available in the experimental data. The cross sections of the resonance interactions were assumed to be equal to the cross sections of interaction of the stable particles with the same quark contents. A coupling of nucleons inside the nuclei and the decays of the excited recoil nuclear fragments were not taken into account in QGSM.

§ 2.3. Phenomenological models and approaches used for description of the pion spectra

The temperatures extracted from kinematical spectra of particles using the thermodynamic relations, derived under assumption of the thermal equilibrium of the source of the particles produced, can be termed as the spectral temperatures of the particles. Produced particles are characterized by the freeze-out temperature, i.e., the temperature at which particles of an expanding fireball stop to interact strongly, or the temperature at which particles become "free" being no longer the part of this fireball. For a gas of a volume V being in a thermal equilibrium, the momentum distribution of different species (particles) $\boldsymbol{i}$ can be expressed as [134–136]:

$$\frac{d^3N}{dp^3} = \frac{(2S_i+1)V}{(2\pi)^3}\left(\exp\left(\frac{E_i-\mu_i}{T}\right)\pm 1\right)^{-1} \tag{2.17}$$

$$\rightarrow \frac{(2S_i+1)V}{(2\pi)^3}\exp\left(\frac{\mu_i-m_i}{T}\right).\exp\left(-\frac{E_{ki}}{T}\right) \tag{2.18}$$

The arrow indicates the classical Boltzmann-statistics limit $E_i-\mu_i >> T$. V is fireball's volume, S_i is spin, μ_i is chemical potential, T is temperature, E_i is particle energy, i.e., $E_i=\sqrt{m_i^2+p_i^2}$, and $E_{ki}=E_i-m_i$ is the kinetic energy of the particle in the net center-of-mass system. The "±" signs refer to fermions and bosons. Using limit of $E_i - \mu_i >> T$ in equation (2.17), the final result can be written as

$$\frac{d^3N}{dp^3} = \frac{d^2N}{p^2\ dp\, d\Omega} = \frac{d^2N}{pE\, dE\, d\Omega} = \text{const}\cdot\exp\left(-\frac{E_k}{T}\right) \tag{2.19}$$

The above equation allows one to extract the particle temperature from the spectral slope. However some factors, which might affect the final result, have to be kept in mind when applying this technique to extract the temperature from a particle spectrum. For example, the net centre-of-mass frame can not be determined exactly in reactions between light projectiles and heavy targets. This depends on the value of impact parameter [137], which itself can not be defined directly. Also the compressional energy acquired at the initial stage of collision followed by the energy flow during expansion stage might affect the spectra of pions, and hence the value of spectral temperature [138]. If we assume that Δ resonances are in thermal equilibrium with surrounding nucleons, then pions will emerge later after these resonances have frozen-out. Thus two-body decay kinematics of Δ resonances ($\Delta \to N\pi$) will also affect the pion energy spectra [139].

Using the global freeze-out model, one can extract the freeze-out temperature by fitting an exponential to the scaled distribution of particles in kinetic energy:

$$(pE)^{-1} dN/dE_k = A\exp\left(-\frac{E_k}{T}\right), \tag{2.20}$$

where A is the fitting constant. Correspondingly, in case of two temperatures the equation (2.20) can be written as

$$(pE)^{-1} dN/dE_k = A_1\ \exp\left(-\frac{E_k}{T_1}\right) + A_2\ \exp\left(-\frac{E_k}{T_2}\right), \tag{2.21}$$

where A_1 and A_2 are the fitting constants, p is the total momentum, E is the total energy in c.m.s., E_k is the kinetic energy in c.m.s., and T_1 and T_2 are temperatures.

The Standard Thermal Model of freeze-out with the c.m.s. predicts that the scaled c.m. kinetic energy spectra of hadrons in the limit $E_k >> T$ can be described as

$$\frac{dN}{N\,pE\,dE_k} = A \cdot \exp\left(-\frac{E_k}{T}\right), \tag{2.22}$$

where p, E, and E_k are the momentum, total energy, and kinetic energy of a hadron in the center-of-mass system of colliding nuclei. The above relation (2.22) will be referred to as one-temperature simple exponential function throughout the present paper. In case of two temperatures, T_1 and T_2, the above expression becomes

$$\frac{dN}{N\,pE\,dE_k} = A_1 \cdot \exp\left(-\frac{E_k}{T_1}\right) + A_2 \cdot \exp\left(-\frac{E_k}{T_2}\right), \tag{2.23}$$

referred to as two-temperature simple exponential function in the present work.
The Hagedorn Thermodynamic Model [77, 140] allows for a set of fireballs to be displaced from each other in the rapidity space. In this model, particles with different momenta freeze-out within a volume which is of universal magnitude when assessed in the rest frame for any given momentum. This model predicts that the p_t distribution of particles can be expressed as

$$\frac{dN}{dp_t} = A \cdot p_t \cdot m_t \cdot K_1\left(\frac{m_t}{T}\right) \approx A \cdot p_t \cdot (m_t T)^{1/2} \exp\left(-\frac{m_t}{T}\right), \tag{2.24}$$

which, in case of two temperatures, can be written as

$$\frac{dN}{dp_t} \approx A_1 \cdot p_t \cdot (m_t T_1)^{1/2} \exp\left(-\frac{m_t}{T_1}\right) + A_2 \cdot p_t \cdot (m_t T_2)^{1/2} \exp\left(-\frac{m_t}{T_2}\right), \tag{2.25}$$

where K_1 is the MacDonald Function, $m_t = \sqrt{m^2 + p_t^2}$ is the transverse mass, and the above approximations (2.24) and (2.25) are valid for $m_t >> T$. Using the Hagedorn Thermodynamic Model, the normalized transverse momentum (p_t) distribution of hadrons can be described using the expression

$$\frac{dN}{N\,p_t dp_t} = A \cdot (m_t T)^{1/2} \exp\left(-\frac{m_t}{T}\right), \tag{2.26}$$

where N, depending on the choice of normalization, is either the total number of inelastic events or the total number of respective hadrons, $m_t = \sqrt{m^2 + p_t^2}$ is the transverse mass, T is the spectral temperature, and A is the fitting constant. This expression (2.26) is referred as the one-temperature Hagedorn function throughout the present work. Correspondingly, in case of two temperatures, T_1 and T_2, the above formula is modified as

$$\frac{dN}{N\,p_t dp_t} = A_1 \cdot (m_t T_1)^{1/2} \exp\left(-\frac{m_t}{T_1}\right) + A_2 \cdot (m_t T_2)^{1/2} \exp\left(-\frac{m_t}{T_2}\right), \tag{2.27}$$

referred to as the two-temperature Hagedorn function in the present dissertation. According to The Boltzmann Model, the transverse momentum spectra of hadrons can be fitted using m_t Boltzmann distribution function given by

$$\frac{dN}{N\,p_t dp_t} = A m_t \exp\left(-\frac{m_t}{T}\right), \tag{2.28}$$

referred to as the one-temperature Boltzmann function in the present work. In case of two temperatures, T_1 and T_2, the above formula is modified as

$$\frac{dN}{N\,p_t dp_t} = A_1 \cdot m_t \exp\left(-\frac{m_t}{T_1}\right) + A_2 \cdot m_t \exp\left(-\frac{m_t}{T_2}\right)., \tag{2.29}$$

referred as the two-temperature Boltzmann function in the present dissertation.

Analysis of rapidity distributions of pions produced in nucleus–nucleus in wide range of collision energies showed that they followed a Gaussian shape [35, 65]. The experimental rapidity spectra of pions in nucleus–collisions can be fitted satisfactorily by Gaussian distribution function given by

$$F(y) = \frac{A_0}{\sigma} \exp\left(\frac{-(y - y_0)^2}{2\,\sigma^2} \right), \tag{2.30}$$

where σ is the standard deviation, referred to as a width of distribution in the present work, y_0 – the center of Gaussian distribution, and A_0 is the fitting constant.

§ 2.4. Selection of central, semicentral, and peripheral collision events

In the present dissertation work, we analyzed quantitatively the change of shapes of transverse momentum and rapidity spectra of negative pions with increase in the collision centrality, which corresponds to decrease in impact parameter of collision. Since impact parameter is not directly measurable, we used the number of participant protons N_p to characterize the collision centrality. We followed the Ref. [65] to define the peripheral collision events to be those in which $N_p \le \langle n_{partprot} \rangle$, and the central collisions as the collision events with $N_p \ge 2\langle n_{partprot} \rangle$, where $\langle n_{partprot} \rangle$ is the mean multiplicity per event of participant protons. Consequently, the semicentral collision events were defined as those in which $\langle n_{partprot} \rangle < N_p < 2\langle n_{partprot} \rangle$. It was shown in early work [141] that the central ^{12}C+^{181}Ta collisions at 4.2 *A* GeV/*c*, selected using the above criterion, were characterized by complete projectile stopping, because in these collisions the average number $\langle \nu^p \rangle$ of interacting projectile nucleons was very close to the total number of nucleons in projectile carbon. Fractions of central and peripheral d+^{12}C,

$^{12}C+^{12}C$, and $^{12}C+^{181}Ta$ collision events, relative to the total inelastic cross section (σ_{in}), obtained in our work [35] for both the experimental and QGSM data are presented in Table 2.1. As seen from Table 2.1, the experimental and corresponding model fractions of central and peripheral $d+^{12}C$, $^{12}C+^{12}C$, and $^{12}C+^{181}Ta$ collision events coincide with each other within two standard errors, with the only exception that the fraction of peripheral $d+^{12}C$ collisions is overestimated by the QGSM. As seen from Table 2.1, the central interactions constitute about 10% in $d+^{12}C$ and $^{12}C+^{12}C$ collisions, whereas it is approximately 15% in $^{12}C+^{181}Ta$ collisions. On the other hand, the fraction of peripheral collisions is roughly 60% in the analyzed collisions. These results for $^{12}C+^{12}C$ and $^{12}C+^{181}Ta$ collisions coincide with the fractions of central and peripheral collision events estimated in Ref. [65], on a significantly lower statistics of $^{12}C+^{12}C$ and $^{12}C+^{181}Ta$ collisions as compared to the corresponding statistics of the present analysis.

Table 2.1

Fractions of central and peripheral $d+^{12}C$, $^{12}C+^{12}C$, and $^{12}C+^{181}Ta$ collisions at 4.2 GeV/*c* per nucleon relative to the total inelastic cross section (σ_{in}) [35]

Type	Central collisions, %		Peripheral collisions, %	
	Experiment	QGSM	Experiment	QGSM
$d+^{12}C$	10±1	12±1	53±1	73±1
$^{12}C+^{12}C$	11±1	8±1	58±1	62±1
$^{12}C+^{181}Ta$	16±1	15±1	60±2	56±1

The further detailed information on description of the experimental data on relativistic hadron-nucleus and nucleus-nucleus collisions (for minimum-bias collisions and different collision centralities) using the FRITIOF, QGSM, and other theoretical models can be found in Refs. [142–157].

III. PRODUCTION OF NEUTRAL Δ^0(1232) RESONANCES

§ 3.1. Reconstruction of Δ(1232) production

In Refs. [39, 41–47] we reconstructed successfully the mass distributions of the Δ^0(1232) resonances, produced in in p+^{12}C, d+^{12}C, ^{4}He+^{12}C, ^{12}C+^{181}Ta collisions at 4.2 A GeV/c, ^{16}Op collisions at 3.25 A GeV/c, and π^{-12}C interactions at 40 GeV/c, using the similar method of analysis of the angles between outgoing protons and negative pions in the collision events. Therefore, as an example, the methodical procedures of the reconstruction of Δ^0(1232) as well as Δ^{++}(1232) production in ^{16}Op collisions at 3.25 A GeV/c [43] is described below.

The identification of the structures in the invariant mass distribution of correlated proton and pion pairs provides the direct proof that nucleons are excited to high-lying resonances [24]. The major obstacle that should be overcome in reconstructing the invariant mass is the large background of non-correlated $p\pi$ pairs [24]. In peripheral reactions with very light projectiles, e.g. p [93, 94] or ^{3}He [95] induced reactions at around 2 GeV bombarding energy, the $p\pi$ correlations were successfully analyzed and the mass distribution of the Δ(1232) resonance was determined. The resonance mass was found to be shifted by about –25 MeV/c^2 to lower masses in reactions on various targets, compared to those on protons [93-95]. The mass reduction of the Δ resonance in $p+A$ collisions ($A =$ C, Nb, Pb) at 0.8 GeV and 1.6 GeV incident energy [93] was traced back to the effects of Fermi motion, NN scattering and pion reabsorption in nuclear matter.

In the model of independent nucleus-nucleus interactions, the Δ resonances are mainly produced in the reaction $NN \to \Delta N$, which competes with the process of direct pion production: $NN \to NN\pi$, $NN \to NN\pi\pi$. In this simple model Δ^{++} resonances are produced via reaction

$$pp \to \Delta^{++} n + k\pi \quad (k = 0,1,...)\,, \tag{3.1}$$

with the subsequent decay $\Delta^{++} \to p\pi^{+}$ and Δ^{0} – in reaction

$$NN \to \Delta^{0} N + k\pi \quad (k = 0,1,...)\,, \tag{3.2}$$

with the later decay $\Delta^{0} \to p\pi^{-}$. To analyze Δ^{++} and Δ^{0} production in the present work, the observed final particles – protons and charged pions were used.

The experimental data were obtained using the 1 m hydrogen bubble chamber of the Laboratory of High Energies of JINR (Dubna, Russia) exposed to a beam of relativistic oxygen nuclei accelerated to the momentum of 3.25 GeV/*c* per nucleon at JINR synchrophasotron. The usage of accelerated nuclear beams impinging on the fixed proton target caused all particles and fragments of the incoming oxygen nucleus to be fast in the laboratory frame and thus one could well measure and identify them practically without losses [144]. On the other hand, almost all the losses due to the chamber threshold are concentrated in the elastic scattering channels. The chamber threshold is the minimal momentum (energy) of the particle that can be detected. This is because the particle tracks shorter than 2 mm (corresponding to a momentum of about 110 MeV/*c* for protons) are not visible in the chamber. That is why practically all the particle losses in our experiment are the losses of short tracks of recoil protons in elastic ^{16}O+*p* interactions. The ionization of the charged secondary particles was estimated visually. The homogeneity and low hydrogen density allowed us to identify with high precision practically all charged secondaries on the basis of ionization and produced measurements [144]. The mean relative errors on momentum measurements for surely identified protons (recoil protons) and $\pi^{\pm}$-mesons, without any restrictions on their track length, proved to be 4.56% and 2.65%, respectively [144]. The absolute mean errors in measuring the azimuthal angle in *XOY* plane proved to be 0.60 ± 0.01 mrad, and 1.50 ± 0.02 mrad for the depth angle [144]. For the reliable separation of fragments by mass we studied the secondary particles with measured length $L \geq 35$ cm in the chamber. For this type of selection, the mean relative errors of momentum measurements did not exceed

3.5% for all charges [144]. During the physical analysis of the experimental data, the corrections accounting for the loss of particles over the length $L = 35$ cm in the chamber were included.

To analyze the production of Δ^{++} and Δ^0 resonances on oxygen nuclei in ^{16}O+*p* collisions at 3.25 *A* GeV/*c*, all the protons coming out of oxygen nuclei and all charged pions were used. The mean multiplicity of protons of oxygen nuclei per event in the momentum range 1.25–4.75 GeV/*c* in the laboratory frame proved to be 1.93 ± 0.02. The mean multiplicity of π^+- and π^--mesons per event in ^{16}O+*p* interactions at 3.25 *A* GeV/*c* proved to be 0.51 ± 0.01 and 0.30 ± 0.01, respectively.

The measured momenta of protons and pions were used to calculate the invariant mass of the $p\pi^{\pm}$ system, M, from the relation

$$M^2 = (E_p + E_\pi)^2 - (\mathbf{p}_p + \mathbf{p}_\pi)^2, \tag{3.3}$$

where E_p, E_π, $\mathbf{p}_p$, $\mathbf{p}_\pi$ – are the energy and momentum of the proton and pion, respectively. The experimental and background invariant mass distributions for $p\pi^+$ and $p\pi^-$ pairs, respectively, in ^{16}O+*p* collisions at 3.25*A* GeV/*c* are shown in Fig. 3.1*a* and Fig. 3.1*b*, respectively.

The experimental distribution was obtained combining protons and pions in each individual event. The background spectrum was obtained by a Monte-Carlo method. That is, the invariant mass of $p\pi$ pairs selected randomly using a proton from one event and a pion from another event was calculated. To take into account the event topology, only events with equal particle multiplicities were combined. As seen from Fig. 3.1, the invariant mass distribution dN/dM for both $p\pi^+$ and $p\pi^-$ pairs does not show a resonance-like structure near M_Δ= 1232 MeV/c^2, expected for Δ resonance, and the maxima of distributions are shifted to the values of $M < 1200$ MeV/c^2. This is, as seen from this figure and shown earlier for C+C [27] and ^{4}He+C [47] collisions at 4.2*A* GeV/*c*, π^-+^{12}C interactions at 40 GeV/*c*

[46], due to a large background contribution from uncorrelated $p\pi$ pairs. To reduce their contribution as much as possible, the method of analyzing an angle between the proton and pion was used as done successfully in [27, 44, 46, 47] to extract the mass distribution of the Δ resonance.

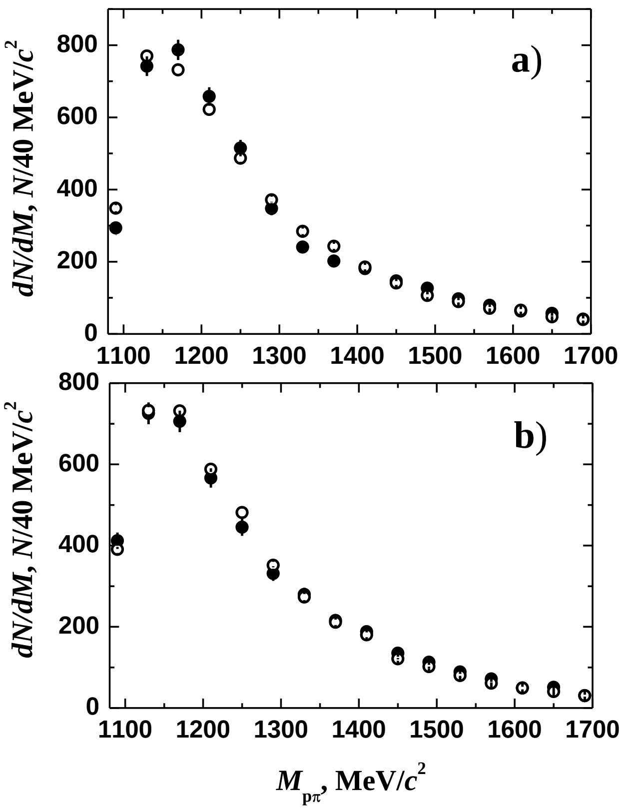

Fig. 3.1. Experimental (●) and background (○) invariant mass distributions of $p\pi^+$ (*a*) and $p\pi^-$ (*b*) pairs in ^{16}O+*p* collisions at 3.25 *A* GeV/*c*

If the Δ resonance decays in flight, the angle α between the outgoing proton and pion, in the laboratory frame, is defined by

$$\cos\alpha = \frac{1}{p_p p_\pi}\left(E_p E_\pi - \frac{M_\Delta^2 - M_\pi^2 - M_p^2}{2}\right), \tag{3.4}$$

where p_p and p_π are the proton and pion momenta, E_p and E_π are the respective energies, and M_Δ= 1232 MeV/c^2. This value was compared with the cosine of experimentally measured angle β,

$$\cos\beta = \frac{\mathbf{p}_p \cdot \mathbf{p}_\pi}{p_p p_\pi}. \quad (3.5)$$

The experimental invariant mass distribution, dn/dM, for $p\pi^\pm$ pairs was constructed using the following criteria:

(i) Only the combinations satisfying the inequality

$$|\cos\beta - \cos\alpha| < \varepsilon \quad (3.6)$$

were kept, where ε is an arbitrary cutoff parameter theoretically lying in the interval [0, 2], while, if the momenta of protons and pions are measured with high precision, the upper limit of the interval should be low;

(ii) The protons emitted from the projectile oxygen nucleus and having momenta $p \le 220$ MeV/*c* in the oxygen nucleus rest frame were treated as evaporated particles and excluded from the further analysis;

(iii) The missing mass for proton-pion pairs should be equal to or greater than the nucleon mass.

It should be mentioned that out of all the criteria, the criterion (i) is the most important [27, 44, 46, 47] resulting in the largest reduction of the spectrum. The background spectrum was obtained by a Monte-Carlo method using the same criteria (i)-(iii) and calculating the invariant mass of $p\pi$ pairs selected randomly taking a proton from one event and a pion from another one. For the pairs measured in a certain event the corresponding mixed pair was chosen from events with identical proton and pion multiplicities. It is necessary to note that the condition of equal multiplicities in the measured and mixed spectra ensures that correlations due to the reaction dynamics and pion rescattering in spectator matter are properly subtracted from the measured spectrum [24, 103, 104].

To make the background distribution as smooth as possible by reducing statistical errors, the number of mixed combinations for each experimental spectrum was 5 times as many as that in experiment. Then the background spectrum was normalized to the total number of pairs in the experimental invariant mass distribution. In such a way, the set of experimental and background invariant mass distributions of $p\pi$ pairs was constructed for different values of the cutoff parameter ε. Analyzing the experimental and background spectra at different values of ε, we found that already at $\varepsilon = 0.15$ (see Fig. 3.2*a* and Fig. 3.2*b*) the experimental spectra for both $p\pi^+$ and $p\pi^-$ pairs became totally suppressed by a large background contribution from uncorrelated $p\pi$ pairs.

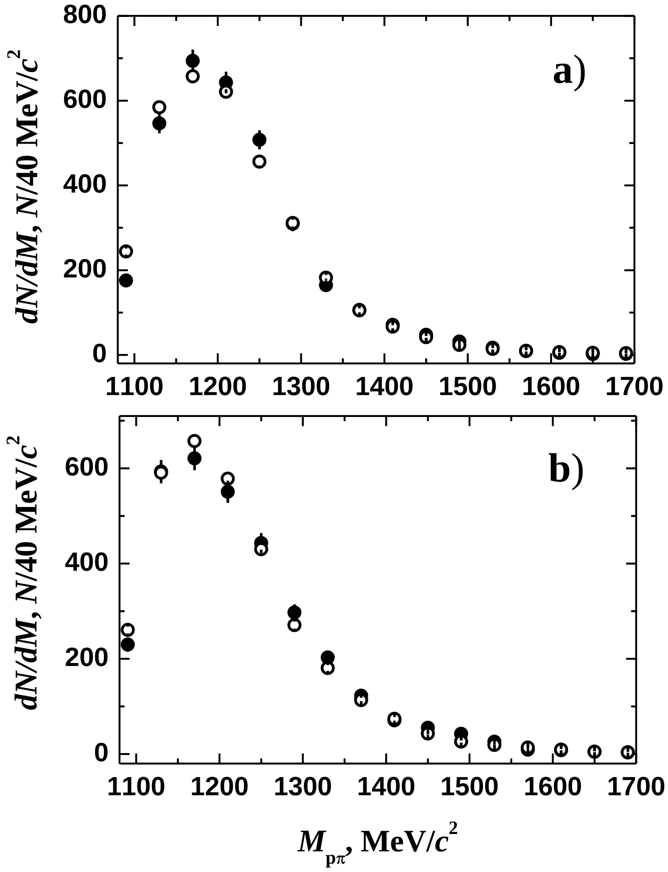

Fig. 3.2. Experimental (●) and background (○) invariant mass distributions of $p\pi^+$ (*a*) and $p\pi^-$ (*b*) pairs in ^{16}O+*p* collisions at 3.25*A* GeV/*c* obtained using the cutoff parameter ε = 0.15

At a further increase of the parameter ε, the experimental spectra become wider approaching more the shape of the invariant mass distributions in Fig. 3.1 obtained without using criteria (i)-(iii). It should be noted that in region $\varepsilon > 0.15$ the value of $\frac{dN_{tot}}{d\varepsilon}$, where N_{tot} is the total number of $p\pi$ combinations in the experimental spectrum at the certain ε, decreases as ε increases. The total number of $p\pi^+$ and $p\pi^-$ combinations in experimental invariant mass distributions at $\varepsilon = 0.15$ makes up already 71% and 73%, respectively, of the total number of respective $p\pi$ combinations in experimental spectra presented in Fig. 3.1*a* and Fig. 3.1*b*, respectively. The latter fact and that the spectra become similar to those in Fig. 3.1 already at $\varepsilon = 0.15$ is explained by the relatively high precision ($\frac{\Delta p}{p} \leq 3.5\%$) on the measurement of proton and pion momenta in the present experiment.

In the light of the above-mentioned, the further search for the mass distributions of Δ resonances, produced on oxygen nuclei in ^{16}O+*p* collisions at 3.25 *A* GeV/*c*, was performed in region $\varepsilon < 0.15$. To extract the mass distribution of the resonance and obtain the best background distribution for each ε value, the following procedures were performed. The distribution of differences between experimental and background invariant mass distribution, given by

$$D(M) = \frac{dn^{\exp}}{dM} - a\frac{dn^{b}}{dM} \tag{3.7}$$

was analyzed, where a is a coefficient varying from 0 to 1.

Interpreting the distribution $D(M)$ as a pure Δ signal, it was approximated in region 1110 ÷ 1350 MeV/c^2 by a relativistic Breit-Wigner function [105]

$$b(M) = C\frac{\Gamma M M_{\Delta}}{(M^2 - M^2{}_{\Delta})^2 + \Gamma^2 M^2{}_{\Delta}}\ , \tag{3.8}$$

where M_{Δ} and Γ are the mass and width of the resonance, and C − the normalization coefficient. The data set $D(M)$ for different values of parameters ε and a was fitted by the Breit-Wigner function $b(M)$ and the value of χ^2 was found for each fit. During these procedures, the parameter ε was varied from the value of 0.010 to 0.150 with the step of 0.001, and a was varied from 0.0 to 1.0 with the step of 0.01 for each ε value. The parameters M_{Δ} and Γ were determined by minimizing the difference $|D(M) - b(M)|$. In this way the set of two parameters was obtained for each experimental spectrum produced for different values of ε and a.

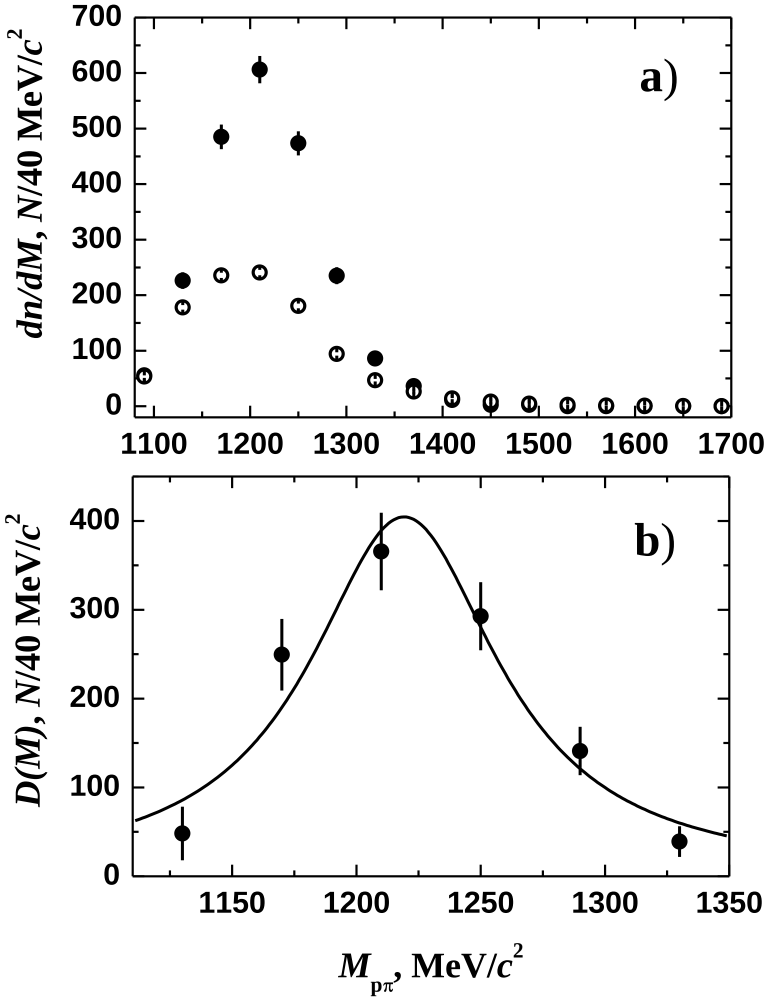

Fig. 3.3. (*a*) − Experimental invariant mass distribution $\frac{dn^{\exp}}{dM}$ (●) and the best background distribution $a\frac{dn^{b}}{dM}$ (○) for $p\pi^{+}$ pairs in ^{16}O+*p* collisions at 3.25*A* GeV/*c* obtained using the best values of parameters ε and a; (*b*) − The corresponding difference (●) between the experimental invariant mass distribution $\frac{dn^{\exp}}{dM}$ and the best background distribution $a\frac{dn^{b}}{dM}$ for $p\pi^{+}$ pairs obtained at the best values of parameters ε and a along with the corresponding Breit-Wigner fit (solid line)

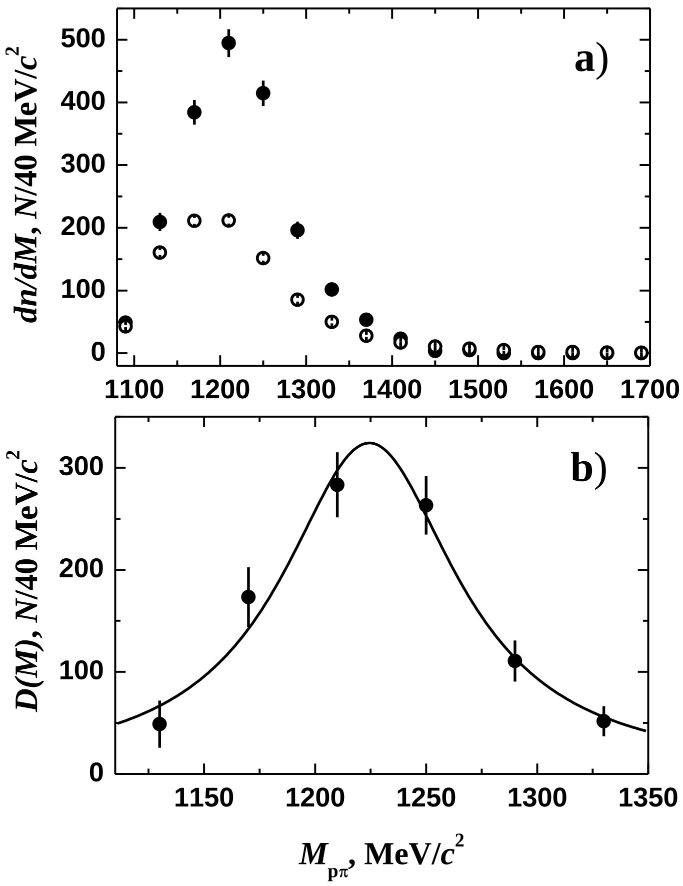

Fig. 3.4. The same as in Fig. 3.3 for $p\pi^-$ pairs

The best values of the parameters ε and a were determined from an analysis of the behavior of the function $\chi^2(\varepsilon, a)$. The minima of χ^2 functions gave the following values: $\varepsilon(\Delta^{++}) =$ 0.071, $\varepsilon(\Delta^0) =$ 0.057, $a(\Delta^{++}) =$ 0.49, and $a(\Delta^0) =$ 0.51. The corresponding experimental invariant mass distribution $\frac{dn^{\exp}}{dM}$ and the best background distribution $a\frac{dn^b}{dM}$ for $p\pi^+$ and $p\pi^-$ pairs using the best values of ε and a are shown in Fig. 3.3*a* and Fig. 3.4*a*, respectively. The difference distributions $D(M)$ for $p\pi^+$ and $p\pi^-$ pairs, using the best values of ε and a, along with the corresponding Breit-Wigner fits are presented in Fig. 3.3*b* and Fig. 3.4*b*, respectively, from where the mass and width of the Δ^{++} and Δ^0 resonances, produced on oxygen nuclei in ^{16}O+*p* collisions at 3.25 *A* GeV/*c*, were obtained. As seen from Fig. 3.3*a* and Fig. 3.4*a*, the experimental invariant mass distributions for both $p\pi^+$ and $p\pi^-$ pairs have a statistically significant resonance-like structures, expected for Δ resonances, at the best values of ε and a.

To estimate the fraction of π^+-mesons coming from Δ^{++} resonance decay relative to the total number of π^+-mesons, produced on oxygen nuclei in ^{16}O+*p* collisions at 3.25 *A* GeV/*c*, the following formula was applied using the above obtained best experimental and background spectra:

$$R(\pi^+/\Delta^{++}) = \frac{\int_{M_p+M_\pi}^{M_x} \left(\frac{dn^{\exp}}{dM} - a \cdot \frac{dn^b}{dM} \right) dM}{N_{in}^{^{16}\mathrm{O}p} \cdot 0.5 \cdot n(\pi^+)}, \tag{3.9}$$

where $M_p + M_\pi$, the sum of proton and pion masses, and $M_x \approx 1400$ MeV/c^2 are the lower and upper limits of integration, respectively, $N_{in}^{^{16}\mathrm{O}p}$ = 7961 − the total number of inelastic ^{16}O+*p* interaction events, $n(\pi^+)$=0.51 ± 0.01 − the mean multiplicity of π^+-mesons per event [144] in ^{16}O+*p* collisions at 3.25 *A* GeV/*c*. The coefficient 0.5 in the formula takes into account that approximately 50% of π^+-mesons in ^{16}O+*p* collisions at 3.25 *A* GeV/*c* are produced on target protons [144]. In the present work we estimate the fraction of π^+-mesons coming from Δ^{++} (produced on oxygen nuclei) decay relative to the total number of π^+-mesons, produced on oxygen nuclei, since we expect that in ^{16}O+*p* collisions at 3.25*A* GeV/*c* Δ^{++} resonances are also produced on target protons. But we did not make any analysis for Δ^{++} produced on target protons, because of the low statistics of target protons (their mean multiplicity per event is 0.60 ± 0.01) compared to the relatively high statistics of protons coming out of oxygen nuclei (their mean multiplicity per event (see the text) is 1.93 ± 0.02). Similarly for the fraction of π^--mesons (relative to the total number of π^--mesons produced in ^{16}O+*p* collisions at 3.25 *A* GeV/*c*) coming from Δ^0 decay we have

$$R(\pi^- / \Delta^0) = \frac{\int_{M_p+M_\pi}^{M_x} \left(\frac{dn^{\exp}}{dM} - a \cdot \frac{dn^b}{dM} \right) dM}{N_{in}^{^{16}\mathrm{O}p} \cdot n(\pi^-)}, \qquad (3.10)$$

where $n(\pi^-)$=0.30 ± 0.01 is the mean multiplicity of π^--mesons per event [144] in ^{16}O+p collisions at 3.25 *A* GeV/*c*. We estimate the fraction of π^--mesons coming from Δ^0 (produced on oxygen nuclei) decay relative to the total number of π^--mesons in ^{16}O+p collisions at 3.25 *A* GeV/*c*, since in ^{16}O+p collisions at 3.25 *A* GeV/*c* production of Δ^0 on target protons is practically impossible, and thus all Δ^0 resonances are produced on oxygen nuclei. The error on the estimation of the fraction of pions coming from Δ decay was estimated to be ~ 10% and is caused by the statistical uncertainties as well as by uncertainties due to overlapping of the tails of the measured momentum distributions of protons and deuterons, and some small admixture of π^+-mesons among protons.

Table 3.1

The experimental values of the masses, widths, fractions of charged pions, $R(\pi / \Delta)$, for Δ^{++} and Δ^0 resonances, produced on oxygen nuclei in ^{16}O+*p* interactions at 3.25 *A* GeV/*c*

Resonance	M (MeV/c^2)	Γ (MeV/c^2)	$R(\pi / \Delta)$ (%)
Δ^{++}	1218 ± 3	93 ± 8	57 ± 6
Δ^0	1224 ± 4	96 ± 10	41 ± 4

The experimental values of the masses, widths, fractions of charged pions, $R(\pi / \Delta)$, for Δ^{++} and Δ^0 resonances, produced on oxygen nuclei in ^{16}O+p collisions at 3.25 *A* GeV/*c*, obtained using the best values of ε and a, are presented in Table 3.1. As seen from Table 3.1, the noticeable diminishing of the masses and widths of Δ^{++} and Δ^0 resonances, produced on oxygen nuclei in ^{16}O+p interactions at 3.25*A* GeV/*c*, relative to those of the free nucleon $\Delta(1232)$ resonance

(M = 1232 and Γ = 115 MeV/c^2) is observed. The values of $R(\pi/\Delta)$ obtained show that (41 ± 4)% of all π^--mesons and (57 ± 6)% of π^+-mesons, produced on oxygen nuclei in ^{16}O+p interactions at 3.25 A GeV/c, are estimated to come from decay of Δ^{++} and Δ^0 resonances, respectively, produced on oxygen nuclei.

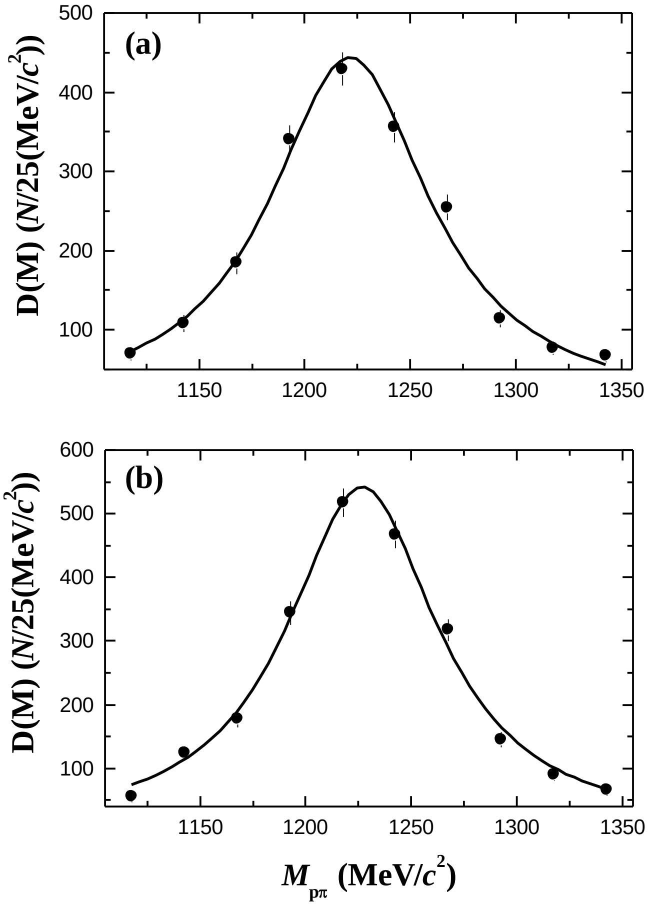

Fig. 3.5. The difference (●) between the experimental invariant mass distribution and background for $p\pi^+$ (*a*) and $p\pi^-$ (*b*) pairs in $\pi^{-\,12}$C interactions at 40 GeV/*c* and the corresponding Breit-Wigner fits (solid lines) at the best values of parameters ε and a: $\varepsilon(\Delta^{++}) =$ 0.63 ± 0.01, $\varepsilon(\Delta^0) =$ 0.57 ± 0.01, $a(\Delta^{++}) =$ 0.63 ± 0.01, and $a(\Delta^0) =$ 0.56 ± 0.01

The lower value of $R(\pi/\Delta)$ obtained for π^--mesons as compared to the fraction of π^+-mesons coming from Δ^{++} decay is probably due to the substantial role of the charge-exchange processes, $pn \to np$, with the transfer of the target-proton charge to a neutron of oxygen nucleus in ^{16}O+p interactions at 3.25 A GeV/c, which can partly suppress Δ^0 production.

Table 3.2

The experimental values for the masses, widths, $R(\pi/\Delta)$, and inclusive cross-sections of production of Δ resonances in $\pi^{-\,12}$C interactions at 40 GeV/*c* [46]

Resonance	M (MeV/c^2)	Γ (MeV/c^2)	$R(\pi/\Delta)$ (%)	$\sigma(\Delta)$ (mb)
Δ^{++}	1220 ± 3	92 ± 8	5.7 ± 0.8	32 ± 5
Δ^{0}	1226 ± 3	87 ± 7	6.1 ± 0.9	105 ± 16

As an example, the reconstructed mass distributions of Δ^{++} and Δ^0 resonances in $\pi^{-\,12}$C interactions at 40 GeV/c [46] along with the corresponding Breit-Wigner fits are shown in Fig. 3.5. The experimental values for the obtained masses, widths, $R(\pi/\Delta)$, and inclusive cross-sections of production of Δ^{++} and Δ^0 resonances in $\pi^{-\,12}$C interactions at 40 GeV/c are presented in Table 3.2.

§ 3.2. Production of Δ^0(1232) resonances in p^{12}C, d^{12}C, α^{12}C and ^{12}C^{181}Ta collisions at 4.2 *A* GeV/*c*, ^{16}O*p* collisions at 3.25 *A* GeV/*c*, and $\pi^{-\,12}$C interactions at 40 GeV/*c*

The mass distributions of Δ^0(1232) resonances produced in p, d(^{12}C) [39, 41, 42], ^{12}C^{12}C [27], α^{12}C [45, 47] and ^{12}C^{181}Ta collisions [44] at 4.2 A GeV/c, ^{16}Op collisions [43] at 3.25 A GeV/c, and in $\pi^{-\,12}$C interactions [46] at 40 GeV/c were extracted from the experimental and background invariant mass distributions of $p\pi^-$ pairs using the similar method of analysis of angle between outgoing protons and negative pions, described above. To extract the mass and width of Δ^0(1232), the reconstructed mass distributions of Δ^0(1232) resonances in these collisions were fitted with the relativistic Breit–Wigner function [105]. The masses and widths of Δ^0(1232) resonances, fractions of π^- mesons coming from Δ^0(1232) decay extracted in the above collisions are presented in Table 3.3.

For a comparison, the average mass shift (relative to the corresponding value (M = 1232 MeV/c^2, Γ=115 MeV/c^2) of the free nucleon $\Delta(1232)$ resonance) and width of the Δ resonance, obtained in Refs. [24, 91] in near-central Ni+Ni and Au+Au collisions at energies between 1 and 2 A GeV, are given in Table 3.4.

As seen from Tables 3.3 and 3.4, the noticeable decrease in the mass and width of Δ resonance produced in hadron-nucleus and nucleus-nucleus collisions at initial energies 1-40 GeV relative to the corresponding values (M = 1232 MeV/c^2, Γ=115 MeV/c^2) of the free nucleon $\Delta(1232)$ resonance is observed. As compared to the light carbon and oxygen involved collisions, the mass and width of Δ resonance produced in near central heavy ion (Ni+Ni and Au+Au) collisions decrease more considerably.

Table 3.3

The masses and widths of Δ^0(1232) resonances, fractions ($R(\Delta^0/\pi^-)$) of π^- mesons coming from Δ^0(1232) decay, in *p, d, α,*^{12}C(^{12}C) and ^{12}C^{181}Ta collisions at 4.2 *A* GeV/*c*, ^{16}O*p* collisions at 3.25 *A* GeV/*c*, and in π^- ^{12}C interactions at 40 GeV/*c*

Reaction, p_0	M (MeV/c^2)	Γ (MeV/c^2)	$R(\Delta^0/\pi^-)$ (%)
d^{12}C, 4.2 A GeV/c	$1230 \pm 4\ ^{+3}_{-6}$	$90 \pm 14\ ^{+19}_{-24}$	$30 \pm 2\ ^{+6}_{-7}$
p^{12}C, 4.2 GeV/c	$1222 \pm 5\ ^{+10}_{-14}$	$89 \pm 14\ ^{+32}_{-43}$	$39 \pm 3\ ^{+10}_{-7}$
π^- ^{12}C, 40 GeV/c	1226 ± 3	87 ± 7	6 ± 1
^{16}Op, 3.25 A GeV/c	1224 ± 4	96 ± 10	41 ± 4
α ^{12}C, 4.2 A GeV/c	1227 ± 2	103 ± 6	48 ± 3
^{12}C^{12}C, 4.2 A GeV/c	1230 ± 4	93 ± 8	50 ± 5
^{12}C^{181}Ta, 4.2 A GeV/c	1224 ± 1	86 ± 5	64 ± 4

This is most probably due to the dense nuclear matter, created in near central heavy ion collisions, in which the properties of Δ resonance can change significantly. As was pointed in [24], there are two conceivable causes for these modifications: The resonance masses are shifted because of their nuclear environment or/and the resonances are in thermal equilibrium with the hadronic matter at a low temperature [24]. The environment causes in general a mass shift which can be either positive or negative and depends on the hadronic density [24].

Table 3.4

The average mass shift and width of the Δ resonance in near-central Ni+Ni and Au+Au collisions at energies between 1 and 2 *A* GeV

Type	$\langle \Delta m_\Delta \rangle$ (MeV/c^2)	$\langle \Gamma_\Delta \rangle$ (MeV/c^2)
Ni+Ni, 1.06 *A* GeV	–59 ± 10	48 ± 5
Ni+Ni, 1.45 *A* GeV	–52 ± 10	49 ± 5
Ni+Ni, 1.93 *A* GeV	–59 ± 10	48 ± 5
Au+Au, 1.06 *A* GeV	–78 ± 10	44 ± 5

For example, as seen from Table 3.4, for near-central Ni+Ni and Au+Au collisions [24, 91] at energies between 1 and 2 *A* GeV the average mass shift of the Δ resonance was about –60 and –80 MeV/c^2, respectively. The mass shift of the Δ resonance in nucleus-nucleus collisions was also found to be roughly proportional to the number of participant nucleons that becomes smaller with increasing impact parameter b [24]. The small mass shift of the Δ resonance for *p*, *α* (^{12}C) and ^{12}C^{181}Ta collisions at 4.2 *A* GeV/*c*, ^{16}O*p* collisions at 3.25 *A* GeV/*c*, and in π^{-} ^{12}C interactions at 40 GeV/*c* and almost no shift observed for *d*^{12}C and ^{12}C^{12}C collisions at 4.2*A* GeV/*c*, as seen from Table 3.3, can be explained by the fact that the colliding nuclei were relatively light and the results averaged over all impact parameter b values [27, 39, 42-47]. As shown in Table 3.3, the average widths of the Δ resonances for collisions of π^{-}-mesons at 40 GeV/*c*, *p*, *d*, ^{4}He, and C nuclei at 4.2 *A* GeV/*c* with the target carbon nucleus coincided within errors, being independent of the mass and energy of the light projectile nucleus (particle). It should be noted that the average width of the Δ resonances for Ni+Ni collisions, as seen from Table 3.4, proved also to be the same within the errors for energies between 1 and 2 *A* GeV and was approximately twice as low as that in carbon involved interactions.

It should be mentioned that in early investigations the quasi-free production of Δ-resonance on a nucleon of a nucleus was considered to be the main mechanism of Δ-excitation in a nucleus [79]. The calculations and specially designed experiments showed that such a mechanism should cause the widening and shift of a Δ-peak to the higher excitation energies as compared to the corresponding values of Δ-resonance produced in collisions of free nucleons [79]. The shift of the Δ-resonance mass to the lower values and diminishing of its width observed in hadron-nucleus and nucleus-nucleus collisions testify, probably, the existence of the mechanism, different from the quasi-free one, which is the collective excitation of Δ-resonance in a nucleus. Thus the origin of the collective excitation of Δ-resonance in a nucleus is connected not to the spin-isospin excitation of one of the nucleons of the nucleus, but to the response of the nucleus as the whole [79, 80]. The modification of the properties of Δ-resonance in a nucleus could also be due to the properties of a tiny local region of a nuclear matter (such as hadronic density, temperature, *etc*.) around the point and at the moment of Δ production, and not due to the response of the nucleus, or the excited hadronic matter, as the whole [59].

We offer the simple interpretation of the diminishing of the masses of the Δ^0(1232) resonances, produced in *p, d, α,*^{12}C(^{12}C) and ^{12}C^{181}Ta collisions at 4.2 *A* GeV/*c*, ^{16}O*p* collisions at 3.25 *A* GeV/*c*, and in $\pi^{-\,12}$C interactions at 40 GeV/*c*. As observed from Table 3.3, the average decrease in the mass of the Δ^0(1232) resonances in these collisions (as compared to the mass of the free nucleon Δ^0(1232)) agrees well within the uncertainties with the average binding energy of the nucleons of the fragmenting nuclei. The largest fraction of the analyzed collisions was the peripheral and semi-central collision events. Therefore, if we assume that the Δ^0(1232) resonances are mainly produced on the bound nucleons at the collective excitations of the fragmenting nuclei, this suggests that the produced Δ^0(1232)'s should have masses smaller than the mass of a Δ^0(1232) resonance, produced in collisions of free nucleons, by approximately the binding energy of a nucleon.

In Ref. [40] we compared the properties and kinematical spectra of Δ^0(1232) resonances produced in *p*C and *d*C collisions at 4.2 *A* GeV/*c*. In Fig. 3.6 the reconstructed transverse momentum distributions of all π^--mesons and π^--mesons coming from Δ^0(1232) decay in d^{12}C and p^{12}C collisions at 4.2 *A* GeV/*c* are presented [40].

As observed from Fig. 3.6, π^--mesons coming from Δ^0(1232) decay occupy mainly the low transverse momentum region (p_t < 0.6 GeV/*c*) and hense are responsible for the low p_t enhancement of π^- spectra in p^{12}C and d^{12}C collisions at 4.2 *A* GeV/*c*, which was also found earlier in Refs. [25, 26] for incident beam energies from 1 to 15 *A* GeV.

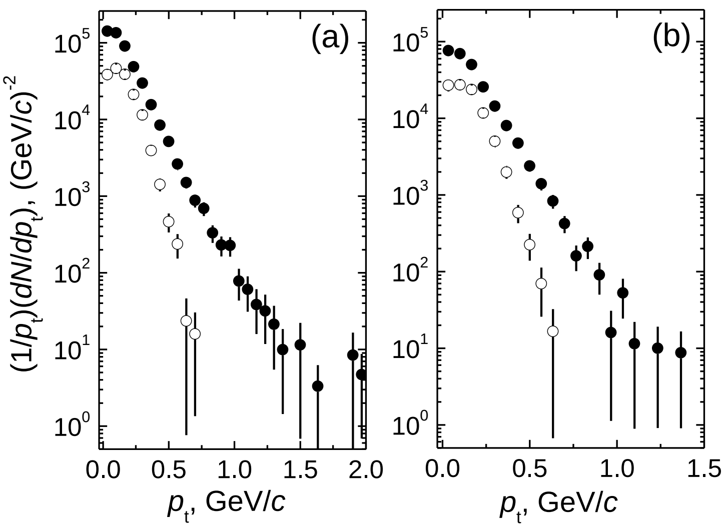

Fig. 3.6. The reconstructed transverse momentum (p_t) spectra of all π^--mesons (●) and π^--mesons coming from Δ^0(1232) decay (○) in d^{12}C (*a*) and p^{12}C (*b*) collisions at 4.2 *A* GeV/*c*

Comparative analysis of the reconstructed rapidity distributions of Δ^0(1232) in d^{12}C and p^{12}C collisions at 4.2 *A* GeV/*c* showed that in d^{12}C collisions a major fraction of Δ^0 is produced on carbon nuclei, while still significant number of Δ^0 resonances originate from the neutrons of the impinging deuterons [40].

In Ref. [37] we analyzed the reconstructed experimental transverse momentum (p_t) distributions of $\Delta^0(1232)$ resonances produced in p^{12}C and d^{12}C collisions at 4.2 *A* GeV/*c* and the corresponding spectra calculated using Modified FRITIOF model in the framework of Hagedorn Thermodynamic Model. The spectral temperatures of $\Delta^0(1232)$ resonances were obtained from fitting their p_t spectra with the one-temperature Hagedorn function. The spectral temperatures of $\Delta^0(1232)$ resonances proved to be compatible with the corresponding temperatures of π^- mesons produced in p^{12}C and d^{12}C collisions at 4.2 *A* GeV/*c*.

§ 3.3. Comparison with the heavy ion collisions

Comparison of the above mentioned fractions of π^--mesons coming from $\Delta^0(1232)$ decays in *p*, *d*(^{12}C) [39, 41, 42], ^{12}C^{12}C [27], α^{12}C [45, 47] and ^{12}C^{181}Ta collisions [44] at 4.2 *A* GeV/*c*, ^{16}O*p* collisions [43] at 3.25 *A* GeV/*c*, and in $\pi^{-\,12}$C interactions [46] at 40 GeV/*c* with those obtained in central heavy ion collisions is presented in Fig. 3.7. As observed from Fig. 3.7, the fraction of π^- coming from $\Delta^0(1232)$ decays on the whole decreases with the increase in the incident energy. As seen from Fig. 3.7, our results for $R(\Delta^0/\pi^-)$ in *p*, *d*(^{12}C), α^{12}C, and ^{12}C^{181}Ta collisions at 4.2 *A* GeV/*c* are compatible with each other and in line with the results of the other experiments with the different sets of colliding nuclei at various incident energies.

As observed from Fig. 3.7, around (40-50)% of the produced negative pions in p^{12}C, d^{12}C, ^{12}C^{12}C, α^{12}C and ^{12}C^{181}Ta collisions at 4.2 *A* GeV/*c*, and in ^{16}O*p* collisions at 3.25 *A* GeV/*c* come from decay of $\Delta^0(1232)$ resonances, whereas only about 6% of the negative pions in $\pi^{-\,12}$C interactions at 40 GeV/*c* originate from $\Delta^0(1232)$ decays. This is due to the fact that at such high energies as 40 GeV the production probability of other heavier resonances and ρ^0, ω^0, and f^0 mesons increases considerably compared to the incident energies of the order of several GeV/nucleon. Indeed, it was estimated in Ref. [146] that around 30% of the charged pions in π^{-12}C interactions at 40 GeV/c come from decays of ρ^0, ω^0, and f^0 mesons.

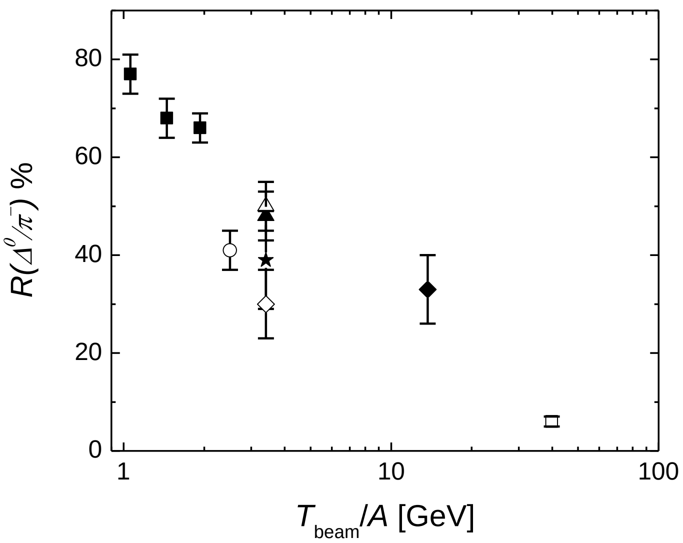

Fig. 3.7. Dependence of fraction of π^- mesons coming from Δ^0 decay on beam kinetic energy per nucleon obtained: (◊) − for d^{12}C collisions at 4.2 *A* GeV/*c* ($T_{\text{beam}} \approx 3.4$ *A* GeV); (★) − for p^{12}C collisions at 4.2 GeV/*c* ($T_{\text{beam}} \approx 3.4$ *A* GeV); (○) − for ^{16}O*p* collisions at 3.25 *A* GeV/*c* ($T_p \approx 2.5$ GeV in oxygen nucleus rest frame); (■) − for central NiNi collisions [91] at 1.06, 1.45, and 1.93 *A* GeV; (♦) – for central ^{28}SiPb collisions [25] at $p_{\text{lab}} = 14.6$ *A* GeV ($T_{\text{beam}} \approx 13.7$ *A* GeV); (▲) and (Δ) – for ^{4}He^{12}C and ^{12}C^{12}C collisions respectively at 4.2 *A* GeV/*c* ($T_{\text{beam}} \approx 3.4$ *A* GeV); (□) – for π^{-12}C collisions at 40 GeV/*c* ($T_{\text{beam}} \approx 39.9$ GeV)

Comparison of our results for the estimated relative number of the nucleons excited to Δ^0 resonances at freeze-out with the results obtained in other works for different sets of colliding nuclei at various incident energies is presented in Fig. 3.8. The estimated relative numbers of nucleons excited to Δ^0 resonances extracted by us for nuclear collisions at 4.2 *A* GeV/*c* are compatible, as observed from Fig. 3.8, with the results of the Refs. [25, 38, 41, 45, 91].

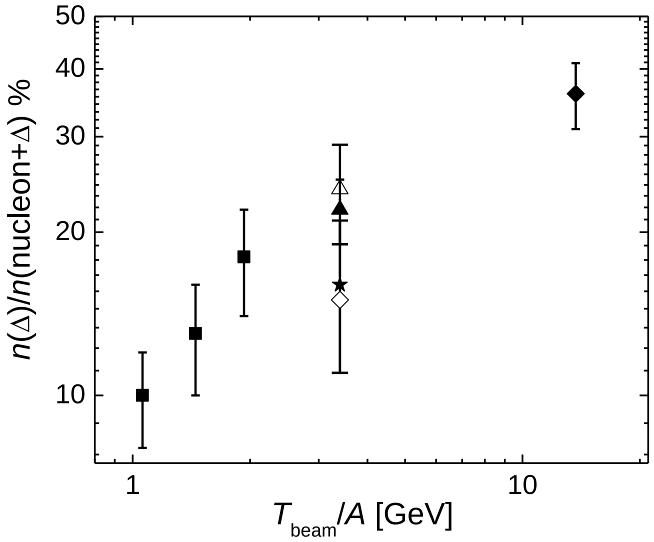

Fig. 3.8. The relative number of nucleons excited to Δ^0 at freeze-out as a function of beam energy obtained: (◊) − for d^{12}C collisions at 4.2 *A* GeV/*c* ($T_{\text{beam}} \approx 3.4$ *A* GeV); (★) − for p^{12}C collisions at 4.2 GeV/*c* ($T_{\text{beam}} \approx 3.4$ *A* GeV); (■) − by FOPI collaboration for central NiNi collisions; (♦) – in E814 experiment for central ^{28}SiPb collisions at $p_{\text{lab}} = 14.6$ *A* GeV/*c*; (▲) and (Δ) – for ^{4}He^{12}C and ^{12}C^{12}C collisions respectively at 4.2 *A* GeV/*c*

In Ref. [91] the freeze-out temperatures of Δ(1232) resonances, produced in NiNi collisions at beam kinetic energies between 1 and 2 *A* GeV, were calculated within the context of hadrochemical equilibrium model [151, 152] using the obtained fractions, $n(\Delta)/n(\text{nucleon}+\Delta)$, of the nucleons excited to Δ(1232). The freeze-out temperatures of Δ(1232), produced in Ni+Ni collisions at 1-2 *A* GeV and Au+Au collisions at 1.06 *A* GeV, were estimated in Refs. [99, 100] from the radial flow analysis. In Ref. [25] the pion enhancement at low transverse momentum was used to estimate the Δ(1232) abundance in central ^{28}Si+Al, Pb collisions at $p_{\text{lab}} = 14.6$ GeV/*c* per nucleon ($T_{\text{beam}} \approx 13.7$ *A* GeV). Then the freeze-out temperature of the system was calculated using the measured Δ(1232) abundance. It was obtained [25] that in central ^{28}Si+Pb collisions at 14.6 *A* GeV/*c* a fireball is created with the significant excitation of the delta baryons, which freezes-out at $T_0 = 138\,^{+23}_{-18}$ MeV. All the above freeze-out temperatures obtained in central heavy ion collisions along with the values of T_0 for $\Delta^0(1232)$ resonances produced in d^{12}C and p^{12}C collisions at 4.2 *A* GeV/*c* ($T_{beam} \approx 3.4$ *A* GeV) are demonstrated in Fig. 3.9. As observed from Fig. 3.9, the freeze-out temperatures of $\Delta(1232)$ resonces produced in central heavy ion collisions increase with the increase in the beam energy.

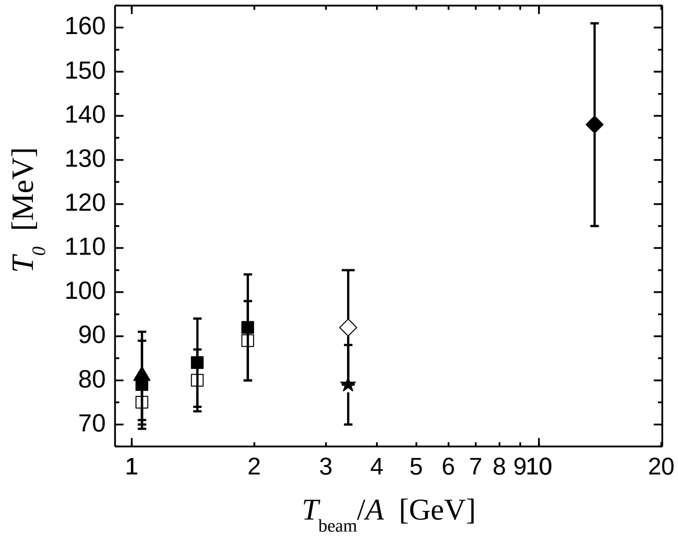

Fig. 3.9. Dependence of T_0 on beam kinetic energy per nucleon: (◊) − obtained for d^{12}C collisions at 4.2 *A* GeV/*c* ($T_{beam} \approx 3.4$ *A* GeV); (★) − obtained for p^{12}C collisions at 4.2 GeV/*c* ($T_{beam} \approx 3.4$ *A* GeV); T_0 obtained from the radial flow analysis (■) and using the hadrochemical equilibrium model (□) for Δ resonances produced in NiNi collisions; (▲) – T_0 obtained from the radial flow analysis for Δ^0 resonances produced in AuAu collisions at 1.06 *A* GeV; (♦) – T_0 obtained for Δ resonances produced in central ^{28}SiPb collisions at p_{lab} = 14.6 *A* GeV/*c*

However the freeze-out temperatures estimated for d^{12}C and p^{12}C collisions do not follow this increasing behavior with the increase in the beam energy, observed in central heavy-ion collisions. This is most probably due to the mainly peripheral character of the collisions of protons and deuterons with the light carbon nuclei and the smallness of the interacting p^{12}C and d^{12}C systems.

§ 3.4. Summary and Conclusions on CHAPTER III

For the first time, the mass distributions of $\Delta^0(1232)$ resonances were reconstructed in p^{12}C, d^{12}C, ^{4}He^{12}C, ^{12}C^{181}Ta collisions at 4.2 *A* GeV/*c*, ^{16}O*p* collisions at 3.25 *A* GeV/*c*, π^{-12}C interactions at 40 GeV/*c* from the experimental and background invariant mass distributions of $p\pi^-$ pairs, using the method of analysis of the angles between outgoing π^- mesons and protons. The masses and widths of the $\Delta^0(1232)$ resonances in the above collisions were extracted from fitting $\Delta^0(1232)$ mass distributions by the relativistic Breit-Wigner function. The fractions of π^--mesons (relative to their total number) coming from $\Delta^0(1232)$ decay as well as the relative number of nucleons excited to Δ^0 at freeze-out were estimated for the above collisions.

It was estimated that around (40-50)% of the produced negative pions in p^{12}C, d^{12}C, α^{12}C and ^{12}C^{181}Ta collisions at 4.2 *A* GeV/*c*, and in ^{16}O*p* collisions at 3.25 *A* GeV/*c* come from decay of $\Delta^0(1232)$ resonances, whereas only about 6% of the negative pions in π^{-12}C interactions at 40 GeV/*c* originate from $\Delta^0(1232)$ decays. This is due to the fact that at such high energies as 40 GeV the production probability of other heavier resonances and ρ^0, ω^0, and f^0 mesons increases considerably compared to the incident energies of the order of several GeV/nucleon.

The average decrease in the mass of the $\Delta^0(1232)$ resonances in the analyzed collisions agreed within the uncertainties with the average binding energy of the nucleons of the fragmenting nuclei, suggesting that the $\Delta^0(1232)$ resonances are mainly produced on the bound nucleons at the collective excitations of the fragmenting nuclei.

IV. RAPIDITY DISTRIBUTIONS OF NEGATIVE PIONS IN *AA* COLLISIONS AT 4.2 *A* GeV/*c*

§ 4.1. Rapidity distributions of negative pions in d^{12}C, ^{12}C^{12}C, and ^{12}C^{181}Ta collisions

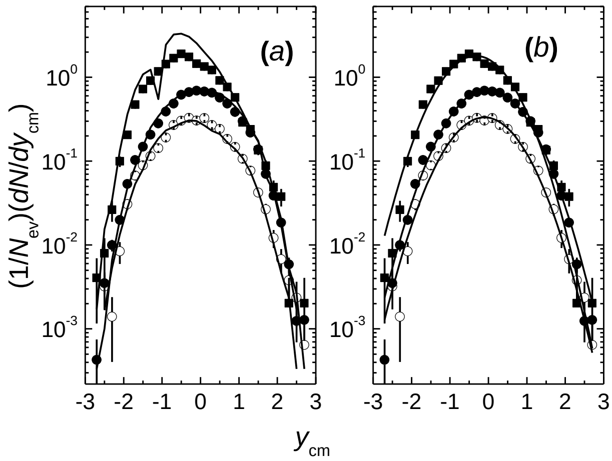

Fig. 4.1. The experimental rapidity distributions of negative pions in d^{12}C (○), ^{12}C^{12}C (●), and ^{12}C^{181}Ta (■) collisions at 4.2 *A* GeV/*c*. The corresponding QGSM spectra (a) and fits by Gaussian function (b) are given by the solid lines. All the spectra are obtained in cms of nucleon–nucleon collisions at 4.2 GeV/*c*. The distributions are normalized per one inelastic collision event

We aim to study the dependences of experimental rapidity distributions of negative pions, produced in d^{12}C, ^{12}C^{12}C, and ^{12}C^{181}Ta collisions at a momentum of 4.2 GeV/*c* per nucleon, as well as the dependences of average transverse momenta of negative pions on their rapidity, on the mass numbers of projectile and target nuclei and the degree of collision centrality [35]. All the experimental results will be systematically compared with the corresponding results extracted using Quark-Gluon-String Model (QGSM) [132–133]. This analysis is important for extracting the valuable information on degree of stopping power of target nuclei and its dependence on the masses of projectile and target nuclei as well as the collision centrality. The experimental results obtained might be useful to help interpret the relevant data on high energy heavy ion collisions.

Comparison of the experimental and QGSM rapidity distributions of negative pions in $d+^{12}C$, $^{12}C+^{12}C$, and $^{12}C+^{181}Ta$ collisions at a momentum of 4.2 GeV/*c* per nucleon is shown in Fig. 4.1*a*. All the spectra in Fig. 4.1 and the figures that follow are obtained in cms of nucleon–nucleon collisions at 4.2 GeV/*c* ($y_{cms} \approx$ 1.1 at this incident momentum). Rapidity distribution of negative pions in $^{12}C+^{12}C$ collisions is symmetric with respect to midrapidity y_{cm}=0 as expected for a system with identical projectile and target nuclei. As seen from Fig. 4.1*a*, the QGSM describes satisfactorily the experimental rapidity distributions of π^- mesons in $d+^{12}C$, $^{12}C+^{12}C$, and $^{12}C+^{181}Ta$ collisions. The mean kinematical characteristics of negative pions and participant protons in $d+^{12}C$, $^{12}C+^{12}C$, and $^{12}C+^{181}Ta$ collisions at 4.2 GeV/*c* per nucleon are given in Table 4.1.

Table 4.1

Mean multiplicities per event of negative pions and participant protons and the average values of rapidity and transverse momentum of π^- mesons in $d^{12}C$, $^{12}C^{12}C$, and $^{12}C^{181}Ta$ collisions at 4.2 GeV/*c* per nucleon. The mean rapidities are calculated in cms of nucleon–nucleon collisions at 4.2 GeV/*c*

Type		$\langle n(\pi^-)\rangle$	$\langle n_{part.prot.}\rangle$	$\langle y_{cms}\rangle$	$\langle p_t(\pi^-)\rangle$, GeV/*c*
$d+^{12}C$	Exper.	0.66±0.01	1.95±0.02	–0.12±0.01	0.252±0.003
	QGSM	0.64±0.01	1.86±0.01	–0.17±0.01	0.222±0.002
$^{12}C+^{12}C$	Exper	1.45±0.01	4.35±0.02	–0.016±0.005	0.242±0.001
	QGSM	1.59±0.01	4.00±0.02	0.007±0.005	0.219±0.001
$^{12}C+^{181}Ta$	Exper	3.50±0.10	13.3±0.2	–0.34±0.01	0.217±0.002
	QGSM	5.16±0.09	14.4±0.2	–0.38±0.01	0.191±0.001

§ 4.2. Centrality and *A* dependencies of rapidity spectra of negative pions in *AA* collisions at 4.2 *A* GeV/*c*

Figure 4.1*b* shows that the experimental rapidity spectra of negative pions in the analyzed collisions can be fitted well by Gaussian distribution function given by

$$F(y) = \frac{A_0}{\sigma} \exp\left(\frac{-(y - y_0)^2}{2\,\sigma^2} \right), \qquad (4.1)$$

where σ is the standard deviation, referred to as a width of distribution in the present work, y_0 – the centre of Gaussian distribution, and A_0 is the fitting constant.

Table 4.2

Parameters extracted from fitting the rapidity spectra of negative pions in $d^{12}C$, $^{12}C^{12}C$, and $^{12}C^{181}Ta$ collisions at 4.2 GeV/*c* per nucleon by Gaussian function

.

Type		A_0	σ	y_0	$\chi^2/$n.d.f.	R^2 value
$d+^{12}C$	Exper.	0.260±0.004	0.78±0.01	–0.10±0.01	2.88	0.983
	QGSM	0.250±0.003	0.80±0.01	–0.17±0.01	5.13	0.986
$^{12}C+^{12}C$	Exper	0.575±0.004	0.793±0.003	–0.016±0.005	8.93	0.992
	QGSM	0.624±0.004	0.786±0.003	0.009±0.005	14.21	0.983
$^{12}C+^{181}Ta$	Exper	1.36±0.02	0.75±0.01	–0.33±0.01	7.66	0.971
	QGSM	1.78±0.02	0.71±0.01	–0.30±0.01	53.43	0.878

Parameters extracted from fitting the rapidity spectra of negative pions in $d+^{12}C$, $^{12}C+^{12}C$, and $^{12}C+^{181}Ta$ collisions at 4.2 GeV/*c* per nucleon by Gaussian function in Eq. (4.1) are presented in Table 4.2. R^2 factor in Table 4.2 is given by relation $R^2 = 1 - \frac{SS_E}{SS_T}$, where $SS_E = \sum_{i=1}^{n} (y_i^{\exp} - y_i^{fit})^2$ is the sum of the squared errors,

$SS_T = \sum_{i=1}^{n} (y_i^{\exp} - \bar{y})^2$ is the total sum of squares, $y_i^{\exp}$ and y_i^{fit} are the original (experimental) and fit (model) data, respectively, and $\bar{y} = \frac{1}{n}\sum_{i=1}^{n} y_i^{\exp}$ is the mean value of the experimental data. As the deviation between the experimental and fit data gets smaller, R^2 factor approaches to 1. Hence, the closer R^2 factor value to 1, the better is the fit quality.

As seen from Table 4.2, the widths of rapidity distributions of π^- mesons practically coincided in d+^{12}C and ^{12}C+^{12}C collisions, whereas σ was slightly lower in case of ^{12}C+^{181}Ta collisions both in the experiment and QGSM. The widths of experimental rapidity spectra of negative pions ($\sigma^{\text{C+C}} = 0.793 \pm 0.003$ and $\sigma^{\text{C+Ta}} = 0.75 \pm 0.01$) extracted in the present analysis proved to be slightly lower than the corresponding widths ($\sigma^{\text{C+C}} \approx 0.82$ and $\sigma^{\text{C+Ta}} \approx 0.79$) estimated in Ref. [65] for ^{12}C+^{12}C and ^{12}C+^{181}Ta collision events at 4.2 GeV/c on a total experimental statistics which was less than half of the corresponding statistics used in the present work. It is evident from Table 4.2 that the locations of centers y_0 extracted from fitting the rapidity spectra of π^- mesons by Gaussian function proved to be equal within uncertainties to the corresponding mean rapidities of negative pions in the analyzed collisions given in Table 4.1. As follows from Table 4.2, the QGSM describes satisfactorily the widths as well as the locations of y_0 of rapidity distributions of negative pions in d+^{12}C, ^{12}C+^{12}C, and ^{12}C+^{181}Ta collisions at 4.2 GeV/c per nucleon.

It is of interest to analyze quantitatively the change of shape of rapidity spectra of negative pions with increase in the collision centrality, which corresponds to decrease in impact parameter of collision. We followed the method, described in subchapter 2.4 of the present dissertation, to select the central and peripheral collision events.

Table 4.3

Fractions of central and peripheral $d^{12}C$, $^{12}C^{12}C$, and $^{12}C^{181}Ta$ collisions at 4.2 GeV/*c* per nucleon relative to the total inelastic cross section (σ_{in})

Type	Central collisions, %		Peripheral collisions, %	
	Experiment	QGSM	Experiment	QGSM
$d+^{12}C$	10±1	12±1	53±1	73±1
$^{12}C+^{12}C$	11±1	8±1	58±1	62±1
$^{12}C+^{181}Ta$	16±1	15±1	60±2	56±1

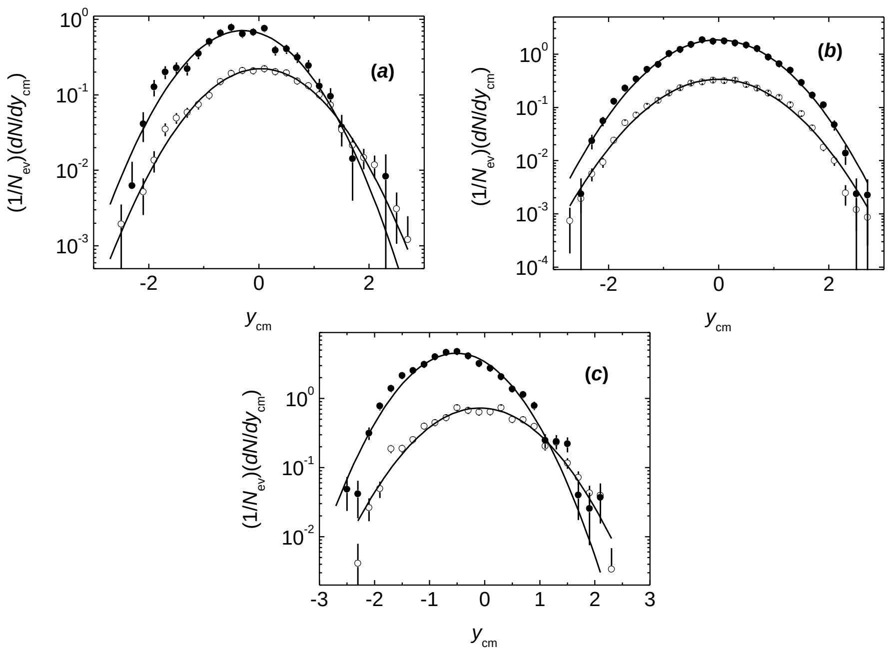

Fig. 4.2. The experimental rapidity distributions of negative pions in central (●) and peripheral (○) collision events in $d^{12}C$ (a), $^{12}C^{12}C$ (b), and $^{12}C^{181}Ta$ (c) collisions at 4.2 *A* GeV/*c*. The corresponding fits by Gaussian function are given by the solid lines. All the spectra are obtained in cms of nucleon–nucleon collisions at 4.2 GeV/*c*

Table 4.4

Parameters obtained from fitting the rapidity spectra of negative pions in central and peripheral d^{12}C, ^{12}C^{12}C, and ^{12}C^{181}Ta collisions at 4.2 GeV/*c* per nucleon by Gaussian function

Type		A_0	σ	y_0	χ^2/n.d.f.	R^2 value
d+^{12}C Central	Exper.	0.52±0.02	0.74±0.02	–0.29±0.03	1.26	0.959
	QGSM	0.55±0.01	0.77±0.01	–0.32±0.02	1.99	0.980
d+^{12}C Peripheral	Exper	0.178±0.004	0.80±0.01	0.03±0.02	0.86	0.986
	QGSM	0.176±0.003	0.80±0.01	–0.10±0.01	2.79	0.985
^{12}C+^{12}C Central	Exper	1.44±0.02	0.774±0.006	–0.021±0.009	2.52	0.990
	QGSM	1.63±0.02	0.794±0.006	0.009±0.009	2.97	0.989
^{12}C+^{12}C Peripheral	Exper.	0.274±0.003	0.813±0.006	–0.008±0.009	2.76	0.991
	QGSM	0.289±0.004	0.797±0.006	–0.006±0.009	7.32	0.972
^{12}C+^{181}Ta Central	Exper	3.10±0.07	0.68±0.01	–0.52±0.01	3.63	0.958
	QGSM	4.02±0.09	0.66±0.01	–0.48±0.01	21.06	0.837
^{12}C+^{181}Ta Peripheral	Exper	0.59±0.01	0.81±0.01	–0.08±0.02	2.82	0.967
	QGSM	0.70±0.01	0.78±0.01	–0.09±0.02	7.19	0.937

Fractions of central and peripheral d+^{12}C, ^{12}C+^{12}C, and ^{12}C+^{181}Ta collision events, relative to the total inelastic cross section (σ_{in}), obtained in the present work for both the experimental and QGSM data are presented in Table 4.3.

In Figs. 4.2 and 4.3, the rapidity distributions of negative pions are compared for central and peripheral d+^{12}C, ^{12}C+^{12}C, and ^{12}C+^{181}Ta collision events in the experiment and QGSM, respectively. All the spectra of Figs. 4.2 and 4.3 are fitted by Gaussian function given in Eq. (4.1). The corresponding parameters extracted from fitting the experimental and QGSM spectra for central and peripheral collisions are given in Table 4.4. In general, as can be seen from Figs. 4.2 and 4.3 and Table 4.4, all the spectra are fitted satisfactorily by Gaussian function. However, as can be seen from $\chi^2/\text{n.d.f.}$ and R^2 values in Table 4.4, the experimental rapidity spectra are fitted significantly better by Gaussian function as compared to the QGSM spectra. As follows from Table 4.4, the widths of the experimental rapidity spectra of negative pions decrease by $(8\pm2)\%$, $(5\pm1)\%$, and $(15\pm2)\%$ in going from peripheral to central d+^{12}C, ^{12}C+^{12}C, and ^{12}C+^{181}Ta collisions, respectively. Similar decrease in the estimated widths of rapidity spectra of negative pions was observed in Ref. [65] in going from peripheral to central ^{12}C+^{12}C and ^{12}C+^{181}Ta collisions at 4.2 *A* GeV/*c*. The widths estimated for peripheral and central ^{12}C+^{12}C and ^{12}C+^{181}Ta collisions ($\sigma^{\mathrm{C+C}}_{\mathrm{periph}} \approx 0.85$ and $\sigma^{\mathrm{C+C}}_{\mathrm{centr}} \approx 0.78$, $\sigma^{\mathrm{C+Ta}}_{\mathrm{periph}} \approx 0.87$ and $\sigma^{\mathrm{C+Ta}}_{\mathrm{centr}} \approx 0.74$) in Ref. [65] proved to be slightly larger as compared to the corresponding widths of the experimental rapidity spectra shown in Table 4.4. The values of σ obtained in the present analysis agree with the results of the Ref. [158], where the width of pseudorapidity distribution for shower particles changed from 0.74 for most central to 0.94 for most peripheral collisions.

As can be seen from Figs. 4.2*a* and 4.2*c* and Table 4.4, the centers y_0 of rapidity distributions of π^- mesons shift by –0.32±0.04 and –0.44±0.02 units towards target fragmentation region while going from peripheral to central *d*+^{12}C and ^{12}C+^{181}Ta collisions, respectively. In case of corresponding QGSM spectra, as seen from Figs. 4.3*a* and 4.3*c* and Table 4.4, the centers y_0 of rapidity distributions of negative pions also shift by –0.22±0.02 and –0.39±0.02 units towards target fragmentation region in *d*+^{12}C and ^{12}C+^{181}Ta, collisions respectively. Such shifts of centers y_0 of rapidity spectra of π^- mesons in *d*+^{12}C and ^{12}C+^{181}Ta collisions are caused by increase in rescattering effects in target nuclei, which are heavier than projectile nuclei, and a subsequent increase in the number of the target participant nucleons (and hence increase in the number of pions produced in target fragmentation region) as the collision centrality increases.

We observe larger shift in case of ^{12}C+^{181}Ta collisions as compared to *d*+^{12}C collisions which is likely due to that $\frac{A(^{181}\mathrm{Ta})}{A(^{12}\mathrm{C})} > \frac{A(^{12}\mathrm{C})}{A(^{2}\mathrm{H})}$. As seen from Figs. 4.2*b* and 4.3*b* and Table 4.4, we do not observe such shift with increasing centrality in case of rapidity spectra of negative pions in ^{12}C+^{12}C collisions in both the experiment and QGSM. This is most likely due to symmetry of the colliding ^{12}C+^{12}C system, in which the effective numbers of participant nucleons from target and projectile

^{12}C nuclei (and hence the numbers of pions produced in target and projectile fragmentation regions) remain practically the same in both central and peripheral collisions. Therefore the rapidity distribution of negative pions in ^{12}C+^{12}C collisions remains symmetric around $y_{\mathrm{cm}} = 0$ with increasing collision centrality.

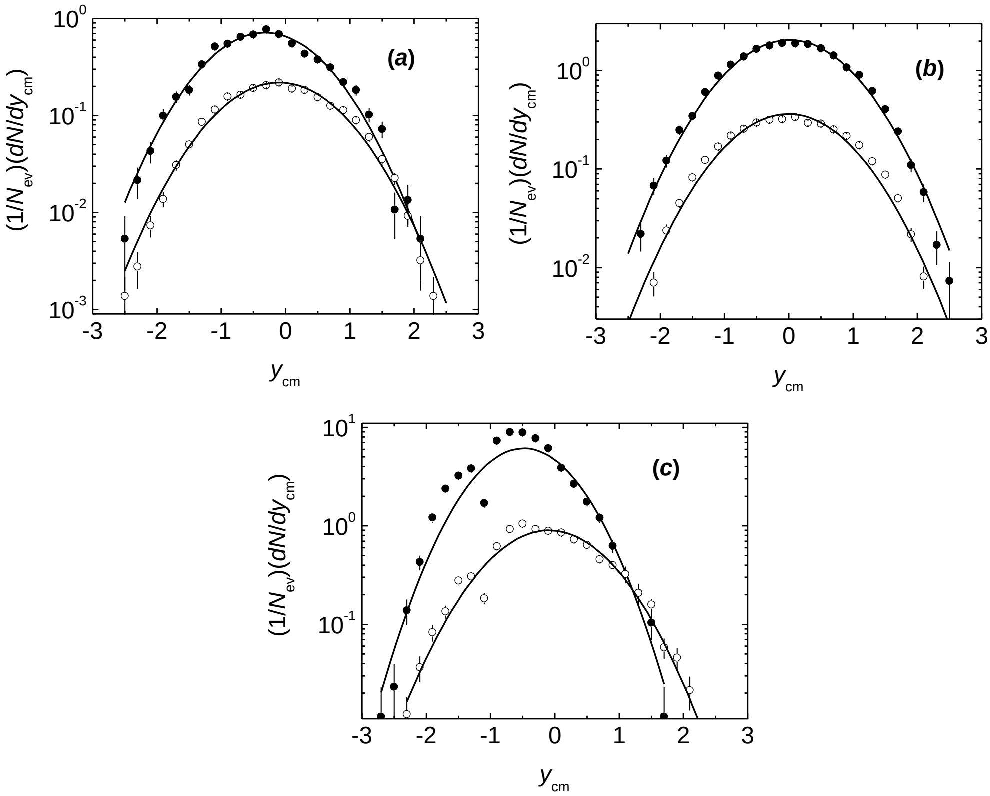

Fig. 4.3. Rapidity distributions of negative pions calculated using QGSM in central (●) and peripheral (○) collision events in d^{12}C (a), ^{12}C^{12}C (b), and ^{12}C^{181}Ta (c) collisions at 4.2 *A* GeV/*c*. The corresponding fits by Gaussian function are given by the solid lines. All the spectra are obtained in cms of nucleon–nucleon collisions at 4.2 GeV/*c*

As observed from Figs. 4.2 and 4.3 and Table 4.4, the peaks and centers y_0 of rapidity spectra of π^- mesons in peripheral d+^{12}C and ^{12}C+^{181}Ta collisions proved to be close to $y_{\mathrm{cm}} = 0$. This can be due to the reason that in case of peripheral collisions the effective volumes of interacting regions in both the target and projectile nuclei (and thus the corresponding numbers of interacting nucleons) are close to each other.

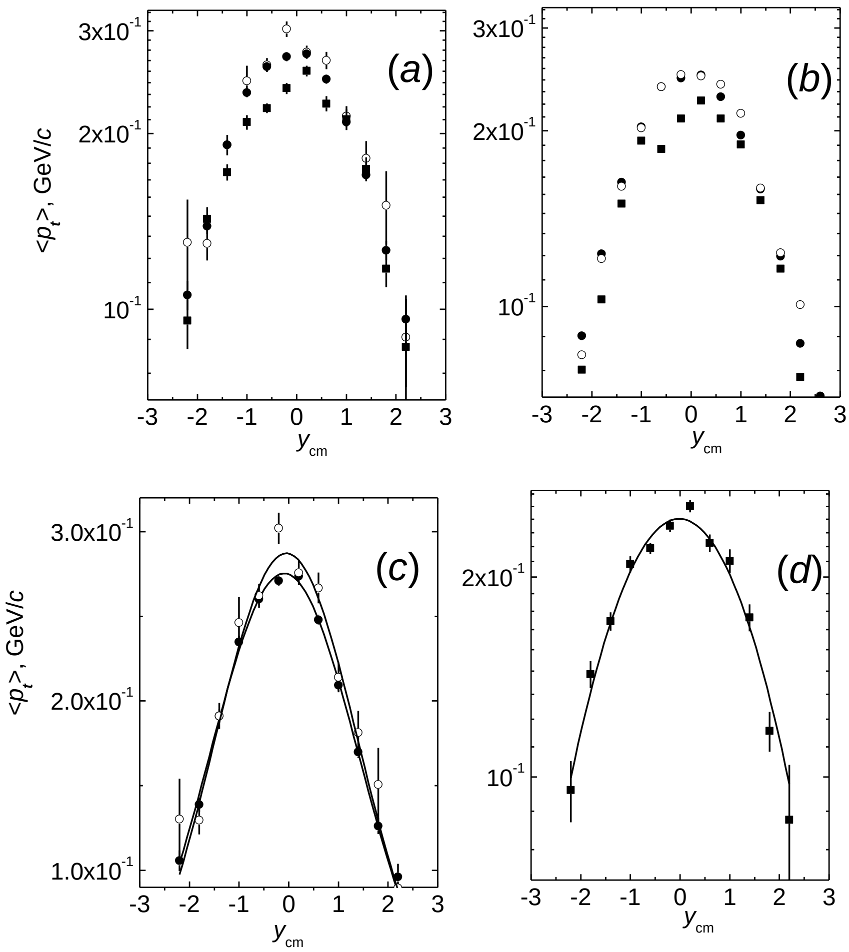

Fig. 4.4. (*a*) – The experimental <p_t> versus y_{cm} spectra of negative pions in d^{12}C (○), ^{12}C^{12}C (●), and ^{12}C^{181}Ta (■) collisions at 4.2 *A* GeV/*c*; (*b*) – The same as in (a) for QGSM spectra; (*c*) – The experimental <p_t> versus y_{cm} spectra of negative pions in d^{12}C (○) and ^{12}C^{12}C (●) collisions at 4.2 *A* GeV/*c* along with the corresponding fits (solid lines) by Gaussian function; (*d*) – The experimental <p_t> versus y_{cm} spectra of negative pions in ^{12}C^{181}Ta (■) collisions at 4.2 *A* GeV/*c* along with the corresponding fit (solid line) by Gaussian function. All the spectra are obtained in cms of nucleon–nucleon collisions at 4.2 GeV/*c*

Figure 4.4*a* shows the comparison of the dependencies of the experimental mean transverse momenta of negative pions on their nucleon–nucleon cms rapidities in d+^{12}C, ^{12}C+^{12}C, and ^{12}C+^{181}Ta collisions at 4.2 GeV/c per nucleon. It is obvious from Fig. 4.4*a* that high p_t π^- mesons are produced in central rapidity region, whereas projectile and target fragmentation regions are occupied by the low p_t negative pions. It can be seen from Fig. 4.4*a* that the height of peak of $<p_t>$ versus rapidity spectrum decreases with increase in projectile or target nucleus mass. As evident from Fig. 4.4*a*, the values of mean transverse momenta of π^- mesons are smaller in target fragmentation region $y_{\text{cm}} < 0$ in ^{12}C+^{181}Ta collisions as compared to d+^{12}C and ^{12}C+^{12}C collisions. This is obviously due to the reason that in case of ^{12}C+^{181}Ta collisions the projectile nucleons have to undergo more collisions (interactions) with more nucleons of heavy ^{181}Ta target as compared to d+^{12}C and ^{12}C+^{12}C collisions at the same incident momentum per nucleon. Therefore the energy transferred during collision is shared among the greater number of participant nucleons (and hence the larger number of produced pions) in ^{12}C+^{181}Ta collisions as compared to d+^{12}C and ^{12}C+^{12}C collisions.

The corresponding to Fig. 4.4*a* dependences calculated using QGSM are presented in Fig. 4.4*b*. As can be seen from Fig. 4.4*b*, the model spectra describe satisfactorily the behavior of the corresponding experimental spectra given in Fig. 4.4*a*.

Table 4.5

Parameters extracted from fitting the $<p_t>$ versus y_{cm} spectra of negative pions in d^{12}C, ^{12}C^{12}C, and ^{12}C^{181}Ta collisions at 4.2 GeV/*c* per nucleon by Gaussian function

Type		A_0	σ	y_0	$\chi^2/\text{n.d.f.}$	R^2 value
d+^{12}C	Exper.	0.42±0.01	1.46±0.04	–0.05±0.03	1.32	0.972
	QGSM	0.381±0.005	1.50±0.02	0.03±0.02	1.29	0.993
^{12}C+^{12}C	Exper	0.416±0.004	1.51±0.02	–0.09±0.01	1.05	0.996
	QGSM	0.376±0.003	1.50±0.02	–0.03±0.01	0.79	0.998
^{12}C+^{181}Ta	Exper	0.40±0.01	1.63±0.04	–0.01±0.03	2.09	0.967
	QGSM	0.354±0.006	1.64±0.03	0.08±0.02	10.63	0.937

Fig. 4.4*b* shows that the height of peak of the model spectrum as well as the values of $<p_t>$ in target fragmentation region $y_{\mathrm{cm}} < 0$ are smaller in case of $^{12}C+^{181}Ta$ collisions as compared to $d+^{12}C$ and $^{12}C+^{12}C$ collisions. The similar behavior was also observed for the experimental spectra illustrated in Fig. 4.4*a*.

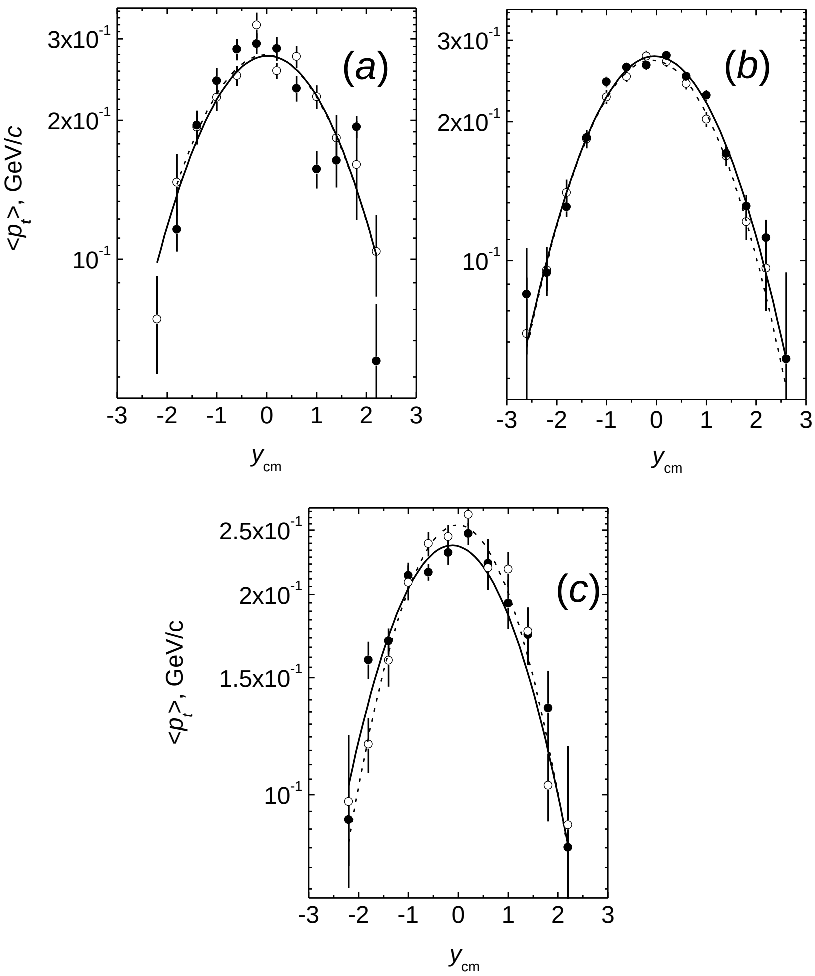

Fig. 4.5. The experimental $<p_t>$ versus y_{cm} spectra of negative pions in central (●) and peripheral (○) collision events in $d^{12}C$ (*a*), $^{12}C^{12}C$ (*b*), and $^{12}C^{181}Ta$ (*c*) collisions at 4.2 *A* GeV/*c*. The corresponding fits by Gaussian function for central and peripheral collisions are given by the solid and dashed lines respectively

The experimental $<p_t>$ versus y_{cm} spectra of negative pions in $d+^{12}C$, $^{12}C+^{12}C$, and $^{12}C+^{181}Ta$ collisions at 4.2 *A* GeV/*c* along with the corresponding fits by Gaussian function are presented in Figs. 4.4*c* and 4.4*d*. The corresponding parameters extracted from fitting the $<p_t>$ versus y_{cm} spectra of negative pions in d+^{12}C, ^{12}C+^{12}C, and ^{12}C+^{181}Ta collisions at 4.2 GeV/c per nucleon by Gaussian function are presented in Table 4.5. As can be seen from Figs. 4.4*c* and 4.4*d* and Table 4.5, all the spectra are fitted quite well by Gaussian function. The values of the widths so obtained, as seen from Table 4.5, are compatible with each other and with the corresponding QGSM results in the analyzed collisions. One can notice that the centers y_0 of $<p_t>$ versus y_{cm} spectra of negative pions in d+^{12}C, ^{12}C+^{12}C, and ^{12}C+^{181}Ta collisions are located very close to midrapidity $y_{cm} = 0$ and do not depend on the masses of target and projectile nuclei.

Table 4.6

Parameters extracted from fitting the $<p_t>$ versus y_{cm} spectra of negative pions in central and peripheral d^{12}C, ^{12}C^{12}C, and ^{12}C^{181}Ta collisions at 4.2 GeV/c per nucleon by Gaussian function

Type		A_0	σ	y_0	$\chi^2/$n.d.f.	R^2 value
d+^{12}C	Exper.	0.43±0.01	1.57±0.07	–0.02±0.05	8.02	0.705
Central	QGSM	0.376±0.009	1.46±0.04	–0.02±0.03	1.67	0.970
d+^{12}C	Exper	0.43±0.02	1.54±0.08	0.02±0.06	1.44	0.924
Peripheral	QGSM	0.377±0.006	1.49±0.03	0.04±0.02	0.95	0.991
^{12}C+^{12}C	Exper	0.42±0.01	1.52±0.03	–0.03±0.02	2.10	0.980
Central	QGSM	0.382±0.005	1.54±0.03	–0.04±0.02	1.19	0.990
^{12}C+^{12}C	Exper.	0.40±0.01	1.49±0.04	–0.08±0.03	0.34	0.993
Peripheral	QGSM	0.371±0.005	1.48±0.03	–0.02±0.02	0.97	0.992
^{12}C+^{181}Ta	Exper	0.38±0.01	1.61±0.04	–0.12±0.04	1.68	0.987
Central	QGSM	0.34±0.02	1.70±0.08	0.03±0.07	5.97	0.903
^{12}C+^{181}Ta	Exper	0.38±0.01	1.48±0.06	–0.01±0.04	1.19	0.955
Peripheral	QGSM	0.371±0.005	1.48±0.03	–0.02±0.02	0.97	0.992

Furthermore we analyzed the dependences of $<p_t>$ versus y_{cm} spectra of negative pions in the analyzed collisions on the collision centrality. The experimental $<p_t>$ versus y_{cm} spectra of negative pions in central and peripheral d+^{12}C, ^{12}C+^{12}C, and ^{12}C+^{181}Ta collisions at 4.2 A GeV/c along with the corresponding fits by Gaussian function are shown in Fig. 4.5. The corresponding parameters extracted from fitting the $<p_t>$ versus y_{cm} spectra of negative pions in central and peripheral $d+^{12}C$, $^{12}C+^{12}C$, and $^{12}C+^{181}Ta$ collisions by Gaussian function in the experiment and QGSM are displayed in Table 4.6. As can be seen from Fig. 4.5, all the spectra are described satisfactorily by Gaussian function. For all the collisions under consideration, as observed from Fig. 4.5, the corresponding spectra for central and peripheral collisions coincide within uncertainties. As seen from Table 4.6, the widths extracted for central and peripheral $d+^{12}C$, $^{12}C+^{12}C$, and $^{12}C+^{181}Ta$ collisions are compatible within uncertainties with each other and with the corresponding QGSM results. It is seen from Table 4.6 that the centers y_0 of $<p_t>$ versus y_{cm} spectra of negative pions in the analyzed central and peripheral collisions are located very close to $y_{cm} = 0$ and do not depend on the collision centrality.

§ 4.3. Rapidity distribution of negative pions in proton-proton collisions at 4.2 GeV/*c*

For sake of comparison, it is interesting to consider the rapidity as well as $<p_t>$ versus y_{cm} spectra of negative pions in nucleon–nucleon collisions at the same incident momentum per nucleon. Therefore we extracted 5023 proton–proton inelastic collision events from the experimental data base of collisions of protons at 4.2 GeV/*c* with C_3H_8 in 2-m propane bubble chamber of JINR (Dubna, Russia). The experimental rapidity as well as $<p_t>$ versus y_{cm} spectra of negative pions in proton–proton collisions at 4.2 GeV/*c* along with the corresponding model spectra and fits by Gaussian function are illustrated in Fig. 4.6. The corresponding parameters extracted from fitting the experimental rapidity and $<p_t>$ versus y_{cm} spectra of negative pions in proton–proton collisions at 4.2 GeV/*c* by Gaussian function are given in Table 4.7.

As seen from Fig. 4.6 and Table 4.7, the experimental rapidity distribution as well as $<p_t>$ versus y_{cm} spectrum of negative pions in proton–proton collisions are fitted well by Gaussian distribution function.

Table 4.7

Parameters extracted from fitting the experimental rapidity and $<p_t>$ versus y_{cm} spectra of negative pions in proton–proton collisions at 4.2 GeV/*c* by Gaussian function

Type	A_0	σ	y_0	$\chi^2/\text{n.d.f.}$	R^2 value
Rapidity spectrum	0.117±0.003	0.79±0.01	–0.12±0.02	1.18	0.989
$<p_t>$ versus y_{cm} spectrum	0.38±0.01	1.33±0.04	–0.13±0.03	1.38	0.966

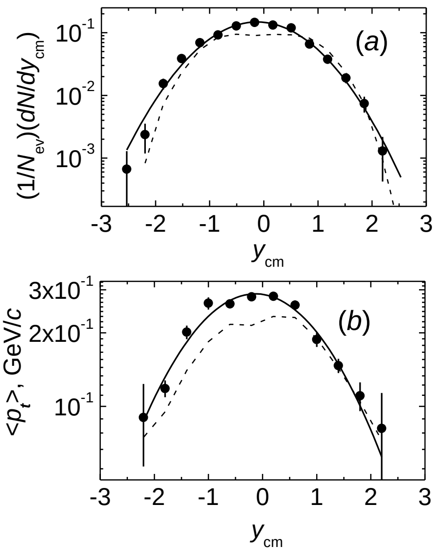

Fig. 4.6. (*a*) – The experimental rapidity distribution of negative pions in proton–proton collisions at 4.2 GeV/*c*; (*b*) – The experimental $<p_t>$ versus y_{cm} spectrum of negative pions in proton– proton collisions at 4.2 GeV/*c*; The model spectra and the fits of experimental spectra by Gaussian function are given by dashed and solid lines respectively. All the spectra are obtained in cms of nucleon–nucleon collisions at 4.2 GeV/*c*

The so obtained value of σ of the rapidity spectrum of π^- mesons in proton–proton collisions proved to be compatible within uncertainties with the corresponding widths of rapidity spectra of π^- in d+^{12}C, ^{12}C+^{12}C, and ^{12}C+^{181}Ta collisions given in Table 4.2.

As can be seen from Tables 4.5 and 4.7, the width of $\langle p_t \rangle$ versus $y_{\rm cm}$ spectrum of negative pions in proton–proton collisions is slightly lower as compared to the corresponding widths in d+^{12}C, ^{12}C+^{12}C, and ^{12}C+^{181}Ta collisions. The slightly larger width extracted in nucleus–nucleus collisions as compared to proton–proton collisions at the same incident momentum per nucleon could be due to the multiple scattering effects in the former collisions.

Table 4.8

The widths of the rapidity spectra of the negative pions and charged kaons in central Pb + Pb collisions at 20*A* and 30*A* GeV extracted from fitting with the Gaussian function by the NA49 Collaboration in Ref. [159]

Type	Central Pb+Pb collisions	
	20 *A* GeV	30 *A* GeV
π^-	0.837 ± 0.007	0.885 ± 0.007
K^+	0.601 ± 0.012	0.722 ± 0.026
K^-	0.642 ± 0.035	0.710 ± 0.032

In the end, it seems interesting to compare the widths of the rapidity spectra of the negative pions extracted in central nucleus–nucleus collisions at 4.2 *A* GeV/*c* with the corresponding widths of the rapidity spectra of the negative pions and charged kaons produced in central Pb + Pb collisions at 20 *A* and 30 *A* GeV, extracted recently in Ref. [159] by the NA49 Collaboration by using the fit with the Gaussian function. The widths of the rapidity spectra of the negative pions and charged kaons in central Pb + Pb collisions at 20 *A* and 30 *A* GeV are presented in Table 4.8.As seen from Tables 4.4 and 4.8, the widths of the rapidity spectra of the π– mesons in central d + ^{12}C, ^{12}C + ^{12}C, and ^{12}C + ^{181}Ta collisions at 4.2 *A* GeV/*c* are noticeably smaller as compared to the corresponding widths of the negative pions in central Pb + Pb collisions at 20 *A* and 30 *A* GeV. This observation agrees with a weak increase in width for $\pi-$ as incident energy increases from 20 *A* to 30 *A* GeV, as seen from Table 4.8. Due to the symmetry of the colliding systems, it seems appropriate to compare the widths extracted in central ^{12}C + ^{12}C collisions at 4.2*A* GeV/*c* with the corresponding widths obtained in central Pb + Pb collisions at 20 *A* and 30 *A* GeV. As observed from Tables 4.4 and 4.8, the width for $\pi-$ in central ^{12}C + ^{12}C collisions is slightly smaller than the corresponding widths for the negative pions in central Pb + Pb collisions, which, as stated above, agrees with a weak growth of the width with an increase in incident energy per nucleon. As seen from Table 4.8, the widths of the rapidity spectra of K^+ and K^- mesons also increase in central Pb + Pb collisions with an increase in incident energy from 20 *A* to 30 *A* GeV. It should be noted that the widths for π^- in both central ^{12}C + ^{12}C and Pb + Pb collisions proved to be noticeably larger than the corresponding widths of the rapidity spectra of K^+ and K^- mesons in central Pb + Pb collisions. This is likely due to the significantly higher-energy threshold for the production of charged kaons as compared to that for pions. Hence, the K^+ and K^- mesons generally are produced at harder collisions with larger momentum transfers as compared to negative pions. Therefore, charged kaons are grouped and are located closer to and around center-of-mass rapidity on the rapidity axis as compared to the negative pions, which results in significantly smaller widths of the rapidity spectra of kaons than that for pions.

§ 4.4. Phenomenological analysis of rapidity distributions of negative pions in ^{12}C^{12}C collisions

We will investigate various aspects of the simple phenomenological model, the Grand Combinational Model (GCM) [160–163], via using it for description of the cm rapidity distribution of the negative pions in ^{12}C+^{12}C collisions at 4.2*A* GeV/*c*. Following the expressions and ideas of Refs. [164–167] based on scaling properties of particle production, the GCM was developed and used [160–163] for the systematic description of the cm rapidity (pseudorapidity) distributions of various particles produced in central symmetric heavy ion collisions at high energies. We will fit the cm rapidity distributions of the negative pions, produced in minimum bias, central, and peripheral $^{12}C+^{12}C$ collisions at 4.2*A* GeV/*c* ($\sqrt{s_{nn}}$ = 3.14 GeV) by GCM. The GCM parameters extracted from fitting the cm rapidity distributions of the negative pions in central $^{12}C+^{12}C$ collisions at $\sqrt{s_{nn}}$ = 3.14 GeV will be compared with those obtained in Ref. [163] from approximation by GCM of the cm experimental rapidity (pseudorapidity) distributions of pions produced in central Pb+Pb collisions at SPS and AGS energies between $\sqrt{s_{nn}}$ = 6.3 GeV and $\sqrt{s_{nn}}$ = 12.3 GeV and in central Au+Au collisions at RHIC energies between $\sqrt{s_{nn}}$ = 19.6 GeV and $\sqrt{s_{nn}}$ = 200 GeV. Based on the analysis and comparison of our results with those obtained in high energy central heavy ion collisions, we aim to give a plausible physical interpretation of the GCM parameters lacking in Refs. [160–163]. The applicability of GCM for adequate description of the experimental data from $^{12}C+^{12}C$ collisions at intermediate energies will also be studied. For the sake of comparison, also the cm rapidity distributions of the negative pions, calculated using Modified FRITIOF model adapted to intermediate energies, in $^{12}C+^{12}C$ collisions at $\sqrt{s_{nn}}$ = 3.14 GeV will be analyzed using GCM.

For the purpose of comparison, we simulated 50 000 $^{12}C+^{12}C$ minimum bias inelastic collision events using Modified FRITIOF model adapted to intermediate energies. The model parameters used for simulation were the same as given in Ref. [157]. Modified FRITIOF model could describe quite satisfactorily many results obtained in hadron−nucleus and nucleus−nucleus collisions at JINR experiments at intermediate energies [38, 118, 156, 157].

Comparison of the mean multiplicities per event of the negative pions and participant protons and the average values of rapidity and transverse momentum of

π^- mesons in ^{12}C+^{12}C collisions at 4.2 A GeV/c in the experiment and Modified FRITIOF model is presented in Table 4.8.

A fairly satisfactory agreement between the experimental and model rapidity distributions of the negative pions, as well as their average characteristics given in Table 4.8, indicates a practical absence of systematic uncertainties in experimental measurements of π^- in ^{12}C+^{12}C collisions.

Table 4.8

Mean multiplicities per event of the negative pions and participant protons and the average values of rapidity and transverse momentum of π^- mesons [38] in minimum bias ^{12}C+^{12}C collisions at 4.2A GeV/c ($\sqrt{s_{nn}}$ = 3.14 GeV). The mean rapidities are calculated in cm of ^{12}C+^{12}C collisions. Only statistical errors are given here and in the tables that follow

Type	$<n(\pi^-)>$	$<n_{part.prot.}>$	$< y_{\text{c.m.}}(\pi^-)>$	$<p_t(\pi^-)>$, GeV/c
Experiment	1.45±0.01	4.35±0.02	–0.016±0.005	0.242±0.001
Mod. FRITIOF	1.42±0.01	3.96±0.01	–0.017±0.003	0.248±0.001

Table 4.9

Fractions of central and peripheral ^{12}C+^{12}C collision events at 4.2 A GeV/c ($\sqrt{s_{nn}}$ = 3.14 GeV), relative to the total inelastic cross section

Peripheral collisions (%)		Central collisions (%)	
Experiment	Mod.	Experiment	Mod.
58±1	62±1	11±1	12±1

We followed the method, described in subchapter 2.4 of the present dissertation, to select the central and peripheral collision events. The same criteria (as given above) were applied separately to the experimental data and Modified FRITIOF model data to determine the number of participant protons in each collision event and select the corresponding peripheral and central collision events in both the experiment and model. Fractions of the central and peripheral $^{12}C+^{12}C$ collision events, relative to the total inelastic cross section, obtained for both experimental and Modified FRITIOF model data are presented in Table 4.9. As observed from Table 4.9, central $^{12}C+^{12}C$ collision events, selected in the present work, corresponded to ~ (0–10)% centrality, and the peripheral ones corresponded to ~ (40–100)% centrality.

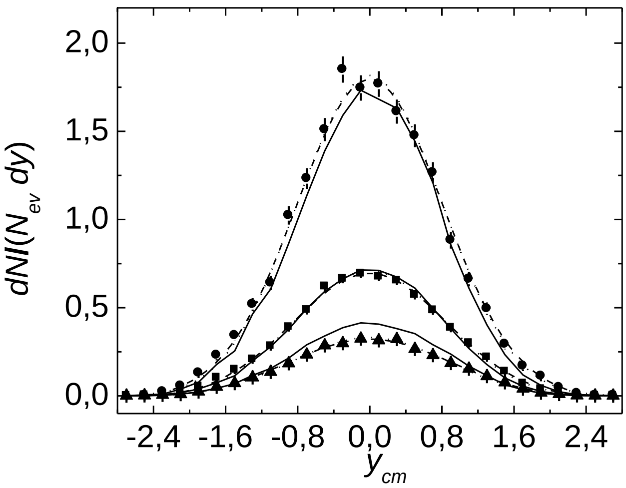

Fig. 4.7. The experimental cm rapidity distributions of the negative pions in central (●), peripheral (▲), and minimum bias (■) $^{12}C^{12}C$ collisions at $\sqrt{s_{nn}}$ = 3.14 GeV along with the modified FRITIOF calculations (solid curves), and fits by the function in (4) for the fixed parameters β = 0, Δ=0.55 (dotted curves) and for the fixed parameter β = 0 only (dashed curves). All the spectra are normalized per one inelastic collision event

In Ref. [164] a working expression was formulated for phenomenological description of the cm rapidity distributions of particles in proton–proton collisions at ISR (Intersecting Storage Rings) energy ranges, given by a three-parameter expression

$$\frac{1}{\sigma}\frac{d\sigma}{dy}=\frac{dN}{N_{ev}dy}=C\left(1+\exp\frac{|y|-y_0}{\Delta}\right)^{-1}, \tag{4.2}$$

where C is a fitting constant, y_0 and Δ are two parameters, dN is the number of particles in the rapidity interval dy, N_{ev} is the total number of inelastic collision events. The term on the left side of Eq. (4.2) represents the rapidity density of particles normalized per one inelastic collision event. The choice of the above form was made to describe conveniently the central plateau and the fall off in the fragmentation region using the parameters y_0 and Δ, respectively. This relation was introduced also to check the concept of both the limiting fragmentation [168] and the hypothesis of Feynman scaling [169]. For all the five cm energies of proton–proton collisions at ISR, between $\sqrt{s}$ = 23 GeV and 63 GeV, the values of Δ were extracted to be ~ 0.55 for pions [161] and kaons [160], ~ 0.35 for protons/antiprotons [160], and ~ 0.70 for Λ, Ξ, ϕ, Σ, and Ω. These values of Δ generally remained almost constant for the ISR cm energy range. Based on the fitting of the cm rapidity spectra of pions in proton–proton collisions at ISR energies, the energy dependence of the parameter y_0 was observed [161] for pions to follow the empirical relationship

$$y_0=0.55\ln\sqrt{s_{nn}}+0.88\,. \tag{4.3}$$

Following the ideas and expressions of Refs. [164–167] on scaling properties of particle production, it was proposed to express the cm rapidity distributions of the particles produced in nucleus–nucleus collisions through Eq. (4.2), using the description of the cm rapidity spectra in proton–proton collisions, as follows

$$\begin{aligned}\left.\frac{dN}{N_{ev}dy}\right|_{AB\to QX}&=C_1(AB)^{f(y)}\left.\frac{dN}{N_{ev}dy}\right|_{pp\to QX}=C_1(AB)^{\alpha+\beta y+\gamma y^2}\left.\frac{dN}{N_{ev}dy}\right|_{pp\to QX}\\&=C(AB)^{\beta y+\gamma y^2}\left(1+\exp\frac{|y|-y_0}{\Delta}\right)^{-1},\end{aligned} \tag{4.4}$$

where Q stands for the studied particle, X represents all the other products of the reaction. C_1 and $C = C_1(AB)^{\alpha}$ are the normalization constants, A and B are the mass numbers of the colliding nuclei, and α, β, and γ are the parameters to be extracted separately for each set of colliding nuclei A and B and cm energy. For the symmetric collisions with identical colliding nuclei (A = B), the final working formula is expressed by

$$\left.\frac{dN}{N_{ev}dy}\right|_{AA\to QX} = C(AA)^{\beta y+\gamma y^2}\left(1+\exp\frac{|y|-y_0}{\Delta}\right)^{-1}, \tag{4.5}$$

which is the final expression for the symmetric collision systems in GCM. The above multiplicative factor $(AA)^{\beta y+\gamma y^2}$ suggests that we could extract the physically meaningful parameters using expression (4) only for central collisions of identical nuclei, i.e. when practically all the nucleons of colliding nuclei participate in collision. The suggested choice of the function $f(y) = \alpha + \beta y + \gamma y^2$ in expressions (4.4) and (4.5) was not accidental. The clue for such an expression was taken from the studies on the behavior of EMC effect in lepton–nucleus collisions, given in Ref. [170]. Similar relationship was also used in Ref. [171] in a somewhat different context. The symmetric cm rapidity distributions of various particles produced in high energy collisions of identical heavy nuclei were analyzed using expression (4.5) in Refs. [162, 163]. Since the particles and collision systems analyzed in Refs. [162, 163] substantially overlap, we will compare our results with those of the final analysis, given in Ref. [163]. The coefficient β in expression (4.5) belongs to a term y, which is not symmetric under $y \to (-y)$ transformation. Based on symmetry of the collision system, resulting in symmetric rapidity distribution, the β = 0 was introduced [162, 163] for the fits of cm rapidity distributions of various particles, produced in high energy collisions of identical nuclei.

The parameters extracted from χ^2 fitting by the expression in (4.5) of the experimental and Modified FRITIOF model cm rapidity distributions of the negative pions in minimum bias, central, and peripheral $^{12}C+^{12}C$ collisions at $\sqrt{s_{nn}}$ = 3.14 GeV for the fixed β = 0 and Δ=0.55, and for the fixed β = 0 only are presented in Tables 4.10 and 4.11, respectively. The corresponding experimental and model cm rapidity distributions along with the two types of fits by the expression in Eq. (4.5) are shown in Fig. 4.7 and Fig. 4.8, respectively. It should be noted that the curves of these two types of fits mostly overlap in Figs. 4.7 and 4.8. As seen from Figs. 4.7 and 4.8, the experimental and model cm rapidity distributions of the negative pions are described quite satisfactorily by the function in (4.5). It is necessary to mention that all the χ^2 fits of the present work were conducted by including the statistical uncertainties.

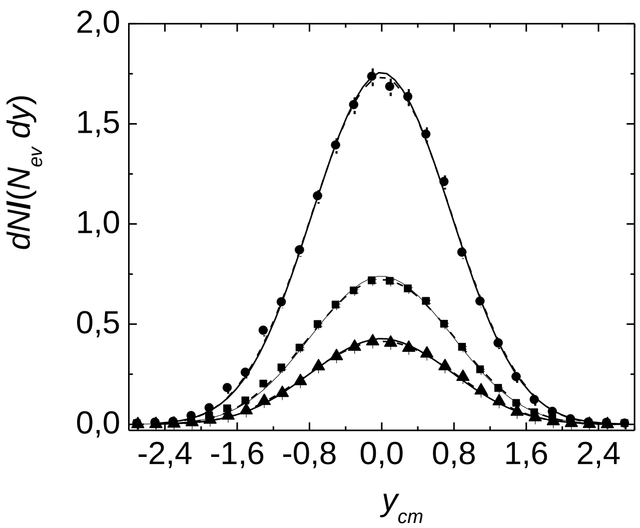

Fig. 4.8. The cm rapidity distributions of the negative pions, calculated using modified FRITIOF model, in central (●), peripheral (▲), and minimum bias (■) $^{12}C+^{12}C$ collisions at $\sqrt{s_{nn}}$ = 3.14 GeV along with the fits by the function in (4.5) for the fixed parameters β = 0, Δ=0.55 (solid curves), and for the fixed parameter β = 0 only (dashed curves). All the spectra are normalized per one inelastic collision event

The parameters extracted in Ref. [163] from χ^2 fitting by the expression in (4.5) of the cm experimental rapidity distributions of the negative pions in central Pb+Pb collisions at various SPS and AGS energies for the fixed β = 0 and Δ = 0.55 are presented in Table 4.12, for a comparison.

Table 4.10

Parameters of approximation by the expression in (4.5) of the cm rapidity distributions of the negative pions in minimum bias, central, and peripheral ^{12}C+^{12}C collisions at $\sqrt{s_{nn}}$ = 3.14 GeV (β = 0, Δ=0.55 are fixed)

Collision Type	Type	C	γ	y_0	$\chi^2/n.d.f.$	R^2
Minimum bias	Experiment	0.73±0.02	–0.13±0.03	2.06±0.71	5.58	0.99
	Mod. FRITIOF	0.76±0.02	–0.15±0.02	2.01±0.56	7.61	0.99
Central ~ (0–10)%	Experiment	1.86±0.08	–0.14±0.04	2.16±1.10	1.99	0.99
	Mod. FRITIOF	1.80±0.11	–0.15±0.05	2.02±1.15	1.97	0.99
Peripheral ~ (40–100)%	Experiment	0.34±0.03	–0.12±0.06	2.00±1.50	1.79	0.99
	Mod. FRITIOF	0.44±0.02	–0.14±0.04	2.00±0.91	3.97	0.99

Table 4.11

Parameters of approximation by the expression in (4.5) of the cm rapidity distributions of the negative pions in minimum bias, central, and peripheral ^{12}C+^{12}C collisions at $\sqrt{s_{nn}}$ = 3.14 GeV (β = 0 is fixed)

Collision Type	Type	C	γ	y_0	Δ	$\chi^2/n.d.f.$
Minimum bias	Experiment	0.69±0.01	–0.140±0.003	2.22±0.05	0.22±0.03	2.72
	Mod. FRITIOF	0.72±0.01	–0.152±0.005	2.08±0.08	0.33±0.04	4.70
Central ~ (0–10)%	Experiment	1.80±0.03	–0.155±0.004	2.33±0.05	0.11±0.04	1.12
	Mod. FRITIOF	1.73±0.02	–0.166±0.008	2.26±0.13	0.31±0.10	1.74
Peripheral ~ (40–100)%	Experiment	0.32±0.01	–0.127±0.008	2.10±0.11	0.26±0.06	0.94
	Mod. FRITIOF	0.41±0.01	–0.147±0.007	2.03±0.09	0.29±0.04	1.72

As seen from Tables 4.10 and 4.11, the values of the fitting constant C proved to be significantly larger in case of central $^{12}C+^{12}C$ collisions at $\sqrt{s_{nn}}$ = 3.14 GeV as compared to the peripheral ones both in the experiment and Modified FRITIOF model. Naturally, it reflected the physical fact that the mean multiplicity of the negative pions produced in central $^{12}C+^{12}C$ collisions was considerably greater compared to that in peripheral ones.

Table 4.12

Parameters extracted in Ref. [163] from approximation by the expression in (4.5) of the cm experimental rapidity distributions of the negative pions in central Pb+Pb collisions at various SPS and AGS energies ($\beta = 0$, $\Delta \approx 0.55$)

$\sqrt{s_{nn}}$ (GeV)	6.3	7.6	8.7	12.3
γ	–0.044±0.0003	–0.037±0.0003	–0.035±0.0003	–0.027±0.0002

Table 4.13

Mean multiplicities of the negative pions and their ratios along with the ratios of the extracted fitting constants C, given in Table 4.11, in central and peripheral $^{12}C+^{12}C$ collisions at $\sqrt{s_{nn}}$ = 3.14 GeV

$\langle n(\pi^-)\rangle_{central}$	Experiment	3.62±0.03
	M. FRITIOF	3.33±0.02
$\langle n(\pi^-)\rangle_{peripheral}$	Experiment	0.70±0.01
	M. FRITIOF	0.83±0.01
$\dfrac{\langle n(\pi^-)\rangle_{central}}{\langle n(\pi^-)\rangle_{peripheral}}$	Experiment	5.2±0.2
	M. FRITIOF	4.0±0.1
$\dfrac{C_{central}}{C_{peripheral}}$	Experiment	5.6±0.2
	M. FRITIOF	4.2±0.1

This is verified by the data of Table 4.13, which presents the mean multiplicities of the negative pions and their ratio along with the ratio of the extracted fitting constants *C*, given in Table 4.11, in the central and peripheral $^{12}C+^{12}C$ collisions at $\sqrt{s_{nn}}$ = 3.14 GeV. As seen from Table 4.13, the ratio of the fitting constants *C* in central and peripheral $^{12}C+^{12}C$ collisions is compatible, within the uncertainties, with the ratio of the mean multiplicities of the negative pions in central and peripheral collisions, both in the experiment and model. This suggests that parameter *C* in expression (4.5) fixes the multiplicity of the studied particles. Tables 4.10 and 4.11 show that the values of *C* are compatible with each other in the experiment and model, whereas the extracted values of the parameter γ are lower in the model compared to experiment. As observed from Tables 4.10 and 4.11, the values of γ were extracted to be consistently lower in central $^{12}C+^{12}C$ collisions as compared to the peripheral ones, both in the experiment and model. It is seen from comparison of Tables 4.10, 4.11 and Table 4.12 that the value of γ proved to be consistently lower (~ more than four times, on the average) in central $^{12}C+^{12}C$ collisions at $\sqrt{s_{nn}}$ = 3.14 GeV as compared to central Pb+Pb collisions at various SPS and AGS energies $\sqrt{s_{nn}}$ $\geq$ 6.3 GeV. This decreasing trend of γ with the decrease of $\sqrt{s_{nn}}$ can also be seen for central Pb+Pb collisions in Table 4.12. As noticed from Tables 4.10 and 4.11, the parameters y_0 (γ) and Δ show some correlation, i.e. y_0 (γ) decreases (increases) weakly with the increase of Δ. Let us recall that the parameters y_0 and Δ were introduced in expression (4.2) to describe conveniently the central plateau and the fall off in fragmentation region of cm rapidity distributions of produced particles in proton–proton collisions. Then, naturally, y_0 could be associated with the quantity related to a rapidity spread (width) (around central rapidity region) in rapidity units of particles originated from expansion and freeze-out of a fireball. It was observed [160, 161] for proton–proton collisions at ISR energies between $\sqrt{s}$ = 23 GeV and 63 GeV that the energy dependence of y_0 for pions, Λ, Ξ, Σ, ϕ, and Ω could be approximated empirically through the relation

$$y_0 = k \ln \sqrt{s_{nn}} + b, \tag{4.6}$$

where k was assumed to vary slowly with the cm energy, and b was a constant. Using empirical relation in (4.3), we obtained y_0 = 1.51 for pions produced in proton–proton collisions at $\sqrt{s_{nn}}$ = 3.14 GeV, which proved to be lower than y_0 values, extracted in the present analysis and given in Tables 4.10 and 4.11, for negative pions in central $^{12}C+^{12}C$ collisions. This result can be understood if we recall that the width of the rapidity distribution of the produced particles should be larger in nucleus–nucleus collisions as compared to that in proton–proton collisions at the same $\sqrt{s_{nn}}$.

At sufficiently high beam energies, the nuclear matter, highly compressed as a result of head-on collision of heavy ions, undergoes a phase transition to a deconfined hot matter, called fireball, or QGP (Quark Gluon Plasma), at energy density about 1 GeV/fm^3 and the temperature ~ 160 MeV [4, 6, 7]. This threshold energy density for deconfinement was shown to be reached already at $\sqrt{s_{nn}} \approx 5$ GeV from the lattice QCD calculations [6].

Obviously, the magnitude of spread around $y_{cm} = 0$ of the rapidities of particles, originated from expansion and freeze-out of a fireball produced in central heavy ion collisions, and so the size of central rapidity region, increases significantly as compared to central nucleus–nucleus collisions at lower energies ($\sqrt{s_{nn}}$ < 5 GeV). For proton–proton collisions at ISR energies, the width of the central plateau region of rapidity distributions of particles, as well as their densities in the central region, increased with increasing $\sqrt{s_{nn}}$ [164].

In Ref. [64], the widths of rapidity distributions of particles produced in nucleus–nucleus collisions at various cm energies, and as a function of centrality at SPS energies, were studied. The rapidity distributions for pions from $\sqrt{s_{nn}}$ = 2 to 200 GeV were fitted with the thermal model function, which took into account a longitudinal flow. It was found that the average longitudinal velocity $\langle \beta_L \rangle$ for pions increased with the cm energy, approaching a value of 1 at maximal RHIC energies from a value of 0.3 at AGS energies [64]. The width of rapidity distributions of particles in heavy ion collisions increased with increasing $\sqrt{s_{nn}}$. It was also observed that, at fixed $\sqrt{s_{nn}}$, the width of rapidity spectra in heavy ion collisions increased with the increase of impact parameter [64]. In Ref. [35], the widths of the cm rapidity distributions of the negative pions were extracted from fitting the pion spectra with a Gaussian given by

$$F(y) = \frac{A_0}{\sigma} \exp\left(\frac{-(y - y_0)^2}{2\,\sigma^2} \right), \tag{4.7}$$

where σ is the standard deviation, referred to as a width of distribution, y_0 – the centre of Gaussian distribution, and A_0 is the fitting constant. As shown in Ref. [35] and presented in Table 4.14, the increase of the width of rapidity distributions of the negative pions with increasing the collision impact parameter was observed also in ^{12}C+^{12}C collisions at $\sqrt{s_{nn}}$ = 3.14 GeV.

Table 4.14

Parameters extracted in Ref. [35] from fitting by Gaussian function, given in expression (4.7), of the experimental cm rapidity distributions of the negative pions in minimum bias, central, and peripheral ^{12}C+^{12}C collisions at $\sqrt{s_{nn}}$ = 3.14 GeV

Collision Type	A_0	σ	y_0	$\chi^2/n.d.f.$	R^2
Minimum bias	0.575±0.004	0.793±0.003	–0.016±0.005	8.93	0.99
Central ~ (0–10)%	1.44±0.02	0.774±0.006	–0.021±0.009	2.52	0.99
Peripheral ~ (40–100)%	0.274±0.003	0.813±0.006	–0.008±0.009	2.76	0.99

The collective flow of protons and negative pions was also observed experimentally in He+C, C+C, C+Ne, C+Cu, and C+Ta collisions at a momentum range of 4.2 A – 4.5 A GeV/c [172–174]. One can have a rough estimate for an average width (Δy_{centr}) of central rapidity region for pions coming from expansion and freeze-out of a compressed nuclear matter in central $^{12}C+^{12}C$ collisions at $\sqrt{s_{nn}}$ = 3.14 GeV. As the longitudinal component of the collective flow of the particles, in the case of central symmetric collisions, expands simultaneously with the same $\langle\beta_L\rangle$ to opposite longitudinal directions from the cm of collision system, the rough estimate for Δy_{centr} can be proposed as follows:

$$\Delta y_{centr} \approx 2\left(\frac{1}{2}\ln\frac{1+\langle\beta_L\rangle}{1-\langle\beta_L\rangle}\right). \tag{4.8}$$

Using the graph of the $\langle\beta_L\rangle$ versus $\sqrt{s_{nn}}$ dependence, given in Ref. [64], we obtained a rough estimate $\langle\beta_L\rangle \approx$ 0.4 at $\sqrt{s_{nn}}$ = 3.14 GeV. Substituting this value into expression (4.8), $\Delta y_{centr} \approx 0.85$ was obtained for the negative pions in $^{12}C+^{12}C$ collisions at $\sqrt{s_{nn}}$ = 3.14 GeV. Interestingly, this estimate of Δy_{centr} for the negative pions proved to be close to the width (σ) of rapidity distribution of π^- in central collisions extracted using Gaussian fits in Ref. [35], and shown in Table 4.14. On the other hand, the full width at half maximum (FWHM) of a Gaussian distribution given in (4.7) is approximately 2.35σ. Using the width (σ) extracted in Ref. [35] for central $^{12}C+^{12}C$ collisions (given in Table 4.14), FWHM ≈ 1.82 was obtained. This value of FWHM came out to be close to the values of y_0, extracted in the present analysis, as seen in Tables 4.10 and 4.11.

The parameter Δ in expression (4.5) could be ascribed to the quantity inversely proportional to the rate of fall off in the rapidity spectra in the fragmentation regions of the colliding nuclei. Indeed, by varying the Δ value and keeping all the other parameters fixed, it can easily be verified from expression

(4.5) that the normalized cm rapidity density decreases (the rate of fall off increases) with decreasing parameter Δ.

Let us revert to the discussion of the factor $(AA)^{f(y)}$ in expression (4.5). It can be assumed initially that, in symmetric central collisions with practically complete overlap of the two colliding identical nuclei, this factor accounts for the degree of involvement of all the constituent nucleons of the colliding nuclei in the creation of a compressed nucleonic matter, or highly excited nuclear matter, at lower energies ($\sqrt{s_{nn}}$ < 5 GeV) or production of a fireball (or QGP) at higher energies ($\sqrt{s_{nn}} > 5$ GeV). As $f(y) = \gamma y^2$ (β = 0) is assumed in symmetric central collisions of identical nuclei, such degree of involvement of the constituent nucleons of colliding nuclei in central nucleus–nucleus collisions would be determined by the parameter γ. As seen from Table 4.12, the value of γ for the negative pions increased quite prominently with the increase of $\sqrt{s_{nn}}$ from 6.3 to 12.3 GeV in central Pb+Pb collisions. As shown in Ref. [163], the value of γ for pions continued to increase with the cm energy even at higher RHIC energies in central Au+Au collisions between $\sqrt{s_{nn}}$ = 19.6 and 200 GeV, reaching the value γ = –0.00890 ± 0.00003 in central Au+Au collisions at $\sqrt{s_{nn}}$ = 200 GeV. The cm energy dependence of the parameter γ, extracted for pions in central $^{12}C+^{12}C$ collisions at $\sqrt{s_{nn}}$ = 3.14 GeV , central Pb+Pb collisions at $\sqrt{s_{nn}}$ between 6.3 and 12.3 GeV, and central Au+Au collisions at $\sqrt{s_{nn}}$ between 19.6 and 200 GeV, is presented in Fig. 4.9. The observed cm energy dependence of γ suggests its approximate ($\gamma \to 0$ as $\sqrt{s_{nn}} \to \infty$) asymptotic behavior.

It is important to mention that also the γ's extracted for the other particles, such as charged kaons and ϕ, produced in central collisions of identical heavy ions, revealed [162, 163] the similar increasing trend with $\sqrt{s_{nn}}$ and showed a tendency to approach approximately zero value asymptotically as $\sqrt{s_{nn}} \to \infty$. This can be observed from Fig. 4.10, which presents the cm energy dependence of the parameter γ extracted [163] for the negative pions, K^+, K^-, and ϕ mesons from their experimental cm rapidity distributions in central Pb+Pb collisions at AGS and SPS energies.

As seen from Fig. 4.10, the gap between γ's, extracted for pions and for the charged kaons and ϕ mesons, reduced quite prominently with the increase of $\sqrt{s_{nn}}$ from 6.3 to 12.3 GeV, and the γ's for the charged kaons and ϕ tended to approach that for the negative pions as $\sqrt{s_{nn}}$ increased. The differences observed between the γ's extracted for various particles and shown in Fig. 4.10 can be explained if the cm energy dependence of γ is related to the cm collision energy dependence of the particle yields at midrapidity $\left(\left. \frac{dN}{dy} \right|_{y_{cm}=0} \right)$ and to the degree of dehadronization of a collision system in central collisions of identical heavy ions.

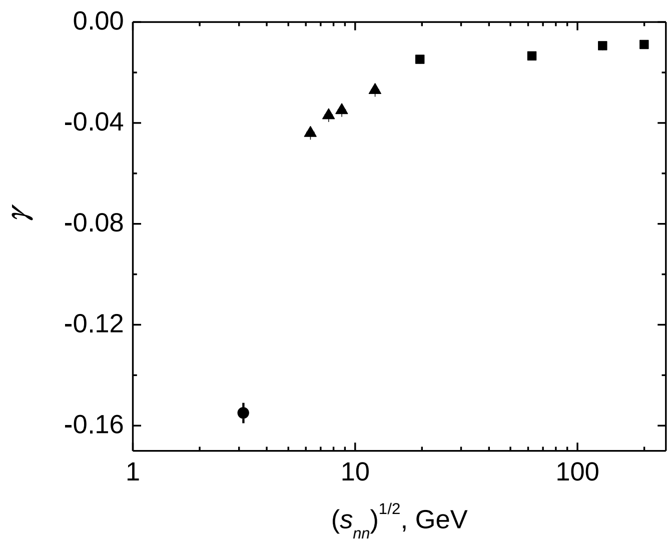

Fig. 4.9. Center-of-mass energy dependence of the parameter γ for pions, extracted in central $^{12}C+^{12}C$ (●), central Pb+Pb [163] (▲), and central Au+Au [163] (■) collisions. The data presented correspond to ~ (0–10)% collision centrality

The differences between γ's for K^+ and K^- can be explained by the differences between K^+ and K^- meson yields at midrapidity at AGS and SPS energies, discussed in Ref. [4]. The difference in yields is determined by the quark content of these hadrons, K^+ ($u\bar{s}$), and K^- ($\bar{u}s$). The availability in a fireball of valence u, d quarks from colliding nucleons "stopped" in the fireball led to a preferential production of hadrons carrying these quarks [4]. These differences vanished at higher RHIC energies, where hadrons were mostly newly created and the production yielded a clear mass ordering [4]. This supports further the statement that both the degree of dehadronization and fraction of constituent nucleons of a collision system, which underwent transition into QGP, along with its energy density, increase as $\sqrt{s_{nn}}$ increases in central heavy ion collisions at high energies.

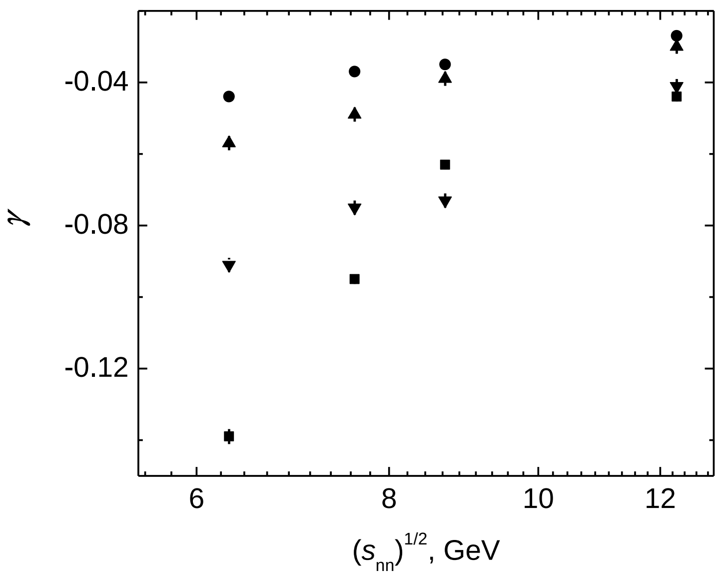

Fig. 4.10. Center-of-mass energy dependence of the parameter γ extracted [163] for the negative pions (●), K^+ (▲), K^- (▼), and ϕ mesons (■) from their experimental cm rapidity distributions in central Pb+Pb collisions at AGS and SPS energies

The differences in Fig. 4.10 between γ for ϕ mesons and γ's for the other particles can be explained by that the ϕ meson ($s\bar{s}$) requires production of both the strange quark and its antiparticle (much heavier than light *u* and *d* quarks), which are not available in the colliding nucleons.

It can easily be verified that, for $\gamma \leq 0$ and finite rapidities, the factor $(AA)^{\gamma y^2}$ reaches its maximum value 1 at $\gamma = 0$. Hence, it can be conjectured that $\gamma \cong 0$ could possibly be related to the complete dehadronization of all the constituent nucleons of a collision system as a result of head-on collision of two identical nuclei, when the whole colliding system undergoes transformation into the state of deconfined quarks and gluons (QGP) and attains its highest possible energy density. At fixed γ ($\gamma < 0$), the factor $(AA)^{\gamma y^2}$ has its maximum value 1 at $y_{cm} = 0$ and falls off rapidly as $|y_{cm}|$ increases towards the fragmentation region of the colliding identical nuclei, which would mean asymptotically $(AA)^{\gamma y^2} \rightarrow 0$ as $|y_{cm}| \rightarrow \infty$. While at $\gamma = 0$, the factor $(AA)^{\gamma y^2}$ would retain its maximum value 1 in the whole cm rapidity range of the produced particles, being independent of y_{cm}. Figure 4.9 shows a large gap between the values of γ for central $^{12}C+^{12}C$ collisions at $\sqrt{s_{nn}}$ = 3.14 GeV and central Pb+Pb collisions at $\sqrt{s_{nn}}$ ≥ 6.3 GeV. This is in line with the above mentioned lattice QCD calculations, predicting the threshold energy density for deconfinement phase transition to be reached already at $\sqrt{s_{nn}} \approx 5$ GeV. Hence, the parameter γ could possibly be sensitive to deconfinement phase transition of a nuclear matter and, as already argued, is possibly an indicator of degree of dehadronization of the whole collision system (or/and an indicator of the fraction of constituent nucleons of the collision system, which underwent transition into the QGP, and its energy density) in central collisions of identical nuclei. We believe that, due to the lowest threshold energy (among hadrons) of pion production (which requires only the lightest *u* and *d* quarks and their antiparticles), an initial onset of deconfinement transition could possibly be deduced from analysis of cm energy dependence of the relevant pion spectra and related phenomenological parameter(s).

Table 4.15

Parameters of approximation by the expression in (4.5) of the cm rapidity distributions of the negative pions in minimum bias, central, and peripheral $^{12}C+^{12}C$ collisions at $\sqrt{s_{nn}}$ = 3.14 GeV (Δ=0.55 is fixed)

Collision Type	Type	*C*	*β*	*γ*	y_0	$\chi^2/n.d.f.$
Minimum bias	Exper.	0.73±0.02	–0.005±0.002	–0.13±0.03	2.07±0.69	5.34
	Mod. FRIT.	0.76±0.02	–0.006±0.001	–0.15±0.02	2.01±0.55	6.35
Central ~ (0–10)%	Exper.	1.86±0.07	–0.007±0.003	–0.14±0.04	2.16±1.08	1.82
	Mod. FRIT.	1.80±0.10	–0.005±0.002	–0.15±0.04	2.03±1.11	1.80
Peripheral ~ (40–100)%	Exper.	0.34±0.03	–0.002±0.003	–0.12±0.06	2.00±1.50	1.85
	Mod. FRIT.	0.44±0.02	–0.002±0.002	–0.14±0.04	2.00±0.91	4.10

Table 4.16

Parameters of approximation by the expression in (4.5) of the cm rapidity distributions of the negative pions in minimum bias, central, and peripheral $^{12}C+^{12}C$ collisions at $\sqrt{s_{nn}}$ = 3.14 GeV

Collision Type	Type	*C*	*β*	*γ*	y_0	Δ	$\chi^2/n.d.f.$
Minimum bias	Exper.	0.69±0.01	–0.005±0.002	–0.141±0.003	2.23±0.05	0.22±0.03	2.38
	Mod. FRIT.	0.72±0.01	–0.006±0.001	–0.154±0.005	2.12±0.08	0.32±0.04	3.41
Central ~ (0–10)%	Exper.	1.79±0.03	–0.008±0.003	–0.155±0.003	2.33±0.05	0.10±0.04	0.87
	Mod. FRIT.	1.73±0.02	–0.005±0.002	–0.167±0.007	2.28±0.11	0.29±0.09	1.55
Peripheral ~ (40–100)%	Exper.	0.32±0.01	–0.0005±0.003	–0.127±0.008	2.10±0.11	0.26±0.06	0.98
	Mod. FRIT.	0.41±0.01	–0.001±0.002	–0.147±0.007	2.04±0.09	0.29±0.04	1.78

For more convincing evidence, one would possibly require 5-6 more experimental data points for γ extracted for pions in central collisions of identical nuclei at $\sqrt{s_{nn}}$ between 3 and 6 GeV. Then, one could possibly identify and estimate the value of cm energy for an abrupt growth of γ in experiment, for a comparison with the existing theoretical expectations.

Due to the estimated threshold cm collision energy $\sqrt{s_{nn}} \approx 5$ GeV, required for reaching the deconfinement threshold energy density, it is expected that quite large fraction of constituent nucleons of a collision system should undergo transition to QGP in central heavy ion collisions at $\sqrt{s_{nn}} \geq 6.3$ GeV. This fraction as well as the energy density of QGP are expected to increase with increasing $\sqrt{s_{nn}}$ in this high energy domain.

Much smaller value of γ extracted for central $^{12}C+^{12}C$ collisions at $\sqrt{s_{nn}}$ = 3.14 GeV than γ's obtained in central heavy ion collisions at $\sqrt{s_{nn}} \geq 6.3$ GeV could then be explained by a very small or practically zero degree of dehadronization of the constituent nucleons, and relatively small energy density, reached in central $^{12}C+^{12}C$ collisions as compared to quite large fraction of constituent nucleons of a collision system, which underwent transition into QGP, and much higher energy densities attained in central Pb+Pb and Au+Au collisions at high energies.

Finally, it is of importance also to check an initial assumption that the parameter β in expression (4.5) should be fixed as $\beta = 0$ due to a symmetry of collision system. For this, all the fits of the experimental and model spectra, presented in Figs. 4.7 and 4.8 and Tables 4.10 and 4.11, have been redone letting the parameter β vary. The parameters extracted from χ^2 fitting by expression in (4.5) of the experimental and Modified FRITIOF model cm rapidity distributions of the negative pions for minimum bias, central, and peripheral $^{12}C+^{12}C$ collisions for the fixed Δ=0.55 only, and allowing all the parameters to vary are presented in

Tables 4.15 and 4.16, respectively. As observed from Tables 4.15 and 4.16, the extracted values of β came out to be essentially zero, within the uncertainties. This validates the initial assumption that $\beta = 0$, made on symmetry consideration, for the cm rapidity distributions of particles produced in collisions of identical nuclei. Comparing Tables 4.10 and 4.15 and Tables 4.11 and 4.16, one can see that the varying of the parameter β practically has no effect on and does not change appreciably any of the other extracted parameters, such as C, γ, y_0, and Δ.

§ 4.5. Summary and Conclusions on CHAPTER IV

The experimental rapidity distributions as well as $<p_t>$ versus $y_{\rm cm}$ spectra of the negative pions in d+^{12}C, ^{12}C+^{12}C, and ^{12}C+^{181}Ta collisions at a momentum of 4.2 GeV/c per nucleon were analyzed and compared systematically with the corresponding spectra calculated using Quark-Gluon String Model. The widths (σ) and centers y_0 of all the experimental and QGSM spectra were extracted from fitting by the Gaussian distribution function. All the rapidity as well as $<p_t>$ versus $y_{\rm cm}$ spectra of negative pions in the analyzed collisions could be fitted quite well by the Gaussian distribution function.

The widths of the experimental rapidity spectra of the negative pions decreased by $(8 \pm 2)\%$, $(5 \pm 1)\%$, and $(15 \pm 2)\%$ in going from peripheral to central d+^{12}C, ^{12}C+^{12}C, and ^{12}C+^{181}Ta collisions, respectively. The centers y_0 of experimental rapidity distributions of π^- mesons shifted by –0.32±0.04 and –0.44±0.02 units towards target fragmentation region while going from peripheral to central d+^{12}C and ^{12}C+^{181}Ta collisions, respectively. Such shifts of y_0 of rapidity spectra of π^- mesons in case of d+^{12}C and ^{12}C+^{181}Ta collisions could be explained by increase in rescattering effects in target nuclei, which are heavier than projectile nuclei, and a subsequent increase in the numbers of target participant nucleons and pions produced in target fragmentation region with increase in collision centrality.

The absolute values of shift of y_0 and decrease in σ of rapidity spectra of π^- mesons increased as this ratio increased in correspondence with the relation $\frac{A(^{12}\mathrm{C})}{A(^{12}\mathrm{C})} < \frac{A(^{12}\mathrm{C})}{A(^{2}\mathrm{H})} < \frac{A(^{181}\mathrm{Ta})}{\mathrm{A}(^{12}\mathrm{C})}$.

The values of σ of $<p_t>$ versus y_{cm} spectra of negative pions in $d+^{12}$C, ^{12}C+^{12}C, and ^{12}C+^{181}Ta collisions proved to be compatible with each other and with the corresponding QGSM results. The centers y_0 of $<p_t>$ versus y_{cm} spectra of negative pions in $d+^{12}$C, ^{12}C+^{12}C, and ^{12}C+^{181}Ta collisions were located very close to midrapidity $y_{\mathrm{cm}} = 0$ and did not depend on the masses of target and projectile nuclei.

The experimental cm rapidity distributions of the negative pions in ^{12}C+^{12}C collisions at 4.2 *A* GeV/*c* ($\sqrt{s_{nn}}$ = 3.14 GeV) were described quite satisfactorily using the simple phenomenological model, the GCM. The GCM parameters extracted from fitting the cm rapidity distributions of the negative pions in central ^{12}C+^{12}C collisions were compared with the corresponding parameters extracted earlier for pions produced in central Pb+Pb collisions at SPS and AGS energies between $\sqrt{s_{nn}}$ = 6.3 GeV and $\sqrt{s_{nn}}$ = 12.3 GeV and in central Au+Au collisions at RHIC energies from $\sqrt{s_{nn}}$ = 19.6 GeV to $\sqrt{s_{nn}}$ = 200 GeV.

By letting the parameter β vary, the initial assumption that $\beta = 0$ in expression (4.5), made on symmetry consideration, for the cm rapidity distributions of particles produced in collisions of identical nuclei was validated. The extracted values of β came out to be practically zero and did not change appreciably any of the other extracted parameters, such as C, γ, y_0, and Δ. The ratio of the fitting constants C, given in expression (4.5), in central and peripheral ^{12}C+^{12}C collisions agreed within the uncertainties with the ratio of the mean multiplicities of the negative pions in central and peripheral collisions, both in the experiment and model. This result showed that the fitting constant C in expression (4.5) fixes the multiplicity of the studied particles.

Approximate ($\gamma \to 0$ as $\sqrt{s_{nn}} \to \infty$) asymptotic behavior of the parameter γ in the $(AA)^{\gamma y^2}$ factor of GCM was deduced from analysis of cm energy dependence of γ, extracted for pions in central ^{12}C+^{12}C collisions at $\sqrt{s_{nn}}$ = 3.14 GeV, central Pb+Pb collisions at $\sqrt{s_{nn}}$ between 6.3 and 12.3 GeV, and central Au+Au collisions at $\sqrt{s_{nn}}$ between 19.6 and 200 GeV. For $\gamma \le 0$ and finite rapidities, the factor $(AA)^{\gamma y^2}$ attains its maximum value 1 at $\gamma = 0$. Physically, $\gamma \cong 0$ could possibly be related to complete dehadronization of all the constituent nucleons of the collision system as a result of head-on collision of two identical nuclei, when the whole colliding system undergoes transformation into the state of free (deconfined) quarks and gluons, and attains its highest possible energy density.

A large gap was observed between the values of γ for central ^{12}C+^{12}C collisions at $\sqrt{s_{nn}}$ = 3.14 GeV and central Pb+Pb collisions at $\sqrt{s_{nn}} \ge 6.3$ GeV. This was in line with the theoretical expectation [6] that the critical energy density for transition of a nuclear matter into the phase of deconfined quarks and gluons should reach already at $\sqrt{s_{nn}} \approx 5$ GeV. Hence, the parameter γ could possibly be sensitive to deconfinement phase transition. Much smaller value of γ extracted in central ^{12}C+^{12}C collisions at $\sqrt{s_{nn}}$ = 3.14 GeV than γ's obtained in central heavy ion collisions at $\sqrt{s_{nn}} \ge 6.3$ GeV could be explained as follows. Very little or practically zero degree of dehadronization of constituent nucleons with relatively low energy density is expected in central ^{12}C+^{12}C collisions at $\sqrt{s_{nn}}$ = 3.14 GeV as compared to quite large degree of dehadronization of the whole collision system with much higher energy densities attained in central Pb+Pb and Au+Au collisions at high energies.

V. SPECTRAL TEMPERATURES OF NEGATIVE PIONS IN *AA* COLLISIONS AT 4.2 *A* GeV/*c*

§ 5.1. Introduction

In Refs. [33, 36] it was shown that non-invariant center-of-mass energy and the p_t spectra of negative pions in d^{12}C, ^{4}He^{12}C, and ^{12}C^{12}C collisions at 4.2 *A* GeV/*c* were characterized by two-temperature shapes and described very well using two-temperature function fits. However the fits of pion spectra with one-temperature Hagedorn (2.26) and simple exponential function (2.22) are also important since they allow one to extract the average spectral temperature of pions.

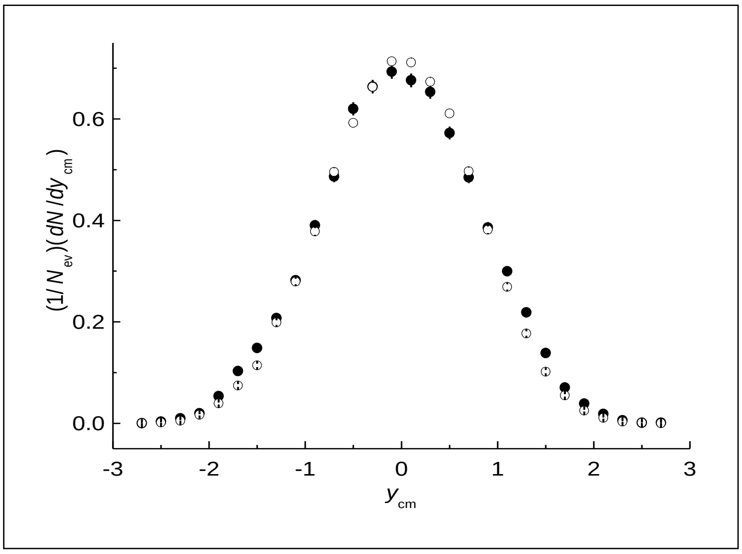

Fig. 5.1. Rapidity distribution of negative pions in the c.m.s. of ^{12}C^{12}C collisions at 4.2 *A* GeV/*c* in experiment (●) and Modified FRITIOF model (○). The distributions are normalized per one inelastic event

The experimental rapidity distribution of negative pions in the c.m.s. of ^{12}C^{12}C collisions at 4.2 *A* GeV/*c* are shown in Fig. 5.1 along with the corresponding spectrum calculated using Modified FRITIOF model. It is seen from this figure that the experimental rapidity distribution is described quite satisfactorily by the model spectrum.

We shall explore how the average spectral temperatures of the negative pions change with the rapidity when one goes from midrapidity (central region) towards fragmentation region of colliding ^{12}C nuclei. The change of the average spectral temperatures of π^- mesons with increase of emission angle of π^- in the c.m.s. of ^{12}C^{12}C collisions from 0 to 90 ± 10 degrees will also be studied. The average spectral temperatures of π^- will be extracted from both the p_t and scaled c.m. E_k spectra of negative pions using fits with the functions, given in equations (2.26) and (2.22), respectively.

§ 5.2. Rapidity and angular dependencies of spectral temperatures of negative pions in ^{12}C^{12}C collisions

The experimental and model p_t distributions of π^- mesons along with the fits by the one-temperature Hagedorn function for the intervals of rapidity $|y| \leq 0.1$ and $1.8 \leq |y| \leq 2.8$ and emission angles $0° \leq \theta \leq 20°$ and $80° \leq \theta \leq 100°$ in the c.m.s. of ^{12}C^{12}C collisions are presented in Figs. 5.2*a*–5.2*d*. As seen from Figs. 5.2*a*–5.2*d*, the experimental p_t distributions of π^- are described satisfactorily by the Modified FRITIOF model calculations. As seen from these figures, both experimental and model p_t spectra are fitted satisfactorily by the one-temperature Hagedorn function. The experimental and model scaled c.m. E_k distributions of π^- mesons with the fits by the one-temperature simple exponential function for the intervals of rapidity $|y| \leq 0.1$ and $1.8 \leq |y| \leq 2.8$ and emission angles $0° \leq \theta \leq 20°$ and $80° \leq \theta \leq 100°$ in the c.m.s. of ^{12}C^{12}C collisions are shown in Figs. 5.3*a*–5.3*d*. As seen from Figs. 5.3*a*–5.3*d*, the experimental scaled c.m. E_k distributions of π^- are reproduced satisfactorily by the model spectra. As seen from these figures, both experimental and model scaled c.m. E_k spectra are fitted satisfactorily by the one-temperature simple exponential function.

The corresponding average spectral temperatures extracted from p_t and scaled c.m. E_k spectra for different intervals of c.m. rapidity and emission angle of π^- mesons in ^{12}C^{12}C collisions at 4.2 *A* GeV/*c* are presented in Tables 5.1 and 5.2.

As seen from Table 5.1, the average spectral temperature of π^- extracted from p_t spectra decreases from the maximal value, 108 ± 2 MeV, to the minimal value, 36 ± 2 MeV, as one goes from c.m. midrapidity towards fragmentation region of colliding ^{12}C nuclei.

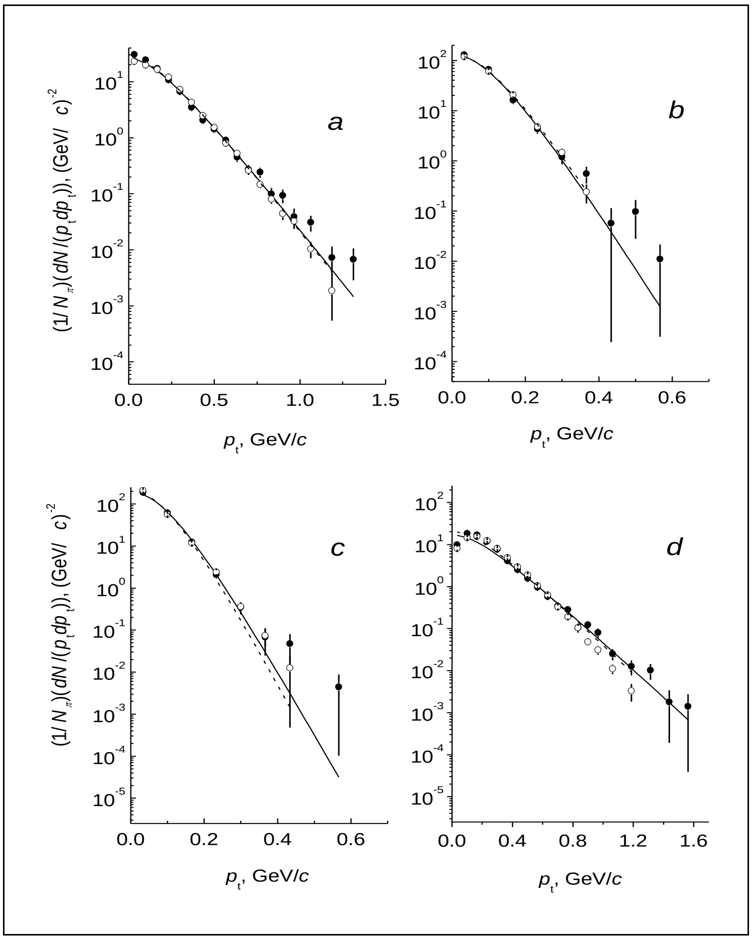

Fig. 5.2. Transverse momentum distributions of negative pions in experiment (●) and Modified FRITIOF model (○) in ^{12}C^{12}C collisions at 4.2 *A* GeV/*c* for the following intervals of rapidity and emission angle of pions in the c.m.s. of ^{12}C^{12}C collisions: $|y|\leq 0.1$ (*a*); $1.8\leq|y|\leq 2.8$ (*b*); $0^o\leq\theta\leq 20^o$ (*c*); $80^o\leq\theta\leq 100^o$ (*d*). Fits of the p_t spectra by the one-temperature Hagedorn function in experiment (solid line) and Modified FRITIOF model (dashed line). All distributions are normalized per one negative pion

This result is expected since pions in central rapidity region are produced mostly in central hard ^{12}C^{12}C collisions, and hence at higher temperatures, as compared to pions in region of fragmentation of colliding nuclei originated predominantly in peripheral soft $^{12}C^{12}C$ interactions, and hence at lower temperatures. This is also confirmed by the c.m. angular dependence of the average spectral temperature of π^-, extracted from p_t spectra, presented in Table 5.2. As seen from Table 5.2, the average spectral temperature of π^- extracted from p_t spectra increases from 27 ± 1 to 126 ± 2 MeV as the c.m. emission angle of π^- increases from 0 to 90 ± 10 degrees.

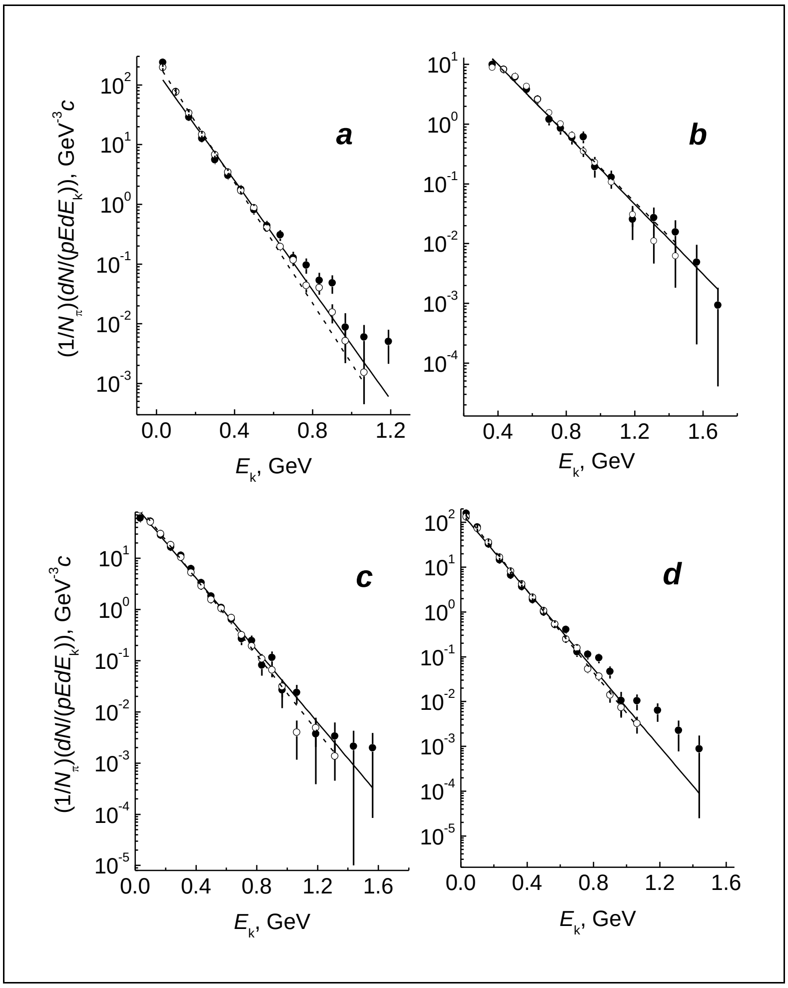

Fig. 5.3. Scaled c.m. kinetic energy distributions of negative pions in experiment (●) and Modified FRITIOF model (○) in $^{12}C^{12}C$ collisions at 4.2 *A* GeV/*c* for the following intervals of rapidity and emission angle of pions in the c.m.s. of $^{12}C^{12}C$ collisions: $|y| \leq 0.1$ (*a*); $1.8 \leq |y| \leq 2.8$ (*b*); $0^o \leq \theta \leq 20^o$ (*c*); $80^o \leq \theta \leq 100^o$ (*d*); Fits of the scaled E_k spectra by the one-temperature simple exponential function: experiment (solid line) and Modified FRITIOF model (dashed line). All distributions are normalized per one negative pion

Table 5.1

Dependence of the average spectral temperatures of negative pions extracted from transverse momentum (p_t) and scaled c.m. kinetic energy (E_k) spectra on the interval of rapidity in the c.m.s. of $^{12}C^{12}C$ collisions at 4.2 *A* GeV/*c*

Interval of y in c.m.s.	Type	N_π	p_t spectra		scaled c.m. E_k spectra	
			T, MeV	χ^2/n.d.f.	T, MeV	χ^2/n.d.f.
$\|y\| \le 0.1$	Experiment	2859	108±2	1.29	95±2	2.99
	FRITIOF	7246	107±1	2.54	86±1	5.24
$0.3 \le \|y\| \le 0.5$	Experiment	5233	103±2	1.41	97±2	2.69
	FRITIOF	12759	103±1	5.50	92±1	2.54
$0.7 \le \|y\| \le 0.9$	Experiment	3575	94±2	2.01	119±2	3.31
	FRITIOF	8814	90±1	5.83	111±1	9.38
$1.2 \le \|y\| \le 1.6$	Experiment	2923	67±2	1.01	127±3	2.41
	FRITIOF	5915	61±1	8.30	118±1	8.49
$1.8 \le \|y\| \le 2.8$	Experiment	628	36±2	1.19	148±5	1.10
	FRITIOF	1038	37±1	0.46	152±3	3.99

Table 5.2

Dependence of the average spectral temperatures of negative pions extracted from transverse momentum (p_t) and scaled c.m. kinetic energy (E_k) spectra on the interval of emission angle in the c.m.s. of $^{12}C^{12}C$ collisions at 4.2 *A* GeV/*c*

Interval of θ in c.m.s., degrees	Type	N_π	p_t spectra		scaled c.m. E_k spectra	
			T, MeV	χ^2/n.d.f.	T, MeV	χ^2/n.d.f.
0—20	Experiment	1547	27±1	0.90	123±3	1.11
	FRITIOF	2802	25±1	4.88	116±1	1.52
20—40	Experiment	3375	68±2	2.16	115±2	0.98
	FRITIOF	7307	67±1	5.11	114±1	3.25
40—60	Experiment	3874	98±2	2.44	106±2	1.17
	FRITIOF	9634	98±1	5.42	105±1	2.08
60—80	Experiment	3893	120±2	2.43	102±2	2.09
	FRITIOF	10323	116±1	6.03	99±1	1.78
80—100	Experiment	3916	126±2	2.94	100±2	2.31
	FRITIOF	10218	121±1	7.37	95±1	1.64

This is because pions emitted at c.m. angles around 0 and 90 degrees are originated at around ^{12}C fragmentation and central rapidity region, respectively. It is interesting to mention that in order to select central collisions some authors [73, 175, 176] restricted particle spectra to c.m.s. emission angles 90 ± 10 or 90 ± 20 degrees since this approach was less affected by nonequilibrium processes [74].

On the other hand, as seen from Tables 5.1 and 5.2, the average spectral temperatures extracted from the scaled c.m. E_k spectra of π^- show the totally opposite behavior as compared to the temperatures extracted from p_t spectra of π^-. As seen from these tables, the temperatures extracted from the scaled c.m. E_k spectra of π^- increase as one goes from cm midrapidity towards fragmentation region of colliding ^{12}C nuclei. Correspondingly, the average temperature of π^- extracted from the scaled c.m. E_k spectra decreases as the c.m. emission angle of π^- increases from 0 to 90 ± 10 degrees. Such behavior of spectral temperatures extracted from c.m. kinetic energy spectra could be explained by the influence of the longitudinal boosts on such spectra. It is important to mention that the average spectral temperatures extracted from the Modified FRITIOF model spectra of π^- mesons, as seen from Tables 5.1 and 5.2, reproduce quite satisfactorily the corresponding temperatures extracted from experimental spectra of negative pions. It follows from above results that p_t spectra of π^- are preferable for estimating adequately the temperatures of π^- as compared to the scaled c.m. E_k spectra. This result agrees with the analogous statements of some authors [77, 177] that transverse momentum distributions of hadrons are preferable for estimating the hadron temperatures due to the Lorentz invariance of such spectra with respect to longitudinal boosts.

We also compared the average spectral temperatures of π^- extracted from the total p_t and total scaled c.m. E_k spectra of π^- in ^{12}C^{12}C collisions at 4.2 A GeV/c using fits by the one-temperature functions (2.26) and (2.22), respectively. The corresponding results are shown in Table 5.3. As seen from this table, the average temperature of π^- extracted from c.m. kinetic energy spectrum is significantly higher than the temperature extracted from the p_t spectrum both in the experiment and Modified FRITIOF model. This confirms that the temperature extracted from c.m. E_k spectra of π^- is affected markedly by the longitudinal boosts along the collision axis.

Table 5.3

Average spectral temperatures of negative pions in $^{12}C^{12}C$ collisions at 4.2 *A* GeV/*c* extracted from total p_t and total scaled c.m. E_k spectra by fitting with the one-temperature Hagedorn and one-temperature simple exponential function, respectively.

Total spectra	Type	*T*, MeV	χ^2/*n.d.f.*
p_t	Experiment	103±2	4.46
	FRITIOF	94±1	2.68
scaled c.m. E_k	Experiment	119±2	3.78
	FRITIOF	106±1	4.17

Table 5.4

Spectral temperatures, T_1 and T_2, and their relative contributions, R_1 and R_2, for negative pions in $^{12}C^{12}C$ collisions at 4.2 *A* GeV/*c* extracted from total p_t and total scaled c.m. E_k spectra by fitting with two-temperature Hagedorn and two-temperature simple exponential function, respectively

Total spectra	T_1	R_1	T_2	R_2	χ^2/*n.d.f.*
p_t	78±4	(87±14)%	146±9	(13±6)%	0.69
scaled c.m. E_k	94±5	(91±8)%	168±12	(9±6)%	0.20

As shown in our paper [36] and earlier works [73–75, 78], the transverse momentum as well as energy spectra of pions, produced in relativistic nuclear collisions, are characterized by two-temperature shapes. For the sake of comparison, in the present work we also fitted the total p_t and total scaled c.m. E_k spectra of π^- in $^{12}C^{12}C$ collisions at 4.2 A GeV/c by two-temperature functions (2.27) and (2.23), respectively.

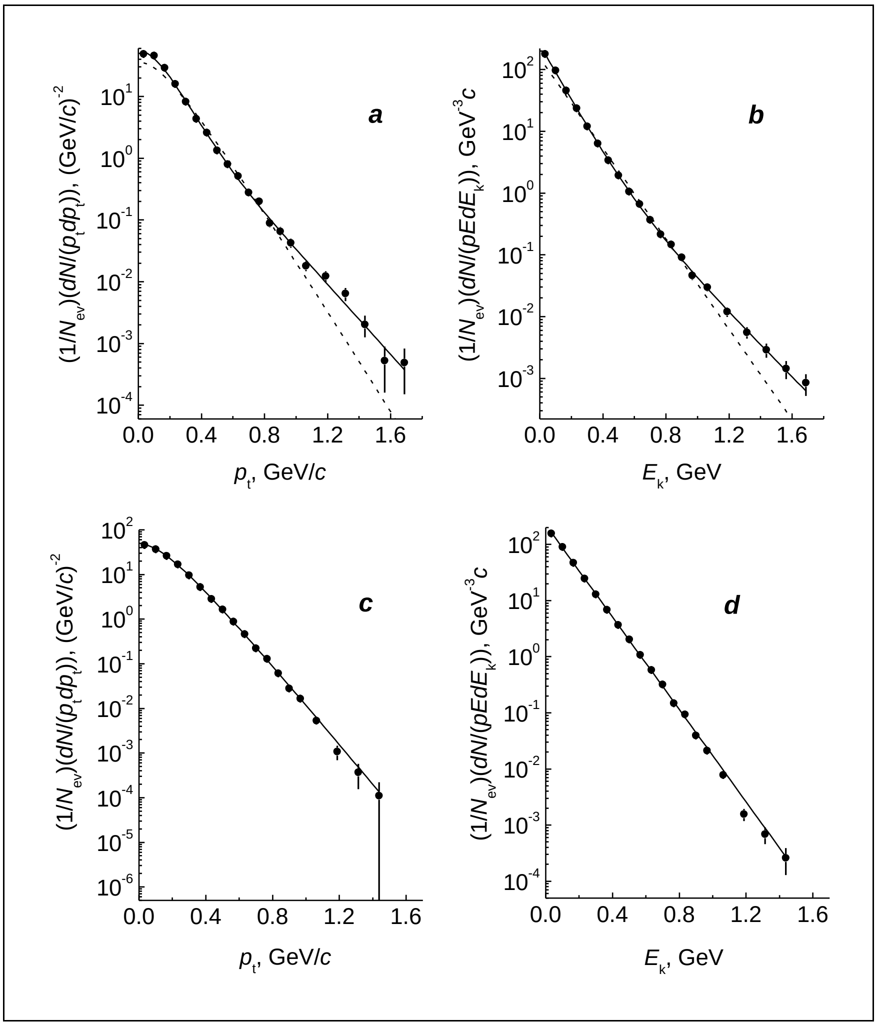

Fig. 5.4. Total transverse momentum distribution of negative pions in experiment (*a*) and Modified FRITIOF model (*c*); total scaled kinetic energy distribution of negative pions in the c.m.s. of $^{12}C^{12}C$ collisions at 4.2 *A* GeV/*c* in experiment (*b*) and Modified FRITIOF model (*d*); Fits by the one-temperature (dashed line) and two-temperature (solid line) Hagedorn function (*a*) and simple exponential function (*b*); Fits (solid line) by the one-temperature Hagedorn function (*c*) and one-temperature simple exponential function (*d*). All distributions are normalized per one inelastic collision event

The corresponding extracted temperatures T_1 and T_2 along with their relative contributions R_1 and R_2 to the total multiplicity of π^- mesons are given in Table 5.4.

As seen from Figs. 5.4*a* and 5.4*b*, the total p_t and total scaled c.m. E_k spectra of π^- in $^{12}C^{12}C$ collisions are fitted very well by two-temperature functions (2.27) and (2.23), respectively, as compared to the one-temperature fits. This is also seen from comparison of the values of $\chi^2/n.d.f.$ given in Tables 5.3 and 5.4. However, as mentioned and seen above, the one-temperature fits of pion spectra are important for extracting the average spectral temperatures of pions. It is also seen from Table 5.4 that the temperatures T_1 and T_2 extracted from the total scaled c.m. E_k spectra of π^- in $^{12}C^{12}C$ collisions proved to be noticeably higher than the corresponding temperatures extracted from the total p_t spectra of π^-, as was also expected. As to the model spectra presented in Figs. 5.4*c* and 5.4*d*, they are reproduced quite well using the fits with the one-temperature functions (2.26) and (2.22), and the fitting of these spectra with two-temperature functions (2.27) and (2.23) leads to almost coinciding temperatures $T_1 \approx T_2$ suggesting that the one-temperature fit is sufficient for the Modified FRITIOF model spectra.

§ 5.3. Spectral temperatures of negative pions in $d^{12}C$, $^4He^{12}C$, and $^{12}C^{12}C$ collisions

We shall obtain [36] the spectral temperatures of π^- mesons in $d^{12}C$, $^4He^{12}C$, and $^{12}C^{12}C$ collisions at 4.2 A GeV/c by fitting the transverse momentum spectra of π^- in the framework of Hagedorn Thermodynamic Model [77, 140]. The extracted temperatures will be compared systematically with the corresponding temperatures estimated in Ref. [72] from analysis of non-invariant center-of-mass (c.m.) energy spectra of π^- mesons. The experimental p_t spectra of π^- mesons will also be compared with those obtained using Quark-Gluon-String Model (QGSM) [132, 133] and Modified FRITIOF model [118, 119, 124–127] adapted to intermediate energies.

Table 5.5

Mean multiplicities per event of π^- mesons produced in d^{12}C, ^{4}He^{12}C, and ^{12}C^{12}C collisions at 4.2 *A* GeV/*c*

Type		$\langle n(\pi^-)\rangle$
d^{12}C	Experiment	0.66±0.01
	Modified FRITIOF	0.70±0.01
	QGSM	0.64±0.01
^{4}He^{12}C	Experiment	1.02±0.01
	Modified FRITIOF	0.95±0.01
	QGSM	0.99±0.01
^{12}C^{12}C	Experiment	1.45±0.01
	Modified FRITIOF	1.42±0.01
	QGSM	1.59±0.01

The experimental mean multiplicities per event of the negative pions in d^{12}C, ^{4}He^{12}C, and ^{12}C^{12}C collisions at 4.2 *A* GeV/*c* along with calculations according to QGSM and Modified FRITIOF models are presented in Table 5.5. As can be seen from Table 5.5, the experimental mean multiplicities of π^- mesons are described satisfactorily by QGSM and Modified FRITIOF model. The experimental mean values of momentum and transverse momentum of negative pions in d^{12}C, ^{4}He^{12}C, and ^{12}C^{12}C collisions at 4.2 *A* GeV/*c* along with the corresponding model calculations are given in Table 5.6. As seen from this table, the mean values calculated using Modified FRITIOF model are compatible with the experimental data. However, as seen from Table 5.6, QGSM noticeably underestimates the experimental mean momenta and transverse momenta of negative pions produced in the analyzed collisions.

A comparison of experimental p_t distributions of π^- mesons in d^{12}C, ^{4}He^{12}C, and ^{12}C^{12}C collisions at 4.2 *A* GeV/*c* with the corresponding spectra calculated using QGSM and Modified FRITIOF model is presented in Figs. 5*a*–5*c*. As seen from these figures, both models describe quite satisfactorily the experimental spectra in region $p_t < 0.8$ GeV/*c*. However, both models underestimate the experimental transverse momentum spectra in region $p_t > 0.8$ GeV/*c*, and experimental spectra are extended towards higher values of p_t as compared to the model spectra. As seen from Fig. 5.5*d*, the p_t spectra of negative pions are characterized by very similar slopes for d^{12}C, ^{4}He^{12}C, and ^{12}C^{12}C collisions.

Table 5.6

Mean momenta and transverse momenta of π^- mesons produced in d^{12}C, ^{4}He^{12}C, and ^{12}C^{12}C collisions at 4.2 *A* GeV/*c*

Type		$\langle p \rangle$, GeV/*c*	$\langle p_t \rangle$, GeV/*c*
d^{12}C	Experiment	0.564±0.007	0.251±0.003
	Modified FRITIOF	0.543±0.002	0.243±0.001
	QGSM	0.507±0.004	0.222±0.002
^{4}He^{12}C	Experiment	0.584±0.004	0.247±0.002
	Modified FRITIOF	0.561±0.002	0.244±0.001
	QGSM	0.541±0.004	0.224±0.001
^{12}C^{12}C	Experiment	0.597±0.003	0.242±0.001
	Modified FRITIOF	0.594±0.002	0.248±0.001
	QGSM	0.571±0.003	0.219±0.001

We shall fit the normalized p_t distributions, $\frac{dN}{N_{\mathrm{ev}} p_{\mathrm{t}} dp_{\mathrm{t}}}$, of negative pions produced in d^{12}C, ^{4}He^{12}C, and ^{12}C^{12}C collisions at 4.2 *A* GeV/*c* by one-temperature (2.26) as well as two-temperature (2.27) Hagedorn function. In Ref. [72] non-invariant c.m. energy spectra of π^- mesons in these collisions were fitted by one-temperature as well as two-temperature Maxwell–Boltzmann distribution function. The experimental statistics used in Ref. [72] was 6684, 4849, and 6806 for d^{12}C, ^{4}He^{12}C, and ^{12}C^{12}C collision events respectively, which is less than half of the statistics used in the present analysis. Two-temperature shape of the non-invariant c.m. energy spectra of π^- mesons was observed for these collisions in Ref. [72].

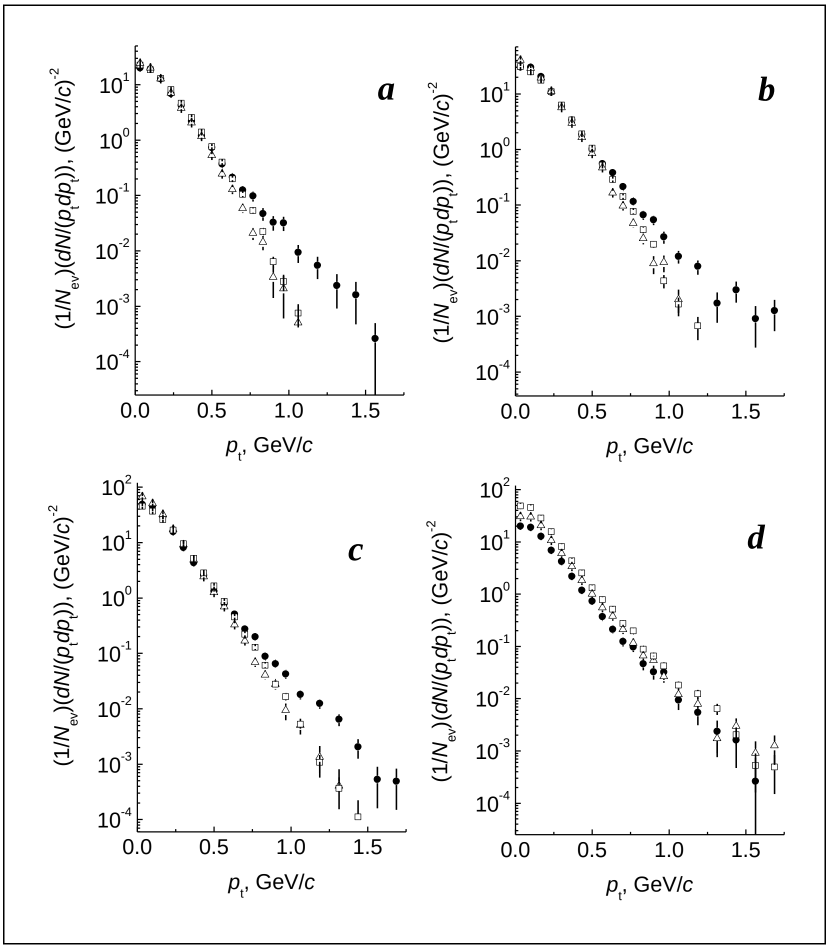

Fig. 5.5. Transverse momentum distributions of π^- mesons in d^{12}C (*a*), ^{4}He^{12}C (*b*), and ^{12}C^{12}C (*c*) collisions at 4.2 *A* GeV/*c* in experiment (●), QGSM (Δ), and Modified FRITIOF model (□); (*d*) – Experimental transverse momentum distributions of π^- mesons in d^{12}C (●), ^{4}He^{12}C (Δ), and ^{12}C^{12}C (□) collisions at 4.2 *A* GeV/*c*. All distributions are normalized by per one inelastic collision event

In Fig. 5.6 the transverse momentum spectra of π^- mesons in ^{4}He^{12}C and ^{12}C^{12}C collisions at 4.2 *A* GeV/*c* are presented along with the fits by one-temperature and two-temperature Hagedorn function. As can be seen from this figure, the two-temperature Hagedorn function fits very well the experimental p_t spectra. On the other hand, one-temperature Hagedorn function fails to fit so well the experimental spectra, especially it underestimates noticeably the experimental spectra in region $p_t > 0.8$ GeV/c. The same two-temperature shape was also observed for p_t spectrum of π^- mesons in d^{12}C collisions at 4.2 A GeV/c.

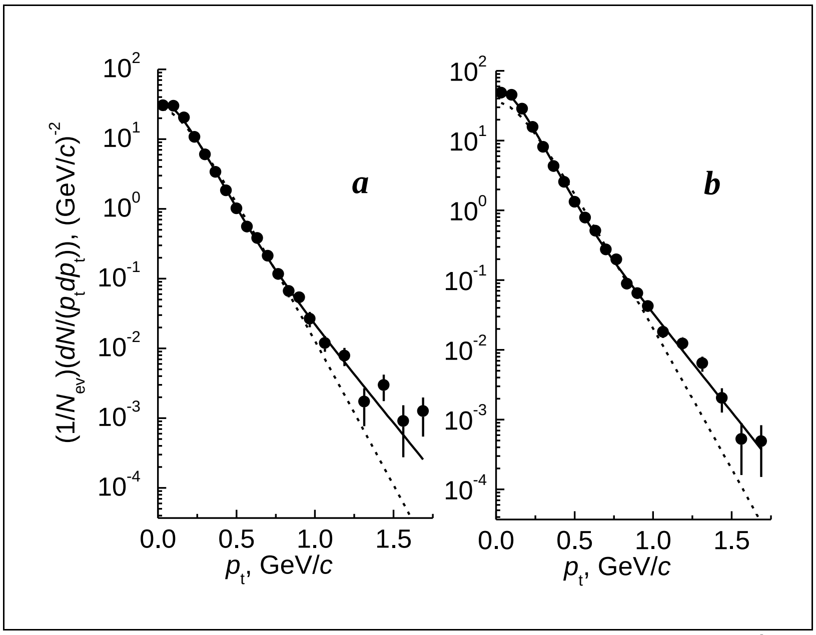

Fig. 5.6. Experimental p_t distributions (●) of π^- mesons in $^4He^{12}C$ (a) and $^{12}C^{12}C$ (b) collisions at 4.2 A GeV/c and the corresponding fits by one-temperature (dashed curve) and two-temperature (solid curve) Hagedorn function

Table 5.7

Spectral temperatures (T) of π^- mesons and their relative contributions (R) extracted in the present work, compared to those obtained in Ref. [72], in d^{12}C, ^{4}He^{12}C, and ^{12}C^{12}C collisions at 4.2 A GeV/c

Type		T_1, MeV	R_1, %	T_2, MeV	R_2, %	$\chi^2/n.d.f.$
d^{12}C	Present work	83±6	89±16	155±21	11±11	0.37
	Ref. [72]	89±4	91±7	190±33	9±7	0.57
^{4}He^{12}C	Present work	84±5	89±14	149±17	11±10	0.73
	Ref. [72]	94±6	85±11	173±22	15±11	0.54
^{12}C^{12}C	Present work	78±4	87±14	146±9	13±6	0.69
	Ref. [72]	83±3	79±6	145±7	21±6	0.72

It should be mentioned that the values of $\chi^2 / n.d.f.$ decrease by about 2 to 4 times when one goes from one-temperature to two-temperature Hagedorn function fits of experimental p_t spectra of π^- mesons in d^{12}C, ^{4}He^{12}C, and ^{12}C^{12}C collisions at 4.2 *A* GeV/*c*.

Spectral temperatures (T_1, T_2) of π^- mesons and their relative contributions (R_1, R_2) extracted in the present work from fitting p_t spectra by two-temperature Hagedorn function are presented in Table 5.7. The corresponding results obtained in Ref. [72] from fitting non-invariant c.m. energy spectra of negative pions by two-temperature Maxwell–Boltzmann distribution function are also shown for a comparison in this table. As seen from Table 5.7, the spectral temperatures, T_1 and T_2, and the corresponding relative contributions, R_1 and R_2, obtained in the present work do not depend on the mass of the projectile nucleus colliding with carbon nuclei. This result is consistent with the earlier work [74], in which the temperatures of π^- mesons produced in central interactions of He, C, and Mg nuclei with Li, C, Ne, Mg, Cu, and Pb nuclei at incident momentum of 4.5 *A* GeV/*c*, obtained using 2-m streamer chamber of JINR, did not depend on the mass numbers of projectile and target nuclei. Our spectral temperatures proved to be compatible with the temperatures extracted in Ref. [74] for collisions of different nuclei at 4.5 *A* GeV/*c*. It is seen from this table that the dominant contribution (R_1 ~ 90%) to the total p_t spectra of π^- mesons comes from spectral temperature T_1 ~ 78–84 MeV, while T_2 ~ 146–155 MeV account for the remaining part (R_2 ~ 10%) of p_t spectra. It is seen from Table 5.7 that the values of T_1 and T_2 obtained in Ref. [72] from non-invariant c.m. energy spectra of π^- mesons are consistently higher (except for T_2 in ^{12}C^{12}C collisions) than the corresponding spectral temperatures deduced from p_t spectra of π^- in the present analysis. As was already discussed, this could be due to the influence of longitudinal motion on energy spectra of π^- mesons, whereas p_t spectra are Lorentz invariant with respect to longitudinal boosts. As seen from Table 5.7, the dominant contribution (R_1 ~ 80–90%) to the total π^- multiplicity, as obtained in Ref. [72], is given by T_1 ~ 83–94 MeV, which is compatible with the results of the present work. The absolute values of T_2 obtained from non-invariant c.m. energy spectra of π^- decrease with an increase of the mass number of projectile nucleus. However these T_2 values coincide with each other within quite large uncertainties, caused most probably by a relatively low experimental statistics used in Ref. [72].

It is of interest to analyze the dependence of spectral temperatures of π^- mesons on the degree of collision centrality for $^{12}C^{12}C$ collisions at 4.2 A GeV/c, for which we have the highest experimental statistics. We analyzed experimental p_t spectra of π^- mesons in $^{12}C^{12}C$ collisions at 4.2 A GeV/c obtained for three groups of collision events characterized by the different numbers of participant protons (N_{part}), as was also done in Ref. [72] for analysis of dependence of the shape of non-invariant c.m. energy spectra on the degree of collision centrality in $^{12}C^{12}C$ collisions. Let us recall that the number of participant protons (N_{part}) correlates with the impact parameter of collision of two nuclei. With an increase of N_{part} the value of impact parameter decreases, which is equivalent to an increase in the degree of collision centrality. Spectral temperatures (T) of π^- mesons and their relative contributions (R) obtained in the present work, compared to those obtained in Ref. [72] in $^{12}C^{12}C$ collisions at 4.2 A GeV/c, for three groups of collision events with different numbers of N_{part} are given in Table 5.8. In case of $^{12}C^{12}C$ collisions the events with $N_{\text{part}} = 0$–2 may be classified as peripheral collisions and those with $N_{\text{part}} \geq 7$ as the central ones, whereas the collision events with $N_{\text{part}} = 3$–6 lie in between [72]. As can be seen from Table 5.8, the spectral temperatures, T_1 and T_2, and the corresponding relative contributions, R_1 and R_2, obtained in the present work do not depend, within fitting errors, on the degree of collision centrality in $^{12}C^{12}C$ collisions at 4.2 A GeV/c. Similar behavior was observed for the spectral temperatures and their relative contributions obtained from c.m. energy spectra of π^- mesons in $^{12}C^{12}C$ in Ref. [72] and shown in Table 5.8. It should be noted that our results for spectral temperatures, T_1 and T_2, obtained for three different groups of $^{12}C^{12}C$ collision events coincide within uncertainties with the corresponding spectral temperatures obtained from c.m. energy spectra of π^- in Ref. [72]. It is also seen from Table 5.8 that the dominant contribution (R_1 ~ 80–90%) to the p_t spectra of π^- mesons comes from spectral temperature T_1 ~ 72–79 MeV, which is compatible with the corresponding results for the total p_t spectra of π^- given in Table 5.7.

Table 5.8

Spectral temperatures (*T*) of π^- mesons and their relative contributions (*R*) extracted in the present work, compared to those obtained in Ref. [72], in $^{12}C^{12}C$ collisions at 4.2 *A* GeV/*c* for three groups of collision events with different numbers of participant protons (N_{part})

N_{part}	Source	T_1, MeV	R_1, %	T_2, MeV	R_2, %	$\chi^2/n.d.f.$
0–2	Present Work	77±6	90±17	144±22	10±12	0.73
	Ref. [72]	89±11	78±26	136±29	22±26	0.95
3–6	Present Work	72±6	78±17	131±9	22±12	0.57
	Ref. [72]	74±7	61±13	128±8	39±13	0.91
$N_{part} \geq 7$	Present Work	79±5	87±15	149±11	13±8	0.70
	Ref. [72]	79±7	72±15	136±13	28±15	0.92

In early work [73] the two-temperature shape of c.m. kinetic energy spectra of negative pions in Ar+KCl at 1.8 GeV/nucleon was obtained. In this work the occurrence of two temperatures, T_1 and T_2, was interpreted as due to two channels of pion production: pions coming from Δ resonance decay (T_1), and directly produced pions (T_2). In Ref. [63] the two-temperature shape of kinetic energy spectrum of pions emitted at 90º in c.m.s. of central La+La collisions at 1.35 GeV/nucleon was interpreted as due to different contributions of deltas originated from the early and later stages of heavy ion reactions. The two-temperature behavior was also observed for c.m. energy as well as p_t spectra of π^- mesons produced in Mg+Mg collisions [75] at incident momentum of 4.2–4.3 *A* GeV/*c*. In Ref. [72] the two-temperature shape of experimental c.m. energy spectra of π^- in

$^{12}C^{12}C$ collisions at 4.2 *A* GeV/*c* was assumed as possibly due to superposition of partial contributions of different sources (decays of resonances, direct reactions, etc), analyzing the spectra of π^- coming from different sources in the framework of QGSM.

§ 5.4 Summary and Conclusions on CHAPTER V

The average spectral temperature of π^- extracted from p_t spectra decreased from 108 ± 2 to 36 ± 2 MeV when going from cm midrapidity towards fragmentation region of colliding ^{12}C nuclei in $^{12}C^{12}C$ collisions at 4.2 *A* GeV/*c*. This result was expected since pions in central rapidity region are produced predominantly in central hard $^{12}C^{12}C$ collisions, and hence at higher temperatures, as compared to pions in region of fragmentation of colliding nuclei originated mostly in peripheral soft $^{12}C^{12}C$ interactions, and hence at lower temperatures. This finding was confirmed by the increase of the average spectral temperature of π^-, extracted from p_t spectra, from 27 ± 1 to 126 ± 2 MeV as the c.m. emission angle of π^- increased from 0 to 90 ± 10 degrees. On the other hand, the average spectral temperatures extracted from the scaled c.m. E_k spectra of π^- showed the totally opposite behavior, which could be explained by the influence of the longitudinal boosts on the kinetic energy spectra of negative pions.

The average spectral temperatures extracted from the Modified FRITIOF model spectra of π^- mesons reproduced quite satisfactorily the corresponding temperatures extracted from the experimental spectra of negative pions.

The transverse momentum as well as energy spectra of negative pions produced in minimum bias $^{12}C^{12}C$ collisions at 4.2 *A* GeV/*c* were fitted noticeably better using the two-temperature thermal model as compared to the one-temperature model. As mentioned earlier, the phenomenon of collective flow has become the well-established and an important feature of relativistic heavy ion collisions. Inverse slope parameter, *T*, or an apparent temperature of the emitting source, of transverse mass spectra of hadrons was shown to consist of two components: a thermal part, $T_{thermal}$, and a second part resembling the collective expansion with an average transverse velocity $\langle\beta_t\rangle$ [178]. Hence the observed two-temperature shape of transverse momentum and energy spectra of negative pions produced in $^{12}C^{12}C$ collisions at 4.2 *A* GeV/*c* can likely be explained by the collective flow effects.

The spectral temperatures of π^- mesons in $d^{12}C$, $^4He^{12}C$, and $^{12}C^{12}C$ collisions at 4.2 *A* GeV/*c* were obtained from fitting transverse momentum spectra of π^- by two-temperature Hagedorn function coming from Hagedorn Thermodynamic Model. Experimental p_t spectra of π^- were fitted significantly better by using Hagedorn function with two temperatures, T_1 and T_2, as compared to the one-temperature fit. The dominant contribution (R_1 ~ 90%) to the total multiplicity of π^- mesons came from spectral temperature T_1 ~ 78–84 MeV, while the relative yield of the high-temperature, T_2 ~ 146–155 MeV, component was much lower (R_2 ~ 10%). The spectral temperatures, T_1 and T_2, and their relative contributions did not depend, within fitting errors, on the degree of collision centrality in $^{12}C^{12}C$ collisions at 4.2 *A* GeV/*c*.

On the whole, the spectral temperatures of π^- mesons in $d^{12}C$, $^4He^{12}C$, and $^{12}C^{12}C$ collisions at 4.2 *A* GeV/*c* ($T_{beam} \approx 3.4$ *A* GeV) extracted in the present analysis from negative pion p_t spectra in the framework of Hagedorn Thermodynamic Model are compatible with the corresponding temperatures of π^- obtained in previous works for different colliding nuclei at comparable incident energies per nucleon.

VI. CENTRALITY AND *A* DEPENDENCIES OF P_t DISTRIBUTIONS OF NEGATIVE PIONS IN *AA* COLLISIONS AT 4.2 *A* GeV/*c*

§ 6.1. P_t distributions of negative pions in $^{12}C^{12}C$ collisions

The transverse momentum and rapidity distributions of the negative pions in minimum bias $^{12}C+^{12}C$ collisions at a momentum of 4.2 GeV/*c* per nucleon are presented in Fig. 6.1. As can be seen from Fig. 6.1*a*, the experimental transverse momentum spectrum of π^- mesons is described satisfactorily by the QGSM [132, 133] calculations. However, Fig. 6.1*a* also shows that the QGSM underestimates the experimental p_t spectrum of π^- mesons in region $p_t > 0.7$ GeV/*c*. It is important to mention that another model − Modified FRITIOF model [118, 119, 43–47], designed also for describing the nucleus-nucleus collisions at incident energies of the order of a few GeV per nucleon, also underestimates this high p_t part of the pion spectra [36, 118]. In Ref. [36] it was observed that the fitting of the p_t spectra of π^- in $d+^{12}C$, $^4He+^{12}C$, and $^{12}C+^{12}C$ collisions at 4.2 *A* GeV/*c* with the two-temperature Hagedorn function resulted in the lower spectral temperatures T_1 and T_2 for both QGSM and Modified FRITIOF model spectra as compared to the experimental p_t distributions.

It is also evident from Fig. 6.1*a* that the inverse slope of the QGSM spectrum is noticeably lesser compared to that of the experimental p_t spectrum. The rapidity spectrum in Fig. 6.1*b* is plotted in cms of nucleon–nucleon collisions at 4.2 GeV/*c* (the rapidity of the cms of nucleon–nucleon collision is $y_{cms} \approx 1.1$ at this incident momentum). As observed from Fig. 6.1*b*, QGSM describes quite well the experimental rapidity spectrum of π^- mesons in $^{12}C+^{12}C$ collisions.

In the present work [33], the transverse momentum spectra of π^- mesons produced in $^{12}C+^{12}C$ collisions at a momentum of 4.2 GeV/*c* per nucleon were fitted by four different functions commonly used for describing the p_t spectra of hadrons.

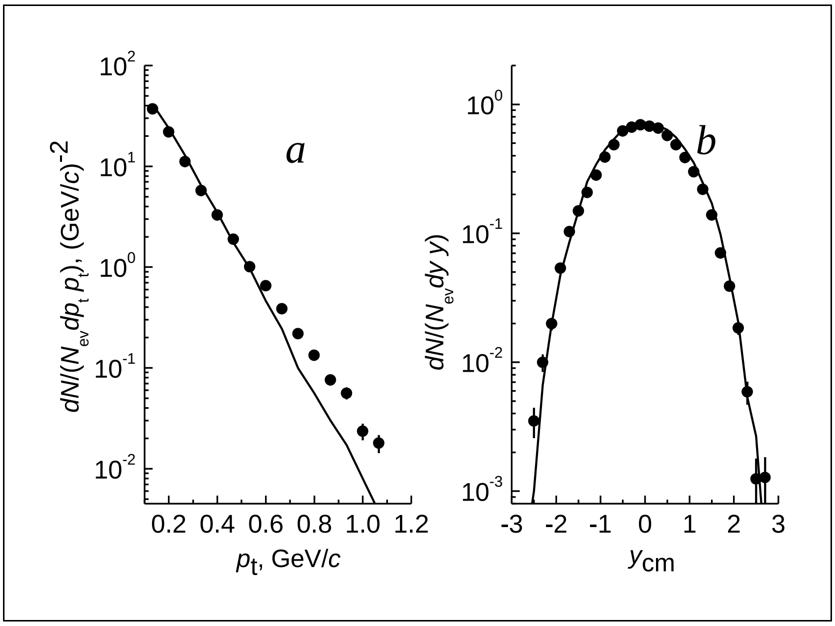

Fig. 6.1. The experimental transverse momentum (a) and rapidity (b) spectra of the negative pions produced in minimum bias $^{12}C^{12}C$ (●) collisions at 4.2 GeV/*c* per nucleon. The corresponding calculated QGSM spectra are given by the solid lines. All the spectra are normalized per one inelastic collision event

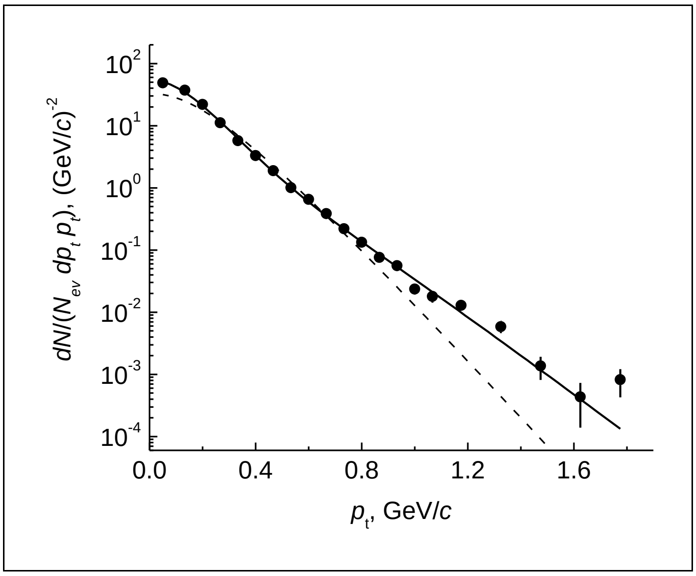

Fig. 6.2. The experimental transverse momentum spectra (●) of the negative pions produced in minimum bias $^{12}C^{12}C$ collisions at 4.2 GeV/*c* per nucleon and the corresponding fits in the whole p_t range by the one-temperature (dashed line) and the two-temperature (solid line) Boltzmann functions. All the spectra are normalized per one inelastic collision event

The transverse momentum spectra of the negative pions were fitted by one-temperature (see eq. 2.26) and two-temperature (see eq. 2.27) Hagedorn, and one-temperature (see eq. 2.28) and two temperature (see eq. 2.29) Boltzmann functions.

The spectra of pions can also be fitted by Simple Exponential function as follows for the one-temperature and two-temperature scenarios, respectively:

$$\frac{dN}{N\,p_t dp_t} = A\exp\left(-\frac{p_t}{T}\right), \tag{6.1}$$

and

$$\frac{dN}{N\,p_t dp_t} = A_1 \cdot \exp\left(-\frac{p_t}{T_1}\right) + A_2 \cdot \exp\left(-\frac{p_t}{T_2}\right). \tag{6.2}$$

Another possibility for fitting the transverse momentum spectra of hadrons could be the Gaussian function given below for the one-temperature and the two-temperature cases as

$$\frac{dN}{N\,p_t dp_t} = A\exp\left(-\frac{p_t^2}{T^2}\right), \tag{6.3}$$

and

$$\frac{dN}{N\,p_t dp_t} = A_1 \cdot \exp\left(-\frac{p_t^2}{T_1^2}\right) + A_2 \cdot \exp\left(-\frac{p_t^2}{T_2^2}\right), \tag{6.4}$$

respectively.

We fitted the total transverse momentum spectra of the negative pions in the whole p_t range in ^{12}C+^{12}C collisions at 4.2 *A* GeV/*c* by the two-temperature and the one-temperature Hagedorn and Boltzmann functions. The experimental p_t spectra of the negative pions produced in minimum bias ^{12}C+^{12}C collisions at 4.2*A* GeV/*c* per nucleon and the respective fits in the whole p_t range by the one-temperature and the two-temperature Hagedorn functions are presented in Fig. 6.2.

As can be seen from Fig. 6.2, the two-temperature Hagedorn function describes the total p_t spectra of the negative pions very well and much better compared to the one-temperature fit. The parameters extracted from fitting the total transverse momentum spectra of the negative pions in the whole range of p_t in $^{12}C+^{12}C$ collisions at 4.2 *A* GeV/*c* by the two-temperature and the one-temperature Hagedorn and Boltzmann functions are shown in Table 6.1.

Table 6.1

The parameters extracted from fitting the total transverse momentum spectra of the negative pions in the whole p_t range in $^{12}C^{12}C$ collisions at 4.2 *A* GeV/*c* by the two-temperature and the one-temperature Hagedorn and Boltzmann functions

Fitting Function	A_1, (GeV)$^{-1}$	T_1, MeV	A_2, (GeV)$^{-1}$	T_2, MeV	$\chi 2/n.d.f.$	R^2 factor
Two Temperature Hagedorn	3097 ± 353	**76 ± 3**	101 ± 38	**142 ± 7**	1.33	0.99
One Temperature Hagedorn	1355 ± 74	**99 ± 1**	N/A	**N/A**	8.17	0.94
Two Temperature Boltzmann	3088 ± 326	**65 ± 2**	95 ± 26	**127 ± 5**	1.40	0.99
One Temperature Boltzmann	1140 ± 62	**89 ± 1**	N/A	**N/A**	11.83	0.92

As can be seen from comparison of $\chi^2/n.d.f.$ and R^2 factor values in Table 6.1, the two-temperature Hagedorn and the two-temperature Boltzmann function fits describe the experimental spectra much better compared to the corresponding one-temperature fits. This result is in line with our recent papers [36, 38] and earlier works, where the transverse momentum as well as energy spectra of pions, produced in relativistic nuclear collisions, were characterized by the two-temperature shapes. In Ref. [73] the two-temperature shape of cm kinetic energy spectra of the negative pions in Ar+KCl collisions at 1.8 GeV/nucleon was revealed. In this work, the occurrence of two temperatures, T_1 and T_2, was explained as due to two channels of pion production: pions coming from Δ resonance decay (T_1), and directly produced pions (T_2). In Ref. [63] the two-temperature shape of kinetic energy spectrum of pions emitted at 90º in cms of central La+La collisions at 1.35 GeV/nucleon was interpreted as due to different contributions of deltas originated from the early and later stages of heavy ion reactions. The two-temperature behavior was also observed for cm energy as well as the p_t spectra of π^- mesons produced in Mg+Mg collisions [75] at incident momentum of 4.2–4.3 *A* GeV/*c*. In Ref. [78] the two-temperature shape of the experimental cm energy spectra of π^- mesons in ^{12}C+^{12}C collisions at 4.2 *A* GeV/*c* was explained by superposition of partial contributions of different sources (decays of resonances, direct reactions, *etc*.) analyzing the spectra of π^- mesons coming from different sources in the framework of QGSM.

Table 6.2

The spectral temperatures (*T*) of the negative pions in $^{12}C^{12}C$ collisions at 4.2 *A* GeV/*c* and their relative contributions (*R*) extracted in the present work from fitting their total transverse momentum spectra in the whole range of p_t by the two-temperature Hagedorn and Boltzmann functions compared to the corresponding values obtained in Ref. [78] from fitting the noninvariant cm energy spectra of the negative pions in $^{12}C^{12}C$ collisions at 4.2 *A* GeV/*c* by Maxwell-Boltzmann distribution function

Fitting Function	**T_1, MeV**	**R_1, %**	**T_2, MeV**	**R_2, %**	**$\chi2/n.d.f.$**	**R^2 factor**
Hagedorn	**76 ± 3**	85 ± 14	**142 ± 7**	15 ± 6	1.32	0.99
Boltzmann	**65 ± 2**	85 ± 13	**127 ± 5**	15 ± 4	1.40	0.99
Maxwell-Boltzmann	**83 ± 3**	79 ± 6	**145 ± 7**	21 ± 6	0.72	-----

The observed two-temperature shape of the transverse momentum spectrum of the negative pions produced in $^{12}C+^{12}C$ collisions at 4.2 *A* GeV/*c* could also be interpreted by the collective flow effects, as was mentioned earlier.

It is important to add that in Ref. [74] the spectral temperature $T = 98 \pm 2$ MeV was extracted from fitting the p_t spectra of the negative pions in $^{4}He+^{12}C$ collisions at 4.5 *A* GeV/*c* by the one-temperature Hagedorn function. This value of T practically coincides with the spectral temperature $T = 99 \pm 1$ MeV extracted from fitting the p_t spectra of π^- mesons in $^{12}C+^{12}C$ collisions at 4.2*A* GeV/*c* by the same one-temperature function and presented in Table 6.1.

The spectral temperatures (T_1, T_2) of π^- mesons in $^{12}C+^{12}C$ collisions at 4.2*A* GeV/*c* and their relative contributions (R_1, R_2) extracted in the present work from fitting the p_t spectra by the two-temperature Hagedorn and the two-temperature Boltzmann functions are given in Table 6.2. The corresponding results obtained in Ref. [78] from fitting the noninvariant cm energy spectra of the negative pions in $^{12}C+^{12}C$ collisions at the same initial momentum using two-temperature Maxwell-Boltzmann distribution function are also given for a comparison in this table. The relative contributions, *R*, of the two temperatures to the total negative pion multiplicity were calculated over the total transverse momentum interval ($R_i = c_i/(c_1+c_2)$, where $c_i = A_i \cdot \int (m_t T_i)^{1/2} \exp\left(-\frac{m_t}{T_i}\right) dp_t$ and $c_i = A_i \cdot \int (m_t \exp\left(-\frac{m_t}{T_i}\right) dp_t$ $(i = 1, 2)$ are for the case of Hagedorn and Boltzmann function fits, respectively). It is necessary to mention that the statistics of $^{12}C+^{12}C$ collisions used in Ref. [78] was 6806 inelastic collision events, which is about three times lesser compared to the statistics used in the present work. As observed from Table 6.2, the values of the spectral temperatures (T_1, T_2) extracted in the present work from fitting the p_t spectra by the two-temperature Hagedorn and the two-temperature Boltzmann functions proved to be noticeably lower compared to the corresponding values obtained in Ref. [78] from fitting the noninvariant cm energy spectra of the negative pions by Maxwell-Boltzmann distribution for $^{12}C+^{12}C$ collisions at 4.2*A* GeV/*c*. As observed from Table 6.2, the dominant contribution (R_1 ~ 85%) to the total π^- multiplicity in $^{12}C+^{12}C$ collisions is given by T_1 ~ (65–76) ± 3 MeV, which is compatible within the uncertainties with the results of the Ref. [78]. It is necessary to note that the fits by Boltzmann function result in somewhat lower values of the spectral temperatures T_1 and T_2 compared to those by Hagedorn function. However, as seen from Table 6.2, the values of the relative contributions (R_1 and R_2) for each temperature term coincided for both Hagedorn and Boltzmann function fits.

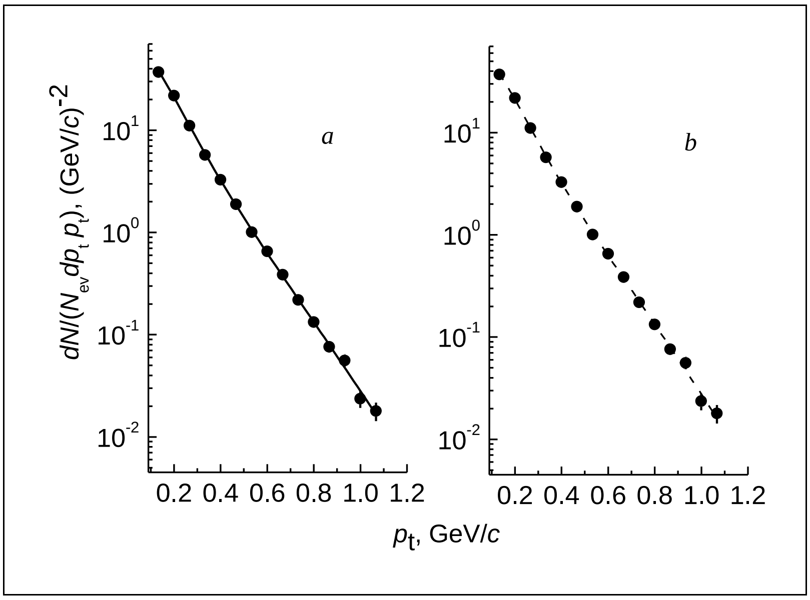

Fig. 6.3. The experimental transverse momentum spectra of the negative pions produced in minimum bias $^{12}C^{12}C$ (●) collisions at 4.2 GeV/*c* per nucleon and the corresponding fits in the range $p_t = 0.1 \div 1.2$ GeV/*c* by the two-temperature Hagedorn (solid line) and the two-temperature Boltzmann (dashed line) functions. All the spectra are normalized per one inelastic collision event

It is seen from Fig. 6.2 that the p_t spectrum of the negative pions with $p_t \leq 1.2$ GeV/*c* is characterized by sufficiently good statistics of π^- mesons, and therefore by quite low statistical errors. Due to the lower momentum threshold of detection of pions $p_{thresh} \approx 70$ MeV/*c*, it is natural to fit the transverse momentum spectra of the pions in range $p_t = 0.1 \div 1.2$ GeV/*c*, where pions are detected and measured with almost 100% efficiency. The transverse momentum spectra of the negative pions in this p_t range in minimum bias $^{12}C+^{12}C$ collisions at 4.2*A* GeV/*c* were fitted by various two-temperature functions.

Table 6.3

The parameters extracted from fitting the total transverse momentum spectra of negative pions in the range $p_t = 0.1 \div 1.2$ GeV/*c* in $^{12}C^{12}C$ collisions at 4.2*A* GeV/*c* by various two-temperature functions (the units of A_1 and A_2 are $(GeV)^{-1}$ in case of Hagedorn and Boltzmann function fits and dimensionless in case of Simple exponential and Gaussian function fits wherever appropriate in the tables that follow)

Fitting function	A_1	T_1, MeV	A_2	T_2, MeV	$\chi2/n.d.f.$	R^2 factor
Hagedorn	6464 ± 2250	**59 ± 6**	378 ± 110	**119 ± 5**	0.44	0.99
Boltzmann	5317 ± 1395	**54 ± 4**	252 ± 63	**111 ± 4**	0.42	0.99
Simple exponential	105 ± 22	**86 ± 19**	44 ± 34	**136 ± 14**	0.61	0.99
Gaussian	4 ± 1	**439 ± 8**	45 ± 3	**212 ± 6**	1.74	0.99

The parameters extracted from fitting the total transverse momentum spectra of the negative pions in range $p_t = 0.1 \div 1.2$ GeV/*c* in $^{12}C+^{12}C$ collisions at 4.2*A* GeV/*c* by these two-temperature functions are given in Table 6.3. As seen from Tables 6.1 and 6.3, the values of T_1 and T_2 extracted from fitting the p_t spectra of the negative pions in range $p_t = 0.1 \div 1.2$ GeV/*c* by the two-temperature Hagedorn and Boltzmann functions are noticeably lower than the corresponding temperature values extracted from fitting in the whole p_t range. This is likely due to the influence of the high p_t tail of the spectrum to the extracted values of the spectral temperatures in case of the fitting in the whole p_t range. It is seen from Table 6.3 that the fits by Hagedorn and Boltzmann functions result in physically acceptable values of T_1 and T_2 with quite small $\chi^2/n.d.f.$ values. The fitting with Simple Exponential function gives significantly larger values of T_1 and T_2 compared to the fits with Hagedorn and Boltzmann functions. The fitting with Gaussian function, as observed from Table 6.3, leads to very large and physically unacceptable values of T_1 and T_2 with the relatively high $\chi^2/n.d.f.$ values.

Table 6.4

Fractions of central, semicentral, and peripheral $^{12}C^{12}C$ collisions at 4.2 GeV/*c* per nucleon relative to the total inelastic cross section

Peripheral collisions (%)		Semicentral collisions		Central collisions (%)	
Experiment	**QGSM**	**Experiment**	**QGSM**	**Experiment**	**QGSM**
58±1	62±1	31±1	30±1	11±1	8±1

Table 6.5

The parameters extracted from fitting the transverse momentum spectra of the negative pions in the range $p_t = 0.1 \div 1.2$ GeV/*c* in peripheral, semicentral, and central $^{12}C^{12}C$ collisions at 4.2*A* GeV/*c* by various two-temperature functions

Fitting function	Collision type	A_1	T_1, MeV	A_2	T_2, MeV	$\chi2/n.d.f.$
Hagedorn	Peripheral	3437 ± 1415	**58 ± 7**	189 ± 82	**117 ± 7**	0.44
	Semicentral	9767 ± 3798	**58 ± 6**	526 ± 183	**121 ± 6**	0.24
	Central	12800 ± 5501	**62 ± 9**	1013 ± 487	**118 ± 8**	1.10
Boltzmann	Peripheral	2864 ± 903	**53 ± 5**	130 ± 47	**108 ± 6**	0.42
	Semicentral	8054 ± 2381	**53 ± 4**	360 ± 107	**111 ± 5**	0.25
	Central	11114 ± 3536	**56 ± 6**	671 ± 265	**109 ± 6**	1.05
Simple exponential	Peripheral	57 ± 16	**88 ± 23**	17 ± 25	**137 ± 26**	0.58
	Semicentral	159 ± 34	**88 ± 20**	53 ± 54	**140 ± 19**	0.31
	Central	208 ± 173	**91 ± 41**	121 ± 223	**132 ± 28**	1.30
Gaussian	Peripheral	2 ± 1	**418 ± 10**	24 ± 2	**201 ± 7**	1.02
	Semicentral	6 ± 1	**432 ± 9**	67 ± 5	**206 ± 6**	1.49
	Central	11 ± 1	**432 ± 11**	110 ± 8	**212 ± 7**	1.23

The experimental transverse momentum spectrum of the negative pions produced in minimum bias $^{12}C+^{12}C$ collisions at 4.2 GeV/*c* per nucleon and the corresponding fits in the range $p_t = 0.1 \div 1.2$ GeV/c by the two-temperature Hagedorn and the two-temperature Boltzmann functions is presented in Fig. 6.3. As can be seen from Fig. 6.3, the two-temperature Hagedorn and the two-temperature Boltzmann functions fit very well the p_t spectrum of the negative pions in $^{12}C+^{12}C$ collisions.

It seems interesting to analyze quantitatively the change in the shape of transverse momentum spectra of the pions with increase in the collision centrality, which corresponds to decrease of the impact parameter of collision. We followed the method, described in subchapter 2.4 of the present dissertation, to select the central, semicentral, and peripheral collision events. Fractions of central, semicentral, and peripheral $^{12}C+^{12}C$ collision events, relative to the total inelastic cross section, obtained for both experimental and QGSM data are presented in Table 6.4.

The p_t spectra of the negative pions in peripheral, semicentral, and central $^{12}C+^{12}C$ collision events in range $p_t = 0.1 \div 1.2$ GeV/c were fitted by the above two-temperature functions given in expressions (2.27), (2.29), (6.2), and (6.4). The parameters extracted from fitting the transverse momentum spectra of the negative pions in range $p_t = 0.1 \div 1.2$ GeV/c in peripheral, semicentral, and central $^{12}C+^{12}C$ collisions at 4.2*A* GeV/c by various two-temperature functions are given in Table 6.5. As observed from Table 6.5, the values of T_1 and T_2 extracted from fitting the p_t spectra by the two-temperature Hagedorn and the two-temperature Boltzmann functions coincide with each other within the errors for peripheral, semicentral, and central $^{12}C+^{12}C$ collisions, and thus do not depend on the collision centrality.

Such independence on the collision centrality of the spectral temperatures extracted from fitting in the whole range of the energy and p_t spectra of the negative pions by the two-temperature Maxwell-Boltzmann distribution and Hagedorn functions, respectively, in $^{12}C+^{12}C$ collisions at 4.2*A* GeV/c was also obtained earlier in Refs. [36, 78]. As observed from Table 6.5, the fitting with

Gaussian function leads to very large and physically unacceptable values of the spectral temperatures.

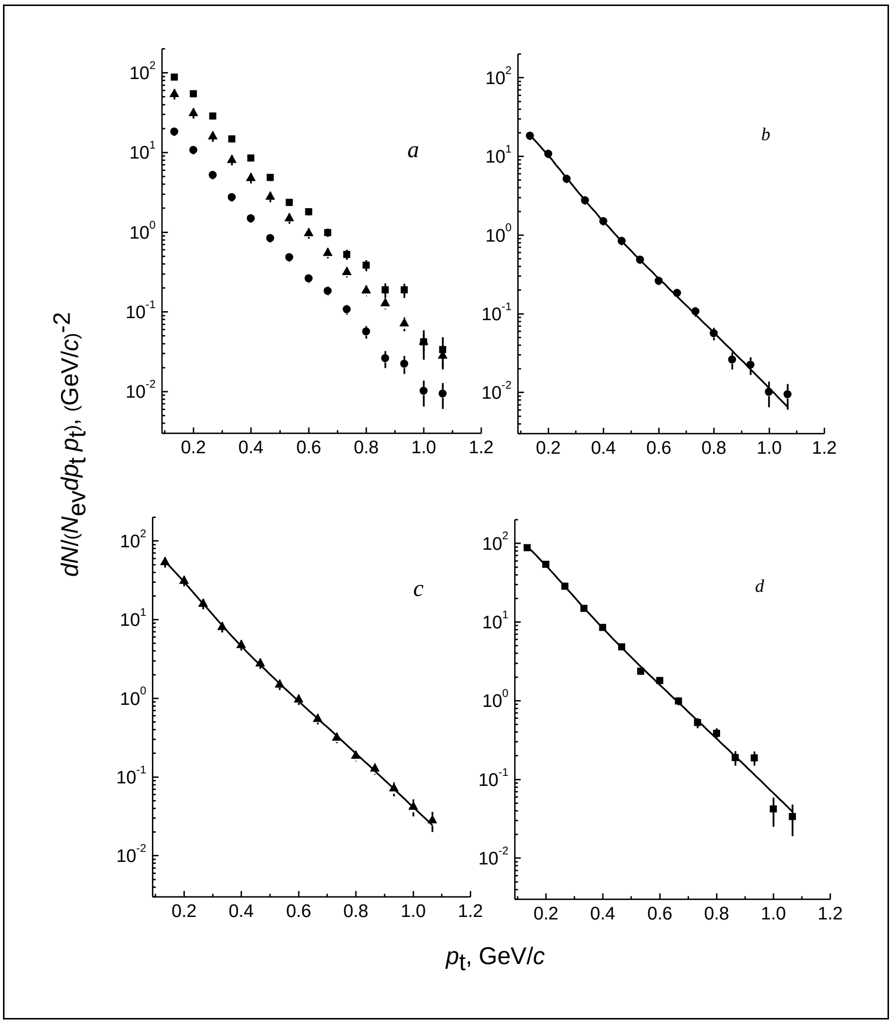

Fig. 6.4. The experimental transverse momentum spectra of the negative pions produced in peripheral (●) ((a) and (b)), semicentral (▲) ((a) and (c)), and central (■) ((a) and (d)) $^{12}C^{12}C$ collisions at 4.2 GeV/*c* per nucleon and the corresponding fits in the range $p_t = 0.1 \div 1.2$ GeV/*c* by the two-temperature Boltzmann function (solid lines). All the spectra are normalized per one inelastic collision event

The experimental transverse momentum spectra of the negative pions produced in peripheral, semicentral, and central ^{12}C+^{12}C collisions at 4.2 GeV/*c* per nucleon and the corresponding fits in range $p_t = 0.1 \div 1.2$ GeV/*c* by the two-temperature Boltzmann function are given in Fig. 6.4. As can be seen from Fig. 6.4, the two-temperature Boltzmann function again fits very well the p_t spectra of the negative pions in peripheral, semicentral, and central $^{12}C+^{12}C$ collisions.

Table 6.6

The parameters extracted from fitting the transverse momentum spectra of negative pions in the range $p_t = 0.1 \div 1.2$ GeV/*c* in $^{12}C+^{12}C$ collisions at 4.2 *A* GeV/*c* by various two-temperature functions for different pion rapidity ranges

Fitting function	Rapidity range	A_1	T_1, MeV	A_2	T_2, MeV	$\chi2/n.d.f.$
Hagedorn	$y_{cm.} \le -0.3$	8463 ± 4016	**53 ± 6**	421 ± 131	**113 ± 5**	0.83
	$\lvert y_{cm.} \rvert \le 0.3$	1896 ± 506	**78 ± 10**	137 ± 109	**142 ± 15**	0.47
	$y_{cm.} \ge 0.3$	10722 ± 6542	**49 ± 8**	661 ± 213	**102 ± 4**	1.04
Boltzmann	$y_{cm.} \le -0.3$	6521 ± 2275	**49 ± 4**	279 ± 78	**105 ± 4**	0.79
	$\lvert y_{cm.} \rvert \le 0.3$	1842 ± 409	**68 ± 6**	109 ± 58	**129 ± 10**	0.42
	$y_{cm.} \ge 0.3$	8094 ± 3502	**46 ± 5**	424 ± 125	**95 ± 4**	1.01
Simple exponential	$y_{cm.} \le -0.3$	95 ± 25	**73 ± 22**	53 ± 29	**126 ± 10**	1.00
	$\lvert y_{cm.} \rvert \le 0.3$	74 ± 9	**122 ± 16**	2 ± 14	**212 ± 205**	0.78
	$y_{cm.} \ge 0.3$	80 ± 33	**69 ± 35**	78 ± 46	**113 ± 9**	1.15
Gaussian	$y_{cm.} \le -0.3$	4 ± 1	**413 ± 9**	44 ± 3	**196 ± 6**	1.52
	$\lvert y_{cm.} \rvert \le 0.3$	3 ± 1	**476 ± 14**	28 ± 2	**235 ± 8**	0.62
	$y_{cm.} \ge 0.3$	5 ± 1	**384 ± 8**	47 ± 4	**189 ± 6**	1.46

It seems interesting also to analyze quantitatively the change in the shape of the p_t spectra of the negative pions with the change of the pion rapidity range. We extracted and fitted, using the above two-temperature functions, the transverse momentum spectra of π^- mesons for three different rapidity intervals in the nucleon-nucleon cms at 4.2 GeV/*c*: $y_{cm} \le -0.3$, $\lvert y_{cm.} \rvert \le 0.3$, and $y_{cm.} \ge 0.3$, which can roughly be classified as target fragmentation, midrapidity, and projectile fragmentation regions, respectively. The parameters extracted from fitting the transverse momentum spectra of the negative pions in range $p_t = 0.1 \div 1.2$ GeV/*c* in $^{12}C+^{12}C$ collisions at 4.2 *A* GeV/*c* by the above mentioned two-temperature functions for different pion rapidity intervals are presented in Table 6.6. It can be noted again that the fitting by Gaussian function results in large and physically unacceptable values of the spectral temperatures. As seen from Table 6.6, the absolute values of T_1 and T_2 were found to be noticeably larger for the midrapidity region than those for the target and projectile fragmentation regions for all the fitting functions, except for Simple Exponential function. This is in agreement with the results of the earlier works [148, 149]: with an increase in transverse momentum of π^- mesons in (p, d, α, C)+C and (d, α, C)+Ta collisions at 4.2 A GeV/c, the fraction of the negative pions in central rapidity region increased and the corresponding fraction in the fragmentation region of colliding nuclei decreased. Central rapidity (or midrapidity) interval was mostly populated with the negative pions with large transverse momenta [148, 149]. The larger spectral temperatures T_1 and T_2 in cm midrapidity region compared to the target and projectile fragmentation regions observed in the present analysis are in agreement with our earlier finding for the average spectral temperatures [38]. The reason for this is that the pions in central rapidity region are produced predominantly in central hard $^{12}C+^{12}C$ collisions, and hence at higher temperatures, as compared to the pions in region of fragmentation of colliding nuclei originated mostly in peripheral soft $^{12}C+^{12}C$ interactions, and hence at lower temperatures [38].

The experimental transverse momentum spectra of the negative pions for the analyzed three rapidity intervals in $^{12}C+^{12}C$ collisions at 4.2 A GeV/c per nucleon and the corresponding fits in range $p_t = 0.1 \div 1.2$ GeV/c by the two-temperature Hagedorn function are presented in Fig. 6.5. As observed from Fig. 6.5, the p_t spectra of the negative pions in peripheral, semicentral, and central $^{12}C+^{12}C$ collisions are described very well by the two-temperature Hagedorn function.

To check the influence of the fitting range of p_t on the extracted values of T_1 and T_2, the total p_t spectra of the negative pions and the respective spectra of π^- mesons for different $^{12}C+^{12}C$ collision centralities and three rapidity regions were also fitted in range $p_t = 0.1 \div 0.7$ GeV/c. The parameters extracted from fitting the total p_t spectra of π^- mesons in range $p_t = 0.1 \div 0.7$ GeV/*c* in ^{12}C+^{12}C collisions at 4.2 *A* GeV/*c* by the considered two-temperature functions are presented in Table 6.7.

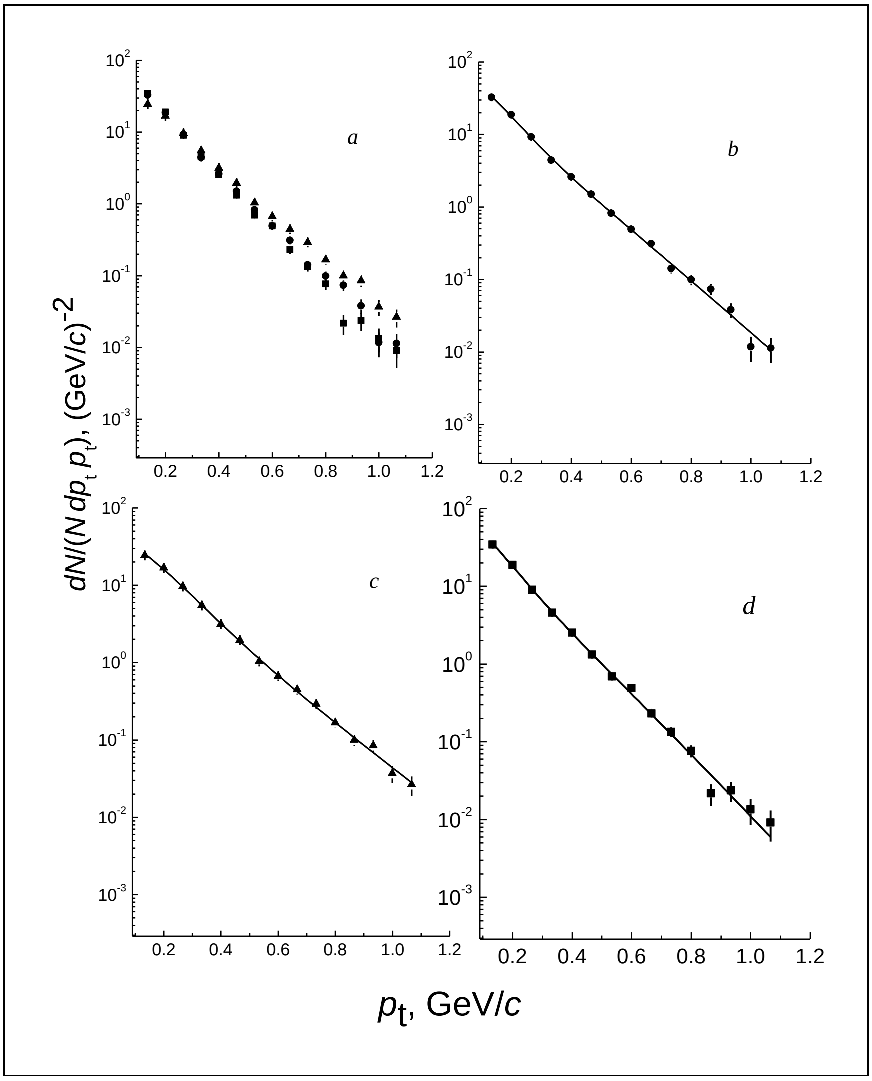

Fig. 6.5. The experimental transverse momentum spectra of the negative pions for rapidity range $y_{cm} \le -0.3$ (●) ((a) and (b)), for rapidity range $|y_{cm.}| \le 0.3$ (▲) ((a) and (c)), and for rapidity range $y_{cm.} \ge 0.3$ (■) ((a) and (d)) in ^{12}C^{12}C collisions at 4.2 GeV/*c* per nucleon and the corresponding fits in the range $p_t = 0.1 \div 1.2$ GeV/*c* by the two-temperature Hagedorn function (solid lines). All the spectra are normalized per one negative pion

It is seen from comparison of Tables 6.3 and 6.7 that the values of the spectral temperatures T_1 and T_2 are compatible within the uncertainties for the fitting ranges $p_t = 0.1 \div 0.7$ GeV/*c* and $p_t = 0.1 \div 1.2$ GeV/*c* for the case of Hagedorn and Boltzmann function fits.

Table 6.7

The parameters extracted from fitting the total transverse momentum spectra of the negative pions in the range $p_t = 0.1 \div 0.7$ GeV/*c* in $^{12}C+^{12}C$ collisions at 4.2 *A* GeV/*c* by various two-temperature functions

Fitting	***A₁***	***T₁*, MeV**	***A₂***	***T₂*, MeV**	***χ2/n.d.f.***
Hagedorn	5461 ± 2189	**64 ± 10**	216 ± 259	**131 ± 26**	0.35
Boltzmann	5006 ± 1679	**56 ± 7**	201 ± 162	**115 ± 15**	0.33
Simple	134 ± 15	**105 ± 10**	0.573 ± 3.4	**499 ± 199**	0.53
Gaussian	7 ± 1	**386 ± 15**	49 ± 4	**191 ± 9**	0.70

Table 6.8

The parameters extracted from fitting the transverse momentum spectra of the negative pions in the range $p_t = 0.1 \div 0.7$ GeV/*c* in peripheral, semicentral, and central $^{12}C^{12}C$ collisions at 4.2 *A* GeV/*c* by various two-temperature functions

Fitting function	**Collision type**	***A₁***	***T₁*, MeV**	***A₂***	***T₂*, MeV**	***χ2/n.d.f.***
Hagedorn	Peripheral	2735 ± 1127	**65 ± 11**	79 ± 130	**136 ± 39**	0.31
	Semicentral	10156 ± 5741	**58 ± 11**	531 ± 480	**121 ± 18**	0.38
	Central	9194 ± 2986	**74 ± 10**	116 ± 325	**174 ± 103**	0.76
Boltzmann	Peripheral	2531 ± 904	**56 ± 7**	84 ± 90	**116 ± 21**	0.31
	Semicentral	8895 ± 3931	**52 ± 7**	421 ± 285	**109 ± 12**	0.35
	Central	8838 ± 2587	**63 ± 8**	204 ± 334	**135 ± 42**	0.76
Simple exponential	Peripheral	60 ± 4	**110 ± 2**	--	**--**	1.06
	Semicentral	191 ± 39	**98 ± 27**	12 ± 67	**185 ± 216**	0.55
	Central	286 ± 19	**115 ± 2**	--	**--**	1.18
Gaussian	Peripheral	4 ± 1	**378 ± 19**	25 ± 2	**187 ± 10**	0.62
	Semicentral	12 ± 2	**377 ± 15**	72 ± 7	**184 ± 9**	0.46
	Central	16 ± 4	**399 ± 26**	112 ± 10	**202 ± 11**	1.03

One can see from Table 6.7 that the values of the spectral temperatures extracted from fitting with the two-temperature Simple Exponential and the two-temperature Gaussian functions are again too large to be acceptable for the colliding system and collision energy under consideration.

The parameters extracted from fitting the transverse momentum spectra of the negative pions in the range $p_t = 0.1 \div 0.7$ GeV/*c* in peripheral, semicentral, and central $^{12}C+^{12}C$ collisions at 4.2 *A* GeV/*c* by the above given two-temperature functions are presented in Table 6.8. As observed from Table 6.8, the absolute values of the spectral temperatures T_1 and T_2 for central $^{12}C+^{12}C$ collisions were consistently higher as compared to the corresponding temperatures for peripheral and semicentral collisions.

Table 6.9

The parameters extracted from fitting the transverse momentum spectra of the negative pions in the range $p_t = 0.1 \div 0.7$ GeV/*c* in $^{12}C^{12}C$ collisions at 4.2*A* GeV/*c* by the various two-temperature functions for different pion rapidity ranges

Fitting function	Rapidity range	A_1	T_1, MeV	A_2	T_2, MeV	χ2/n.d.f.
Hagedorn	$y_{cm.} \leq -0.3$	6639 ± 3151	**59 ± 9**	224 ± 232	**126 ± 22**	0.40
	$\lvert y_{cm.} \rvert \leq 0.3$	1155 ± 96	**101 ± 2**	---	**---**	1.63
	$y_{cm.} \geq 0.3$	7735 ± 4112	**56 ± 10**	349 ± 354	**114 ± 18**	0.71
Boltzmann	$y_{cm.} \leq -0.3$	5780 ± 2241	**52 ± 6**	193 ± 146	**112 ± 15**	0.37
	$\lvert y_{cm.} \rvert \leq 0.3$	1020 ± 79	**89 ± 1**	---	**---**	2.87
	$y_{cm.} \geq 0.3$	6636 ± 2827	**50 ± 6**	275 ± 207	**102 ± 12**	0.69
Simple exponential	$y_{cm.} \leq -0.3$	131 ± 14	**97 ± 15**	3 ± 13	**238 ± 316**	0.62
	$\lvert y_{cm.} \rvert \leq 0.3$	77 ± 5	**128 ± 3**	---	**---**	0.78
	$y_{cm.} \geq 0.3$	140 ± 17	**93 ± 20**	6 ± 33	**180 ± 221**	0.87
Gaussian	$y_{cm.} \leq -0.3$	7 ± 1	**378 ± 16**	47 ± 4	**182 ± 9**	0.49
	$\lvert y_{cm.} \rvert \leq 0.3$	5 ± 2	**423 ± 36**	30 ± 2	**220 ± 14**	0.48
	$y_{cm.} \geq 0.3$	7 ± 1	**363 ± 15**	49 ± 4	**181 ± 8**	0.94

The parameters extracted from fitting the transverse momentum spectra of the negative pions in range $p_t = 0.1 \div 0.7$ GeV/*c* in $^{12}C+^{12}C$ collisions at 4.2 *A* GeV/*c* by the same two-temperature functions for different pion rapidity ranges are given in Table 6.9. The fitting of the p_t spectra of π^- mesons coming from midrapidity range ($|y_{cm.}| \le 0.3$) with the two-temperature Hagedorn, Boltzmann, and Simple Exponential functions resulted in the negative values of the parameter A_2 with the extracted temperatures T_2 practically coinciding with the corresponding values of T_1. Therefore it was natural for these three cases to fit the p_t spectra of π^- from midrapidity range with the one-temperature functions. As seen from Tables 6.6 and Table 6.9, the extracted values of the spectral temperatures T_1 and T_2 practically coincided for the target and projectile fragmentation regions. The obvious reason for this is the symmetry of the colliding $^{12}C+^{12}C$ system with identical target and projectile nuclei.

§ 6.2. P_t distributions of negative pions in $^{12}C^{181}Ta$ collisions

To examine quantitatively the change in the shape of the p_t spectra of π^- mesons in $^{12}C+^{181}Ta$ collisions at 4.2 *A* GeV/*c* with the change of the collision centrality and pion rapidity range, all the extracted p_t spectra were fitted [32] by four different functions commonly used for describing the hadron spectra.

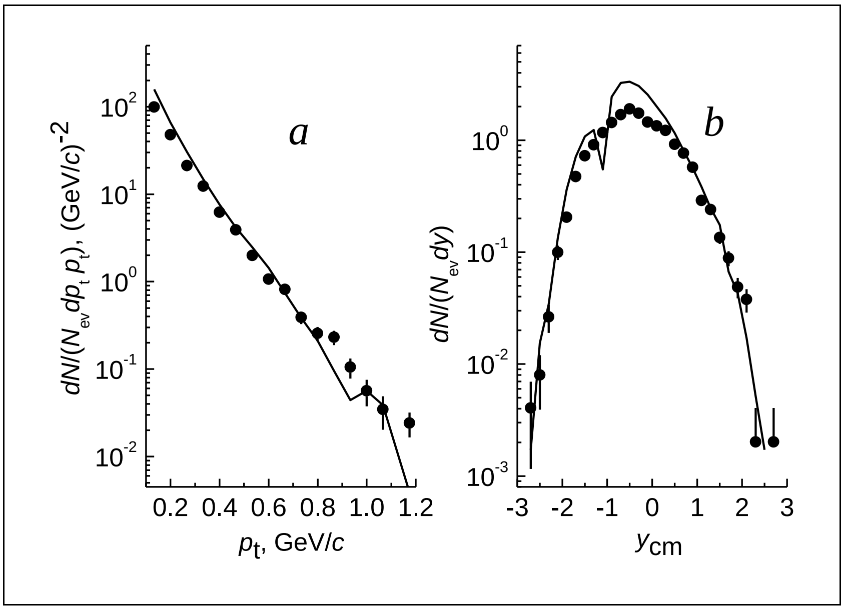

Fig. 6.6. The experimental transverse momentum (a) and rapidity (b) spectra of negative pions produced in minimum bias $^{12}C^{181}Ta$ (●) collisions at 4.2 GeV/*c* per nucleon. The corresponding calculated QGSM spectra are given by the solid lines. All the spectra are normalized per one inelastic collision event

It is also of interest to check which of these commonly used functions would be more appropriate for fitting the transverse momentum spectra of the negative pions.

The total transverse momentum and rapidity distributions of the negative pions in minimum bias $^{12}C+^{181}Ta$ collisions at a momentum of 4.2 GeV/*c* per nucleon are shown in Fig. 6.6. As seen from Fig. 6.6*a*, the experimental transverse momentum spectrum of π^- mesons is described satisfactorily by the QGSM [132, 133] calculations. The rapidity spectrum in Fig. 6.6*b* is plotted in cms of nucleon–nucleon collisions at 4.2 GeV/*c* (the rapidity of the cms of nucleon–nucleon collision is $y_{cms} \approx 1.1$ at this incident momentum).

It was observed earlier [20] that the fitting of the p_t spectrum of π^- in $d+^{12}C$, $^4He+^{12}C$, and $^{12}C+^{12}C$ collisions at 4.2*A* GeV/*c* with the two-temperature Hagedorn function resulted in the lower spectral temperatures T_1 and T_2 for both QGSM and Modified FRITIOF model spectra as compared to the experimental ones. As seen from Fig. 6.6*b*, QGSM describes satisfactorily the experimental rapidity spectrum of π^- mesons in $^{12}C+^{181}Ta$ collisions.

In the present analysis we fitted the transverse momentum spectra of π^- mesons produced in $^{12}C+^{181}Ta$ collisions at a momentum of 4.2 GeV/*c* per nucleon by four different functions commonly used for describing the p_t spectra of hadrons**.** We used one-temperature Hagedorn, Boltzmann, Simple exponential, and Gaussian functions and the corresponding two-temperature functions given in expressions (2.26), (2.28), (6.1), and (6.3), and in expressions (2.27), (2.29), (6.2), and (6.4), respectively.

We fitted the total transverse momentum spectra of the negative pions in the whole range of p_t in $^{12}C+^{181}Ta$ collisions at 4.2 *A* GeV/*c* by the two-temperature and the one-temperature Hagedorn and Boltzmann functions. The experimental transverse momentum spectra of the negative pions produced in minimum bias $^{12}C+^{181}Ta$ collisions at 4.2 *A* GeV/*c* per nucleon and the corresponding fits in the whole p_t range by the one-temperature and the two-temperature Hagedorn functions are given in Fig. 6.7. As can be seen from Fig. 6.7, the two-temperature Hagedorn function fits the total p_t spectra of the negative pions very well as compared to the one-temperature fit. Parameters extracted from fitting the total transverse momentum spectra of the negative pions in the whole range of p_t in $^{12}C+^{181}Ta$ collisions at 4.2 *A* GeV/*c* by the two-temperature and the one-temperature Hagedorn and Boltzmann functions are presented in Table 6.10.

As can be seen from comparison of $\chi^2/n.d.f.$ and R^2 factor values in Table 6.10, the two-temperature Hagedorn and the two-temperature Boltzmann function fits describe the experimental spectra much better as compared to the one-temperature fits. This is in agreement with our recent papers [36, 38] and earlier works [63, 73, 75, 78], where the transverse momentum as well as energy spectra of pions, produced in relativistic nuclear collisions, were characterized by the two-temperature shapes.

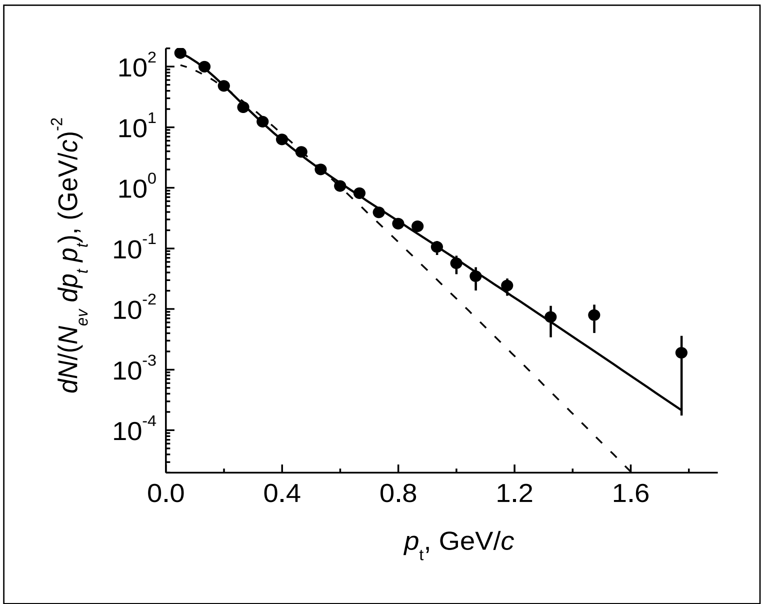

Fig. 6.7. The experimental transverse momentum spectra (●) of the negative pions produced in minimum bias $^{12}C^{181}Ta$ collisions at 4.2 GeV/*c* per nucleon and the corresponding fits in the whole p_t range by the one-temperature (dashed line) and the two-temperature (solid line) Hagedorn functions. All the spectra are normalized per one inelastic collision event

The spectral temperatures (T_1, T_2) of π^- mesons in ^{12}C+^{181}Ta collisions at 4.2A GeV/c and their relative contributions (R_1, R_2) extracted in the present work from fitting the p_t spectra by the two-temperature Hagedorn and the two-temperature Boltzmann functions are presented in Table 6.11. The corresponding results obtained in Ref. [78] from fitting the non-invariant cm energy spectra of the negative pions in ^{12}C+^{181}Ta collisions at the same initial momentum using two-temperature Maxwell-Boltzmann distribution function are also shown for a comparison in this table.

Table 6.10

The parameters extracted from fitting the total transverse momentum spectra of negative pions in the whole range of p_t in ^{12}C^{181}Ta collisions at 4.2 A GeV/c by the two-temperature and the one-temperature Hagedorn and Boltzmann functions

Fitting Function	A_1, (GeV)$^{-1}$	T_1, MeV	A_2, (GeV)$^{-1}$	T_2, MeV	$\chi2/n.d.f.$
Two Temperature Hagedorn	21715 ± 4335	**57 ± 3**	494 ± 149	**128 ± 6**	0.93
One Temperature Hagedorn	5040 ± 391	**88 ± 1**	N/A	**N/A**	7.79
Two Temperature Boltzmann	19069 ± 3229	**50 ± 2**	385 ± 98	**116 ± 5**	1.02
One Temperature Boltzmann	4296 ± 322	**78 ± 1**	N/A	**N/A**	10.03

It should be mentioned that the statistics of ^{12}C+^{181}Ta collisions used in Ref. [78] was 1989 inelastic collisions, which is about 20% lesser compared to the statistics used in the present analysis. As seen from Table 6.11, the values of the spectral temperatures (T_1, T_2) extracted in the present work from fitting the p_t spectra by the two-temperature Hagedorn and the two-temperature Boltzmann functions proved to be noticeably lower compared to the corresponding values obtained in Ref. [78]

from fitting the noninvariant cm energy spectra of negative pions by Maxwell-Boltzmann distribution for $^{12}C+^{181}Ta$ collisions at 4.2 *A* GeV/*c*. Especially the value of T_2 obtained in Ref. [78] seems to be quite high for such relatively small collision energy.

Table 6.11

The spectral temperatures (*T*) of the negative pions in $^{12}C^{181}Ta$ collisions at 4.2 *A* GeV/*c* and their relative contributions (*R*) extracted in the present work from fitting their total transverse momentum spectra in the whole range of p_t by the two-temperature Hagedorn and Boltzmann functions compared to the corresponding values obtained in Ref. [78] from fitting the noninvariant cm energy spectra of the negative pions by Maxwell-Boltzmann distribution function for $^{12}C^{181}Ta$ collisions at 4.2 *A* GeV/*c*

Fitting Function	T_1, MeV	R_1, %	T_2, MeV	R_2, %	$\chi2/n.d.f.$	R^2 factor
Hagedorn	**57 ± 3**	80 ± 22	**128 ± 6**	20 ± 7	0.92	0.99
Boltzmann	**50 ± 2**	83 ± 20	**116 ± 5**	17 ± 5	1.02	0.99
Maxwell-Boltzmann	**66 ± 2**	88 ± 3	**159 ± 6**	12 ± 3	0.58	N/A

This is likely due to the influence of longitudinal motion on the energy spectra of π^- mesons, whereas p_t spectra are Lorentz invariant with respect to longitudinal boosts. As seen from Table 6.11, the dominant contribution (R_1 ~ 80–83%) to the total π^- multiplicity in $^{12}C+^{181}Ta$ collisions is given by T_1 ~ (50–57) ± 3 MeV, which is compatible within the uncertainties with the results of the Ref. [78]. It is worth mentioning that the fits by Boltzmann function give slightly lower values of the spectral temperatures compared to those by Hagedorn function.

It is evident from Fig. 6.7 that the p_t spectrum of the negative pions with $p_t \leq 1.2$ GeV/*c* is characterized by a good enough statistics of π^- and therefore by sufficiently low statistical errors. Due to the lower momentum threshold of detection of pions $p_{thresh} \approx 80$ MeV/c, it is natural to fit the transverse momentum spectra of the pions in the range $p_t = 0.1 \div 1.2$ GeV/c, where pions are detected and measured with almost 100% efficiency. We fitted the transverse momentum spectra of π^- in this p_t range in minimum bias ^{12}C+^{181}Ta collisions at 4.2A GeV/c by different two-temperature functions.

Table 6.12

The parameters extracted from fitting the total transverse momentum spectra of the negative pions in the range $p_t = 0.1 \div 1.2$ GeV/*c* in ^{12}C^{181}Ta collisions at 4.2 *A* GeV/*c* by various two-temperature functions (the units of A_1 and A_2 are (GeV)$^{-1}$ in case of Hagedorn and Boltzmann function fits and dimensionless in case of Simple exponential and Gaussian function fits wherever appropriate in the tables that follow)

Fitting function	A_1	T_1, MeV	A_2	T_2, MeV	$\chi 2/n.d.f.$	R^2 factor
Hagedorn	28312 ± 10614	**53 ± 5**	641 ± 204	**123 ± 6**	0.91	0.99
Boltzmann	21121 ± 6359	**49 ± 3**	449 ± 127	**113 ± 5**	1.02	0.99
Simple exponential	417 ± 72	**76 ± 10**	67 ± 35	**144 ± 12**	0.73	0.99
Gaussian	8 ± 1	**436 ± 11**	121 ± 10	**196 ± 6**	3.03	0.97

Parameters extracted from fitting the total transverse momentum spectra of the negative pions in the range $p_t = 0.1 \div 1.2$ GeV/c in ^{12}C+^{181}Ta collisions at 4.2 A GeV/c by different two-temperature functions are presented in Table 6.12. As seen from Tables 6.10 and 6.12, the values of T_1 and T_2 obtained from fitting the p_t spectra of the negative pions in the range $p_t = 0.1 \div 1.2$ GeV/c by the two-temperature Hagedorn and Boltzmann functions are compatible within the uncertainties with the corresponding temperature values extracted from fitting in the whole p_t range. It is observed from Table 6.12 that the fits by Hagedorn and Boltzmann functions give reasonably acceptable values for T_1 and T_2 with quite small values of $\chi^2/n.d.f.$. The fitting with Simple Exponential function leads to significantly higher values of T_1 and T_2 compared to the fits with Hagedorn and Boltzmann functions. Moreover, the fitting with Gaussian function results in too large and unphysical values of T_1 and T_2 with quite high value of $\chi^2/n.d.f.$.

The experimental transverse momentum spectrum of the negative pions produced in minimum bias ^{12}C+^{181}Ta collisions at 4.2 GeV/c per nucleon and the corresponding fits in the range $p_t = 0.1 \div 1.2$ GeV/c by the two-temperature Hagedorn and the two-temperature Boltzmann functions is presented in Fig. 6.8. As seen from Fig. 6.8, the two-temperature Hagedorn and the two-temperature Boltzmann functions fit very well the p_t spectrum of the negative pions in ^{12}C+^{181}Ta collisions.

It is of interest to analyze quantitatively the change in the shape of transverse momentum spectra of the pions with increase in the collision centrality, which corresponds to decrease of the impact parameter of collision. We followed the method, described in subchapter 2.4 of the present dissertation, to select the central, semicentral, and peripheral collision events. Fractions of central, semicentral, and peripheral ^{12}C+^{181}Ta collision events, relative to the total inelastic cross section, obtained for both experimental and QGSM data are presented in Table 6.13. As seen from Table 6.13, the experimental and corresponding model fractions of peripheral and central ^{12}C+^{181}Ta collision events coincide with each other within the two standard errors. However, the fraction of semicentral ^{12}C+^{181}Ta collision is slightly overestimated by QGSM.

We fitted the p_t spectra of the negative pions in peripheral, semicentral, and central ^{12}C+^{181}Ta collision events in the range $p_t = 0.1 \div 1.2$ GeV/c by the above given two-temperature functions. The parameters extracted from fitting the transverse momentum spectra of the negative pions in the range $p_t = 0.1 \div 1.2$

GeV/c in peripheral, semicentral, and central ^{12}C+^{181}Ta collisions at 4.2 A GeV/c by various two-temperature functions are given in Table 6.14. As seen from Table 6.14, the fits of the p_t spectra by the two-temperature Hagedorn and the two-temperature Boltzmann functions are compatible with each other within the errors for peripheral, semicentral, and central ^{12}C+^{181}Ta collisions.

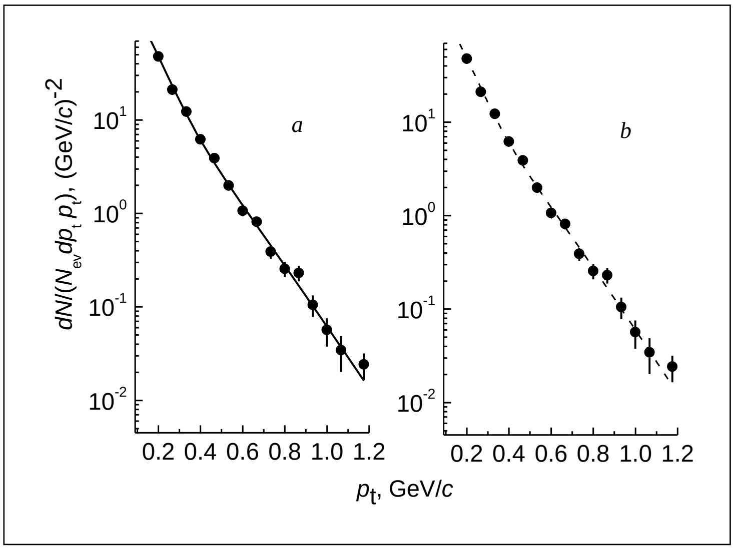

Fig. 6.8. The experimental transverse momentum spectrum of the negative pions produced in minimum bias ^{12}C+^{181}Ta (●) collisions at 4.2 GeV/*c* per nucleon and the corresponding fits in the range $p_t = 0.1 \div 1.2$ GeV/*c* by the two-temperature Hagedorn (solid line) and the two-temperature Boltzmann (dashed line) functions. All the spectra are normalized per one inelastic collision event

The experimental transverse momentum spectra of the negative pions produced in peripheral, semicentral, and central ^{12}C+^{181}Ta collisions at 4.2 GeV/c per nucleon and the corresponding fits in the range $p_t = 0.1 \div 1.2$ GeV/c by the two-temperature Boltzmann function are given in Fig. 6.9. As observed from Fig. 6.9*a*, the p_t spectra of the negative pions for the central and semicentral ^{12}C+^{181}Ta collisions are located considerably above the corresponding spectrum for the peripheral ^{12}C+^{181}Ta collisions.

This result could be understood if we recall that in case of central $^{12}C+^{181}Ta$ collisions, the collision energy is distributed among significantly larger number of pions (due to a larger number of nucleon-nucleon collisions) compared to peripheral $^{12}C+^{181}Ta$ collisions, which results in lower mean kinetic energies of the negative pions in central $^{12}C+^{181}Ta$ collisions as compared to the peripheral ones.

Table 6.13

Fractions of central, semicentral, and peripheral $^{12}C^{181}Ta$ collisions at 4.2 GeV/*c* per nucleon relative to the total inelastic cross section

Type	Peripheral collisions (%)		Semicentral collisions (%)		Central collisions (%)	
	Experiment	QGSM	Experiment	QGSM	Experiment	QGSM
$^{12}C+^{181}Ta$	60±2	56±1	24±1	29±1	16±1	15±1

Table 6.14

The parameters extracted from fitting the transverse momentum spectra of the negative pions in the range $p_t = 0.1 \div 1.2$ GeV/*c* in peripheral, semicentral, and central $^{12}C^{181}Ta$ collisions at 4.2 *A* GeV/*c* by various two-temperature functions

Fitting function	Collision centrality	A_1	T_1, MeV	A_2	T_2, MeV	$\chi 2/n.d.f.$
Haged.	Peripheral	6214 ± 2326	**63 ± 7**	138 ± 101	**139 ± 16**	0.85
	Semicentral	74329 ± 53202	**46 ± 7**	1766 ± 629	**112 ± 6**	0.50
	Central	93566 ± 49847	**49 ± 6**	1624 ± 740	**119 ± 8**	1.11
Boltz.	Peripheral	5465 ± 1785	**56 ± 5**	120 ± 71	**123 ± 12**	0.93
	Semicentral	50087 ± 27017	**44 ± 5**	1196 ± 398	**104 ± 5**	0.49
	Central	67136 ± 28885	**46 ± 4**	1138 ± 468	**109 ± 7**	1.17
Simple exponential	Peripheral	146 ± 19	**95 ± 10**	6 ± 10	**193 ± 58**	0.65
	Semicentral	714 ± 364	**60 ± 18**	220 ± 90	**126 ± 9**	0.55
	Central	1146 ± 285	**71 ± 12**	159 ± 108	**140 ± 16**	1.01
Gaussian	Peripheral	4 ± 1	**441 ± 22**	48 ± 5	**202 ± 9**	2.04
	Semicentral	20 ± 3	**404 ± 13**	213 ± 25	**180 ± 8**	0.86
	Central	22 ± 4	**414 ± 17**	326 ± 38	**182 ± 8**	2.27

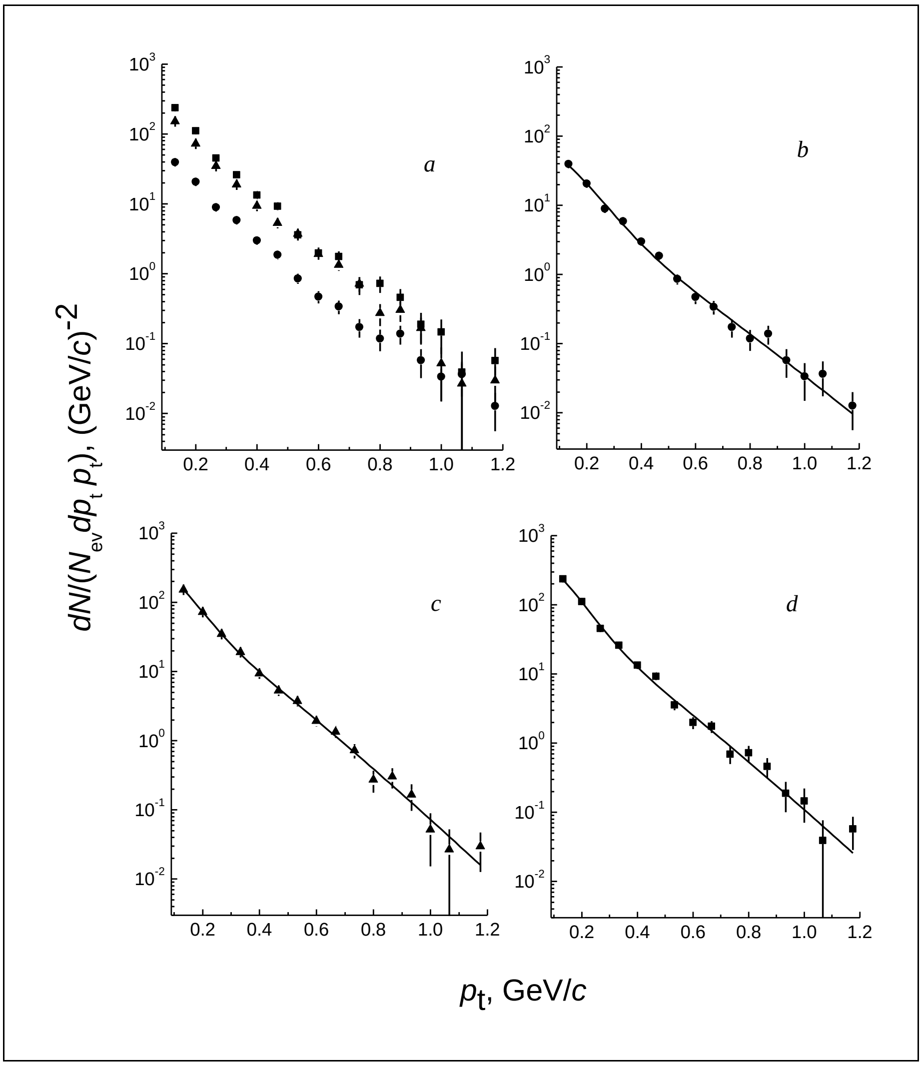

Fig. 6.9. The experimental transverse momentum spectra of the negative pions produced in peripheral (●) ((a) and (b)), semicentral (▲) ((a) and (c)), and central (■) ((a) and (d)) $^{12}C+^{181}Ta$ collisions at 4.2 GeV/*c* per nucleon and the corresponding fits in the range $p_t = 0.1 \div 1.2$ GeV/*c* by the two-temperature Boltzmann function (solid lines). All the spectra are normalized per one inelastic collision event

This is obviously due to the known fact that, with an increase in the collision centrality, the number of nucleon-nucleon collisions and, hence, the number of the participant nucleons and produced pions increase. As can be seen from Fig. 6.9*a*, the two-temperature Boltzmann function again fits very well the p_t spectra of the negative pions in peripheral, semicentral, and central $^{12}C+^{181}Ta$ collisions.

Table 6.15

Parameters extracted from fitting the transverse momentum spectra of the negative pions in the range $p_t = 0.1 \div 1.2$ GeV/*c* in ^{12}C^{181}Ta collisions at 4.2 *A* GeV/*c* by various two-temperature functions for different pion rapidity intervals

Fitting function	Rapidity range	A_1	T_1, MeV	A_2	T_2, MeV	$\chi 2/n.d.f.$
Hagedorn	$y_{cm.} \le -0.3$	18533 ± 7825	**48 ± 4**	247 ± 96	**119 ± 7**	1.46
	$\lvert y_{cm.} \rvert \le 0.3$	5556 ± 3859	**56 ± 11**	337 ± 162	**122 ± 9**	0.62
	$y_{cm.} \ge 0.3$	9183 ± 6549	**53 ±11**	415 ± 303	**111 ± 12**	0.76
Boltzmann	$y_{cm.} \le -0.3$	13521 ± 4778	**44 ± 3**	183 ± 64	**108 ± 6**	1.58
	$\lvert y_{cm.} \rvert \le 0.3$	4478 ± 2210	**52 ± 7**	229 ± 98	**113 ± 7**	0.61
	$y_{cm.} \ge 0.3$	7475 ± 4182	**48 ± 7**	296 ± 185	**102 ± 10**	0.77
Simple exponential	$y_{cm.} \le -0.3$	211 ± 36	**73 ± 8**	17 ± 11	**150 ± 17**	1.16
	$\lvert y_{cm.} \rvert \le 0.3$	65 ± 27	**80 ± 43**	46 ± 40	**137 ± 18**	0.68
	$y_{cm.} \ge 0.3$	121 ± 37	**85 ± 26**	27 ± 56	**136 ± 40**	0.76
Gaussian	$y_{cm.} \le -0.3$	4 ± 1	**391 ± 13**	62 ± 6	**171 ± 6**	3.31
	$\lvert y_{cm.} \rvert \le 0.3$	4 ± 1	**442 ± 17**	36 ± 4	**204 ± 10**	0.90
	$y_{cm.} \ge 0.3$	6 ± 1	**373 ± 18**	49 ± 6	**178 ± 11**	1.16

It seems interesting also to analyze quantitatively the change in the shape of transverse momentum spectra of the negative pions with the change in the pion rapidity range. Therefore, we extracted and fitted, using the above two-temperature functions, the transverse momentum spectra of the negative pions for three different rapidity intervals in the nucleon-nucleon cms at 4.2 GeV/*c*: $y_{cm} \le -0.3$, $\lvert y_{cm.} \rvert \le 0.3$, and $y_{cm.} \ge 0.3$, which can roughly be classified as target fragmentation, midrapidity, and projectile fragmentation regions, respectively. The parameters extracted from fitting the transverse momentum spectra of the negative pions in the range $p_t = 0.1 \div 1.2$ GeV/*c* in ^{12}C+^{181}Ta collisions at 4.2 *A* GeV/*c* by various two-temperature functions for different pion rapidity intervals are displayed in Table 6.15.

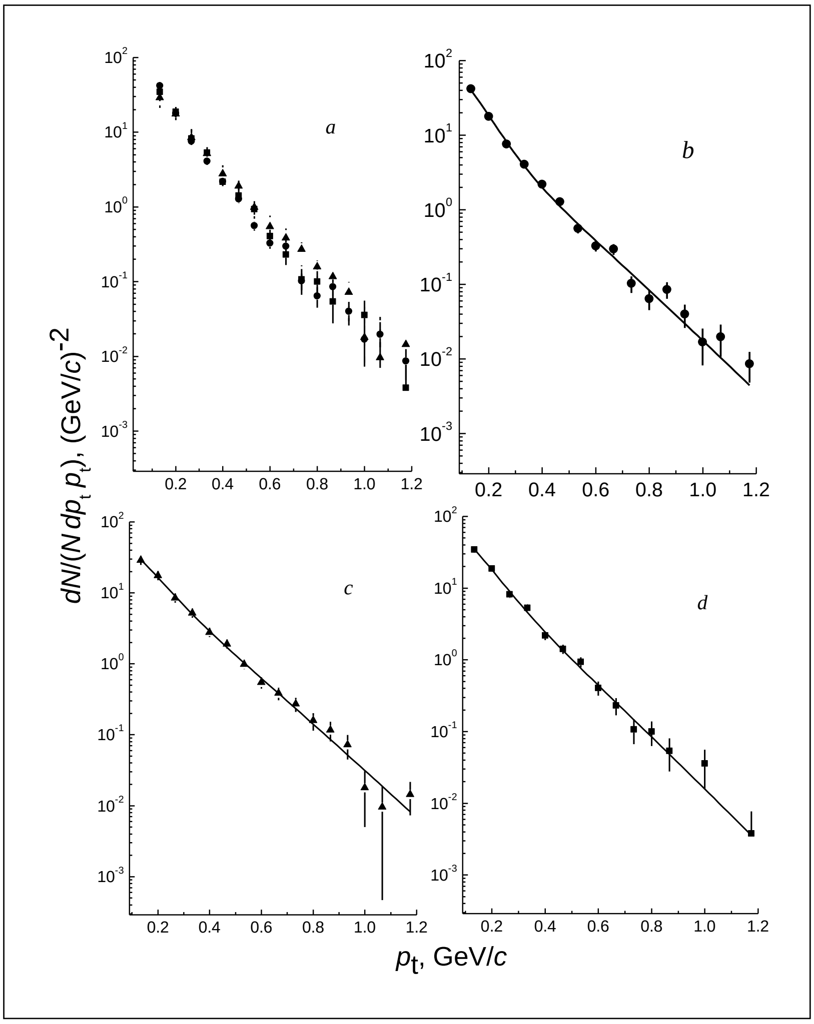

Fig. 6.10. The experimental transverse momentum spectra of the negative pions for rapidity range $y_{cm} \leq -0.3$ **(●) ((a) and (b)), for rapidity range** $|y_{cm.}| \leq 0.3$ **(▲) ((a) and (c)), and for rapidity range** $y_{cm.} \geq 0.3$ **(■) ((a) and (d)) in** ^{12}**C**^{181}**Ta collisions at 4.2 GeV/*c* per nucleon and the corresponding fits in the range** $p_t = 0.1 \div 1.2$ **GeV/*c* by the two-temperature Hagedorn function (solid lines). All the spectra are normalized per one negative pion**

As can be seen from Table 6.15, the absolute values of T_1 and T_2 proved to be consistently larger for the midrapidity region compared to the target and projectile fragmentation regions in case of all the fitting functions used here, except for the Simple Exponential function. However, as observed from Table 6.15, the extracted values of T_1 and T_2 are compatible with each other within the errors for the analyzed three rapidity regions of the negative pion spectra. It can be noticed once again that the fitting by the Gaussian function results in unphysically large values of the spectral temperatures.

The experimental transverse momentum spectra of the negative pions for the analyzed three rapidity ranges in $^{12}C+^{181}Ta$ collisions at 4.2 GeV/*c* per nucleon and the corresponding fits in the range $p_t = 0.1 \div 1.2$ GeV/*c* by the two-temperature Hagedorn function are shown in Fig. 6.10. It is important to note that the p_t spectra of the negative pions for different rapidity ranges were normalized per one pion, because pions produced in one collision event may belong to different rapidity regions, i.e. the same collision event may contribute to the p_t spectra of the negative pions from different rapidity intervals. As can be seen from Fig. 6.10, the p_t spectra of the negative pions in peripheral, semicentral, and central $^{12}C+^{181}Ta$ collisions are fitted very well by the two-temperature Hagedorn function.

Table 6.16

Parameters extracted from fitting the total transverse momentum spectra of the negative pions in the range $p_t = 0.1 \div 0.7$ GeV/*c* in $^{12}C^{181}Ta$ collisions at 4.2 *A* GeV/*c* by various two-temperature functions

Fitting function	A_1	T_1, MeV	A_2	T_2, MeV	$\chi2/n.d.f.$
Hagedorn	60366 ± 48300	**44 ± 8**	1401 ± 667	**108 ± 9**	1.01
Boltzmann	42464 ± 26279	**41 ± 6**	1038 ± 436	**98 ± 7**	1.04
Simple exponential	438 ± 126	**67 ± 23**	111 ± 112	**131 ± 26**	0.99
Gaussian	22 ± 3	**353 ± 12**	154 ± 18	**161 ± 8**	1.83

To check the influence of the fitting range of p_t on the extracted spectral temperatures T_1 and T_2, the total p_t spectra of the negative pions and the respective spectra of π^- mesons for different $^{12}C+^{181}Ta$ collision centralities and three rapidity regions considered in this analysis were also fitted in the range $p_t = 0.1 \div 0.7$ GeV/*c*. It is necessary to mention that a similar analysis was done in our recent paper [33] where the centrality and rapidity dependences of transverse momentum spectra of the negative pions produced in $^{12}C+^{12}C$ collisions at 4.2*A* GeV/*c* were investigated. While comparing fit results for $p_t = 0.1 \div 0.7$ and $p_t = 0.1 \div 1.2$ GeV/*c* ranges, it was observed [33] that high p_t ($p_t > 0.7$ GeV/*c*) and high temperature part of the pion spectra with quite large statistical errors influences significantly the extracted values of T_1 and T_2, masking and suppressing the centrality dependence of the spectral temperatures. The parameters extracted from fitting the total transverse momentum spectra of the negative pions in the range $p_t = 0.1 \div 0.7$ GeV/*c* in $^{12}C+^{181}Ta$ collisions at 4.2 *A* GeV/*c* by the considered two-temperature functions are given in Table 6.16. From comparison of Tables 6.12 and 6.16 one can deduce that the values of the spectral temperatures T_1 and T_2 are consistently lower for the fitting range $p_t = 0.1 \div 0.7$ GeV/*c* compared to the fitting interval $p_t = 0.1 \div 1.2$ GeV/*c*. The similar trend was also observed in our recent work [33]. This could be likely due to the reason that the p_t spectra in the former transverse momentum fitting range are lesser affected by the high temperature tail of the pion spectra as compared to the latter fitting range.

As expected, Table 6.16 shows that the values of T_1 and T_2 extracted from fitting with the two-temperature Hagedorn and the two-temperature Boltzmann functions are compatible with each other within the uncertainties.

The parameters extracted from fitting the transverse momentum spectra of the negative pions in the range $p_t = 0.1 \div 0.7$ GeV/*c* in peripheral, semicentral, and central $^{12}C+^{181}Ta$ collisions at 4.2 *A* GeV/*c* by the above considered two-temperature functions are shown in Table 6.17. As can be seen from Table 6.17, the extracted values of the spectral temperatures T_1 and T_2 coincided within the errors for peripheral, semicentral, and central $^{12}C+^{181}Ta$ collisions when fitted by the two-temperature Hagedorn, Boltzmann, and Simple Exponential functions.

Table 6.17

The parameters extracted from fitting the transverse momentum spectra of negative pions in the range $p_t = 0.1 \div 0.7$ GeV/*c* in peripheral, semicentral, and central $^{12}C+^{181}Ta$ collisions at 4.2 *A* GeV/*c* by various two temperature functions

Fitting function	Collision centrality	A_1	T_1, MeV	A_2	T_2, MeV	χ2/n.d.f.
Hagedorn	Peripheral	38798 ± 71350	**38 ± 14**	982 ± 506	**100 ± 9**	0.85
	Semicentral	79014 ± 65917	**45 ± 8**	1899 ± 915	**111 ± 9**	0.54
	Central	262592 ± 329768	**39 ± 9**	4224 ± 2391	**101 ± 10**	1.45
Boltzmann	Peripheral	24118 ± 31482	**36 ± 10**	717 ± 348	**91 ± 8**	0.84
	Semicentral	54634 ± 34661	**43 ± 6**	1341 ± 585	**102 ± 7**	0.51
	Central	169975 ± 165624	**37 ± 7**	3094 ± 1590	**92 ± 8**	1.46
Simple exponential	Peripheral	156 ± 288	**49 ± 51**	93 ± 51	**116 ± 14**	0.91
	Semicentral	702 ± 361	**61 ± 23**	215 ± 136	**126 ± 15**	0.61
	Central	1352 ± 931	**55 ± 27**	362 ± 303	**119 ± 20**	1.49
Gaussian	Peripheral	13 ± 3	**335 ± 15**	62 ± 11	**153 ± 13**	1.01
	Semicentral	25 ± 5	**382 ± 15**	222 ± 28	**173 ± 9**	0.58
	Central	57 ± 11	**333 ± 14**	415 ± 69	**150 ± 11**	1.77

It is observed from comparison of Tables 6.14 and 6.17 that in general the absolute values of T_1 and T_2 are noticeably lower in case of fitting in the range $p_t = 0.1 \div 0.7$ GeV/*c* as compared to the fitting interval $p_t = 0.1 \div 1.2$ GeV/*c*. The largest reduction in the extracted spectral temperatures T_1 and T_2 is observed for the p_t spectra of π^- in peripheral collisions when going from fitting in the range $p_t = 0.1 \div 1.2$ GeV/*c* to $p_t = 0.1 \div 0.7$ GeV/*c*. This is likely due to the influence of the high temperature p_t part of π^- spectra to the extracted values of T_1 and T_2 in case of the fitting range $p_t = 0.1 \div 1.2$ GeV/*c* compared to the fitting interval $p_t = 0.1 \div 0.7$ GeV/*c*.

Table 6.18 displays the parameters extracted from fitting the transverse momentum spectra of the negative pions in the range $p_t = 0.1 \div 0.7$ GeV/*c* in $^{12}C+^{181}Ta$ collisions at 4.2 *A* GeV/*c* by the same two-temperature functions for different pion rapidity intervals. As can be seen from Table 6.18, the extracted values of the spectral temperatures T_1 and T_2 are consistently larger for the p_t spectra of π^- mesons coming from midrapidity range ($|y_{cm.}| \leq 0.3$) as compared to the transverse momentum spectra of the negative pions generated in the target ($y_{cm.} \leq -0.3$) and projectile ($y_{cm.} \geq 0.3$) fragmentation regions.

Table 6.18

The parameters extracted from fitting the transverse momentum spectra of the negative pions in the range $p_t = 0.1 \div 0.7$ GeV/*c* in $^{12}C+^{181}Ta$ collisions at 4.2*A* GeV/*c* by various two-temperature functions for different pion rapidity intervals

Fitting function	**Rapidity range**	A_1	T_1**, MeV**	A_2	T_2**, MeV**	$\chi 2/n.d.f.$
Hagedorn	$y_{cm.} \leq -0.3$	50595 ± 44736	**39 ± 7**	627 ± 303	**102 ± 8**	1.44
	$\lvert y_{cm.}\rvert \leq 0.3$	6199 ± 7228	**54 ± 21**	445 ± 496	**117 ± 22**	0.51
	$y_{cm.} \geq 0.3$	12410 ± 14196	**48 ± 15**	593 ± 599	**105 ± 17**	1.06
Boltzmann	$y_{cm.} \leq -0.3$	32851 ± 23205	**36 ± 5**	465 ± 202	**93 ± 7**	1.49
	$\lvert y_{cm.}\rvert \leq 0.3$	5395 ± 4574	**49 ± 13**	341 ± 302	**106 ± 16**	0.50
	$y_{cm.} \geq 0.3$	9756 ± 8301	**44 ± 10**	429 ± 364	**96 ± 13**	1.05
Simple exponential	$y_{cm.} \leq -0.3$	266 ± 101	**59 ± 17**	45 ± 38	**126 ± 22**	1.37
	$\lvert y_{cm.}\rvert \leq 0.3$	91 ± 128	**102 ± 82**	14 ± 158	**166 ± 334**	0.57
	$y_{cm.} \geq 0.3$	111 ± 105	**76 ± 68**	48 ± 166	**125 ± 69**	1.13
Gaussian	$y_{cm.} \leq -0.3$	9 ± 2	**334 ± 12**	77 ± 10	**148 ± 8**	2.41
	$\lvert y_{cm.}\rvert \leq 0.3$	9 ± 2	**368 ± 22**	40 ± 6	**176 ± 16**	0.54
	$y_{cm.} \geq 0.3$	9 ± 2	**350 ± 21**	52 ± 7	**169 ± 13**	1.04

As observed from Table 6.18, the absolute values of the spectral temperatures T_1 of the negative pions coming from projectile fragmentation region ($y_{cm.} \geq 0.3$) proved to be consistently larger than the respective temperatures of the negative pions coming from target fragmentation region ($y_{cm.} \leq -0.3$). This is, as was already mentioned above, due to the high asymmetry of collision system ($A_{proj} << A_{target}$) and that pions coming from projectile fragmentation region are produced in first single collisions (interactions) of projectile nucleons with target nucleons, whereas pions coming from target fragmentation are produced mostly at lesser energy transfers in secondary nucleon-nucleon collisions in heavy tantalum nuclei. As seen from comparison of Tables 6.15 and 6.18, the extracted absolute values of T_1 and T_2 are generally lower in case of fitting in the range $p_t = 0.1 \div 0.7$ GeV/c as compared to the fitting interval $p_t = 0.1 \div 1.2$ GeV/c. The differences in the spectral temperatures extracted in these two fitting ranges are quite small in case of fitting by the two-temperature Hagedorn and the two-temperature Boltzmann functions, as observed from Tables 6.15 and 6.18. As was noticed earlier, the fitting of the p_t spectra of the negative pions with the Gaussian function gives unphysically large values of T_1 and T_2.

§ 6.3. Collision centrality and *A* dependencies of soft and hard components of *P*$_t$ distributions of negative pions in *AA* collisions at 4.2 *A* GeV/*c*

This work [28] is a further continuation of our papers [30–36, 38] on analysis of various features of pion spectra in nucleus–nucleus collisions at 4.2*A* GeV/*c*. The aim of the present paper is to study and reveal the centrality and system-size dependencies of the temperatures of soft (p_t = 0.1–0.5 GeV/c) and hard (p_t = 0.5–1.2 GeV/c) parts of the experimental p_t distributions of the negative pions produced in ^{4}He+^{12}C, ^{12}C+^{12}C, and ^{12}C+^{181}Ta collisions at 4.2*A* GeV/*c* ($\sqrt{s_{nn}}$ =

3.14 GeV). For these collision systems and selected collision centralities, the temperatures will be extracted from fitting separately the soft and hard p_t components of π^- mesons by one temperature Hagedorn and one temperature Boltzmann functions, given in expressions (2.26) and (2.28), respectively. It is of interest to ascertain whether there is any observable dependence of the temperature of both soft and hard p_t components of π^- on the size and degree of overlap of colliding nuclei in peripheral, semicentral, and central nucleus–nucleus collisions at $\sqrt{s_{nn}}$ = 3.14 GeV.

Table 6.19

Mean multiplicities per event of the negative pions and participant protons and the average values of rapidity and transverse momentum of π^- mesons in ^{4}He^{12}C [31], ^{12}C^{12}C [34, 35] and ^{12}C^{181}Ta [32, 35] collisions at 4.2 *A* GeV/*c* per nucleon. The mean rapidities are calculated in c.m. of nucleon–nucleon collisions at 4.2 GeV/*c*

Type		$\langle n(\pi^-)\rangle$	$\langle n_{part.prot.}\rangle$	$\langle y_{\mathrm{c.m.}}(\pi^-)\rangle$	$\langle p_t(\pi^-)\rangle$ (GeV/c)
^{4}He +^{12}C	Exper	1.02±0.01	2.83±0.02	–0.090±0.007	0.247±0.002
	QGSM	0.99±0.01	2.60±0.01	–0.082±0.007	0.224±0.001
^{12}C+^{12}C	Exper	1.45±0.01	4.35±0.02	–0.016±0.005	0.242±0.001
	QGSM	1.59±0.01	4.00±0.02	0.007±0.005	0.219±0.001
^{12}C+^{181}Ta	Exper	3.50±0.10	13.3±0.2	–0.34±0.01	0.217±0.002
	QGSM	5.16±0.09	14.4±0.2	–0.38±0.01	0.191±0.001

As seen from Table 6.19, on the whole, the QGSM describes qualitatively all the average characteristics of the negative pions in experiment, except for the mean multiplicity of π^- mesons in ^{12}C+^{181}Ta collisions and their $<p_t>$ in all three collisions systems. The QGSM overestimates significantly the multiplicity of π^- in ^{12}C+^{181}Ta collisions at 4.2 *A* GeV/*c*. This could be explained by that the QGSM simplifies the nuclear effects, which are more pronounced in heavy nuclei [179, 180]. It was suggested in Ref. [180] that this model could be improved by taking into account a possible increase of the pion absorption cross section in dense baryon medium, as well as by including the higher mass baryon resonances. As observed from Table 6.19, QGSM underestimates noticeably the average values of p_t of the negative pions in all three collisions systems. The experimental transverse momentum and rapidity distributions of π^- along with the corresponding QGSM spectra in minimum bias ^{4}He+C, ^{12}C+^{12}C and ^{12}C+^{181}Ta collisions at 4.2*A* GeV/*c* are presented in Fig. 6.11. Figure 6.11*a* shows that the QGSM [132, 133] underestimates the experimental p_t spectrum of π^- mesons in region $p_t > 0.8$ GeV/*c*. It is worth mentioning that another model − Modified FRITIOF model [118, 119, 124–127], specifically modified for describing the nucleus–nucleus collisions at incident energies of the order of a few GeV per nucleon, also underestimates this high p_t part of the pion spectra [36, 118]. As observed from Fig. 6.11*b*, the QGSM describes satisfactorily the experimental rapidity distributions in the studied collision systems.

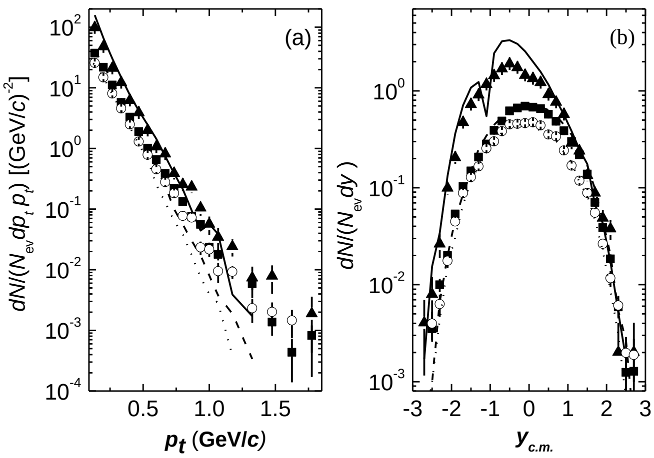

Fig. 6.11. The experimental transverse momentum (a) and rapidity (b) distributions of the negative pions produced in minimum bias ^{4}He^{12}C (○), ^{12}C^{12}C [34] (■), and ^{12}C^{181}Ta [32] (▲) collisions at 4.2 GeV/*c* per nucleon. The rapidity distributions were plotted in c.m. of nucleon–nucleon collisions at 4.2 GeV/*c*. The corresponding calculated QGSM spectra are given by the dotted (^{4}He^{12}C), dashed (^{12}C^{12}C), and solid (^{12}C^{181}Ta) curves. All the spectra are normalized per one inelastic collision event

To analyze quantitatively the change in the shape of p_t distributions of the negative pions in $^{12}C+^{12}C$ [34] and $^{12}C+^{181}Ta$ [32] collisions with an increase in collision centrality (which corresponds to decrease of the impact parameter of collision), the number of participant protons (N_p) was used to characterize the collision centrality. We followed the method, described in subchapter 2.4 of the present dissertation, to select the central, semicentral, and peripheral collision events. Fractions of central, semicentral, and peripheral $^{4}He+C$, $^{12}C+^{12}C$ [34, 35] and $^{12}C+^{181}Ta$ [32, 35] collision events, relative to the total inelastic cross section, obtained for both experimental and QGSM data are presented in Table 6.20. As seen from Table 6.20, on the whole, the experimental fractions of peripheral, semicentral, and central $^{4}He+C$, $^{12}C+^{12}C$ and $^{12}C+^{181}Ta$ collision events are reproduced quite satisfactorily by the QGSM calculations. Table 6.20 shows that the selected central collision events correspond to ~ (0–10)% centrality in $^{4}He+C$ and $^{12}C+^{12}C$ collisions and to ~ (0–15)% centrality in $^{12}C+^{181}Ta$ collisions.

Table 6.20

Fractions of peripheral, semicentral, and central $^{4}He^{12}C$, $^{12}C^{12}C$, and $^{12}C^{181}Ta$ collisions at 4.2 *A* GeV/*c* per nucleon, relative to the total inelastic cross section

Type	Peripheral collisions (%)		Semicentral collisions (%)		Central collisions (%)	
	Experiment	QGSM	Experiment	QGSM	Experiment	QGSM
$^{4}He+^{12}C$	54 ± 1	54 ± 1	37 ± 1	38 ± 1	9 ± 1	8 ± 1
$^{12}C+^{12}C$	58 ± 1	62 ± 1	31 ± 1	30 ± 1	11 ± 1	8 ± 1
$^{12}C+^{181}Ta$	60 ± 2	56 ± 1	24 ± 1	29 ± 1	16 ± 1	15 ± 1

Table 6.21 presents the spectral temperatures of the negative pions in minimum bias $^{4}He+^{12}C$, $^{12}C+^{12}C$ [34], and $^{12}C+^{181}Ta$ [32] collisions at 4.2 *A* GeV/*c* and their relative contributions (R_1 and R_2) extracted from fitting their transverse momentum spectra in the whole p_t range by two temperature Hagedorn and Boltzmann

functions. They were compared with the corresponding results obtained in Ref. [78] from fitting the non-invariant c.m. energy spectra of the negative pions in the studied collisions at the same initial momentum (on about two times lesser statistics of collision events) using two temperature Maxwell-Boltzmann distribution function.

Table 6.21

Spectral temperatures (*T*) of the negative pions in minimum bias $^{4}He^{12}C$, $^{12}C^{12}C$ [34], and $^{12}C^{181}Ta$ [32] collisions at 4.2 *A* GeV/*c* and their relative contributions (R_1 and R_2) extracted from fitting their experimental transverse momentum distributions in the whole p_t range by two temperature Hagedorn and Boltzmann functions compared to the corresponding values obtained in Ref. [78] from fitting the noninvariant c.m. energy spectra of the negative pions by Maxwell-Boltzmann distribution function. (*n.d.f.* denotes the number of degrees of freedom)

Fitting Function	Collision Type	T_1 (MeV)	R_1 (%)	T_2 (MeV)	R_2 (%)	$\chi2/n.d.f.$	R^2 factor
Hagedorn	HeC	**83 ± 4**	89 ± 14	**150 ± 15**	11 ± 8	1.43	0.99
	CC	**76 ± 3**	85 ± 14	**142 ± 7**	15 ± 6	1.32	0.99
	CTa	**57 ± 3**	80 ± 22	**128 ± 6**	20 ± 7	0.92	0.99
Boltzmann	HeC	**68 ± 3**	85 ± 13	**124 ± 8**	15 ± 7	1.44	0.99
	CC	**65 ± 2**	85 ± 13	**127 ± 5**	15 ± 4	1.40	0.99
	CTa	**50 ± 2**	83 ± 20	**116 ± 5**	17 ± 5	1.02	0.99
Maxwell-Boltzmann	HeC	**94 ± 6**	85 ± 11	**173 ± 22**	15 ± 11	0.54	N/A
	CC	**83 ± 3**	79 ± 6	**145 ± 7**	21 ± 6	0.72	N/A
	CTa	**66 ± 2**	88 ± 3	**159 ± 6**	12 ± 3	0.58	N/A

As seen from Table 6.21, the values of the temperatures (T_1, T_2) extracted from fitting the p_t spectra by two temperature Hagedorn and two temperature Boltzmann functions proved to be noticeably lower [32, 34] compared to the corresponding values, obtained [78] from fitting the noninvariant c.m. energy spectra of the negative pions by Maxwell-Boltzmann distribution function. This was likely due to influence of longitudinal motion on the energy spectra of π^- mesons, in contrast to their p_t spectra, which are Lorentz invariant with respect to longitudinal boosts [36, 73, 75, 77].

As observed from Table 6.21, the dominant contribution (R_1 ~ 80–90%) to the total π^- multiplicity in the studied collision systems was given by T_1, which was compatible within the uncertainties with the results of Ref. [78]. The fits by Boltzmann function resulted in slightly lower values of the temperatures compared to those by Hagedorn function [32, 34].

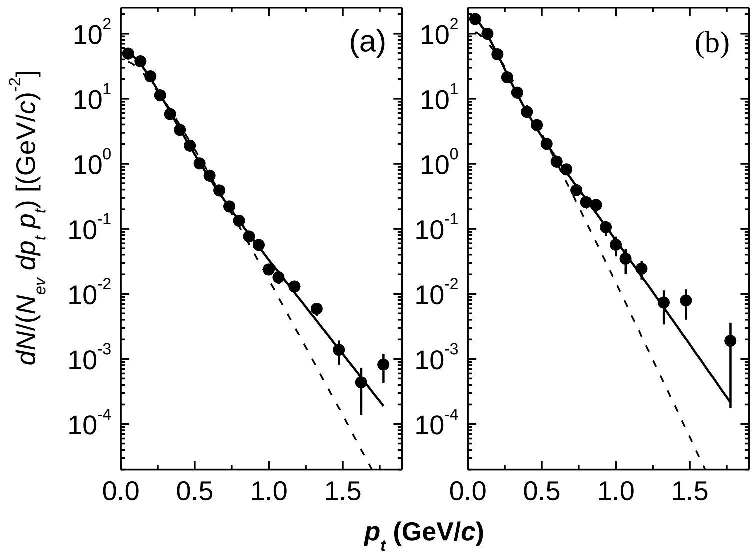

Fig. 6.12. The experimental transverse momentum spectra (●) of the negative pions produced in minimum bias $^{12}C^{12}C$ [34] (a) and $^{12}C^{181}Ta$ [32] (b) collisions at 4.2 GeV/*c* per nucleon and the corresponding fits in the whole p_t range by one temperature (dashed lines) and two temperature (solid lines) Hagedorn functions. All the spectra are normalized per one inelastic collision event

Figure 6.12 shows, as an example, the experimental p_t distributions of π^- mesons produced in minimum bias $^{12}C+^{12}C$ [34] and $^{12}C+^{181}Ta$ [32] collisions at 4.2 GeV/*c* per nucleon along with the corresponding fits in the whole p_t range by one temperature and two temperature Hagedorn functions. It was concluded earlier [72, 78, 32, 34, 36], which can also be seen from Fig. 6.12, that the p_t as well as noninvariant c.m. energy distributions of the negative pions in minimum bias ^{4}He+^{12}C, ^{12}C+^{12}C, and ^{12}C+^{181}Ta collisions at 4.2*A* GeV/*c* exhibit two temperature shapes.

The two temperature shape of pion spectra was observed also in other experiments in relativistic collisions of different sets of nuclei at various energies in the past [73, 74, 75, 31]. The phenomenon of collective flow has become the well established and important feature of relativistic heavy ion collisions. Inverse slope parameter, T, or an apparent temperature of the emitting source, of transverse mass spectra of hadrons was shown to consist of two components: a thermal part (T_{thermal}), and a second part resembling the collective expansion with an average transverse velocity $<\beta_t>$ [178]. It is necessary to mention that the collective flow of protons and negative pions was observed experimentally also in He+C, C+C, C+Ne, C+Cu, and C+Ta collisions within the momentum range of 4.2–4.5 *A* GeV/*c* [172–174]. The two temperature shape of pion spectra could also be explained qualitatively as due to two pion types: pions, emitted from the “hot” core of collision zone at initial collision stage, and other pions, coming later from expansion and freeze-out of a highly compressed nuclear matter, or a fireball, created in central or semicentral nucleus–nucleus collisions. The low temperature part of pion spectra can also be thought as due to contribution of mixture of pions, originated from expansion and freeze-out of a fireball, with “cold” pions coming from decay of resonances at a later stage of collision. And, the high temperature part of spectra can certainly be due to pions produced in semi(hard) nucleon–nucleon collisions.

Hence, the observed two temperature shape of the p_t distribution of pions, produced in minimum bias nucleus–nucleus collisions at 4.2 *A* GeV/*c*, is likely to be due to contribution of combination of pions coming from collective flow, pions generated from decay of various resonances, and pions produced in semi(hard) nucleon–nucleon collisions. Each of the above plausible sources should contribute to pion p_t distribution with a certain weight, which is expected likely to depend on collision centrality as well as mass numbers and geometry of colliding nuclei.

It is evident from Figs. 6.11 and 6.12 that the p_t spectra of the negative pions with $p_t \leq 1.2$ GeV/*c* are characterized by a good enough statistics of π^- and, therefore, by sufficiently low statistical errors. On the other hand, as seen from Figs. 6.11 and 6.12, $p_t > 1.2$ range displays quite poor statistics of produced pions and, hence, quite large statistical uncertainties. Due to the lower momentum threshold of detection of pions $p_{t\,hresh} \approx 70-80\,\text{MeV}/c$, it was natural [32, 34] to fit the p_t distributions of pions in range $p_t = 0.1-1.2$ GeV/*c*, where they were detected and measured with practically 100% efficiency.

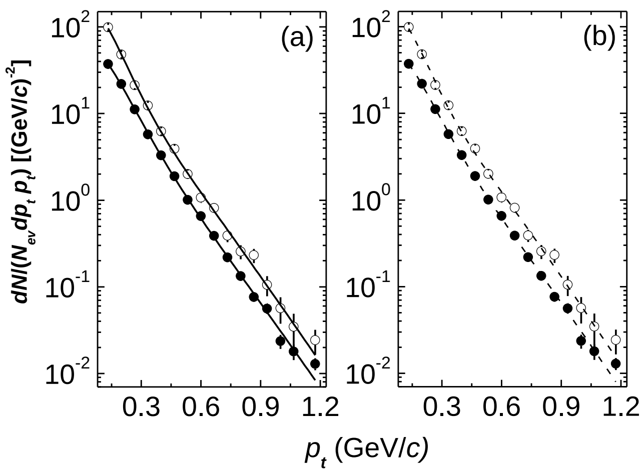

Fig. 6.13. The experimental transverse momentum spectra of the negative pions produced in minimum bias ^{12}C^{12}C [34] (●) and ^{12}C^{181}Ta [32] (○) collisions at 4.2 GeV/*c* per nucleon and the corresponding fits in the range $p_t = 0.1-1.2$ GeV/*c* by two temperature Hagedorn (a) (solid lines) and two temperature Boltzmann (b) (dashed lines) functions. All the spectra are normalized per one inelastic collision event

Table 6.22

Spectral temperatures (*T*) of the negative pions in minimum bias $^{4}He^{12}C$, $^{12}C^{12}C$ [34], and $^{12}C^{181}Ta$ [32] collisions at 4.2 *A* GeV/*c* and their relative contributions (R_1 and R_2) extracted from fitting their experimental transverse momentum distributions in range $p_t = 0.1 - 1.2$ GeV/*c* by two temperature Hagedorn and Boltzmann functions

Fitting function	Collision Type	T_1 (MeV)	R_1 (%)	T_2 (MeV)	R_2 (%)	$\chi^2/n.d.f.$	R^2 factor
Hagedorn	HeC	**67 ± 8**	70 ± 30	**122 ± 8**	30 ± 18	1.15	0.99
	CC	**59 ± 6**	68 ± 33	**119 ± 5**	32 ± 14	0.44	0.99
	CTa	**53 ± 5**	77 ± 40	**123 ± 6**	23 ± 11	0.91	0.99
Boltzmann	HeC	**59 ± 5**	75 ± 26	**112 ± 6**	25 ± 12	1.17	0.99
	CC	**54 ± 4**	74 ± 27	**111 ± 4**	26 ± 9	0.42	0.99
	CTa	**49 ± 3**	81 ± 34	**113 ± 5**	19 ± 8	1.02	0.99

Table 6.22 presents the spectral temperatures of the negative pions in minimum bias $^{4}He+^{12}C$, $^{12}C+^{12}C$ [34], and $^{12}C+^{181}Ta$ [32] collisions at 4.2 *A* GeV/*c* and their relative contributions extracted from fitting their experimental p_t distributions in range $p_t = 0.1 - 1.2$ GeV/*c* by two temperature Hagedorn and Boltzmann functions. Figure 6.13 shows, as an example, the experimental transverse momentum distributions of the negative pions produced in minimum bias $^{12}C+^{12}C$ [34] and $^{12}C+^{181}Ta$ [32] collisions at 4.2 GeV/*c* per nucleon and the corresponding fits in range $p_t = 0.1 - 1.2$ GeV/*c* by two temperature Hagedorn and two temperature Boltzmann functions. As seen from Fig. 6.13 and Table 6.22, the experimental p_t distributions of π^- exhibited two temperature shapes, being described quite well by two temperature Hagedorn and Boltzmann functions in minimum bias $^{4}He+^{12}C$, $^{12}C+^{12}C$ [34] and $^{12}C+^{181}Ta$ [32] collisions at 4.2 GeV/*c* per nucleon.

As observed from Table 6.22, the lower temperature T_1 part dominates the p_t distributions of π^- mesons in range $p_t = 0.1-1.2$ GeV/c, as was also the case for the whole p_t range. Spectral temperatures of π^- in peripheral, semicentral, and central ^{4}He+^{12}C, ^{12}C+^{12}C [34], and ^{12}C+^{181}Ta [32] collisions at 4.2 *A* GeV/*c* and their relative contributions, extracted from fitting their experimental transverse momentum spectra in range $p_t = 0.1-1.2$ GeV/c by two temperature Hagedorn and Boltzmann functions, are presented in Table 6.23.

Table 6.23

Spectral temperatures (*T*) of the negative pions in peripheral, semicentral, and central ^{4}He^{12}C, ^{12}C^{12}C [34], and ^{12}C^{181}Ta [32] collisions at 4.2 *A* GeV/*c* and their relative contributions (R_1 and R_2) extracted from fitting their experimental transverse momentum distributions in range $p_t = 0.1-1.2$ GeV/*c* by two temperature Hagedorn and Boltzmann functions

Fitting function	Centrality Type	Collision Type	T_1 (MeV)	R_1 (%)	T_2 (MeV)	R_2 (%)	χ^2/n.d.f.
Hagedorn	Peripheral	HeC	**67 ± 8**	77 ± 35	**125 ± 12**	23 ± 19	0.99
		CC	**62 ± 6**	74 ± 34	**123 ± 8**	26 ± 15	0.73
		CTa	**63 ± 7**	83 ± 43	**139 ± 16**	17 ± 14	0.85
	Semicentral	HeC	**57 ± 5**	54 ± 45	**112 ± 6**	46 ± 32	1.53
		CC	**60 ± 6**	70 ± 33	**123 ± 6**	30 ± 14	0.27
		CTa	**46 ± 7**	70 ± 69	**112 ± 6**	30 ± 24	0.50
	Central	HeC	**59 ± 20**	48 ± 58	**109 ± 10**	52 ± 55	0.97
		CC	**65 ± 8**	70 ± 33	**124 ± 8**	30 ± 18	1.42
		CTa	**49 ± 6**	78 ± 58	**119 ± 8**	22 ± 15	1.11
Boltzmann	Peripheral	HeC	**60 ± 5**	81 ± 30	**115 ± 9**	19 ± 12	0.95
		CC	**55 ± 4**	78 ± 29	**112 ± 6**	22 ± 10	0.76
		CTa	**56 ± 5**	85 ± 39	**123 ± 12**	15 ± 10	0.93
	Semicentral	HeC	**53 ± 7**	65 ± 37	**104 ± 5**	35 ± 19	1.52
		CC	**55 ± 4**	77 ± 28	**113 ± 5**	23 ± 9	0.31
		CTa	**44 ± 5**	76 ± 57	**104 ± 5**	24 ± 15	0.49
	Central	HeC	**54 ± 11**	60 ± 50	**100 ± 8**	40 ± 32	0.98
		CC	**58 ± 5**	76 ± 28	**114 ± 6**	24 ± 12	1.40
		CTa	**46 ± 4**	82 ± 50	**109 ± 7**	18 ± 10	1.17

As seen from Table 6.23, practically no centrality dependence of the extracted temperatures T_1 and T_2 was observed, which is likely due to interplay between the temperatures of soft and hard components of pion p_t spectra while performing combined two temperature model fits, and partly due to significant fitting errors of T_1 and T_2. We, therefore, studied the centrality as well as system-size dependencies of the shapes (temperatures) of p_t distributions of π^- mesons by fitting separately their soft ($p_t = 0.1 - 0.5$ GeV/c) and hard ($p_t = 0.5 - 1.2$ GeV/c) p_t components by one temperature Hagedorn and one temperature Boltzmann functions, in the present work.

Table 6.24 presents the parameters extracted from fitting by one temperature Hagedorn and one temperature Boltzmann functions of the experimental p_t distributions of the negative pions in peripheral, semicentral, and central ^{4}He+^{12}C, ^{12}C+^{12}C, and ^{12}C+^{181}Ta collisions at 4.2 A GeV/c in the fitting ranges $p_t = 0.1 - 0.5$ GeV/c and $p_t = 0.5 - 1.2$ GeV/c.

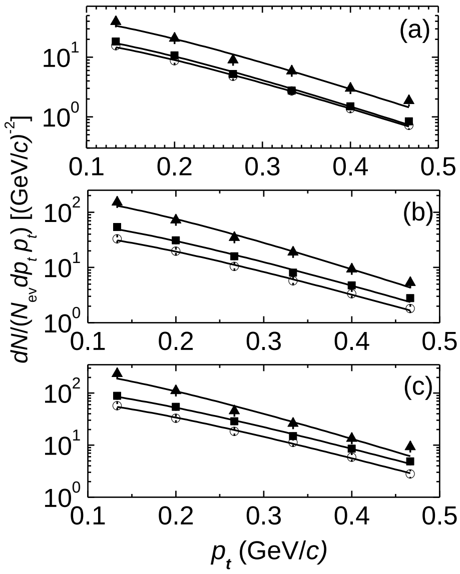

Fig. 6.14. Soft component of the experimental transverse momentum distributions of the negative pions in peripheral (a), semicentral (b), and central (c) – ^{4}He^{12}C (○), ^{12}C^{12}C (■), and ^{12}C^{181}Ta (▲) collisions at 4.2 *A* GeV/*c* along with the corresponding fits (solid lines) by one temperature Hagedorn function in p_t range 0.1 – 0.5 GeV/*c*

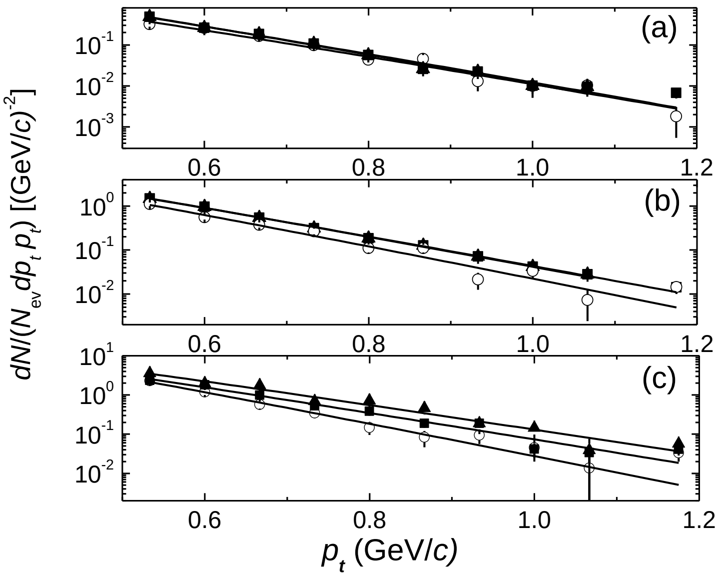

Fig. 6.15. Hard component of the experimental transverse momentum distributions of the negative pions in peripheral (a), semicentral (b), and central (c) – ^{4}He^{12}C (○), ^{12}C^{12}C (■), and ^{12}C^{181}Ta (▲) collisions at 4.2 *A* GeV/*c* along with the corresponding fits (solid lines) by one temperature Hagedorn function in p_t range 0.5 – 1.2 GeV/*c*

As can be seen from comparison of Tables 6.23 and 6.24, the separate fitting of the soft (0.1–0.5 GeV/*c*) and hard (0.5–1.2 GeV/*c*) p_t components of the negative pions resulted in significantly lower fitting uncertainties of the extracted temperatures as compared to combined two temperature fits in range $p_t = 0.1 - 1.2$ GeV/*c*.

Soft components of the experimental p_t distributions of the negative pions in peripheral, semicentral, and central ^{4}He+^{12}C, ^{12}C+^{12}C, and ^{12}C+^{181}Ta collisions at 4.2 *A* GeV/*c* along with the corresponding fits by one temperature Hagedorn function in p_t range 0.1 – 0.5 GeV/*c* are presented in Fig. 6.14. Figure 6.15 presents hard components of the experimental p_t distributions of the negative pions in peripheral, semicentral, and central ^{4}He+^{12}C, ^{12}C+^{12}C, and ^{12}C+^{181}Ta collisions at 4.2 *A* GeV/*c* along with the corresponding fits by one temperature Hagedorn function in p_t range 0.5 – 1.2 GeV/*c*. As seen from Figs. 6.14 and 6.15 and Table

6.24, both one temperature Hagedorn and one temperature Boltzmann functions describe quite satisfactorily the soft as well as hard components of p_t distributions of π^- in three centrality groups in the studied collision systems.

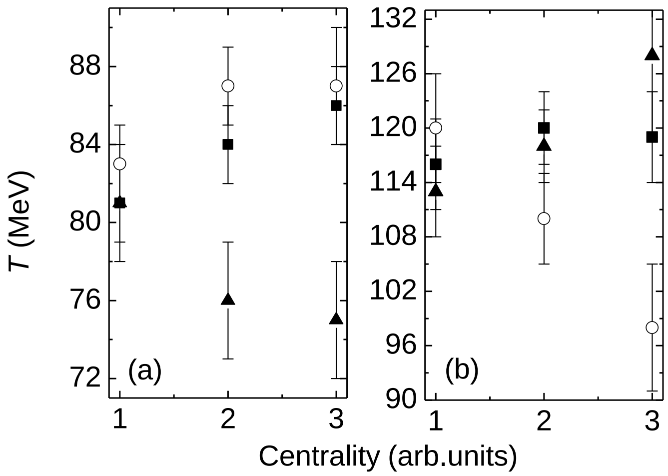

Fig. 6.16. Collision centrality dependence of the temperature of soft (a) and hard (b) component of the experimental transverse momentum distributions of the negative pions in ^{4}He^{12}C (○), ^{12}C^{12}C (■), and ^{12}C^{181}Ta (▲) collisions at 4.2 *A* GeV/*c*, extracted from fitting by one temperature Hagedorn function in p_t range 0.1 – 0.5 GeV/*c* and 0.5 – 1.2 GeV/*c*, respectively. The numbers 1, 2, and 3 on *x* axis correspond to the group of peripheral, semicentral, and central collision events, respectively

Figure 6.16 demonstrates collision centrality dependencies of the temperatures of soft and hard components of the experimental p_t distributions of π^- in ^{4}He+^{12}C, ^{12}C+^{12}C, and ^{12}C+^{181}Ta collisions at 4.2 *A* GeV/*c*, extracted from fitting by one temperature Hagedorn function in p_t ranges 0.1 – 0.5 GeV/*c* and 0.5 – 1.2 GeV/*c*, respectively. As seen from Fig. 6.16, the temperatures of soft as well as hard components of p_t distributions of the negative pions in peripheral collisions are very close to each other for collision systems under consideration. As observed from Fig. 6.16*a*, on the whole, the gap between the temperatures of soft p_t component in ^{4}He+^{12}C, ^{12}C+^{12}C, and ^{12}C+^{181}Ta collisions increases with an increase in collision centrality. The behavior of centrality dependence of T of soft p_t component is, to certain extent, close to each other for ^{4}He+^{12}C and ^{12}C+^{12}C collisions.

Table 6.24

Parameters extracted from fitting by one temperature Hagedorn and one temperature Boltzmann functions of the experimental transverse momentum distributions of the negative pions in peripheral, semicentral, and central ^{4}He^{12}C, ^{12}C^{12}C, and ^{12}C^{181}Ta collisions at 4.2*A* GeV/*c* in the fitting ranges $p_t = 0.1-0.5$ GeV/*c* and $p_t = 0.5-1.2$ GeV/*c*

Type			Fitting Range					
			$p_t = 0.1-0.5$ GeV/c			$p_t = 0.5-1.2$ GeV/c		
Fit. funct.	**Centr. Type**	**Coll. Type**	***A***	***T* (MeV)**	**χ^2/ *n.d.f.***	***A***	***T* (MeV)**	**χ^2/ *n.d.f.***
Hag.	Periph.	HeC	1173 ± 148	**83 ± 2**	0.36	140 ± 47	**120 ± 6**	0.97
		CC	1467 ± 170	**81 ± 2**	1.59	210 ± 57	**116 ± 5**	1.08
		CTa	2894 ± 474	**81 ± 3**	3.41	249 ± 72	**113 ± 5**	0.57
	Semicen.	HeC	2207 ± 267	**87 ± 2**	0.85	657 ± 194	**110 ± 5**	2.22
		CC	3819 ± 431	**84 ± 2**	2.73	573 ± 121	**120 ± 4**	0.28
		CTa	13710 ± 2179	**76 ± 3**	1.90	624 ± 144	**118 ± 4**	0.19
	Centr.	HeC	3908 ± 563	**87 ± 3**	0.44	2506 ± 1229	**98 ± 7**	0.93
		CC	6230 ± 738	**86 ± 2**	1.05	1023 ± 256	**119 ± 5**	1.88
		CTa	20167 ± 3589	**75 ± 3**	5.06	980 ± 428	**128 ± 9**	0.71
Bolt.	Periph.	HeC	1019 ± 116	**74 ± 2**	0.78	93 ± 29	**111 ± 5**	0.91
		CC	1258 ± 133	**72 ± 2**	2.51	140 ± 35	**108 ± 4**	1.14
		CTa	2496 ± 372	**72 ± 2**	4.30	164 ± 44	**105 ± 4**	0.58
	Semicen.	HeC	1951 ± 213	**76 ± 2**	1.55	423 ± 117	**102 ± 4**	2.22
		CC	3315 ± 341	**74 ± 2**	3.95	381 ± 76	**111 ± 3**	0.35
		CTa	11373 ± 1654	**68 ± 2**	2.63	417 ± 90	**109 ± 4**	0.22
	Centr.	HeC	3449 ± 448	**76 ± 2**	0.67	1575 ± 729	**92 ± 6**	0.97
		CC	5482 ± 589	**75 ± 2**	1.77	683 ± 160	**110 ± 4**	1.87
		CTa	16722 ± 2730	**67 ± 2**	6.09	670 ± 272	**118 ± 8**	0.71

For ^{12}C+^{12}C collisions, the T of soft p_t component increases with increasing centrality, whereas that for ^{4}He+^{12}C collisions first increases in going from peripheral to semicentral collisions, then remains almost constant in semicentral and central collisions. The centrality dependence of T of soft p_t component for

$^{12}C+^{181}Ta$ collisions demonstrates quite opposite behavior, it decreases noticeably in going from peripheral to semicentral and central collisions. On the other hand, as can be noticed from Fig. 6.16*b*, the temperature of hard p_t component for $^{12}C+^{181}Ta$ collisions increases consistently with an increase in collision centrality, whereas that for $^{12}C+^{12}C$ collisions first increases in going from peripheral to semicentral collisions, then remains approximately constant in semicentral and central collisions. For $^{4}He+^{12}C$ collisions, the T of hard p_t component decreases consistently with an increase in centrality. The observed differences between behaviors of centrality dependencies of T of both soft and hard p_t components of light and heavy collision systems could be analyzed in terms of geometry and degree of overlap of colliding nuclei. The latter can be deduced from the numbers of participant projectile and target nucleons, and the corresponding number of binary (nucleon–nucleon) collisions.

The average numbers of participant nucleons from the projectile (A) and target (B) nuclei, and the corresponding average number of binary (nucleon–nucleon) collisions in the studied collision systems can be estimated by using the relations [181–183]

$$\langle \nu_A \rangle = \frac{A\sigma_{pB}^{inel}}{\sigma_{AB}^{inel}}, \tag{6.5}$$

$$\langle \nu_B \rangle = \frac{B\sigma_{pA}^{inel}}{\sigma_{AB}^{inel}}, \text{ and} \tag{6.6}$$

$$\langle \nu_{AB} \rangle = \frac{AB\sigma_{pp}^{inel}}{\sigma_{AB}^{inel}}, \tag{6.7}$$

respectively, where A and B are the total numbers of nucleons in projectile and target nucleus, respectively, σ_{pp}^{inel}, σ_{pA}^{inel}, σ_{pB}^{inel}, and σ_{AB}^{inel} are the inelastic cross sections of proton–proton, $p+A$, $p+B$, and $A+B$ collisions, taken from Refs. [120, 184]. These relations were obtained [181, 182] from the model of independent collisions of projectile nucleons with the target nucleons. This simple model accounts for only primary nucleon–nucleon collisions and disregards the cascading of the secondary nucleons.

Table 6.25

The inelastic cross sections [120, 184] and the average numbers of nucleon–nucleon collisions $\langle \nu_{AB} \rangle$, interacting projectile $\langle \nu_A \rangle$ and target $\langle \nu_B \rangle$ nucleons, calculated using simple model of independent nucleon collisions [181, 182], and the estimated average numbers of participant nucleons in nucleus–nucleus collisions at 4.2 *A* GeV/*c* in experiment

Type	p+p	$^4He+^{12}C$	$^{12}C+^{12}C$	$^{12}C+^{181}Ta$
$\sigma^{inel}(A+B)$ (mb)	28 ± 1	450 ± 20	830 ± 50	3445 ± 140
$\langle \nu_A \rangle$	1	2.4 ± 0.2	3.8 ± 0.3	5.9 ± 0.3
$\langle \nu_B \rangle$	1	2.7 ± 0.2	3.8 ± 0.3	14.0 ± 1.0
$\langle \nu_{AB} \rangle$	1	3.0 ± 0.2	4.9 ± 0.3	18.0 ± 1.0
$\langle \nu_A \rangle + \langle \nu_B \rangle$	2	5.1 ± 0.3	7.6 ± 0.4	20.0 ± 1.0
$<n_{part..nucl..}>^{exper}$	2	5.66 ± 0.04	8.70 ± 0.04	32.5 ± 0.5

Table 6.25 presents the inelastic cross sections and the average numbers of ν_A, ν_B, and ν_{AB}, calculated using formulas in (6.5)–(6.7), along with the estimated average numbers of participant nucleons in experiment in the studied collision systems at 4.2 *A* GeV/*c*. The average numbers of participant nucleons in the studied nucleus–nucleus collisions at 4.2 *A* GeV/*c* were estimated from the mean multiplicity per event of the participant protons in Table 6.19, taking into account the corresponding ratio of neutrons and protons in each collision system. As noticed from Table 6.25, $^{12}C+^{181}Ta$ collisions are characterized by significantly larger average numbers of binary (nucleon–nucleon) collisions, participant projectile and target nucleons, as compared to those in $^4He+^{12}C$ and $^{12}C+^{12}C$ collisions. As seen from comparison of the calculated and experimental average numbers of participant nucleons in Table 6.25, the contribution of the secondary cascading

processes, neglected in the model, increases with an increase in size of a collision system. From comparison of the numbers of participant nucleons in this simple model and experiment in Table 6.25, we estimated that the secondary cascading processes contribute approximately 10%, 13%, and 38% to formation of participant nucleons in ^{4}He+^{12}C, ^{12}C+^{12}C, and ^{12}C+^{181}Ta collisions, respectively.

As deduced from analysis of relativistic heavy ion collisions [185], the contribution of soft processes scales with the number of participant nucleons and that of semi(hard) scattering processes scales with the number of binary (nucleon–nucleon) collisions. Hence, it is expected that contribution of both soft and hard processes should be significantly larger in case of heavy ^{12}C+^{181}Ta collision system as compared to the light ^{4}He+^{12}C and ^{12}C+^{12}C systems. This supports our observation that the temperature of hard p_t component for ^{12}C+^{181}Ta collisions increases with an increase in collision centrality (which corresponds to an increase of binary collisions, resulting in significant increase of probability of (semi)hard nucleon–nucleon scatterings). The pions in this hard p_t range originate mostly from an early fast stage of nuclear collisions. In terms of collective flow effects, these pions are thought to come from the early stage of collision (before chemical freeze-out) from the initial fast component of collective flow, built up by the high pressure in a core of collision zone [185]. According to the QGSM calculations for nucleus–nucleus collisions at 4.2*A* GeV/*c* [148, 149], the major fraction of pions (≈ 70% on the average) in soft p_t range originates at a later stage from decays of Δ resonances and vector mesons, such as ρ, ω and η, when the collision system cools down noticeably. In soft p_t range (p_t < 0.5 GeV/*c*), according to QGSM, fraction of pions, coming from Δ and vector meson decays, increases with increasing the collision system-size in nucleus–nucleus collisions at 4.2 *A* GeV/*c* [148, 149]. On the other hand, the hard p_t range (p_t > 0.5 GeV/*c*), in this model, is dominated (≈ 55% on the average) by pions produced directly in nucleon–nucleon collisions as $NN \to NN\pi$ [148, 149].

The observed centrality dependence of T in soft p_t range in the studied reactions could be interpreted in terms of fireball creation, expansion, and its chemical and final kinetic freeze-out, as was discussed for Au+Au collisions at RHIC energies in Ref. [185]. The main difference is that, at our collision energy ($\sqrt{s_{nn}} = 3.14$ GeV), the fireball is expected to be compressed and dense nuclear (nucleon) matter, whereas at RHIC energies the fireball can be associated with the Quark Gluon Plasma, a state of deconfined quarks and gluons. The threshold c.m. collision energy $\sqrt{s_{nn}} \approx 5$ GeV was estimated for reaching the deconfinement threshold energy density from lattice QCD calculations [6]. Therefore, it is expected that a significant fraction of collision system should undergo transition to the QGP in central heavy ion collisions at RHIC energies, much larger than $\sqrt{s_{nn}} = 5$ GeV. After the expansion and chemical freeze-out of a compressed nuclear matter, or a nuclear (nucleon) fireball, created in central $^{12}C+^{181}Ta$ collisions, the produced pions undergo multiple elastic scatterings with the surrounding nucleons of a heavy target medium and, hence, their temperature drops noticeably at the final kinetic freeze-out.

The observed centrality dependence of T in soft p_t range in $^{12}C+^{181}Ta$ collisions could be explained qualitatively in a simpler way. As $A_p << A_t$ in $^{12}C+^{181}Ta$ collisions, the energy of impinging projectile nucleons has to be distributed among more and more nucleons of heavy ^{181}Ta target as the collision centrality increases. In case of central $^{12}C+^{181}Ta$ collisions, each of incoming projectile nucleons invokes at least several nucleon–nucleon collisions (interactions) with heavy target nucleons, which results in significantly higher multiplicity of pions produced on tantalum nuclei in central $^{12}C+^{181}Ta$ collisions as compared to peripheral $^{12}C+^{181}Ta$ collisions, where significantly lesser pions are produced, mostly in the first single collisions (interactions) of projectile nucleons with target nucleons [32]. Indeed, as observed in Fig. 6.11*b*, the significantly larger number of π^- mesons is produced in around heavy target fragmentation region as compared to light projectile fragmentation region. Hence, in case of central

$^{12}C+^{181}Ta$ collisions, the collision energy is distributed among significantly larger number of pions compared to peripheral $^{12}C+^{181}Ta$ collisions, which results in lower mean kinetic energies of π^- in central $^{12}C+^{181}Ta$ collisions as compared to the peripheral ones [32]. Hence, the *T* of soft p_t component decreases with increasing centrality of $^{12}C+^{181}Ta$ collisions.

In contrast to $^{12}C+^{181}Ta$ collisions, quite opposite trend in behavior of centrality dependence of *T* of soft p_t component in $^{4}He+^{12}C$ and $^{12}C+^{12}C$ collisions, observed in Fig. 6.16*a*, could be interpreted as due to the much smaller system-size and, hence, much lesser probability of multiple rescatterings of pions after chemical freeze-out stage. The small difference in behavior of centrality dependence of *T* of soft p_t component in $^{4}He+^{12}C$ and $^{12}C+^{12}C$ collisions in Fig. 6.16*a* can be explained by the difference in geometry of these collision systems. As $A_p < A_t$ in $^{4}He+^{12}C$ collisions, we expect a complete overlap of these colliding nuclei already in semicentral collisions. Therefore, after the initial growth of *T* of soft p_t component in $^{4}He+^{12}C$ collisions in going from peripheral to semicentral collisions, practically no more appreciable energy can be transferred from target to projectile nucleons in the range from semicentral to central collisions. Hence, the temperature of soft p_t component remains constant for semicentral and central $^{4}He+^{12}C$ collisions. As $A_p = A_t$ in $^{12}C+^{12}C$ collisions, we expect the consistent growth of degree of overlap of these colliding nuclei with an increase in centrality in going from peripheral to central collisions. Therefore, the energy transferred from projectile to target nucleons and *T* of soft p_t component increases with increasing centrality of $^{12}C+^{12}C$ collisions. In above, an increase of the energy, transferred from projectile to target nucleons with increasing centrality, could also be thought as an increase in compressional energy of compressed nuclear matter (or nuclear (nucleon) fireball) in semicentral and central $^{12}C+^{12}C$ collisions.

In $^{4}He+^{12}C$ and $^{12}C+^{12}C$ collision systems, both projectile and target nuclei have equal numbers of protons and neutrons. On the other hand, in $^{12}C+^{181}Ta$ collision system, the number of neutrons is almost 1.5 times greater than that of protons in the heavy ^{181}Ta target nucleus. Hence, the fraction as well the number of interactions (collisions) of projectile nucleons with target neutrons is significantly greater in ^{12}C+^{181}Ta collisions as compared to ^{4}He+^{12}C and ^{12}C+^{12}C collisions. This increases significantly the fraction of π^- coming from decay of neutral baryon resonances in case of ^{12}C+^{181}Ta collisions as compared to those in ^{4}He+^{12}C and ^{12}C+^{12}C collisions. Indeed, it was estimated experimentally that about half of the negative pions come from decay of Δ^0 resonances in ^{12}C+^{12}C [27] and ^{4}He+^{12}C [47] collisions at 4.2 *A* GeV/*c*, whereas the corresponding estimated fraction of π^- from Δ^0 decay was around $2/3$ in ^{12}C+^{181}Ta collisions [44] at 4.2*A* GeV/*c*. As shown in Table 6.25, the average number of binary collisions in ^{12}C+^{181}Ta collisions is at least around 5 to 6 times greater than that in ^{4}He+^{12}C and ^{12}C+^{12}C collisions. In addition, the contribution of the secondary cascading processes to formation of participant nucleons was significantly larger in ^{12}C+^{181}Ta collisions (38%), as compared to ^{4}He+^{12}C (10%) and ^{12}C+^{12}C (13%) collisions. Hence, it is expected that the fraction of the negative pions coming from decay of Δ resonances will increase with increasing centrality of ^{12}C+^{181}Ta collisions.

As already mentioned, the consistent increase of T of hard p_t component in ^{12}C+^{181}Ta collisions, observed in Fig. 6.16*b*, can be explained either by the early fast component of collective flow resulting from the high pressure, built up in a core of collision zone, in central collisions or by an increase of probability of semi(hard) scatterings with an increase in collision centrality, which scales with the number of binary collisions. In case of ^{12}C+^{12}C collisions, the temperature of hard p_t component first increases in going from peripheral to semicentral collisions, then it remains almost constant for semicentral and central collisions. This is likely due to the relative smallness of both identical projectile and target nucleus. And, hence, we do not expect any appreciable increase in the pressure, built up in a core of collision zone, in going from semicentral to central ^{12}C+^{12}C collisions. For even smaller ^{4}He+^{12}C collision system, the probability of production of a dense nuclear (nucleon) fireball in semicentral and central collisions is expected to be extremely low, if not zero. Therefore, the decrease of T of hard p_t component with increasing centrality of ^{4}He+^{12}C collisions can be explained in terms of simple semi(hard) nucleon–nucleon collisions. In case of peripheral ^{4}He+^{12}C collisions, quite energetic pions produced in semi(hard) nucleon–nucleon collisions (from small overlap zone at periphery of colliding nuclei) would most probably escape the collision zone without further rescattering. With an increase in collision centrality, the path to be traversed through target ^{12}C nucleus, along the direction of the impinging projectile nucleon, increases from zero to $2R(^{12}\mathrm{C})$ (where $R(^{12}\mathrm{C})$ is the radius of ^{12}C nucleus) in going from most peripheral to most central ^{4}He+^{12}C collisions.

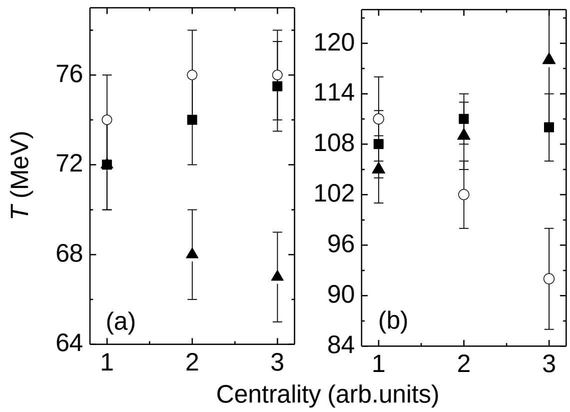

Fig. 6.17. The same as in Fig. 6.16, but extracted from fitting by the one temperature Boltzmann function

Hence, the rescattering probability of a pion, produced in semi(hard) nucleon–nucleon collision, on surrounding target nucleons increases with increasing centrality of ^{4}He+^{12}C collisions. This could explain qualitatively the decrease of T of hard p_t component with increasing centrality of ^{4}He+^{12}C collisions, observed in Fig. 6.16*b*.

As seen from Fig. 6.17, the temperatures extracted using one temperature Boltzmann function reproduce completely the behavior of centrality dependences of T of both soft and hard p_t components of π^-, observed in Fig. 6.16.

Figure 6.18 presents collision system-size dependencies of the temperatures of soft and hard components of the experimental p_t distributions of π^- in peripheral, semicentral, and central nucleus–nucleus collisions at 4.2 *A* GeV/*c*, extracted from fitting by one temperature Hagedorn function in p_t ranges 0.1 – 0.5 GeV/*c* and 0.5 – 1.2 GeV/*c*, respectively. As observed from Fig. 6.18*a*, the temperatures of soft p_t component for semicentral and central collisions decrease consistently with an increase in system size ($(A_p A_t)^{1/2}$), or, in other words, with an increase in the number of participant nucleons in collision systems. On the other hand, the temperature of soft p_t component for peripheral collisions does not change appreciably with an increase in collision system-size. The decrease of *T* in semicentral and central collisions in going from ^{4}He+^{12}C to ^{12}C+^{12}C and ^{12}C+^{181}Ta collisions could be interpreted in terms of the nuclear (nucleon) fireball creation as well as by an increase of fraction of the "cold" negative pions, coming from decay of delta resonances. As already mentioned, with an increase in system-size, the pions undergo more and more elastic rescaterrings on the nucleons of the surrounding medium until they reach the final kinetic freeze-out stage, where the system is cooled down significantly. Evidently, no nuclear (nucleon) fireball is expected to be produced in peripheral nucleus–nucleus collisions. Peripheral interactions of nuclei proceed at significantly lower momentum–energy transfers with markedly lesser number of pions (as well as with considerably smaller fraction of π^- from resonance decays) as compared to semicentral and central collisions. Due to short range of strong interactions, only relatively small fractions (at periphery of nuclei) of colliding nuclei can be involved in strong interaction in peripheral collisions. Hence, the size of the colliding nuclei does not play noticeable role in peripheral collisions and, therefore, the temperature of soft p_t component does not vary appreciably with an increase in $(A_p A_t)^{1/2}$ in these interactions.

Here it is worth mentioning the results of Ref. [179], where the light front analysis of the negative pions in central He+(Li, C), C+Ne, C+Cu, and O+Pb collisions at 4.5 A GeV/c was performed. The phase space of secondary pions was divided into two parts, and in one of which the thermal equilibrium assumption seemed to be in good agreement with the data. The thermal equilibrium region corresponded to lower p_t range ($p_t < 0.4$ GeV/c) [179]. The corresponding temperatures were extracted from fitting the data by the Boltzmann distribution function. The dependence of obtained T on $(A_p A_t)^{1/2}$ was studied. The temperature decreased consistently with an increase in $(A_p A_t)^{1/2}$ [179]. This is in agreement with a decrease of T of soft p_t component of π^- with increasing of the system-size in semicentral and central nucleus–nucleus collisions at 4.2 A GeV/c, obtained in present work. The temperatures of soft p_t component extracted in the present analysis are comparable with the corresponding temperatures obtained in Ref. [179]. However, no physical interpretation for decrease of T with an increase in $(A_p A_t)^{1/2}$ was given in Ref. [179].

As observed from Fig. 6.18*b*, the T of hard p_t component in central collisions increases consistently with an increase in system size. This can be understood in terms of semi(hard) nucleon–nucleon collisions. Such an increase of the temperature of hard p_t component in central collisions with increasing of the system size can be explained as follows. This is, as already mentioned, because the probability of semi(hard) nucleon–nucleon collisions increases significantly as the number of binary collisions increases quite prominently in going from central ^{4}He+^{12}C to central ^{12}C+^{12}C collisions, and further to central ^{12}C+^{181}Ta collisions. Indeed, since $A(^{181}\mathrm{Ta}) >> A(^{12}\mathrm{C}) > A(^{4}\mathrm{He})$, the probability of semi(hard) scattering of projectile nucleon with target nucleon will be greater in case of central ^{12}C+^{181}Ta collisions as compared to central ^{12}C+^{12}C and ^{4}He+^{12}C collisions.

Hence, the T of hard p_t component in central collisions increases with an increase in $(A_p A_t)^{1/2}$. This could also be explained by an increase in pressure, built up in a core of collision zone (and, hence, by an increase of T of “hot” pions coming out of this core at initial collision stage), with an increase in $(A_p A_t)^{1/2}$ in central nucleus–nucleus collisions. Indeed, since ^{181}Ta target is much heavier than light ^{12}C target, the extent of compressibility of a nuclear matter, and hence the pressure attained in central nucleus–nucleus collisions, is expected to be larger in case of central ^{12}C+^{181}Ta collisions as compared to central ^{12}C+^{12}C and ^{4}He+^{12}C collisions.

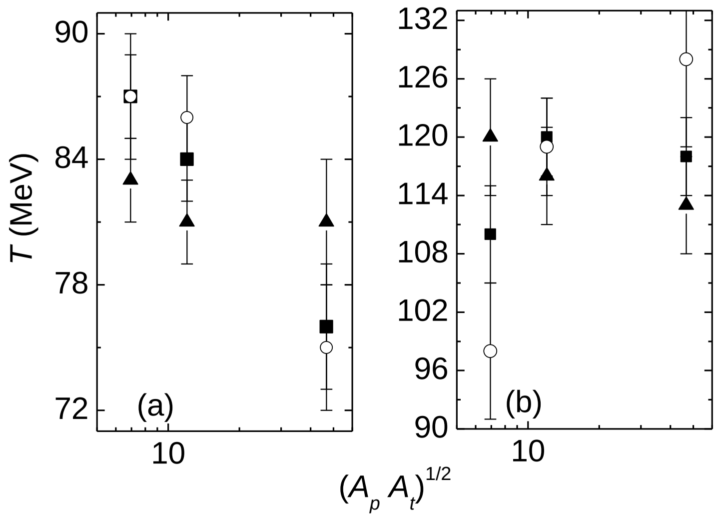

Fig. 6.18. Collision system-size dependence of the temperature of soft (a) and hard (b) component of the experimental transverse momentum distributions of the negative pions in peripheral (▲), semicentral (■), and central (○) nucleus–nucleus collisions at 4.2 *A* GeV/*c*, extracted from fitting by one temperature Hagedorn function in p_t range 0.1 – 0.5 GeV/*c* and 0.5 – 1.2 GeV/*c*, respectively

As seen from Fig. 6.18*b*, the *T* of hard p_t component shows only weak decrease with an increase in $(A_p A_t)^{1/2}$ in peripheral nucleus–nucleus collisions at 4.2 *A* GeV/*c*. Such a weak dependence of *T* on $(A_p A_t)^{1/2}$, as already discussed, is likely due to small degree of overlap, at periphery of colliding nuclei, in peripheral interactions. Though an overlap of colliding nuclei is relatively small in peripheral collisions, the probability of further rescattering of pions, produced in semi(hard) nucleon–nucleon collisions, on target nucleons is greater in ^{12}C+^{181}Ta as compared to $^{12}C+^{12}C$ and $^{4}He+^{12}C$ collisions due to still some differences in the sizes of overlap regions in peripheral interactions since $A(^{181}\mathrm{Ta}) >> A(^{12}\mathrm{C}) > A(^{4}\mathrm{He})$. In semicentral collisions, as observed from Fig. 6.18*b*, the T of hard p_t component is larger in heavier $^{12}C+^{12}C$ and $^{12}C+^{181}Ta$ collision systems as compared to the lighter $^{4}He+^{12}C$ system, which is likely due to the larger size of overlap region in the heavier systems as compared to the lighter one.

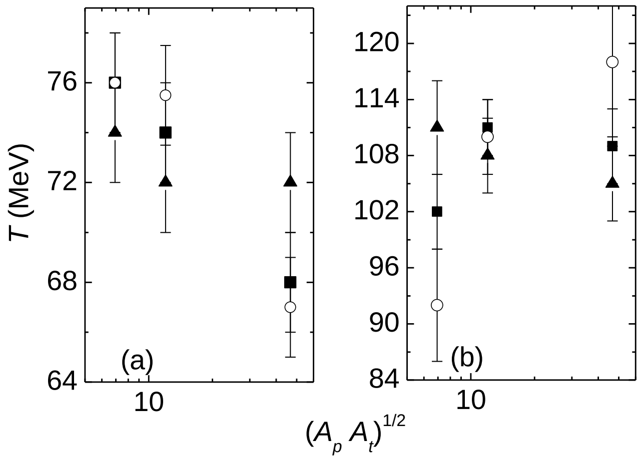

Fig. 6.19. The same as in Fig. 6.18, but extracted from fitting by the one temperature Boltzmann function

Figure 6.19 shows that the temperatures extracted using one temperature Boltzmann function reproduce completely the behavior of system size dependences of T of both soft and hard p_t components of π^-, observed in Fig. 6.18.

Finally, it is of importance to discuss some quantitative results on values of T, obtained for pions in other JINR, GSI and SPS experiments in order to link the quantitative findings of the present work with those obtained at lower, intermediate, and higher energies. In Ref. [186] the temperatures of the negative pions in central Mg+Mg collisions at 4.3 *A* GeV/*c* (GIBS set-up of JINR) were estimated from inclusive kinetic energy and transverse momentum spectra of π^- mesons using two different selection criteria: in the rapidity interval 0.5–2.1 (corresponding to π^- pionization region) and at c.m.s. angles (90±10) degrees.

The pion spectra were fitted by a sum of two exponentials with two temperatures, T_1 = 55 ± 1 MeV and T_2 = 113 ± 2 MeV. The relative yield of the second exponential term having a temperature T_2 was about 22%. These values of T_1 and T_2 are comparable with the corresponding T_1 and T_2 values extracted in central nucleus–nucleus collisions at 4.2 *A* GeV/*c* in the present analysis (see Table 6.23). The light front analysis of the negative pions in central He (Li, C), C+Ne, C+Cu and O+Pb collisions at 4.5*A* GeV/*c* was made in Ref. [179]. The phase space of secondary pions was divided into two parts, into one of which the thermal equilibrium seemed to be in a good agreement with the data. The thermal equilibrium region corresponded to lower p_t range (p_t < 0.4 GeV/*c*) [179]. The extracted temperatures proved to be 81 ± 2, 79 ± 3, 72 ± 2, and 55 ± 3 MeV in central He(Li, C), C+Ne, C+Cu, and O+Pb collisions at 4.5 *A* GeV/*c*, respectively [179]. The temperature obtained in central He(Li, C) collisions at 4.5*A* GeV/*c* is compatible with the temperature of soft p_t component of π^- mesons in central ^{4}He+^{12}C collisions at 4.2 *A* GeV/*c*, extracted in the present analysis (see Table 6.24). Also the temperatures extracted in central C+Ne and C+Cu collisions at 4.5 *A* GeV/*c* [179] are comparable with the corresponding temperatures of soft p_t component of π^- mesons in central ^{12}C+^{12}C and ^{12}C+^{181}Ta collisions, respectively, extracted in the present work (see Table 6.24).

The values of *T* for pions were extracted also in GSI experiments (FOPI, FRS, KAON and TAPS Collaborations) [187–193]. It was deduced that the spectra of π^- mesons in central Ni+Ni collisions at incident (kinetic) energies E_{kin} = 1.06 *A* GeV, 1.45 *A* GeV, and 1.93 *A* GeV (FOPI Collaboration [187]) required the sum of two exponentials with independent yields and inverse slope parameters T_l and T_h describing mainly the low and high momentum part of the spectrum, respectively. T_l = 55 ± 3 MeV and T_h = 93 ± 5 MeV, and T_l = 56 ± 3 MeV and T_h = 100 ± 5 MeV, and T_l = 61 ± 3 MeV and T_h = 115 ± 6 MeV were extracted at E_{kin} = 1.06 *A* GeV, 1.45 *A* GeV, and 1.93 *A* GeV, respectively. In Ne+NaF collisions (FRS Collaboration) the *T* for π^- mesons ranged from 78 ± 2 MeV to 96 ± 3 MeV for projectile energies from 1.34 *A* to 1.94 *A* GeV. The KAON Collaboration extracted the value of T for π^+ mesons to be 71 ± 3 MeV and 95 ± 3 MeV for projectile energies 1 *A* GeV and 1.8 *A* GeV, respectively. The TAPS Collaboration obtained T value for π^0 mesons to be 83 ± 3 MeV in C+C collisions at E_{kin} = 2 *A* GeV and T = 70 ± 1 MeV in Ar+Ca collisions at E_{kin} = 1.5 *A* GeV. Significantly larger inverse slope parameters (apparent temperatures) T ranging from around 140 to 160 MeV were extracted in SPS experiments by NA44 Collaboration [178, 193] for charged pions from fitting their transverse mass spectra with simple Boltzmann distribution in central Pb+Pb and S+S collisions at 158 *A* GeV/*c* and 200 *A* GeV/*c*, respectively. On the whole, the temperatures extracted from pion spectra in central nucleus–nucleus collisions (GSI, JINR, SPS experiments) depended on collision energy and sizes (geometry) of the colliding nuclei.

§ 6.4 Summary and Conclusions on CHAPTER VI

We studied the dependencies of the p_t spectra of the negative pions produced in minimum bias $^{12}C^{12}C$ collisions at 4.2 *A* GeV/*c* on the collision centrality and pion rapidity range. The extracted transverse momentum spectra were analyzed using fits by Hagedorn, Boltzmann, Simple Exponential, and Gaussian functions. We observed that the p_t spectra of π^- mesons are described much better by the two-temperature Hagedorn and Boltzmann functions compared to the fitting done by the one-temperature functions, which is in line with the earlier papers [36, 38, 63, 73, 75, 78]. Out of the four fitting functions used, Hagedorn and Boltzmann functions gave significantly better fits of the experimental p_t spectra with the physically acceptable values of the extracted spectral temperatures, compared to Simple Exponential, and Gaussian functions. The fitting of the p_t spectra of π^- with Boltzmann function resulted in slightly lower values of the spectral temperatures compared to those by Hagedorn function. It was found that the dominant contribution (R_1 ~ 85%) to the total π^- multiplicity in $^{12}C^{12}C$ collisions at

4.2 A GeV/c is given by the spectral temperature T_1 ~ (65–76) ± 3 MeV, which agrees within the uncertainties with the results of Ref. [78].

We extracted and fitted the p_t spectra of the negative pions for peripheral, semicentral, and central $^{12}C^{12}C$ collisions as well as for three rapidity regions of π^- in the fitting ranges $p_t = 0.1 \div 1.2$ GeV/c and $p_t = 0.1 \div 0.7$ GeV/c. The extracted values of the spectral temperatures T_1 and T_2 were consistently larger for the p_t spectra of π^- mesons coming from midrapidity range ($|y_{cm.}| \leq 0.3$) as compared to those of transverse momentum spectra of the negative pions generated in the target ($y_{cm.} \leq -0.3$) and projectile ($y_{cm.} \geq 0.3$) fragmentation regions. The spectral temperatures T_1 and T_2 of the p_t spectra of π^- mesons extracted from fitting in range $p_t = 0.1 \div 1.2$ GeV/c were very close to each other for the group of peripheral, semicentral, and central $^{12}C^{12}C$ collision events, selected using the number of participant protons, and thus practically did not depend on the collision centrality. However, the values of T_1 and T_2 extracted from fitting in range $p_t = 0.1 \div 0.7$ GeV/c were consistently and noticeably larger in case of the central collisions as compared to peripheral and semicentral collisions. Possible reason for that could be that the higher p_t and high temperature part of the pion spectra with quite large statistical errors influences significantly the extracted T_1 and T_2 values masking and suppressing the centrality dependence of the spectral temperatures. This is likely to be the reason for not observing the centrality dependence of the extracted temperatures in the earlier works [36, 78], where the pion p_t spectra for peripheral, semicentral, and central collisions were fitted in the whole transverse momentum range.

The transverse momentum spectra of the negative pions produced in minimum bias $^{12}C^{181}Ta$ collisions at 4.2 A GeV/c were analyzed by fitting with the four different commonly used functions: Hagedorn, Boltzmann, Simple Exponential, and Gaussian functions. It was observed that the p_t spectra of π^- mesons are fitted much better using the two-temperature Hagedorn and Boltzmann functions as compared to the fitting done by the one-temperature functions, which is in agreement with the earlier works [38, 73, 78, 63, 75, 36]. Out of the above four fitting functions, Hagedorn and Boltzmann functions provide better fits of the experimental p_t spectra giving the physically acceptable values of the spectral temperatures, compared to the other two functions. The fitting of the p_t spectra of pions with Boltzmann function gives noticeably lower values of the spectral temperatures compared to that by Hagedorn function. It was found that the dominant contribution (R_1 ~ 80–83%) to the total π^- multiplicity in ^{12}C^{181}Ta collisions at 4.2 A GeV/c is given by the spectral temperature T_1 ~ (50–57) ± 3 MeV, which is compatible within the uncertainties with the results of Ref. [78].

We extracted and fitted the p_t spectra of the negative pions for peripheral, semicentral, and central ^{12}C^{181}Ta collisions as well as for three rapidity regions of π^- in the fitting ranges $p_t = 0.1 \div 1.2$ GeV/c and $p_t = 0.1 \div 0.7$ GeV/c. In general the absolute values of T_1 and T_2 were lower in case of fitting in the range $p_t = 0.1 \div 0.7$ GeV/c as compared to the fitting interval $p_t = 0.1 \div 1.2$ GeV/c. The extracted values of the spectral temperatures T_1 and T_2 were consistently larger for the p_t spectra of π^- mesons coming from midrapidity range ($|y_{cm.}| \le 0.3$) as compared to those of transverse momentum spectra of the negative pions generated in the target ($y_{cm.} \le -0.3$) and projectile ($y_{cm.} \ge 0.3$) fragmentation regions. The spectral temperatures of the negative pions coming from projectile fragmentation region ($y_{cm.} \ge 0.3$) proved to be consistently larger compared to the respective temperatures of the negative pions coming from target fragmentation region ($y_{cm.} \le -0.3$). The extracted spectral temperatures T_1 and T_2 of the p_{t} spectra of π^- mesons were compatible within the uncertainties for the group of peripheral, semicentral, and central ^{12}C^{181}Ta collision events, selected using the number of participant protons in collision events.

We analyzed the collision centrality as well as the system-size dependencies of the temperatures of soft (p_t = 0.1–0.5 GeV/c) and hard (p_t = 0.5–1.2 GeV/c) parts of the experimental transverse momentum distributions of the negative pions in ^{4}He^{12}C, ^{12}C^{12}C, and ^{12}C^{181}Ta collisions at 4.2 *A* GeV/*c* ($\sqrt{s_{nn}}$ = 3.14 GeV). For the studied collision systems and selected collision centralities, the temperatures were extracted from fitting separately the soft and hard components of the p_t distributions of π^- mesons by the one temperature Hagedorn and one temperature Boltzmann functions. The temperatures extracted using one temperature Boltzmann function reproduced completely the observed collision centrality and system-size dependencies of the temperatures of both soft and hard p_t components, obtained from fitting by the one temperature Hagedorn function.

The extracted temperatures of both soft and hard components of p_t distributions of π^- depended on the geometry (size) and degree of overlap of colliding nuclei in peripheral, semicentral, and central ^{4}He^{12}C, ^{12}C^{12}C, and ^{12}C^{181}Ta collisions at $\sqrt{s_{nn}}$ = 3.14 GeV. The differences between the extracted temperatures in the studied collision systems increased with an increase in collision centrality.

The temperature of the soft p_t component of the negative pions in ^{12}C^{12}C (^{12}C^{181}Ta) collisions increased (decreased) with increasing of collision centrality. The temperature of the hard p_t component of π^- in ^{12}C^{181}Ta (^{4}He^{12}C) collisions increased (decreased) consistently with an increase in collision centrality.

The temperature of the soft p_t component for π^- decreased consistently with an increase in system-size ($(A_p A_t)^{1/2}$) in the semicentral and central nucleus–nucleus collisions at 4.2 *A* GeV/*c*. This agreed with the decrease of *T* of π^- with increasing $(A_p A_t)^{1/2}$ obtained in Ref. [179] using the light front analysis of the negative pions in central He+(Li, C), C+Ne, C+Cu, and O+Pb collisions at 4.5 *A* GeV/*c*. The decrease of *T* of the soft p_t component in semicentral and central collisions in going from ^{4}He^{12}C to ^{12}C^{12}C and to ^{12}C^{181}Ta collisions could be interpreted as follows: with an increase in system-size, the pions have to undergo more and more rescatterings on nucleons of the surrounding medium until they reach the final kinetic freeze-out stage, where the system is cooled down appreciably.

Such decrease of T of soft p_t component of π^- with an increase in $(A_p A_t)^{1/2}$ can also be interpreted qualitatively in a simpler way. In contrast to semicentral and central ^{4}He^{12}C and ^{12}C^{12}C collisions, in semicentral and central ^{12}C^{181}Ta collisions, the energy of the impinging (projectile) nucleons has to be distributed among significantly larger numbers of participant (target) nucleons and produced pions. Hence, this resulting in lesser average kinetic energy of π^- in soft p_t range in ^{12}C^{181}Ta collisions as compared to those in ^{4}He^{12}C and ^{12}C^{12}C collisions.

In central collisions, the temperature of the hard p_t component of π^- mesons increased consistently with an increase in system-size. This hard p_t component can be explained as mainly due to pions produced in semi(hard) nucleon–nucleon collisions. Such increase of T of hard p_t component in central collisions with increasing of the system-size is in line with the following: the probability of semi(hard) nucleon–nucleon collisions increases as the number of binary collisions increases quite prominently in going from central ^{4}He^{12}C to central ^{12}C^{12}C collisions, and further to central ^{12}C^{181}Ta collisions. Indeed, since $A(^{181}\mathrm{Ta}) >> A(^{12}\mathrm{C}) > A(^4\mathrm{He})$, the probability of the semi(hard) scattering of a projectile nucleon with a target nucleon will be greater in case of the central ^{12}C^{181}Ta collisions as compared to the central ^{12}C^{12}C and ^{4}He^{12}C collisions. Increase of T of the hard p_t component in central collisions could also be interpreted by an increase in a pressure, built up in a core of collision zone (and, hence, by an increase of T of the “hot” pions emitted from this core at initial collision stage), with an increase in $(A_p A_t)^{1/2}$ in central nucleus–nucleus collisions.

CONCLUSIONS

For the first time, the mass distributions of Δ^0(1232) resonances were reconstructed in minimum bias p^{12}C, d^{12}C, ^{4}He^{12}C, ^{12}C^{181}Ta collisions at 4.2 A GeV/c, ^{16}Op collisions at 3.25 A GeV/c, π^{-12}C interactions at 40 GeV/c from experimental and background invariant mass distributions of $p\pi^-$ pairs, using the method of analysis of the angles between outgoing π^- mesons and protons. The masses and widths of the Δ^0(1232) resonances in the above collisions were extracted from fitting Δ^0(1232) mass distributions by the relativistic Breit-Wigner function. The fractions of π^--mesons coming from Δ^0(1232) decay as well as the relative number of nucleons excited to Δ^0 at freeze-out were estimated for the above collisions.

It was obtained that around (40-50)% of the produced negative pions in p^{12}C, d^{12}C, α^{12}C and ^{12}C^{181}Ta collisions at 4.2 A GeV/c, and in ^{16}Op collisions at 3.25 A GeV/c come from decay of Δ^0(1232) resonances, whereas in $\pi^{-\,12}$C interactions at 40 GeV/c this fraction was about 6%.

The average decrease in the mass of the Δ^0(1232) resonances in the analyzed collisions agreed within the uncertainties with the average binding energy of the nucleons of the fragmenting nuclei, suggesting that the Δ^0(1232) resonances are mainly produced on the bound nucleons at the collective excitations of the fragmenting nuclei in the analyzed minimum bias collisions.

The widths of the experimental rapidity spectra of the negative pions were found to decrease by $(8\pm2)\%$, $(5\pm1)\%$, and $(15\pm2)\%$ in going from peripheral to central d^{12}C, ^{12}C^{12}C, and ^{12}C^{181}Ta collisions, respectively, and the centers of the experimental rapidity distributions of π^- mesons were found to shift by –0.32±0.04 and –0.44±0.02 units towards target fragmentation region while going from peripheral to central d^{12}C and ^{12}C^{181}Ta collisions, respectively. On the whole, the degree of shift of y_0 and decrease in the width of rapidity spectra of negative pions in going from peripheral to central collisions correlated with the ratio of the mass numbers of target and projectile nuclei.

The experimental cm rapidity distributions of the negative pions in $^{12}C^{12}C$ collisions at 4.2 *A* GeV/*c* ($\sqrt{s_{nn}}$ = 3.14 GeV) were described quite satisfactorily using the simple phenomenological model, the GCM. Approximate ($\gamma \to 0$ as $\sqrt{s_{nn}} \to \infty$) asymptotic behavior of the parameter γ of GCM function was revealed from analysis of the cm energy dependence of γ, extracted for pions in central $^{12}C^{12}C$ collisions at $\sqrt{s_{nn}}$ = 3.14 GeV, central Pb+Pb collisions at $\sqrt{s_{nn}}$ between 6.3 and 12.3 GeV, and central Au+Au collisions at $\sqrt{s_{nn}}$ between 19.6 and 200 GeV. For $\gamma \le 0$ and finite rapidities, the factor $(AA)^{\gamma y^2}$ attains its maximum value 1 at $\gamma=0$. Physically, $\gamma \cong 0$ could possibly be related to complete dehadronization of all the constituent nucleons of the collision system as a result of head-on collision of two identical nuclei, when the whole colliding system undergoes transformation into the state of free (deconfined) quarks and gluons, and attains its highest possible energy density.

A large gap was observed between the values of γ for central $^{12}C^{12}C$ collisions at $\sqrt{s_{nn}}$ = 3.14 GeV and central PbPb collisions at $\sqrt{s_{nn}}$ ≥ 6.3 GeV. This is in line with the theoretical expectation [6] that the critical energy density for transition of a nuclear matter into the phase of deconfined quarks and gluons should reach already at $\sqrt{s_{nn}} \approx 5$ GeV. Hence, the parameter γ could possibly be sensitive to deconfinement phase transition. Much smaller value of γ extracted in central $^{12}C+^{12}C$ collisions at $\sqrt{s_{nn}}$ = 3.14 GeV than γ's obtained in central heavy ion collisions at $\sqrt{s_{nn}}$ ≥ 6.3 GeV could be explained by the relatively low energy density attained in central $^{12}C+^{12}C$ collisions at $\sqrt{s_{nn}}$ = 3.14 GeV as compared to quite large degree of dehadronization of the whole collision system with much higher energy densities attained in central Pb+Pb and Au+Au collisions at high energies.

Experimental p_t spectra of π^- were fitted significantly better by using Hagedorn function with two temperatures, T_1 and T_2, as compared to the one-temperature fit in d^{12}C, ^{4}He^{12}C, and ^{12}C^{12}C collisions at 4.2 A GeV/c. The dominant contribution (R_1 ~ 90%) to the total multiplicity of π^- mesons came from spectral temperature T_1 ~ 78–84 MeV, while the relative yield of the high-temperature, T_2 ~ 146–155 MeV, component was much lower (R_2 ~ 10%). The spectral temperatures, T_1 and T_2, and their relative contributions did not depend, within fitting errors, on the degree of collision centrality in ^{12}C^{12}C collisions at 4.2 A GeV/c.

It was deduced that the extracted temperatures of both soft (p_t = 0.1–0.5 GeV/c) and hard (p_t = 0.5–1.2 GeV/c) components of p_t distributions of π^- depended on the geometry (size) and degree of overlap of colliding nuclei in peripheral, semicentral, and central ^{4}He^{12}C, ^{12}C^{12}C, and ^{12}C^{181}Ta collisions at 4.2 A GeV/c ($\sqrt{s_{nn}}$ = 3.14 GeV). The differences between extracted temperatures in the studied collision systems increased with an increase in collision centrality. The temperature of the soft p_t component of the negative pions in ^{12}C+^{12}C (^{12}C+^{181}Ta) collisions increased (decreased) with increasing of collision centrality. The temperature of the hard p_t component of π^- in ^{12}C+^{181}Ta (^{4}He+^{12}C) collisions increased (decreased) consistently with an increase in collision centrality. The temperature of soft p_t component for π^- decreased consistently with an increase in system-size ($(A_pA_t)^{1/2}$) in the semicentral and central nucleus–nucleus collisions at 4.2 A GeV/c. This agreed with decrease of T of π^- with increasing $(A_pA_t)^{1/2}$ obtained in Ref. [179] using the light front analysis of the negative pions in central He+(Li, C), C+Ne, C+Cu, and O+Pb collisions at 4.5 A GeV/c. The decrease of T of soft p_t component in semicentral and central collisions in going from ^{4}He^{12}C to ^{12}C^{12}C and to ^{12}C^{181}Ta collisions could be interpreted in terms of the nuclear (nucleon) fireball creation, expansion, and its chemical and final kinetic freeze-out. With an increase in system-size, the pions have to undergo more and more rescatterings on nucleons of the surrounding medium until they reach the final kinetic freeze-out stage, where the system is cooled down appreciably.

It was obtained that the temperature of the hard p_t component of π^- increased consistently with an increase in system-size in central collisions. This hard p_t component can be explained as mainly due to pions produced in semi(hard) nucleon–nucleon collisions. Such increase of T of hard p_t component in central collisions with increasing of the system-size is in line with the following: the probability of semi(hard) nucleon–nucleon collisions increases as the number of binary collisions increases quite prominently in going from central ^{4}He^{12}C to central ^{12}C^{12}C collisions, and further to central ^{12}C^{181}Ta collisions. Increase of T of hard p_t component in central collisions could also be interpreted by an increase in pressure, built up in a core of collision zone (and, hence, by an increase of T of "hot" pions emitted from this core at initial collision stage), with an increase in $(A_p A_t)^{1/2}$ in central nucleus–nucleus collisions.

In the end, I would like to thank sincerely my official scientific consultant Prof. S. L. Lutpullaev. I am grateful to Academician B. S. Yuldashev and Professor Kosim Olimov for the fruitful discussions of the results of the present doctoral (Doctor of Science) dissertation and useful suggestions and comments, which helped to make the dissertation more presentable and clear. Therefore, I consider Academician Bekhzod S. Yuldashev and Professor Kosim Olimov as the scientific consultants of my Doctor of Science dissertation equally as my official scientific consultant, Professor S. L. Lutpullaev.

REFERENCES

1. Karsch F. Lattice Results on QCD Thermodynamics // Nucl. Phys. A. – Elsevier (Holland), 2002. – Vol. 698. – pp. 199-208.
2. STAR Collaboration (Abelev B. I. *et al*.) Systematic Measurements of Identified Particle Spectra in pp, d+Au, and Au+Au Collisions from STAR // Phys. Rev. C – American Physical Society (USA), 2009. – Vol. 79. –id.034909. – p.034909-1.
3. LHC experiments make progress in our understanding of the early universe's state of matter // CERN Press Release, February 9, 2017. – Geneva (Switzerland), 2017. **(**https://press.cern/update/2017/02/lhc-experiments-make-progress-our-understanding-early-universes-state-matter)
4. Adronic A. An overview of the experimental study of quark-gluon matter in high energy nucleus-nucleus collisions // Int. J. Mod. Phys. A. – World Scientific (Singapore), 2014. – Vol. 29. – id.1430047. – p. 1430047-1.
5. Chapline G.F., Johnson M.H., Teller E., and Weiss M.S. Highly Excited Nuclear Matter // Phys. Rev. D. – American Physical Society (USA), 1973. – Vol. 8. – p. 4302.
6. Karsch F. Lattice QCD at high temperature and density // Lect. Notes Phys. A. – Springer (Germany), 2002. – Vol. 583. – pp. 209-249.
7. Yasumichi Aoki, Szabolcs Borsanyi, Stephan Durr, Zoltan Fodor, Sandor D. Katz, Stefan Krieg, and Kalman Szabo The QCD transition temperature: results with physical masses in the continuum limit II // J. High Energy Phys. – IOP Publishing (UK), 2009. – Vol. 06 (2009). – id.088. – p. 17.
8. Bazavov A. and Berg B.A. Deconfining phase transition on lattices with boundaries at low temperature // Phys. Rev. D. – American Physical Society (USA), 2012. – Vol. 85. – id.054503. – p. 054503-1.

9. E802 Collaboration (Ahle L. *et al.*) Particle production at high baryon density in central Au+Au reactions at 11.6A GeV/c // Phys. Rev. C. – American Physical Society (USA), 1998. – Vol. **57.** – pp. 466-470.

10. BRAHMS Collaboration (Arsene I. *et al.*) Quark gluon plasma and color glass condensate at RHIC? The Perspective from the BRAHMS experiment // Nucl. Phys. A. – Elsevier (Holland), 2005. – Vol. 757. – pp. 1-27.

11. PHENIX Collaboration (Adcox K. *et al.*) Formation of dense partonic matter in relativistic nucleus-nucleus collisions at RHIC: Experimental evaluation by the PHENIX collaboration // Nucl. Phys. A. – Elsevier (Holland), 2005. – Vol. 757. – pp. 184-283.

12. Back B., Backer M., Ballintijn M., Barton D., Becker B. The PHOBOS perspective on discoveries at RHIC // Nucl. Phys. A. – Elsevier (Holland), 2005. – Vol. 757. – pp. 28-101.

13. STAR Collaboration (Adams J. *et al.*) Experimental and theoretical challenges in the search for quark gluon plasma: The STAR Collaboration's critical assessment of the evidence from RHIC collisions // Nucl. Phys. A. – Elsevier (Holland), 2005. – Vol. 757. – pp. 102-183.

14. ALICE Collaboration (Aamodt K. *et al*.) Elliptic Flow of charged particles in Pb-Pb collisions at 2.76 TeV // Phys. Rev. Lett. – American Physical Society (USA), 2010. – Vol. 105. – id.252302. – p. 252302-1.

15. ALICE Collaboration (Aamodt K. *et al*.) Suppression of Charged Particle Production at Large Transverse Momentum in Central Pb-Pb collisions at $\sqrt{s_{nn}}$=2.76 TeV // Phys. Lett. B. – Elsevier (Holland), 2011. – Vol. 696. – pp. 30-39.

16. ALICE Collaboration (Abelev B. *et al.*) J/Ψ suppression at forward rapidity in Pb-Pb collisions at $\sqrt{s_{nn}}$=2.76 TeV // Phys. Rev. Lett. – American Physical Society (USA), 2012. – Vol. 109. – id.072301. p. 072301-1.

17. ATLAS Collaboration (Aad G. *et al.*) Observation of a Centrality-Dependent Dijet Asymmetry in Lead-Lead Collisions at $\sqrt{s_{nn}}$=2.77 TeV with the

ATLAS Detector at the LHC // Phys. Rev. Lett. – American Physical Society (USA), 2010. – Vol. 105. – id.252303. – p. 252303-1.

18. CMS Collaboration (Chatrchyan S. *et al.*) Observation and studies of jet quenching in PbPb collisions at nucleon-nucleon center-of-mass energy = 2.76 TeV // Phys. Rev. C. – American Physical Society (USA), 2011. – Vol. 84. – id.024906. – p. 024906-1.
19. By ATLAS Collaboration, Probing physics beyond the Standard Model with heavy vector bosons // CERN Press Release, July 8, 2017. – Geneva (Switzerland), 2017. (https://atlas.cern/updates/physics-briefing/probing-heavy-vector-bosons)
20. Gazdzicki Marek, Roehrich Dieter Pion multiplicity in nuclear collisions // Z. Phys. C. – Springer (Germany), 1995. – Vol. 65. – pp. 215-223.
21. Stock R. Compression effects in relativistic nucleus-nucleus collisions // Phys. Rev. Lett. – American Physical Society (USA), 1982. – Vol. 49. – p. 1236.
22. Bao-An Li and Che Ming Ko Formation of superdense hadronic matter in high energy heavy-ion collisions // Phys. Rev. C. – American Physical Society (USA), 1995. – Vol. 52. – p. 2037.
23. Ehehalt W., Cassing W., Engel A., Mosel U., Wolf Gy. Effects of pion and delta selfenergies in nucleus–nucleus reactions // Phys. Lett. B. – Elsevier (Holland), 1993. – Vol. 298. – p. 31.
24. FOPI Collaboration (Eskef M. *et al.*) Identification of baryon resonances in central heavy-ion collisions at energies between 1 and 2 *A* GeV // Eur. Phys. J. A – Springer (Germany), 1998. – Vol. 3. – p. 335.
25. E814 Collaboration (Barrette J. *et al.*) Measurement of pion enhancement at low transverse momentum and of the Δ resonance abundance in Si-nucleus collisions at AGS energy // Phys. Lett. B. – Elsevier (Holland), 1995. – Vol. 351. – p. 93.

26. Brown G. E., Stachel J., and Welke G. M. Pions from resonance decay in Brookhaven relativistic heavy-ion collisions // Phys. Lett. B. – Elsevier (Holland), 1991. – Vol. 253. – p. 19.
27. Krpic D., Skoro G., Picuric I., Backovic S., and Drndarevic S. Baryon resonances in carbon–carbon collisions at 4.2 GeV/*c* per nucleon // Phys. Rev. C. – American Physical Society (USA), 2002. – Vol. 65. – id.034909. – p. 034909-1.
28. Olimov Kh.K., Iqbal A., Haseeb M.Q., Lutpullaev S.L., Yuldashev B.S. Centrality and system-size dependencies of temperatures of soft and hard components of p_t distributions of negative pions in ^{4}He+^{12}C, ^{12}C+^{12}C and ^{12}C+^{181}Ta Collisions at $\sqrt{s_{nn}}$ =3.14 GeV // Physical Review C. – American Physical Society (USA), 2015. – Vol. 92, N. 2– id.024909. – 16 p.
29. Olimov Kh. K.,Olimov K., Gulamov K. G., Olimov A.K., Lutpullaev S.L., Yuldashev B.S., Haseeb M.Q. Partial inelasticity coefficients of negative pions in p, d, α, ^{12}C+^{12}C and p, ^{12}C+^{181}Ta at 4.2 GeV/c per nucleon // International Journal of Modern Physics E. – World Scientific (Singapore), 2015. – Vol. 24, N.10 – id.1550070– 9 p.
30. Olimov Kh. K., Ali Q., Haseeb M.Q., Arif A., Lutpullaev S.L., and Yuldashev B.S. Phenomenological analysis of rapidity distributions of negative pions in central ^{12}C+^{12}C collisions at $\sqrt{s_{nn}}$ =3.14 GeV// International Journal of Modern Physics E. – World Scientific (Singapore), 2015–Vol. 24, N. **7** –id.1550049– 21 p.
31. Olimov Kh.K., Iqbal A., Lutpullaev S.L., Hadi S.A., Glagolev V.V., Yuldashev B.S., Haseeb M.Q. Centrality dependences of soft and hard components of p_t distributions of negative pions in ^{4}He+^{12}C collisions at4.2AGeV/c // International Journal of Modern Physics E. – World Scientific (Singapore), 2015**.** –Vol. 24, N. 5. – id.1550036. – 24 p.
32. Olimov Kh.K., Iqbal A., Lutpullaev S.L., Khan I., Glagolev V.V. Haseeb M.Q., On transverse momentum spectra of negative pions in ^{12}C+^{181}Ta

collisions at 4.2A GeV/c per nucleon // International Journal of Modern Physics E. – World Scientific (Singapore), 2014. –Vol. 23, N. 12. –id.1450084. – 22 p.

33. Iqbal A., Olimov Kh.K., Khan I., Yuldashev B.S., Haseeb M.Q. On centrality and rapidity dependences of transverse momentum spectra of negative pions in $^{12}C+^{12}C$ collisions at 4.2 GeV/c per nucleon // International Journal of Modern Physics E. – World Scientific (Singapore), 2014. – Vol. 23, N. 9.–id.1450047. – 19 p.
34. Olimov Kh.K., Hadi S.A., Haseeb M.Q. Centrality Dependence of Rapidity Spectra of Negative Pions in $^{12}C+^{12}C$ and $^{12}C+^{181}Ta$ Collisions at 4.2 GeV/c per Nucleon // Physics of Atomic Nuclei. – Pleiades Publishing (USA), 2014. – Vol. 77, N. 5. – pp. 613-622.
35. Olimov Kh.K.,Iqbal A., Glagolev V.V., Haseeb M.Q. Analysis of rapidity spectra of negative pions in $d+^{12}C$, $^{12}C+^{12}C$, and $^{12}C+^{181}Ta$ collisions at 4.2 GeV/c per nucleon // Physical Review C. – American Physical Society (USA), 2013. – Vol. 88. –id.064903. – 11 p.
36. Olimov Kh.K., Haseeb M.Q. On spectral temperatures of negative pions produced in $d^{12}C$, $^{4}He^{12}C$, and $^{12}C^{12}C$ collisions at 4.2 A GeV/c // Physics of Atomic Nuclei. – Pleiades Publishing (USA), 2013. – Vol. 76, N. 5. –pp. 595-601.
37. Khan I., Olimov Kh.K. Spectral temperatures of $\Delta^0(1232)$ resonances produced in $p^{12}C$ and $d^{12}C$ collisions at 4.2 GeV/c per nucleon. // Physics of Atomic Nuclei. – Pleiades Publishing (USA), 2013. – Vol. 76, N. 7. – pp. 883-887.
38. Olimov Kh.K., Haseeb M.Q., Hadi S.A. Rapidity and angular dependences of spectral temperatures of negative pions produced in $^{12}C^{12}C$ collisions at 4.2 A GeV/c // International Journal of Modern Physics E. – World Scientific (Singapore), 2013. – Vol. 22, N. 4. – id.1350020. – 14 p.
39. Olimov Kh.K., Haseeb M.Q., Khan I., Olimov A.K., Glagolev V.V. $\Delta^0(1232)$ production in $d+^{12}C$ collisions at 4.2 A GeV/c. // Physical Review C. – American Physical Society (USA), 2012. – Vol. 85. – id.014907. – 14 p.

40. Olimov Kh.K., Haseeb M.Q., Khan I. Comparison of characteristics of Δ^0(1232) produced in $p^{12}C$ and $d^{12}C$ collisions at 4.2 A GeV/c // Physics of Atomic Nuclei. – Pleiades Publishing (USA), 2012. –Vol. 75, N. 4. – pp. 479-487.
41. Olimov Kh.K., Haseeb M.Q. Production of Δ^0(1232)-resonances in $p+^{12}C$ collisions at a momentum of 4.2 GeV/c // The European Physical Journal A – Springer Verlag, 2011. –Vol. 47. – id.79. – p. 16.
42. Olimov Kh.K., Haseeb M.Q., Olimov A.K., Khan I. Analysis of Δ^0(1232) production in collisions of protons with carbon nuclei at 4.2 GeV/*c* // Central European Journal of Physics. – Springer Verlag (Germany), 2011. – Vol. 9. – pp. 1393-1409.
43. Olimov Kh.K., Lutpullaev S.L., Yuldashev B.S., Huseynaliyev Y.H., Olimov A.K. Production of Δ(1232) resonances on oxygen nuclei in ^{16}O+p collisions at a momentum of 3.25 GeV/c per nucleon // The European Physical Journal A. – Springer Verlag (Germany), 2010. – Vol. 44. – pp. 43-54.
44. Olimov Kh.K. Production of delta isobars on tantalum nuclei in CTa-collisions at a projectile momentum of 4.2 GeV/c per nucleon // Physics of Atomic Nuclei. – Pleiades Publishing (USA), 2010. – Vol. 73, N 3. – pp. 433-442.
45. Olimov Kh.K. Production of baryon resonances in collisions of ^{4}He nuclei with carbon nuclei at 4.2 GeV/c per nucleon // Physics of Atomic Nuclei. – Pleiades Publishing (USA), 2008. – Vol. 71, N 1. – pp. 93-97.
46. Olimov Kh.K. Production of baryon resonances in $\pi^- +^{12}C$ interactions at 40 GeV/c // Physical Review C. – American Physical Society (USA), 2007. – Vol. 76. – id.055202. – 7 p.
47. Olimov Kh.K., Lutpullaev S.L., Olimov K., Gulamov K.G., Olimov J.K. Production of Δ^0 and Δ^{++} resonances in collisions of ^{4}He nuclei with carbon nuclei at 4.2 GeV/c per nucleon // Physical Review C. – American Physical Society (USA), 2007. – Vol. 75. – id.067901. – 4 p.
48. Olimov Kh.K. Recent results on investigation of relativistic hadron-nucleus and nucleus-nucleus collisions //“Fundamental and Applied Problems of

Physics": International Conference Tashkent (Conference Programme, Plenary Section), June 13-14, 2017. - Tashkent, 2017. - p. 3.

49. Olimov Kh.K., Lutpullaev S.L., Olimov K., Yuldashev B.S., Gulamov K.G. Recent results on relativistic hadron-nucleus and nucleus-nucleus collisions obtained from bubble chamber experiments //"New Tendencies of Developing Fundamental and Applied Physics: Problems, Achievements, Prospectives": Proceedings of the International Symposium November 10-11, 2016. - Tashkent, 2016. - pp. 10-12.

50. Olimov Kh., Lutpullaev S., Kanokova Sh., Yuldashev B. Phenomenological analysis of rapidity distributions of negative pions in symmetric $^{12}C+^{12}C$ collisions at $\sqrt{s_{nn}}$ = 3.14 GeV //"Fundamental and Applied Problems of Physics": Proceedings of the International Conference November 5-6, 2015.- Tashkent, 2015.- pp. 4-9.

51. Olimov Kh., Lutpullaev S., Kanokova Sh., Yuldashev B. System-size and centrality dependencies of temperatures of soft and hard components of p_t distributions of negative pions in $^{4}He+^{12}C$, $^{12}C+^{12}C$ and $^{12}C+^{181}Ta$ collisions at $\sqrt{s_{nn}}$ = 3.14 GeV // "Fundamental and Applied Problems of Physics": Proceedings of the International Conference November 5-6, 2015.- Tashkent, 2015. - pp. 10-14.

52. Olimov Kh.K.,Lutpullaev S.L., Olimov K., Petrov V.I., Gulamov K.G., Olimov J.K., Yuldashev B.S. The comparative analysis of production of the cumulative π^{+} and π^{-} mesons in interactions of protons and nuclei with nuclei at high energies// "Nuclear and Radiation Physics": Book of Abstracts of the VI International Conference June 4-7, 2007. - Almaty (Kazakhstan), 2007. - pp. 75-77.

53. Olimov Kh.K., Khan I. About spectral temperatures of $\Delta^{0}(1232)$ produced in $p^{12}C$ and $d^{12}C$ collisions at 4.2 *A* GeV/*c* // "Nuclear Science and Its Applications": Book of Abstracts of the VI Eurasian Conference September 25-28, 2012. – Samarkand, 2012.- pp. 135-137.

54. Olimov Kh.K., Haseeb M.Q. Spectral temperatures of π^- mesons produced in d^{12}C ^{4}He^{12}C, and ^{12}C^{12}C collisions at 4.2 A GeV/c //“Nuclear Science and Its Applications”: Book of Abstracts of the VI Eurasian Conference September 25-28, 2012. – Samarkand, 2012. - pp. 137-139.

55. Huseynaliyev Y.H., Suleymanov M.K., Khan. I., Olimov K., Olimov Kh.K. Production of Δ^0-isobar in multi-nucleon π^{-12}C interactions at the momentum of 40 GeV/*c*// “Modern Problems of Nuclear Physics”: Book of Abstracts of the VII International ConferenceSeptember 22-25, 2009. - Tashkent, 2009.- pp. 73-74.

56. Olimov Kh.K. Production of baryon resonances on tantalum nuclei in CTa-collisions at the momentum of 4.2 GeV/*c* per nucleon // “Modern Problems of Nuclear Physics”: Book of Abstracts of the VII International Conference September 22-25, 2009. - Tashkent, 2009. - p. 81.

57. Olimov Kh.K., Lutpullaev S.L., Yuldashev A.A., Olimov A.K., Huseynaliyev Y.H. Production of Δ-resonances in ^{16}Op interactions at a momentum of 3.25 GeV/c per nucleon // “Modern Problems of Nuclear Physics”: Proceedings of the VII International Conference September 22-25, 2009. - Tashkent, 2010. - pp. 269-279. (published in Uzbek Journal of Physics. – 2010. – Vol.12, N 4-6. – pp. 269-279.)

58. Huseynaliev Y.H., Olimov Kh.K., Sattarov A.R. Production of Δ^0-isobars on oxygen nuclei in ^{16}O*p*-interactions at the momentum of 3.25 GeV/*c* per nucleon // “Modern Problems of Nuclear Physics”: Book of Abstracts of the VII International Conference September 22-25, 2009. - Tashkent, 2009. - p. 20.

59. Olimov Kh.K., Olimov K. Correlations in azimuthal plane in production of cumulative pions in relativistic hadron-nucleus and nucleus-nucleus collisions // “Fundamental and applied problems of physics”: Proceedings of the international conference, dedicated to 80th anniversary of academician M. S. Saidov (in Russian) 24-25 November, 2010. - Tashkent, 2010.- pp. 36-38.

60. Лутпуллаев С.Л., *Олимов Х.К.*, Олимов К., Петров В.И. Образование Δ^0 -и Δ^{++}-изобар в адрон- и ядро-ядерных соударениях при высоких энергиях // “Фундаментальные и прикладные вопросы физики”: Сборник обзорных статей республиканской конференции, посвящённой 100-летию академика С.А. Азимова 6–7 ноября, 2014. – Ташкент, 2014. – с. 9-21.
61. Gazdzicky Marek, Gorenstein Mark I., Mrowczynski Stanislaw Pion suppression in nuclear collisions // Eur. Phys. J. C. – Springer (Germany), 1998. – Vol. 5. – p. 129.
62. Gazdzicki M. Entropy in nuclear collisions // Z. Phys. C. – Springer (Germany), 1995. – Vol. 66. – pp. 659-662.
63. Li Bao-An and Bauer Wolfgang Pion spectra in a hadronic transport model for relativistic heavy ion collisions // Phys. Rev. C. – American Physical Society (USA), 1991. – Vol. 44. – p. 450.
64. Netrakanti P. K. and Mohanty B. The width of rapidity distribution in heavy ion collisions // Phys. Rev. C. – American Physical Society (USA), 2005. – Vol. 71. – id.047901.
65. Simic Lj., Backovic S., Salihagic D. Centrality dependence of pion and proton spectra in C+C and C+Ta interactions at 4.2 GeV/*c* per nucleon // Phys. Rev. C. – American Physical Society (USA), 1995. – Vol. 52. – p. 356.
66. Bekmirzaev R.N., Kladnitskaya E.N., and Sharipova S.A. Rapidity distributions of π^- mesons in (p, d, α, C) C interactions at 4.2 GeV/*c* per nucleon // Phys. Atom. Nucl. – Pleiades Publishing (USA), 1995. – Vol. 58. – p. 58.
67. Bekmirzaev R.N., Kladnitskaya E.N., and Sharipova S.A. Rapidity distributions of π^- in (d, α, C) Ta collisions at 4.2 GeV/*c* per nucleon // Phys. Atom. Nucl. – Pleiades Publishing (USA), 1995. – Vol. 58. – p. 1721.
68. Chkhaidze L., Djobava T., Kharkhelauri L., and Mosidze M. The comparison of characteristics of π^- mesons produced in central Mg+Mg interactions with

the quark gluon string model predictions // Eur. Phys. J. A. – Springer (Germany), 1998. – Vol. 1. – p. 299.

69. E895 Collaboration (Klay J. L. *et al.*) Longitudinal Flow of Protons from (2–8) *A* GeV Central Au + Au Collisions // Phys. Rev. Lett. – American Physical Society (USA), 2002. – Vol. 88. – id.102301. – p. 102301-1.

70. Aichelin J. and Werner K. A novel approach to rescattering in ultrarelativistic heavy ion collisions // Phys. Lett. B – Elsevier (Holland), 1993. – Vol. 300. – p. 158.

71. Mohanty B. and Alam J. Velocity of sound in relativistic heavy-ion collisions // Phys. Rev. C – American Physical Society (USA), 2003. – Vol. 68. – id.064903. – p.064903-1.

72. Backovic S. Temperature of negative pions in inelastic (d, α, C) + (C, Ta) collisions at 4.2A GeV/c // Phys. Rev. C. – American Physical Society (USA), 1992. – Vol. 46. – p. 1501.

73. Brockmann R. Pion and Proton "Temperatures" in Relativistic Heavy-Ion Reactions // Phys. Rev. Lett. – American Physical Society (USA), 1984. – Vol. 53. – p. 2012.

74. Chkhaidze L. The temperatures of protons and π^- mesons in central nucleus-nucleus interactions at a momentum of 4.5 GeV/c per incident nucleon // Z. Phys. C. – Springer (Germany), 1992. – Vol. 54. – p. 179.

75. Chkhaidze Lida, Djobava Tamar, Kharkhelauri Lali Temperatures of Λ hyperons, K^0 and π^- mesons produced in C-C and Mg-Mg collisions at 4.2–4.3 A GeV/c // Bull. Georg. Natl. Acad. Sci. – National Academy of Sciences (Georgia), 2010. – Vol. 4. – p. 41.

76. Chkhaidze L. Anisotropic collective flow of Λ-hyperons produced in C+C collisions at 4.2A GeV/c // Nucl. Phys. A. – Elsevier (Holland), 2009. – Vol. 831. – p. 22.

77. Hagedorn R. and Rafelski J. Hot hadronic matter and nuclear collisions // Phys. Lett. B. – Elsevier (Holland), 1980. – Vol. 97. – p. 136.

78. Backovic S. The Boltzmann temperature of negative pions in inelastic (d, α, C) + (C, Ta) collisions at 4.2 A GeV/c // JINR Rapid Communications. – Dubna, 1992. – № 2 [53]-92 – pp. 58-70.
79. Mukhin K. N. and Patarakin O. O. // Phys. Uspekhi. – Moscow, 1995.– Vol. 38. – p. 803.
80. Strokovsky E. A. // Phys. Part. Nucl. – JINR Publishing (Russia), 1993.– Vol. 24. – p. 255. (http://wwwinfo.jinr.ru/publish/Archive/Pepan/1993-v24/v-24-3.htm).
81. Bertsch G. F., Das Gupta S. Phys. Rep. – Elsevier (Holland), 1988. – Vol. 160. – p. 189.
82. Cassing W., Niita K., Wang S.J. // Z. Phys. A. – Springer (Germany), 1988. – Vol. 331. – p. 439..
83. Cassing W., Metag V., Mosel U., Niita K. // Phys. Rep. – Elsevier (Holland), 1990. – Vol. 188. – p. 363.
84. Aichelin J. // Phys. Rep. – Elsevier (Holland), 1991. – Vol. 202. – p. 233.
85. Bass S. A., Hartnack C., Stocker H., Greiner W. // Phys. Rev. C. – American Physical Society (USA), 1994. – Vol. 50. – p. 2167.
86. Bass S. A., Hartnack C., Stocker H., Greiner W. // Phys. Rev. C. – American Physical Society (USA), 1995. – Vol. 51. – p. 3343.
87. Danielewicz P. // Phys. Rev. C. – American Physical Society (USA), 1995. – Vol. 51. – p. 716.
88. Teis S., Cassing W., Effenberger M., Hombach A. // Z. Phys. A. – Springer (Germany), 1997. – Vol. 356. – p. 421.
89. Senger P. in *Multiparticle Correlations and Nuclear Reactions* (edited by Aichelin J. and Ardouin D.) // World Scientific (Singapore), 1994. – p. 285.
90. EOS Collaboration (Hjort E.L. *et al*.) // Phys. Rev. Lett. – American Physical Society (USA), 1997. – Vol. 79. – p. 4345.
91. FOPI Collaboration (Hong B. *et al*.) // Phys. Lett. B. – Elsevier (Holland), 1997. – Vol. 407. – p. 115.
92. Pelte D., arXiv: nucl-ex/9902006v1.

93. DIOGENE Collaboration (Trzaska M. *et al*.) // Z. Phys. A. – Springer (Germany), 1991. – Vol. 340. – p. 325.
94. Chiba J., Kobayashi T., Nadae T. // Phys. Rev. Lett. – American Physical Society (USA), 1991. – Vol. 67. – p. 1982.
95. Hennino T., Ramstein B., Bachalier D. // Phys. Lett. B. – Elsevier (Holland), 1992. – Vol. 42. – p. 42.
96. Pascalutsa Vladimir // Phys. Rep. – Elsevier (Holland), 2007. – Vol. 437. – p. 125.
97. Hacker C. // Phys. Rev. C. – American Physical Society (USA), 2005. – Vol. 72. – id.055203. – p. 055203-1.
98. Simic Lj. // Phys. Rev. C. – American Physical Society (USA), 2009. – Vol. 80. – id.017901. – p. 017901-1.
99. FOPI Collaboration (Hong B. *et al*.) // Phys. Rev. C. – American Physical Society (USA), 1998. – Vol. 57. – p. 244.
100. EOS Collaboration (Lisa M. A. *et al*.) // Phys. Rev. Lett. – American Physical Society (USA), 1995. – Vol. 75. – p. 2662.
101. Ko C. M., Li G. Q. // J. Phys. G. – IOP Publishing (UK), 1996. – Vol. 22. – p. 1673.
102. Weinhold W., Friman B.L., Nörenberg W. // Acta Phys. Pol. B. – Polish Physical Society (Poland), 1996. – Vol. **27**. – p. 3249.
103. FOPI Collaboration (Pelte D. *et al*.) // Z. Phys. A. – Springer (Germany), 1997. – Vol. 357. – p. 215.
104. FOPI Collaboration (Pelte D. *et al*.) // Z. Phys. A. – Springer (Germany), 1997. – Vol. 359. – p. 55.
105. Higgins D. // Phys. Rev. D. – American Physical Society (USA), 1979. – Vol. 19. – p. 731.
106. Particle Data Group (Nakamura K. *et al*.) // J. Phys. G. – IOP Publishing (UK), 2010. – Vol. 37. – id.075021. – p. 075021-1.
107. Brown G. E. and Rho M. // Phys. Rev. Lett. – American Physical Society (USA), 1991. – Vol. 66. – p. 2720.

108. E. V. Shuryak and G. Brown // Nucl. Phys. A. – Elsevier (Holland), 2003. – Vol. 717. – p. 322.
109. Malakhov A. I., Sissakian A. N., Sorin A. S. and Vokal S. Relativistic Nuclear Physics at the Joint Institute for Nuclear Research // Physics of Elementary Particles and Nuclei**.** – JINR Publishing (Dubna, Russia), 2007. – Vol. 38. – p. 407.
110. Baldin A. M. Cumulative meson production // Sov. J. Nucl. Phys. – Nauka (Moscow), 1973. – Vol. 18. – p. 53.
111. Issinsky I. B., Kirillow A. D., Kovalenko A. D. and Rukoyatkin P. A. Beams of the Dubna Synchrophasotron and Nuclotron // ACTA Physica Polonica B. – Polish Physical Society (Poland), 1994. – Vol. 25. – p. 3.
112. Perkins Donald H. Introduction to high energy physics (4th Edition) // Cambridge University Press, 2000. – Cambridge (UK), 2000 – pp. 366-368.
113. Gron Tudor Jones. Archived Bubble Chamber Teaching Materials developed by HST participants //University of Birmingham (UK), Compiled by Karl Sarnow K., Gymnasium Isernhagen (Germany) and Recompiled by Grejtak V. (Slovakia);
(http://teachers.web.cern.ch/teachers/archiv/HST2005/bubble_chambers)
114. Armutlisky D. Multiplicity, Momentum and Angular Distributions of Protons from the Interactions of *p, d, α* and C with Carbon at 4.2 GeV/*c*/Nucleon Momentum // Z. Phys. A. – Springer (Germany), 1987. – Vol. 328. – p. 455.
115. Agakishiyev H. N. Multiplicity, momentum and angular characteristics of π^- mesons for *p*C, *d*C, *α*C and CC interactions at 4.2 GeV/*c* per nucleon // Z. Phys. A. – Springer (Germany), 1985. – Vol. 27. – p. 177.
116. Bondarenko A. I., Bondarenko R. A., Kladnitskaya E. N., Kuznetsov A. A., Toneeva G. P. and Yuldashev B. S. The Ensemble of interactions on carbon and hydrogen nuclei obtained using the 2 m propane bubble chamber exposed to the beams of protons and H-2, He-4, C-12 relativistic nuclei at the Dubna Synchrophasotron // JINR Communications. – Dubna, 1998. – № P1-98-292.

117. Flaminio V., Moorhead W.G., Morrison D.R.O., Rivoi N. Compilation of cross sections // CERN-HERA Reports. – CERN (Geneva), 1983. – № 83-02.

118. Baatar Ts. Analyzing the Features of π^- Mesons and Protons from *A*C Interactions at a Momentum of p = 4.2 GeV/*c* per Projectile Nucleon on the Basis of the FRITIOF Model // Phys. At. Nucl. – Pleiades Publishing (USA), 2000. – Vol. 63. – p. 839.

119. Galoyan A. S., Kladnitskaya E. N., Rogachevsky O. V., Togoo R., and Uzhinskii V. V. Features of *p*C Interactions at a Momentum of 4.2 GeV/*c* versus the Degree of Centrality of a Collisions between a Proton and a Carbon Nucleus: Kinematical Features of Secondaries // Phys. At. Nucl. – Pleiades Publishing (USA), 2004. – Vol. 67. – p. 256.

120. Angelov N. Interaction Cross Sections and Negative pion Multiplicities in Nucleus-Nucleus Collisions at 4.2 GeV/*c* Per Nucleon // JINR Preprint. – Dubna, 1979. – № E1-12548.

121. Batskovich S., Boldea V., Grishin V. G. // JINR Preprint. – Dubna, 1988. – № P1-88-858.

122. Agakishiev G. N. // JINR Preprint. – Dubna, 1981. – № P1-81-176.

123. Agakishiev G. N. // JINR Preprint. – Dubna, 1982. – № 1-82-235.

124. Gankhuyag B. and Uzhinskii V. V. Modified FRITIOF code: Negative charged particle production in high-energy nucleus-nucleus interactions // JINR Preprint. – Dubna, 1996. – № P2-96-419.

125. Uzhinskii V. V. MODIFIED CODE FRITIOF. User's Guide // JINR Communications. – Dubna, 1996. – № E2-96-192.

126. Gankhuyag B. Description of π^- meson and proton characteristics in *np* interactions at $P(n)$=1.25-GeV/*c*–5.1-GeV/*c* within the framework of FRITIOF model // JINR Preprint. – Dubna, 1998. – № P2-98-26.

127. Abdel Waged K. and Uzhinskii V. V. Model of nuclear disintegration in high-energy nucleus-nucleus interactions // Phys. At. Nucl. – Pleiades Publishing (USA), 1997. – Vol. 60. – p. 828.

128. Shmakov S. Yu. DIAGEN - Generator of inelastic nucleus-nucleus interaction diagrams // Comp. Phys. Commun. – Elsevier (Holland), 1989. – Vol. 54. – p. 125.

129. EMU-01 Collaboration (Adamovich M. I. *et al*.) Complex analysis of gold interactions with photoemulsion nuclei at 10.7 GeV/nucleon within the framework of cascade and FRITIOF models // Z. Phys. A. – Springer (Germany), 1997. – Vol. 358. – p. 337.

130. Weisskopf V. Statistics and Nuclear Reactions // Phys. Rev. – American Physical Society (USA), 1937. – Vol. 52. – p. 295.

131. Barashenkov V.S. and Toneev V. D. Interactions of High-Energy Particles and Nuclei with Nuclei // Atomizdat (Moscow), 1972.

132. Amelin N. S., Gudima K. K., Sivoklokov S. Yu., and Toneev V. D. Further Development Of A Quark-Gluon-String Model For Describing High-Energy Collisions With A Nuclear Target // Sov. J. Nucl. Phys. – Nauka (Moscow, USSR), 1990. – Vol. 52. – p. 172.

133. Amelin N. S., Staubo E. F., Csernai L. P., Toneev V. D., and Gudima K. K. Strangness production in proton and heavy ion collisions at 14.6 *A* GeV // Phys. Rev. C. – American Physical Society (USA), 1991. – Vol. 44. – p. 1541.

134. Stock R. Particle production in high energy nucleus–nucleus collisions // Phys. Rep. – Elsevier (Holland), 1986. – Vol. 135. – pp. 259–315.

135. Nagamiya S. Role of Mean Free Paths of Product Particles in High-Energy Nucleus-Nucleus Collisions // Phys. Rev. Lett. – American Physical Society (USA), 1982. – Vol. 49. – pp. 1383-1386.

136. Kapusta J. Particle production in the nuclear fireball model // Phys. Rev. C. – American Physical Society (USA), 1977. – Vol. 16. – pp. 1493-1498.

137. Gosset J. Calculations with the nuclear firestreak model // Phys. Rev. C. – American Physical Society (USA), 1978. – Vol. 18. – pp. 844-855.

138. Nagamiya S. Single-Particle Spectra Associated with High-Multiplicity Events in 800 MeV/Nucleon Ar on KCl and Pb // Phys. Rev. Lett. – American Physical Society (USA), 1980. – Vol. 45– pp. 602-605.

139. Bohrmann S. and Knoll J. Finite number of effects in high-energy nuclear collision: Implications on pion spectra // Nucl. Phys. A. – Elsevier (Holland), 1981. – Vol. 356. – pp. 498-516.

140. Hagedorn R. *in* Cargese Lectures in Physics VI (ed. by Schatzman E.) // Gordon and Breach (New York), 1973 – p. 643.

141. Backovic S., Boldea V., Grishin V. G., Ditza S. // Sov. J. Nucl. Phys. – Nauka (Moscow, USSR), 1989. – Vol. 50. – p. 1001.

142. Galoyan A. S. // Phys. At. Nucl. – Pleiades Publishing (USA), 2003. – Vol. 66. – p. 836.

143. Galoyan A. S. Simulation of Nucleus-Nucleus Interactions in the Framework of the FRITIOF Model at the Energy of 3.3 GeV/Nucleon // JINR Preprint. – Dubna, 2000. – № E2-2000-306.

144. Glagolev V. V., Gulamov K. G., Lipin V. D. // Eur. Phys. J A. – Springer (Germany), 2001. – Vol. 11. – p. 285.

145. Weinhold W., Friman B.L., Nörenberg W. // Acta Phys. Pol. B. – Polish Physical Society (Poland), 1996. – Vol. 27. – p. 3249.

146. Olimov K., Yuldashev A. A., Yuldashev B. S. // JETP Lett. – Moscow, 1980. – Vol. 32. – p. 604.

147. Gudima K. K., Toneev V. D. // Nucl. Phys. A. – Elsevier (Holland), 1983. – Vol. 400. – p. 173.

148. Bekmirzaev R. N., Kladnitskaya E. N., Muminov M. M., and Sharipova S. A. // Phys. At. Nucl. – Pleiades Publishing (USA), 1995. – Vol. 58. – p. 1548.

149. Bekmirzaev R. N., Kladnitskaya E. N., and Sharipova S. A. // Phys. At. Nucl. – Pleiades Publishing (USA), 1995. – Vol. 58. – p. 58.

150. Didenko L. A., Grishin V. G., and Kuznetsov A. A. // Nucl. Phys. A. – Elsevier (Holland), 1991. – Vol. 525. – p. 653.
151. Braun-Munzinger P. // Phys. Lett. B. – Elsevier (Holland), 1995. – Vol. 344. – p. 43.
152. Braun-Munzinger P. // Phys. Lett. B. – Elsevier (Holland), 1996. – Vol. 356. – p. 1.
153. Andersson B. // Nucl. Phys. B. – Elsevier (Holland), 1987. – Vol. 281. – p. 289.
154. Nilsson-Almquist B. and Stenlund E. // Comput. Phys. Commun. – Elsevier (Holland), 1987. – Vol. 43. – p. 387.
155. EMU-01 Collab. (Adamovich M. I. *et al*.) // Z. Phys. A. – Springer (Germany), 1997. – Vol. 358. – p. 337.
156. Bondarenko A. I. // Phys. At. Nucl. – Pleiades Publishing (USA), 2002. – Vol. 65. – p. 90.
157. Galoyan A. S., Melkumov G. L., and Uzhinskii V. V., // Phys. At. Nucl. – Pleiades Publishing (USA), 2002. – Vol. 65. – p. 1722.
158. EMU01 Collaboration (Adamovich M. I. *et al*.) // Phys. Rev. Lett. – American Physical Society (USA), 1992. – Vol. 69. – p. 745.
159. NA49 Collaboration (Alt C. *et al*.) // Phys. Rev. C. – American Physical Society (USA), 2008. – Vol. 77. – id. 024903. – p. 024903-1.
160. De B. and Bhattacharyya S. // Int. J. Mod. Phys. A. – World Scientific (Singapore), 2004. – Vol. 19. – p. 2313.
161. De B., Bhattacharyya S. and Guptaroy P. // Int. J. Mod. Phys. A. – World Scientific (Singapore), 2002. – Vol. 17. – p. 4615.
162. Sau G. // Il Nuovo Cimento B. – Italian Physical Society (Italy), 2010. – Vol. 125. – p. 833.
163. Sau G. // J. Mod. Phys., 2011 – Vol. 2. – p. 1354.
164. Thome W. // Nuclear Physics B. – Elsevier (Holland), 1977. – Vol. 129. – p. 365.
165. Faessler M. A. // Phys. Rep. – Elsevier (Holland), 1984. – Vol. 115. – p. 1.

166. Schmidt H. R., Schukraft J. // J. Phys. G. – IOP Publishing (UK), 1993. – Vol. 19. – p. 1705.
167. Peitzmann T. // Physics Letters B. – Elsevier (Holland), 1999. – Vol. 450. – p. 7.
168. Benecke J. // Phys. Rev. – American Physical Society (USA), 1969. – Vol. 188. – p. 2159.
169. Feynmann R. P. // Phys. Rev. Lett. – American Physical Society (USA), 1969. – Vol. 23. – p. 1415.
170. S. Bhattacharyya // Lett. Nuovo Cimento. – Italian Physical Society (Italy), 1985. – Vol. 44 – p. 119.
171. Hwa R. C. // Phys. Rev. C. – American Physical Society (USA), 2001. – Vol. 64. – id. 054611. – p. 054611-1.
172. Chkhaidze L., Danielewicz P., Djobava T., Kharkhelauri L., and Kladnitskaya E. // Nucl. Phys. A. – Elsevier (Holland), 2007. – Vol. 794. – p. 115.
173. Chkhaidze L., Djobava T., Galoyan A. // Phys. Rev. C. – American Physical Society (USA), 2011. – Vol. 84. – id. 064915. – p. 064915-1.
174. Chkhaidze L. V. // Phys. Atom. Nucl. – Pleiades Publishing (USA), 2004. – Vol. 67. – p. 693.
175. Nagamiya S. // Phys. Rev. C. – American Physical Society (USA), 1987. – Vol. 24. – p. 971.
176. Grishin V. G. // JINR Preprint. – Dubna, 1986. – № P1-86-639.
177. Gudima V. D. // Phys. Elem. Part. At. Nucl. – JINR Publishing (Russia), 1986. – Vol. 17 – p. 1093.
178. NA44 Collaboration (Bearden I. *et al.*) // Phys. Rev. Lett. – American Physical Society (USA), 1997. – Vol. 78. – p. 2080.
179. Anikina M. The analysis of π^- mesons produced in nucleus-nucleus collisions at a momentum of 4.5 GeV/c nucleon in light front variables // Eur. Phys. J. A. – Springer (Germany), 2000. – Vol. 7. – p. 139.

180. Bravina L. Fluid dynamics and quark gluon string model: What we can expect for Au+Au collisions at 11.6 *A* GeV/*c* // Nucl. Phys. A. – Elsevier (Holland), 1994. – Vol. 566. – p. 461.

181. Bialas A. Multiplicity distributions in nucleus-nucleus collisions at High-Energies // Nucl. Phys. B. – Elsevier (Holland), 1976. – Vol. 111. – p. 461.

182. Shabelsky Y. M. On the multiplicity of the secondaries produced in collisions of relativistic nuclei // Acta Phys. Pol. B. – Polish Physical Society (Poland), 1979. – Vol. 10. – p. 1049.

183. Simic Lj. Dependence of average characteristics of π^- mesons on number of interacting protons in nucleus-nucleus collisions at 4.2 GeV/*c* per nucleon // Phys. Rev. D. – American Physical Society (USA), 1986. – Vol. 34. – p. 692.

184. Flaminio V., Moorhead W.G., Morrison D.R.O., Rivoi N. Compilations of cross sections III – p and $\bar{p}$ induced reactions // CERN-HERA Report. – CERN (Geneva), 1984. – № 84-01 – 328 p.

185. STAR Collaboration (Abelev B. I. *et al.*) Systematic measurements of identified particle spectra in *pp*, *d*+Au, and Au+Au collisions at the STAR detector // Phys. Rev. C. – American Physical Society (USA), 2009. – Vol. 98. – id.034909. – p. 034909-1.

186. Chkhaidze L., Djobava T., Gogiberidze G. // Study of the inclusive reaction Mg+Mg$\rightarrow\pi^-+X$ at a momentum of 4.3 GeV/*c* per incident nucleon // J. Phys. G. – IOP Publishing (UK), 1996. – Vol. 22. – p. 641.

187. FOPI Collaboration (Hong B. *et al*.) Stopping and radial flow in central ^{58}Ni+^{58}Ni collisions between 1 *A* and 2 *A* GeV // Phys. Rev. C. – American Physical Society (USA), 1998. – Vol. 57. – p. 244.

188. Gilg A. // GSI Scientific Report. – Darmstadt, 1996. – № 96-1. – p. 52.

189. Pfeiffer M. // GSI Scientific Report. – Darmstadt, 1993. – № 93-1. – p. 58.

190. Schwalb O. // GSI Scientific Report. – Darmstadt, 1993. – № 93-1. – p. 62.

191. Appenheimer M. // GSI Scientific Report. – Darmstadt, 1997. – № 97-1. – p. 58.

192. Muntz C. // GSI Scientific Report. – Darmstadt, 1995. – № 95-1. – p. 77.

193. Herrmann N., Wessels J. P., Wienold T. Collective Flow in Heavy-Ion Collisions // Annu. Rev. Nucl. Part. Sci. – Annual Reviews (USA), 1999. – Vol. 49. – p. 581.